

DOI: <https://doi.org/10.15388/vu.thesis.705>
<https://orcid.org/0000-0001-5398-8225>

VILNIUS UNIVERSITY

Daina Bujanauskienė (*née* Pamedytytė)

Molecular profiling of synapses during brain circuit refinement

DOCTORAL DISSERTATION

Natural Sciences,
Biochemistry (N 004)

VILNIUS 2024

The dissertation was prepared between 2018 and 2024 at the Institute of Biosciences Life Sciences Center of Vilnius University (Vilnius, Lithuania). The research was supported by the European Regional Development Fund under grant agreement No. 01.2.2-CPVA-V-716-01-0001 with the Central Project Management Agency (CPVA), private support grant from UAB Realinija and The Boehringer Ingelheim Fonds (BIF).

Academic supervisor –

Dr. Urtė Neniškytė (Vilnius University, Natural Sciences, Biochemistry, N 0004).

This doctoral dissertation will be defended in a public meeting of the Dissertation Defence Panel:

Chairman – Prof. Dr. Vilmantė Borutaitė (Lithuanian University of Health Sciences, Life Sciences, Biochemistry – N 004).

Members:

Dr. Etienne Herzog (University of Bordeaux, France, Life Sciences, Biophysics - N 011),

Dr. Giancarlo Russo (Vilnius University, Life Sciences, Biochemistry – N 004),

Dr. Giedrius Steponaitis (Lithuanian University of Health Sciences, Life Sciences, Biology – N 010),

Dr. Giedrė Valiulienė (Vilnius University, Life Sciences, Biochemistry – N 004).

The dissertation shall be defended at a public meeting of the Dissertation Defence Panel at 13:00 on the 12th of December 2024 in meeting room R401 of the VU Life Sciences Center.

Address: Saulėtekio al. 7, LT-10257, Vilnius, Lithuania

Tel. +370 5 223 4419; e-mail: info@gmc.vu.lt

The text of this dissertation can be accessed at the library of Vilnius University, as well as on the website of Vilnius University:

www.vu.lt/lt/naujienos/ivykiu-kalendorius

VILNIAUS UNIVERSITETAS

Daina Bujanauskienė (Pamedytytė)

Sinapsių molekulinų profilių nustatymas smegenų tinklų genėjimo metu

DAKTARO DISERTACIJA

Gamtos mokslai,
Biochemija (N 004)

VILNIUS 2024

Disertacija rengta 2018–2024 metais Vilniaus universiteto Gyvybės mokslų centro Biomokslų institute. Mokslinius tyrimus rėmė Europos regioninės plėtros fondas (Finansavimo Nr. 01.2.2-CPVA-V-716-01-0001) su Centrine Projektų Valdymo Agentūra (CPVA), privatus finansavimas iš UAB Realinija ir Boehringer Ingelheim Fondas (BIF).

Mokslinis (-ė) vadovas (-ė) – dr. Urtė Neniškytė (Vilniaus universitetas, gamtos mokslai, biochemija, N-004).

Gynimo taryba:

Pirmininkė – prof. dr. Vilmantė Borutaitė (Lietuvos sveikatos mokslų universitetas, gamtos mokslai, biochemija – N 004).

Nariai:

dr. Etienne Herzog (Bordo universitetas, Prancūzija, gamtos mokslai, biofizika – N 011),

dr. Giancarlo Russo (Vilniaus universitetas, gamtos mokslai, biochemija – N 004),

dr. Giedrius Steponaitis (Lietuvos sveikatos mokslų universitetas, gamtos mokslai, biologija – N 010),

dr. Giedrė Valiulienė (Vilniaus universitetas, gamtos mokslai, biochemija – N 004).

Disertacija ginama viešame Gynimo tarybos posėdyje 2024 m. gruodžio mėn. 12 d. 13:00 val. Gyvybės mokslų centro R401 auditorijoje. Adresas: Saulėtekio al. 7, LT-10257, Vilnius, Lietuva, tel. +370 5 223 4419; el. paštas info@gmc.vu.lt.

Disertaciją galima peržiūrėti Vilniaus universiteto bibliotekoje ir Vilniaus universiteto interneto svetainėje adresu:

<https://www.vu.lt/naujienos/ivykiu-kalendorius>

CONTENTS

ABBREVIATIONS.....	9
INTRODUCTION.....	10
SCIENTIFIC NOVELTY	12
DEFENDING STATEMENTS	14
1. LITERATURE REVIEW.....	15
1.1. The critical period of plasticity and its mechanisms	15
1.1.1. Visual cortex as a system to study critical period plasticity....	16
1.1.2. Molecular and cellular mechanisms of synaptic plasticity and network refinement.....	18
1.1.3. Local protein synthesis and its impact on plasticity	22
1.2. Research challenges of local protein synthesis.....	24
1.2.1. Lack of appropriate quality controls for synaptic mRNA samples 26	
1.2.2. Current tools to label PS externalizing synapses destined for elimination.....	28
2. MATERIALS AND METHODS	31
2.1. Animals	31
2.2. Human samples	31
2.3. Human brain tissue preparation.....	32
2.4. Mouse brain slice preparation	32
2.5. Fluorescence imaging and quantification.....	33
2.6. PGK1 cDNA Plasmids	33
2.7. Crude synaptosome sample preparation.....	34
2.8. Fluorescence Activated Synaptosome Sorting (FASS).....	34
2.9. Synaptosome analysis using Cytex Amnis FlowSight imaging flow cytometer35	
2.10. RNA extraction	35
2.11. Preparation of heat-degraded RNA samples	35

2.12. Evaluation of RNA concentration and rRNA integrity	35
2.13. cDNA synthesis and RT-qPCR	36
2.14. Integrity value correction for difference in amplification efficiency 36	
2.15. RNA next-generation sequencing	37
2.16. RNA sequencing data analysis	37
2.17. C2 cloning and fusion with tags	38
2.18. The mutagenesis of C2 domain	39
2.19. pAAV plasmid for virus production	39
2.20. Protein expression and purification	39
2.21. Cultivation of mammalian cell lines	40
2.22. Apoptosis assay	40
2.23. Cell image analysis	41
2.24. Adeno-associated virus production	41
2.25. The modelling of the structure of fused recombinant proteins	42
2.26. Organotypic hippocampus slice culture preparation	42
2.27. PS labelling in AAV-transduced OHSC	43
2.28. OHSC immunofluorescence labelling	43
2.29. OHSC image analysis	44
2.30. AAV transduction in vivo	45
2.31. Statistical analysis	45
3. RESULTS	47
3.1. The analysis of axonal boutons during cortex maturation	47
3.1.1. Axon bouton and C1q dynamics during the critical period of plasticity in mouse visual cortex	47
3.1.2. Implementation of Fluorescence Activated Synaptosome Sorting (FASS) for local transcriptome assessment	49
3.2. 5':3' assay for direct mRNA integrity evaluation	53
3.2.1. 5':3' assay is based on PGK1 cDNA	55
3.2.2. The integrity value of 5':3' assay should be corrected to reflect primer pair amplification efficiency	56

3.2.3. The integrity value of 5':3' assay accurately represents different ratios of primer binding sites.....	58
3.2.4. 5':3' integrity value and RIN value correlate well in heat-treated RNA samples.....	59
3.2.5. In human post-surgical brain tissue samples, 5':3' integrity value represents the RNA integrity better than RIN	62
3.2.6. 5':3' assay can be used to measure RNA integrity in synaptosomal preparations	64
3.3. Local synaptic transcriptome	64
3.3.1. Synaptic RNA-sequencing and data quality control	65
3.3.2. Local excitatory synaptic transcriptome and its changes during cortex maturation.....	69
3.3.3. Development of genetically encoded tool for the labelling of exposed synaptic phosphatidylserine	77
3.4. Local synaptic presence of transcripts involved in "don't eat-me" and "eat-me" signaling	78
3.4.1. PS labeling protein modelling suggests structural integrity of fused proteins	79
3.4.3. C2-mKate and C2-SNAP label apoptotic cells <i>in vitro</i>	81
3.4.4. Expression of genetically encoded C2 probes in tissue culture	84
3.4.5. AAV-encoded C2 probes label apoptotic cells in tissue culture	86
3.4.6. AAV-C2-SNAP efficiently transduce the central nervous system <i>in vivo</i>	87
4. DISCUSSION	90
4.1. Dynamics of axonal bouton changes during critical periods and these changes can be studied by using extracted labelled synaptosome population.....	90
4.2. Developed 5':3' assay can be applied to assess synaptic mRNA integrity	91
4.3. Local transcriptomic changes during visual cortex refinement	94
4.4. Genetically encoded PS labeling tool efficiently identifies exposed PS in the neurons.....	97
CONCLUSIONS.....	99

BIBLIOGRAPHY	100
SANTRAUKA	129
ACKNOWLEDGEMENTS	164
LIST OF PUBLICATIONS	165
CONFERENCE PROCEEDINGS	166
CURRICULUM VITAE	168

ABBREVIATIONS

Bp	base pairs
C1q	complement component 1q
cDNA	copy DNA
CNS	central nervous system
CP	critical period
CPM	counts per million
GO	gene ontology
IR	insulin receptor
LGNd	lateral geniculate nucleus, pars dorsalis
LTD	long-term depression
LTP	long-term potentiation
mRNA	messenger RNA
Pgk1	phosphoglycerate kinase 1
PNNs	perineuronal nets
PS	phosphatidylserine
qPCR	quantitative polymerase chain reaction
RIN	RNA integrity number
RNA-seq	RNA sequencing
rRNA	ribosomal RNA
RT	reverse transcription
TPM	transcripts per million
V1	primary visual cortex

INTRODUCTION

The development of the brain relies heavily on critical periods (CPs) characterized by heightened synaptic plasticity, facilitating structural and functional alterations in response to sensory stimuli. This early plasticity makes experiences critical for developing complex skills such as language and musical abilities, which become harder to acquire in adulthood due to the more stable but less flexible nature of the adult brain's circuits (Skoe and Kraus 2013; White et al. 2013; Hartshorne, Tenenbaum, and Pinker 2018). Once critical period closes, synaptic plasticity significantly declines. Recent investigations underscore the role of neuronal interactions with glial cells, the balance between inhibition and excitation, the development of myelin and perineuronal nets and local synaptic protein synthesis in regulating this process (Takesian and Hensch 2013; Schafer et al. 2012; Reichelt et al. 2019; Stedehouder et al. 2018; Rajgor, Welle, and Smith 2021). During critical periods of plasticity, the dynamic formation and elimination of synapses is also needed and relies on molecular signals denoted as "don't eat-me" and "eat-me" signals. Among these signals are externalized phosphatidylserine (PS) and complement opsonins C1q and C3 that can be recognized by microglia (Mordelt and de Witte 2023). Lastly, local protein synthesis at synaptic terminals plays a pivotal yet poorly understood role in synaptic plasticity. Neurons, with their complex and polarized structures, require local protein synthesis at presynaptic and postsynaptic sites to update the synaptic proteome, supporting rapid changes in synaptic function essential for plasticity during critical periods (Rajgor, Welle, and Smith 2021). However, the local synaptic biochemical processes initiating synapse elimination remain elusive.

The study of local protein synthesis and mRNA presence in axons was previously challenging due to the delicate nature of axonal processes and the difficulty in isolating pure axonal material. Synaptosome preparations have been immensely helpful in studying nerve terminals and local protein synthesis, despite the drawback of significant contamination from non-synaptic compartments (Bai and Witzmann 2007; Burré, Zimmermann, and Volknandt 2007; Boyken et al. 2013; Weingarten et al. 2014; Wilhelm et al. 2014). Fluorescence Activated Synaptosome Sorting (FASS) improved the specificity and purity of synaptosome samples, facilitating discoveries about local protein synthesis and synapse-specific proteomes (Biesemann et al. 2014). Nevertheless, appropriate RNA quality control methods for such samples are lacking. Traditionally, RNA integrity evaluation is based on ribosomal RNAs (rRNAs). However, gene expression studies are usually

focused on protein coding messenger RNAs (mRNAs). As rRNA and mRNA have significant structural and functional differences, the assumption that rRNA integrity properly represents mRNA integrity may not be accurate (Fleige and Pfaffl 2006; Sidova et al. 2015; Sonntag et al. 2016). Moreover, contrary to whole tissue RNA samples, subcellular preparations such as synaptosomes contain almost no rRNA, thus prohibiting the use of traditional rRNA-based methods to assess sample RNA integrity. Moreover, as additional crucial "eat-me" signals are identified for the remodelling and optimization of neural networks through synaptic pruning, there is an increasing need for sensitive tools to study these signals at synaptic connections. Genetically encoded biosensors are needed for visualizing one such signal, phosphatidylserine (PS) exposure, within synapses. Promising candidates for this purpose include the PS-binding domains of proteins like MFG-E8, which are recognized for their high sensitivity and specificity (Reddy Nanga, Vivekanandan, and Yoon 2007; Ye et al. 2013). Such improved methods and biosensors have the potential to significantly advance research on local transcriptomic changes and synaptic pruning during critical periods of neural plasticity.

Study aim

The aim of this study was to characterize the local transcriptome and its changes in excitatory synapses during visual cortex refinement and to develop a tool to label and study synapses destined for elimination.

Objectives

1. To characterize axon bouton dynamics and implement FASS for synaptic transcriptome assessment in the critical period of plasticity of mouse visual cortex.
2. To develop a method for direct mRNA integrity evaluation suitable for synaptosomal preparations lacking the prominent rRNA representation.
3. To define local synaptic transcriptome changes during mouse visual cortex maturation.
4. To develop a genetically encoded phosphatidylserine (PS) probe to label synapses destined for elimination during cortical refinement.

SCIENTIFIC NOVELTY

In the study of neuronal plasticity during development, both dendritic spines and axonal boutons are frequently examined; however, dendritic spines are more commonly studied (Majewska and Sur 2003; Tropea et al. 2010; Zhou, Lai, and Gan 2017; Y. J. Sun et al. 2019). Therefore, despite their importance in understanding synaptic connections and plasticity, axonal boutons appear to be understudied. Notably, only a few studies have investigated axonal changes in the visual cortex during development, primarily focusing on changes following monocular visual deprivation (Y. J. Sun et al. 2019; Sammons, Clopath, and Barnes 2018). Consequently, there is a lack of knowledge regarding axonal bouton changes during the normal, unperturbed critical period. This study aimed to investigate changes in visual cortex bouton size and density during normal brain maturation. Additionally, while it is well established that C1q plays a role in labelling unnecessary synapses for refinement in the retinogeniculate system and hippocampus during early development (Presumey, Bialas, and Carroll 2017), there is a gap

in knowledge regarding network refinement during the critical period of plasticity. Therefore, this study also assessed C1q labelling in the visual cortex before, during, and after the critical period to address this gap.

Local protein synthesis is now recognized as a critical component in synaptic transmission and plasticity (Holt, Martin, and Schuman 2019; Cioni, Koppers, and Holt 2018). Consequently, this study not only delineates the general local transcriptome of excitatory neurons in the visual cortex but also examines its alterations during cortical refinement. Previous studies have characterized the local synaptic transcriptome (Cajigas et al. 2012; Hafner et al. 2019). However, the precision of some of these findings is questionable. For example, utilized micro dissected neuropil comprises a mixture of axonal and dendritic projections, and glial cells making it a tricky sample to draw conclusions about local presynaptic transcriptome. Additionally, synaptosomal preparations in prior research were limited to adult mice, focusing solely on synaptic transcripts in this age group. Therefore, this study uniquely investigates the developmental changes in the local synaptic transcriptome.

Research on the local synaptic transcriptome presents several challenges, one of which is ensuring appropriate quality control for extracted RNA. Traditional methods for evaluating RNA integrity rely on ribosomal RNA (rRNA). However, subcellular samples like synaptosomes contain less rRNA compared to whole tissue lysates, and studies indicate that rRNA levels decrease even further as axons mature (Costa et al. 2019). Additionally, the RNA quality of synaptosomal preparations has not been previously reported, likely due to the absence of suitable methods. To address this, a novel 5':3' assay was developed in this study to directly measure mRNA integrity, providing an appropriate quality control method for synaptosomal preparations.

Lastly, to advance the research on brain development and refinement, it is essential to utilize highly sensitive tools that can effectively label and visualize synapses along with their exposed "eat-me" signals for synaptic pruning. One such signal is phosphatidylserine (PS), which is known to be externalized on synaptic terminals marked for elimination by microglia (Schafer et al. 2012; Neniskyte et al. 2023a). Although some tools, such as Annexin V (Hu et al. 2008), exist for labeling exposed PS, they lack sensitivity and are unsuitable for *in vivo* applications. Consequently, during this study a novel genetically encoded and modifiable PS labelling probe was developed based on the C2 domain of MFG-E8 protein for use *in vitro*, *ex vivo*, and *in vivo*. This new tool demonstrated higher selectivity and sensitivity for PS detection compared to

other commercially available labelling tools, offering significant potential for studying network refinement through synaptic pruning.

DEFENDING STATEMENTS

1. The enrichment of excitatory synaptosomes exceeding 70% can be attained through the utilization of FASS methodology, enabling the collection and analysis of bouton alterations during the maturation of the cortex.
2. The developed 5':3' assay exhibits robustness in evaluating mRNA integrity within mouse brain tissue and synaptosome samples lacking the prominent ribosomal RNA representation.
3. Local synaptic transcripts are implicated in cellular transport, regulation of synaptic transmission, and localized protein synthesis, while synaptic transcriptomic profile is modulated to support plasticity mechanisms and network refinement.
4. The designed PS probe effectively labels exposed PS, thereby enabling its visualization and quantification across diverse assays, including those conducted *in vivo*.

1. LITERATURE REVIEW

1.1. The critical period of plasticity and its mechanisms

The brain's natural ability to adapt and change shifts drastically over the course of a lifetime. The brain exhibits very high plasticity during early development before essential neural circuits are fully established. This characteristic makes early experiences critical for the development of certain complex skills like language and musical abilities, explaining why acquiring these skills is much more difficult in adulthood (Skoe and Kraus 2013; White et al. 2013; Hartshorne, Tenenbaum, and Pinker 2018). Unlike the developing brain, the circuits in the adult brain are more stable but less adjustable for learning new complicated skills. This shift from a flexible to a more stable state is beneficial as it enables the progressive consolidation and retention of new and increasingly complex perceptual, motor, and cognitive functions (Cisneros-Franco et al. 2020). However, establishing a stable neural network limits the ability to make substantial changes to the circuitry in the future.

It is now well known that brain plasticity reaches its peak during certain time windows in early development, known as critical periods (CPs) (Hensch 2005). A critical period is an exceptionally sensitive period where sensory experiences are essential for shaping neural circuits for basic sensory processing. During this time, the brain establishes an optimal neural representation of the environment (Hensch 2005; Hubel and Wiesel 1970). Abnormal or absent sensory experiences can have lasting effects, leading to partly permanent adaptations that hinder learning certain skills or processing stimuli later in life. Even if sensory input is restored later, its processing is suboptimal and results in permanent functional deficits (Fine et al. 2003; Lewis and Maurer 2005). A good example of this would be infant cataracts. If they are removed early during the high plasticity period, individuals can develop near-normal vision. However, if untreated until adulthood, people will have significantly diminished visual abilities (Martins Rosa et al. 2013).

Critical periods have been documented across various systems in a wide range of species. Primary sensory areas, as the brain's gateway to external stimuli, have been studied the most (Zhang, Bao, and Merzenich 2002; Villers-Sidani et al. 2007; Erzurumlu and Gaspar 2012; Hooks and Chen 2007). It is now evident that multiple distinct CPs exist, with each distinct brain area having a specific narrow window of maximal plasticity (Figure 1.1.) (Hooks and Chen 2007; Villers-Sidani et al. 2007; Reh et al. 2020). Critical periods for different domains emerge at various times during development,

and their proper sequencing is crucial for acquiring higher-order functions (Werker and Hensch 2015). These well-timed critical periods refine neural circuits, integrating intrinsic maturation programs with environmental input to build complex cognitive abilities.

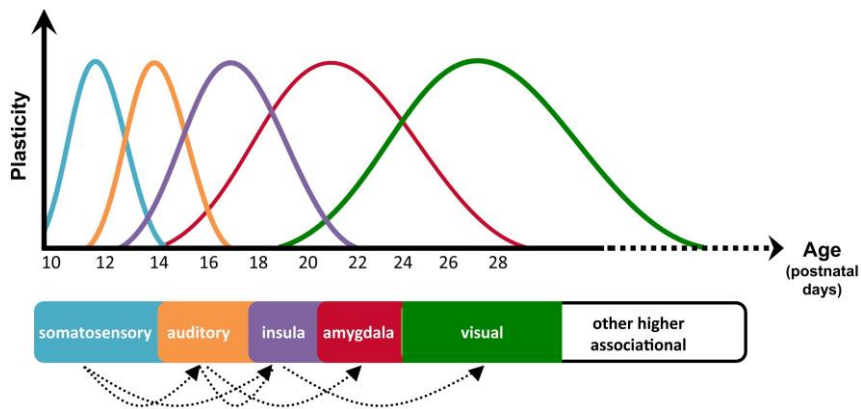


Figure 1.1. Sequential critical periods of plasticity are observed in the mouse brain. Time windows for peak plasticity in barrel cortex, auditory cortex, insular cortex, amygdala, visual cortex, and higher cognitive areas (Reh et al. 2020).

The critical period for the somatosensory cortex begins earliest, typically occurring between postnatal day (P) 3 to P14. During this time, the somatosensory cortex exhibits a high degree of plasticity, with sensory inputs from the mouse whiskers playing a crucial role in shaping the development and organization of the barrel fields (Erzurumlu and Gaspar 2012). Similarly, the subsequent critical period for the auditory cortex is marked by heightened synaptic plasticity which is essential for refining the tonotopic map based on the auditory experiences of the animal (Barkat, Polley, and Hensch 2011). The insula and amygdala are both integral parts of the brain's emotional and sensory processing networks and there is evidence suggesting that early life experiences can have lasting effects on their function. For example, it has been shown that fear memories in young animals can be permanently erased, but in adults when critical period has been closed fear memories can be easily recovered after extinction training (Gogolla et al. 2009). However, the critical period of plasticity for these cortex areas is less well-defined and studied compared to sensory areas like the visual, auditory, or somatosensory cortices.

1.1.1. Visual cortex as a system to study critical period plasticity

The critical period of the primary visual cortex (V1) has been studied the most by far. The discoveries of Hubel and Wiesel (1962) about visual cortex development sixty years ago laid the ground for much of our current understanding of the development and plasticity of the brain. It all started with series of experiments, now considered as classic, which showed that monocular deprivation (sensory deprivation that is restricted to one eye) of kittens during a brief period at the onset of vision is enough to disrupt the normal segregated response of neurons in the visual cortex. This disruption occurs by reducing the number of neurons activated by the closed eye and shifting them to respond to the open eye instead (Wiesel and Hubel 1963b; 1963a). In contrast, three month-long monocular deprivation during adulthood had no significant effect on visual processing once normal vision was regained (Hubel and Wiesel 1970). With their studies Hubel and Wiesel made the visual cortex perhaps the most intensely studied and best understood area of the forebrain in terms of development and plasticity.

Although initial discoveries regarding the critical period of the visual cortex were made using cats and monkeys, similar patterns were soon identified in mice (Wagor, Mangini, and Pearlman 1980; Dräger 1975). Subsequently, numerous significant findings about synaptic plasticity during the critical period have been achieved using mice, owing to their genetic similarities to humans and other mammals, small size, short reproductive cycles, and the accessibility of advanced genetic manipulation techniques.

Development of the V1 neural circuitry in mice takes place in a series of stages, which appear to proceed similarly both in mouse and human brain (Figure 1.2). Before eye opening, axonal projections from the lateral geniculate nucleus, pars dorsalis (LGNd) form precise topographic maps by establishing high-resolution connections with cells in layer 4 of V1 (retinotopy). This process is guided by molecular signaling in the cortex and spontaneous neural activity. During the subsequent stage of V1 development, orientation selectivity in V1 neurons emerges around the time when the eyes open, shortly after the retina first begins to respond to visual stimuli. Experiments indicate that visual experience is not essential for this development, spontaneous activity alone is sufficient. In the third stage of V1 development, the selective properties of neurons are refined to become consistent between both eyes. This phase is called the "critical period" because visual deprivation leads to swift and significant changes in the strength and organization of inputs from both eyes to cortical cells. Numerous experiments have explored the plasticity triggered by abnormal visual experiences during this period and have shed light on its underlying mechanisms. After the critical

period, V1 circuitry and responses mature and typically stay stable for life (Espinosa and Stryker 2012).

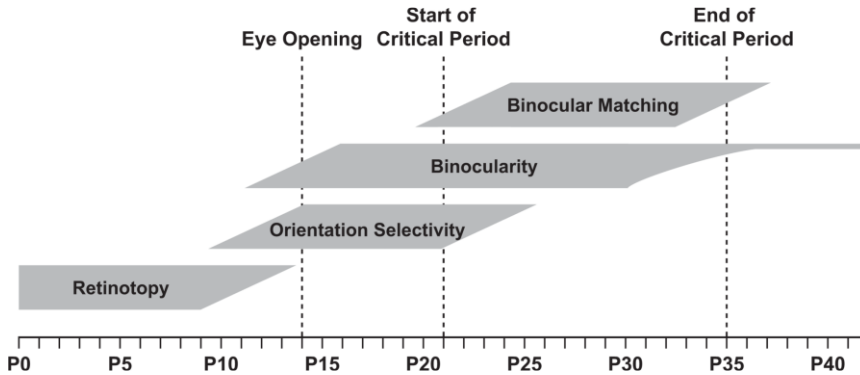


Figure 1.2. Timeline of the Development of Mouse V1. Retinotopic maps are established before eye opening, with orientation-selective and contralateral-eye-driven neurons already present. In the following days, neurons enhance their visual responsiveness and orientation selectivity, also responding stronger to inputs from the ipsilateral eye. At the onset of the critical period, neurons exhibit mismatched eye-specific preferred orientations. This binocular mismatch decreases throughout the critical period, culminating in adult-level responses (Espinosa and Stryker 2012).

1.1.2. Molecular and cellular mechanisms of synaptic plasticity and network refinement

For the critical period to start and end many cellular mechanisms are required. While many of them remains a mystery, some of them are now known and their interaction is demonstrated to form so called “plasticity breaks” that limit neural plasticity in the brain before and after the critical periods of development. These “plasticity brakes” ensure that the neural circuits become stable and functional, preserving the integrity of established networks while preventing excessive rewiring that could disrupt learned functions and behaviours.

The balance between excitation and inhibition is one of the best known “plasticity break” crucial for regulating CPs in the brain, with the onset of plasticity being controlled by the maturation of inhibitory cells in the cortex (Takesian and Hensch 2013). Parvalbumin-positive (PV) inhibitory neurons

are especially important in this process. They are GABAergic neurons that are found throughout the brain and have a unique ability to fire at high frequencies. They also generate gamma oscillations associated with CP plasticity and play a pivotal role in this process (Reh et al. 2020). Inhibitory circuit formation typically lags behind excitatory pyramidal cells, with interneuron migration continuing postnatally for several months in humans (Lodato et al. 2011; Paredes et al. 2016). PV circuits emerge sequentially across brain regions, contributing to the staggered nature of CPs (Condé, Lund, and Lewis 1996). Interestingly, introducing immature inhibitory cells from the medial ganglionic eminence into the visual cortex of adult mice reactivates CP plasticity. This new CP begins only when the transplanted cells reach an age equivalent to the onset of CP plasticity in the donor's visual system, indicating that intrinsic maturational programs within inhibitory neurons govern the timing of plasticity (Tang et al. 2014; Southwell et al. 2010).

This maturation of the cortex and the closing of CP also involves the development of functional perineuronal nets (PNNs) around PV inhibitory neurons (Pizzorusso et al. 2002). PNNs are specialized extracellular matrix structures that densely surround inhibitory neurons and restrict synaptic plasticity by providing a physical barrier, stabilizing synapses, and limiting their ability to form new connections (Reichelt et al. 2019). The formation and maintenance of PNNs are also dependent on neuronal activity. When intracortical inhibition is reduced by administering GABA antagonists in the V1, it enhances ocular dominance (OD) plasticity and is associated with a decrease of PNNs (Harauzov et al. 2010). Similarly, the removal of PNNs disrupts the excitation/inhibition balance by lowering the activity of PV neurons which reactivates OD plasticity in V1 (Pizzorusso et al. 2002; Rowlands et al. 2018).

After the closure of the critical period, the increased activity of pyramidal and PV neurons dynamically influences the myelination of axons. The development of myelin sheaths around axons increases the speed and efficiency of neural transmission but also reduces the ability of axons to form new connections, thereby limiting plasticity (Stedehouder et al. 2018). For example, mice lacking a functional myelin-related gene retain developmental plasticity into adulthood, whereas myelin production following brain injury hinders axonal regeneration and functional recovery (S. Li et al. 2004; McGee et al. 2005).

Glial cells including astrocytes and microglia are being increasingly attributed to synaptic plasticity by monitoring extracellular matrix and absorbing and releasing signalling molecules like cytokines and complement

proteins. During critical periods of plasticity, excessive or weak synaptic connections are pruned in an activity-dependent manner, a process that is heavily regulated by all glial types (Allen and Eroglu 2017; Wilton, Dissing-Olesen, and Stevens 2019; Faust, Gunner, and Schafer 2021; Auguste et al. 2022; Xiao et al. 2022). Microglia are specialized population of macrophages-like cells in the central nervous system that play a prominent role in monitoring the brain, recognizing “eat-me” and “don’t eat-me” signals and pruning the connections to optimize the network (Figure 1.3.) (Schafer, Lehrman, and Stevens 2013). In addition to classical phagocytosis, emerging evidence suggests that microglia may also engage in trogocytosis, a process where they partially nibble away at synapses without fully engulfing them, leading to synaptic weakening rather than complete elimination (Weinhard et al. 2018; Lim and Ruthazer, 2021). This more refined mechanism could allow for targeted removal of parts of synaptic boutons, preserving surrounding structures like axons. Overall, all these mechanisms reflect the complexity of glial involvement in synaptic remodeling and suggest that multiple forms of pruning may co-exist to fine-tune neural circuits.

While microglial pruning can involve a variety of mechanisms beyond full phagocytosis, its role in activity-dependent synaptic refinement has been well established in key neural circuits. Landmark studies from the Barres and Stevens labs showed that neuronal activity influences microglial refinement of retinogeniculate synapses during an early postnatal pruning period. Microglial engulfment of synapses requires the complement signalling cascade, specifically CR3/C3 (Schafer et al. 2012; Stevens et al. 2007). Retinogeniculate synapse pruning peaks prior to the eye opening, and thus is outside of the classic visual critical period defined by Hubel and Wiesel (the peak of critical period at ~P28) (Wiesel and Hubel 1963b). Nevertheless, it has been shown that pharmacological depletion of microglia using a colony stimulating factor 1 receptor inhibitor PLX3397 during the visual critical period (P14 through P28) increases spine density on L5 pyramidal (excitatory) neurons, presumably due to lack of microglial synaptic pruning. Accordingly, ocular dominance plasticity is diminished during the visual critical period (Ma et al. 2020). This demonstrates the importance of microglial synaptic pruning for activity-dependent synapse refinement during the visual critical period.

More recently, it has been found that externalised phosphatidylserine (PS) mediates synaptic pruning signalling on the neuronal side and interacts with the microglial receptor GPR56 and the complement component C1q (Scott-Hewitt et al. 2020; T. Li et al. 2020; Kurematsu et al. 2022; T. Li et al. 2020). Also, complement receptor 3 (CR3), made up of CD11b and CD18 and expressed on microglia, detects C3 located at synapses, triggering microglia

to engulf the synapse. Moreover, it has been shown that TREM2, a microglial innate immune receptor, is essential for microglia-mediated synaptic refinement during the early stages of brain development (Filipello et al. 2018). Finally, CX3CR1, a receptor on microglia, has been shown to interact with its neuronal ligand fractalkine (CX3CL1) to regulate microglial activity and synapse surveillance (Ball, Green-Fulgham, and Watkins 2022). These findings underscore the intricate and essential roles that various microglial receptors play in synaptic pruning, highlighting the complexity of glial contribution to neural circuit refinement and brain development.

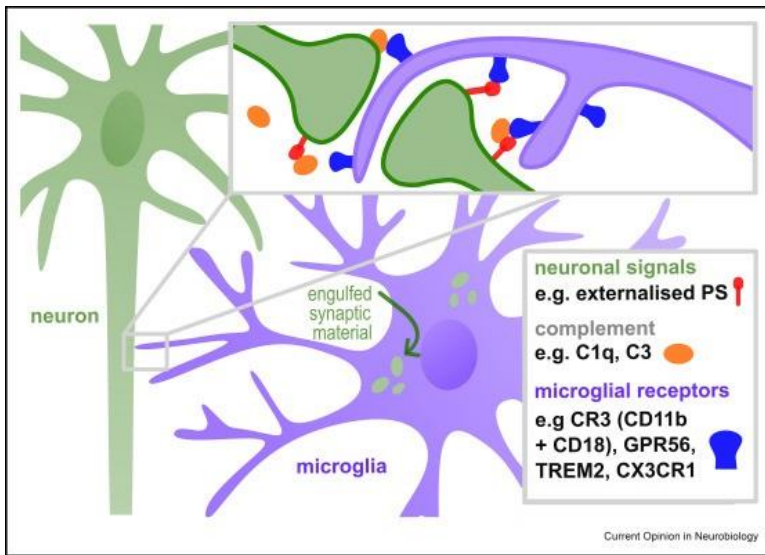


Figure 1.3. Regulatory mechanisms of synaptic pruning by microglia involve various signaling interactions. Microglia express the complement receptor 3 (CR3), which binds to C3 at the synapse to facilitate synapse engulfment. Also, recent findings emphasize the importance of externalized phosphatidylserine (PS) on neurons, which interacts with secreted proteins like complement component C1q. This externalized PS is detected by the microglial receptor GPR56. Other receptors that play a role in microglia-mediated synaptic pruning include TREM2 and CX3CR1. (Mordelt and de Witte 2023).

Another glial cell type, astrocytes, are the most abundant glial cells in the brain, where they extend many fine processes to simultaneously interact with thousands to millions of neuronal synapses as part of the tripartite synapse (Perez-Catalan, Doe, and Ackerman 2021). These astrocyte processes are

structural and signalling partners of the synapses that help regulate neurotransmission and plasticity (Dallérac, Zapata, and Rouach 2018). Moreover, astrocytes also contribute to synaptic pruning through the secretion of complement proteins that tag synapses for full or partial microglial clearance or engulf the synapses themselves. This suggests a potential collaborative role between astrocytes and microglia in synaptic pruning (Mordelt and de Witte 2023; Chung et al. 2013; Faust, Gunner, and Schafer 2021). It is also known that in the mouse visual cortex, astrocytes are involved in closing critical period by regulating the extracellular matrix and allowing interneuron maturation. Astrocytes achieve this through a developmental increase in Cx30 expression. Cx30 functions to regulate extracellular matrix maturation around developing PV neurons. Although Cx30 is better known for mediating astrocyte-astrocyte communication as a gap junction protein, Cx30 also signals through RhoA/ROCK pathway to suppress expression of MMP9, a matrix metalloprotease that degrades PNNs (Ribot et al. 2021). Thus, astrocytes not only influence the activity of single synapses but also are key elements in the experience-dependent wiring of brain circuits.

1.1.3. Local protein synthesis and its impact on plasticity

Neurons are morphologically complex and polarized cells with extensively branched dendrites and axons, providing spatial compartmentalization that facilitates their primary roles in neurotransmission and circuit connectivity. At presynaptic and postsynaptic sites, far from the cell body, local protein synthesis is needed to continuously update the synaptic proteome, which enables rapid protein production changes to support synaptic function. During critical periods synapses experience various forms of plasticity – long-term potentiation (LTP), long-term depression (LTD), and short-term plasticity. These processes lead to long-term changes in synapse strength, which are crucial for learning, memory, and cognition. It is now well-established that local translation of numerous synaptic proteins is essential for these processes, and considerable effort has been devoted to understanding how neurons regulate activity-dependent protein synthesis. Recent studies suggest the coordination of local mRNA translation needed for synaptic plasticity and the trafficking of membranous organelles in neurons. This includes the co-transport of RNAs to their action sites using endosome/lysosome transports, regulation of activity-dependent translation at synapses, and the role of mitochondria in supporting synaptic translation (Citri and Malenka 2008; Rajgor, Welle, and Smith 2021).

Localizing and translating mRNA in distal neuronal dendrites and axons is faster, more specific, and more energy-efficient than long-range trafficking of mature proteins from the soma. On-demand protein synthesis near synapses quickly produces new synaptic components, enhancing or reducing synaptic efficacy as needed (Williams et al. 2016; Fonkeu et al. 2019). Rapid local translation at synapses is essential for synaptic plasticity, enabling neurons to respond quickly to neural stimulation, sometimes producing new proteins within minutes (Ouyang et al. 1999). This localized translation ensures synaptic specificity, allowing neurons to fine-tune synaptic strength in response to local signals, as seen in input-specific long-term potentiation (LTP) (Govindarajan et al. 2011). Consequently, inducing protein translation at activated synapses while avoiding nearby inactivated ones prevents aberrant, non-specific synaptic potentiation. Local protein synthesis at presynaptic and postsynaptic sites is now well-established process with protein synthesis components such as mRNA, ribosomes and regulatory elements demonstrated to be present in both dendritic and axonal compartments (Cajigas et al. 2012; Scarnati et al. 2018; Hafner et al. 2019; Biever et al. 2020). However, the involvement and importance of local protein synthesis in modulating synaptic plasticity remain under-researched, and current understanding of these novel and nuanced regulatory processes is limited.

Numerous mRNAs encoding synaptic proteins are highly prevalent in neuronal dendrites (Cajigas et al. 2012), and recent research has demonstrated their local translation at synaptic sites (Biever et al. 2020). Key proteins involved in synaptic plasticity, such as CaMKII and PSD95, are well-documented to undergo activity-dependent translation at glutamatergic postsynaptic sites (Muddashetty et al. 2007; Aakalu et al. 2001; Nihonmatsu et al. 2020). CaMKII is an essential kinase that is highly expressed in the brain, particularly abundant in dendritic spines, and necessary for both LTP and long-term depression (LTD) (Bayer and Schulman 2019). In addition to the local translation of these molecules, glutamate, and GABAA receptors (GABAARs) are also locally translated in dendrites following synaptic stimulation (Rajgor et al. 2020). The abundance and composition of neurotransmitter receptors at synapses are critical determinants of synaptic strength, and it appears that synapses can locally produce these receptors to facilitate synaptic plasticity.

Initially, most of research of activity-dependent local translation in distal neuronal compartments was centred on dendrites and postsynaptic regions. However, there is now plenty of evidence that local translation also occurs in presynaptic compartments (Younts et al. 2016; Scarnati et al. 2018; Hafner et

al. 2019). Studies using invertebrates have shown that presynaptic protein synthesis is essential for various forms of synaptic plasticity, as demonstrated with long-term facilitation in *Aplysia*, which required CREB-mediated gene expression and local translation in presynaptic neurons (K. C. Martin et al. 1997). More recent studies in mature mammalian neurons have confirmed the necessity of presynaptic translation for long-term plasticity identifying the axonal translome and functional ribosomes in presynaptic terminals (Shigeoka et al. 2016; Scarnati et al. 2018). A recent study using expansion microscopy visualized newly synthesized proteins in both excitatory and inhibitory presynaptic and postsynaptic compartments, revealing that translation is compartment-specific and regulated by different forms of plasticity (Hafner et al. 2019). These studies contribute to a refined model of plasticity, showing that local translation at both presynaptic and postsynaptic sites can modify synaptic strength during various forms of activity-dependent modulation.

1.2. Research challenges of local protein synthesis

Previously studies of local protein synthesis and mRNA presence in the axons were challenging due to the delicate nature of axonal processes and the difficulty in isolating pure axonal material. Early studies involved using explant tissue to investigate the physiological relevance of local protein production. For example, sensory ganglia can be dissected and cultured in the presence of embryonic limb buds to allow for sensory axon extension (Tucker, Meyer, and Barde 2001). Several strategies, such as using compartmentalized chambers and microfluidic culturing devices, have been also developed to achieve purer axon preparations or to specifically label ribosomes. These methods have uncovered a complex array of several thousand transcripts localized to axons (Taylor et al. 2005; Deglincerti and Jaffrey 2012). For an *in vivo* experimental system, an animal model utilizing the RiboTag method for cell-type specific tagging and polysome isolation was developed and used to compare ribosome-bound mRNAs, or so called translomes, in axons of developing and adult RGCs (Sanz et al. 2009; Shigeoka et al. 2016; 2018).

Synaptosome preparations are also widely utilized systems for studying the functions of nerve terminals and the mechanisms of local protein synthesis. Synaptosomes are isolated nerve endings produced by the shearing forces during the homogenization of neuronal tissue (Whittaker, Michaelson, and Kirkland 1964). Prepared synaptosomes are functional synaptic connections consisting of a resealed presynaptic compartment and part of the postsynaptic

element. They retain the same subcellular organelles, proteins, cytoplasm, cytoskeleton, synaptic vesicles and mitochondria that are normally found at the nerve endings *in vivo* (Figure 1.4). Synaptosome preparations have significantly advanced our understanding of synaptic structure, composition, and function, contributing to the generation of general synaptic proteomes (Bai and Witzmann 2007; Burré, Zimmermann, and Volknandt 2007; Boyken et al. 2013; Weingarten et al. 2014; Wilhelm et al. 2014). However, conventional synaptosome isolation has a major drawback. The prepared sample consists of a diverse array of synapse types, accounting for 49.1% of all particles, alongside a substantial presence of neuronal and non-neuronal contaminants, comprising 50.9% of the total particles (Henn, Anderson, and Rustad 1976; Luquet et al. 2017). This significant contamination by non-synaptic compartments in synaptosome preparations complicates data interpretation and hinders the discovery of new synapse-specific proteins, necessitating the development of highly specific methods for studying functional synaptic populations in neurobiological research. To reach specificity and significantly higher purity of unfixed synaptosome samples, Fluorescence Activated Synaptosome Sorting (FASS) technique has been established that allowed to sort out fluorescently labelled synaptosomes and collect enriched synaptic population (Biesemann et al. 2014). Since then FASS-enriched synaptic populations have been used to describe many more discoveries about local protein synthesis at presynaptic compartments and synapse type-specific proteomes (Biesemann et al. 2014; Hafner et al. 2019; Hobson et al. 2022; Paget-Blanc et al. 2022; Oostrum et al. 2023). However, acquiring a substantial and highly enriched synaptosome population for quantitative analysis requires the use of genetically engineered mice, an extremely sensitive cell sorter, extensive sorting procedures, and a highly skilled researcher, all of which still restrict widespread adoption of FASS in research.

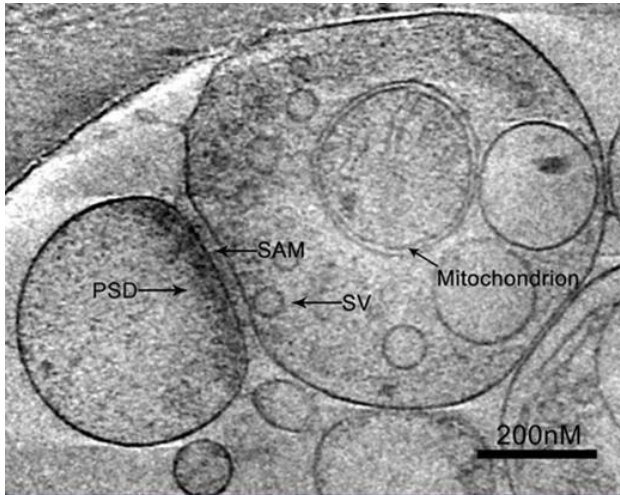


Figure 1.4. Structure of a synaptosome with part of the postsynaptic element still attached. Cryo-ET of the synaptosome shows the structure of the neural terminals: post-synaptic density (PSD), synaptic vesicle (SVs), mitochondria, and synaptic adhesion molecules (SAM). Scale bar = 200 nm. (Shi et al. 2014).

1.2.1. Lack of appropriate quality controls for synaptic mRNA samples

Good RNA quality is essential for acquiring reliable and replicable data from any gene expression analysis (Fleige and Pfaffl 2006). Purified RNA is quite sensitive to environmental factors and is prone to the degradation due to its single-stranded structure and abundant RNases in the environment. Therefore, measuring RNA integrity is established as a ubiquitous step to check RNA quality before any further downstream analysis. First methods to test RNA integrity were based on RNA electrophoresis, where some of RNA sample was run on denaturing agarose gel, and RNA integrity was evaluated by comparing the intensity of visible small 18S and large 28S ribosomal RNA (rRNA) bands (Green and Sambrook 2012). However, this method requires at least a few hundred nanograms of RNA, is difficult to standardize and the conclusions heavily depends on subjective visual interpretation. Since 2006, microfluidic capillary electrophoresis has become a gold standard for RNA integrity measurements assigning an RNA integrity number (RIN) to an assayed RNA sample (Schroeder et al. 2006). However, both RNA gel and capillary electrophoresis predominantly evaluate rRNA integrity, assuming

that it reflects the integrity of all other sample RNAs, including messenger RNA (mRNA).

Meanwhile, gene expression studies are mainly concerned with the quality of mRNA and not rRNA. It has been shown that because of structural and functional differences between them, rRNA cannot represent the integrity of mRNA accurately enough (Fleige and Pfaffl 2006; Sidova et al. 2015; Sonntag et al. 2016). In the cells, rRNAs are compact and contain many post-transcriptional modifications to form complex and functional ribosomes, which grants them exceptional stability (Noller 2005). In contrast, mRNA has a more linear structure and is more prone to degradation (Andrzejewska, Zawadzka, and Pachulska-Wieczorek 2020). Therefore, RNases and any environmental factors such as temperature affect the stability and degradation rates of rRNA and mRNA differently (Sonntag et al. 2016). Moreover, rRNA-based methods have not been used to evaluate RNA integrity in subcellular extracts like purified synaptosomes, most likely because rRNA content is reduced or completely lacking.

The integrity of mRNA in RNA samples can be measured directly using real-time quantitative reverse transcription PCR (RT-qPCR). This approach, called 3':5' assay, has been first proposed in 2006 by Nolan and colleagues (Nolan, Hands, and Bustin 2006). The 3':5' assay measures the integrity of the ubiquitously expressed mRNA of choice, independently of rRNAs. By now a few versions of the 3':5' assay have been published that used different template mRNAs for different species (Nolan, Hands, and Bustin 2006; Schaeck et al. 2016; Padhi et al. 2018; Du Cheyne et al. 2021). However, 3':5' assays accuracy has not been sufficiently explored as the few existing studies validate the assay only by comparing 3':5' assays integrity values to RIN values. There has been no validation modelling different availability of 3' and 5' binding sites to show how the integrity values of 3':5' assays represent degraded mRNA. Furthermore, recent studies demonstrated that even minor differences of primer efficiencies result in significant under- or overestimation of mRNA levels, which should be accounted for in a qPCR based assay (Damgaard and Treebak 2022). Thus, a convenient and reliable method for directly assessing mRNA integrity, applicable to RNA samples lacking ribosomal RNA, would greatly benefit the expanding research field utilizing subcellular fractions like synaptosomes.

1.2.2. Current tools to label PS externalizing synapses destined for elimination

Local translation is crucial for neuronal functions such as axon growth and guidance, synapse formation, synaptic pruning, and synaptic plasticity processes like long-term potentiation (LTP) and long-term depression (LTD). Synaptic elimination in particular is essential for developing a healthy, adaptive brain, with synapses being selectively removed during brain development to refine neural circuits. Phosphatidylserine (PS) is an important membrane phospholipid that acts as an "eat-me" signal for brain phagocytes such as microglia to engulf certain unnecessary synapses. Normally located on the inner leaflet of the cellular membrane, PS is exposed on the outer side of the membrane due to caspase- and calcium-induced inactivation of flippases and activation of scramblases on the synaptic terminals destined for elimination. Due to the contribution of PS to synaptic pruning, an efficient PS probe is needed to study this dynamic process.

Currently, a few commercial PS labelling tools are available. The most commonly used PS label is fluorescently tagged annexin A5. Annexin A5 can successfully detect and quantify externalized PS during cell death (Crowley et al. 2016) or platelet activation (Prinzen et al. 2007) and has been used to study the activity of procoagulants (Dachary-Prigent et al. 1993). However, annexin A5 requires a relatively high concentration of calcium ions for its binding (1-3 mM) (Logue, Elgendy, and Martin 2009), thus preventing the detection of internal PS in live cells or its application for *in vivo* assays (Hu et al. 2008). Furthermore, it has been reported that annexin A5 has limited specificity for PS, as it binds to the phosphatidylethanolamine – the second most abundant phospholipid in eukaryotic cell membranes (Meers and Mealy 1994). Therefore, alternative annexins have been explored as potential tools for more specific PS detection. Modified annexin B12 has been fused to polarity-sensitive fluorophores to develop the pSIVA probe that exhibits a significant increase in fluorescence upon binding to the membrane and displays low fluorescence when not bound (Kim, Chen, Chan, et al. 2010). However like annexin A5, this probe also requires calcium (~1–2 mM) and has a limited signal-to-noise ratio for *in vivo* applications (Kim, Chen, Langen, et al. 2010). Alternatively, PS can be visualized by PS-specific antibodies (Maneta-Peyret et al. 1989); however, antibodies exhibit cross-reactivity with other phospholipids, diminishing the specificity of such labelling techniques (Yeung et al. 2009).

Small organic compounds have also been developed for PS labelling and include TNBS (2,4,6-trinitrobenzenesulfonate) (Schick, Kurica, and Chacko

1976) or Zn-DPA (bis(zinc-dipicolylamine)) and Zn-DPA-based fluorescent imaging reagent PSVue® (Kwong et al. 2014). Such compounds can detect PS on apoptotic cells *in vitro* when used either directly or delivered by liposomes (Cho et al. 2013). However, these tools have significant limitations. TNBS is not suitable for live cell imaging (Boon and Smith 2002) and shows limited selectivity to PS due to the reaction with phosphatidylethanolamine and other amines (Scott et al. 2019). Meanwhile, PSVue demonstrates a significant background signal (Scott-Hewitt et al. 2020). Finally, the distribution and dynamics of PS can be visualized by fluorescent PS analogues, such as aromatic fluorescent compound 7-nitro-2-1,3-benzoxadiazol-4-yl (NBD) attached to the acyl chain (Martin and Pagano 1987). Unfortunately, PS analogues photo bleach extremely rapidly (Nichols 2002) and can cause membrane distortion, thus modifying the behaviour of the lipid bilayer (O. C. Martin and Pagano 1987).

The need to visualize the exposure of PS on the synapse in undamaged brain *in vivo*, has promoted the development of genetically encoded biosensors. These biosensors are typically based on the PS-binding domains of various PS-recognizing proteins. For instance, milk fat globule-epidermal growth factor-factor 8 (MFG-E8), also known as lactadherin, is an opsonin expressed by a variety of cells, including both professional and non-professional phagocytes. MFG-E8 consists of four functional domains: two epidermal growth factor domains (EGF1 and EGF2), as well as C1 and C2 domains like those found in coagulation factors V and VIII (Oshima et al. 2014). MFG-E8 tightly binds to exposed PS through its C2 domain in a calcium-independent manner (Reddy Nanga, Vivekanandan, and Yoon 2007; Ye et al. 2013). Therefore, the C2 domain of MFG-E8 can be used to develop a sensitive probe for PS exposed on cell surfaces, overcoming several challenges presented by the aforementioned tools. It has been demonstrated that the C2 domain binds to PS more sensitively and efficiently than annexin A5, enabling the detection of lower levels of PS and cell apoptosis at earlier stages compared to other available tools (Hu et al. 2008). The microinjection of a plasmid encoding MFG-E8 fused to red fluorescent protein mCherry into *C. elegans* has allowed visualization of PS *in vivo* on necrotic neurons after dysregulated Ca²⁺ influx, which induced excitotoxicity (Furuta et al. 2021). PS labelling on living cells has also been achieved using the C2 domain alone. The fusion of the C2 domain with green fluorescent protein enabled the monitoring of the endogenous distribution of PS in intact *S. cerevisiae* and various mammalian cells (Kay et al. 2012; Yeung et al. 2008). However, this method is unsuitable for labelling phosphatidylserine (PS) on the external surface of neurons, thus impeding the investigation of PS exposure

mechanisms and roles during critical periods of plasticity. Consequently, it cannot be used to explore local synaptic mechanisms that involve the release of "eat-me" signals such as PS for synaptic pruning.

2. MATERIALS AND METHODS

2.1. Animals

C57BL/6J and *Thy1::EGFP* mice were obtained from the local Life Sciences Center colonies. VGLUT1^{mVenus} mice¹⁸ were used in the homozygous state. *Thy1::EGFP;Cx3cr1::CreER;RC::LSL-tdTomato* triple transgenic mouse were homozygous for *Thy1::EGFP* and heterozygous for *Cx3cr1::CreER* and *RC::LSL-tdTomato*. *Thy1::EGFP* mice were used in the heterozygous state. Animal studies were conducted in accordance with the requirements of the Directive 2010/63/EU and were approved by the Lithuanian State Food and Veterinary Service (permit No. G2-92). All mice were bred and kept at the animal facility of the Life Sciences Center of Vilnius University. For total brain RNA extraction, mouse brains were harvested from adult C57BL/6 mouse after cervical dislocation. The cortex was immediately dissected, homogenized in Trizol and stored at -80 °C until RNA isolation. VGLUT1^{mVenus} mice aged P21, P28 or P35 were used for synaptosomal preparations.

2.2. Human samples

Permission to use human brain tissue was obtained from Vilnius Regional Biomedical Research Ethics Committee (Approval No. 2020/2-1202-687). Human brain tissue specimens were obtained with the informed consent as requested by the Regional Ethics Committee (No. 2/2020 02 18). Human neocortical access tissue (n=16) was sampled from either glioma tumor resection surgery (n=6), using distant cortex without tumor infiltration, or access cortex tissue from epilepsy surgery (n=5) obtained during the resection of epileptic foci. Human hippocampus tissue (n=5) were samples resected during epilepsy surgery. Detailed information regarding the donors used in this study is provided in Table 1.

Table 1. Donor tissue used in the study.

ID	Sex	Age, yr	Region of origin	Diagnosis
#02	Female	10	Cortex	Hemisphere glioma
#03	Male	61	Cortex	Supratentorial ependymoma
#04	Male	46	Cortex	GBM
#05	Female	48	Cortex	Epilepsy with hippocampal changes
#06	Female	44	Cortex	Astrocytoma
#07	Male	40	Cortex	GBM
#08	Female	28	Cortex	Epilepsy with hippocampal sclerosis
#08a	Female	28	Hippocampus	Epilepsy with hippocampal sclerosis
#09	Male	23	Cortex	Epilepsy
#09a	Male	23	Hippocampus	Epilepsy
#10a	Female	29	Hippocampus	Epilepsy
#11	Male	44	Cortex	Oligodendroglioma
#12a	Female	27	Hippocampus	Epilepsy with hippocampal sclerosis
#12	Female	27	Cortex	Epilepsy with hippocampal sclerosis
#13	Male	40	Cortex	Epilepsy
#13a	Male	40	Hippocampus	Epilepsy
#14	Male	55	Cortex	Oligodendroglioma

2.3. Human brain tissue preparation

Tissue was immersed in 4 °C Artificial Cerebrospinal Fluid (aCSF) immediately post-resection and transferred for homogenization in Trizol (#15596026, ThermoFisher Scientific). Homogenized samples were stored at -80 °C until further procedures.

ACSF used for tissue transport was prepared as previously reported²⁹. Shortly, the solution contained 0.5 mM calcium chloride (dehydrate), 25 mM D-glucose, 20 mM HEPES, 10 mM magnesium sulfate, 1.2 mM sodium phosphate monobasic monohydrate, 92 mM N-methyl-d-glucamine chloride (NMDG-Cl), 2.5 mM potassium chloride, 30 mM sodium bicarbonate, 5 mM sodium L-ascorbate, 3 mM sodium pyruvate, and 2 mM thiourea. Osmolality was verified to be between 295–305 mOsm/kg, pH was adjusted to 7.3 using HCl. Prior to use, the solution was equilibrated with 95% O₂, 5% CO₂.

2.4. Mouse brain slice preparation

Thy1::EGFP;Cx3cr1::CreER;RC::LSL-tdTomato mice at P21, P28 and P35 were anesthetized with intraperitoneal injection of 2.5% Avertin (Sigma-Aldrich) and perfused transcardially with 4% paraformaldehyde (PFA). Brains were removed and post-fixed in 4% PFA overnight at 4 °C. Coronal 100 µm sections were cut on a vibratome (Leica Microsystems) and permeabilized in 20% normal goat serum with 0.4% Triton X-100 in PBS for 2 h at room temperature.

2.5. Fluorescence imaging and quantification

To visualize EGFP fluorescent neuronal axons and C1q labelling the coronal brain sections of *Thy1::EGFP;Cx3cr1::CreER;RC::LSL-tdTomato* mice were stained with DAPI (1 µg/ml), primary rabbit anti-C1q antibodies (ab182451) and secondary monoclonal anti-rabbit Alexa Fluor Plus 647 antibodies (A32733), and mounted with Mowiol. Brains sections were imaged on TCS SP8 resonant scanner confocal microscope (Leica Microsystems) using 63×/1.4 NA oil-immersion objective. To evaluate axonal bouton size and C1q labelling a z-stack images encompassing an axon at visual cortex layer 2/3 were acquired with 0.3 µm z-step. The images were analysed using optimized binary-processed image analysis with ImageJ. After background processing, mean axonal branch intensity was calculated, and multiplied by 1.4. Then after applying “Watershed and “Fill holes” functions, “Analyze Particles” function parameters were set to size 0.06-infinity and circularity 0.02-1.00 to calculate bouton size and density. 180 images were analysed in each age group (P21, P28 and P35) with 30 images from one mouse. These experiments were done together with bachelor student Monika Kušeliauskė.

2.6. PGK1 cDNA Plasmids

Mouse and human *PGK1* cDNA fragments were copied and amplified by PCR using Thermo Scientific Phusion High-Fidelity DNA polymerase from mouse or human brain total RNA sample. The following primers were used: *Pgk1_For_MMPCR*: 5'- GGAGGCCCGGCATTCTGCAC-3' and *Pgk1_Rev_MMPCR*: 5'- ACCGCCCCAGTGCTCACATG-3' for mouse gene and *PGK1_For_HSPCR*: 5'- GGCAGTCGGCTCCCTCGTTG-3', *PGK1_Rev_HSPCR*: 5'- CCACCCCCAGTGCTCACATG-3' for human gene. The PCR fragments were then ligated into pJET1.2/blunt plasmid using CloneJET PCR cloning Kit (Thermo Scientific). To generate plasmids containing 3'-end of *PGK1* cDNA 5' part of *PGK1* was excised by NcoI from

previously generated full-length *PGK1* cDNA plasmids. All plasmids were linearized by *XhoI* for experiments.

2.7. Crude synaptosome sample preparation

Fresh mouse brain was cleaned and cooled in ice cold PBS. All the following steps were carried on ice. Mouse visual cortex was dissected and placed into a 2 ml clean ice-cold glass-Teflon potter. The tissue was then homogenized in 1 ml of ice-cold 0.32 M sucrose buffer (0.32 M sucrose, 4 mM HEPES, 4 U/ μ L Ribolock, pH 7.4) at 900 rpm for 15 s moving the pestle up and down. The homogenate was centrifuged at 1000 \times g for 5 min at 4 °C. The supernatant was then centrifuged at 12,500 \times g for 8 min at 4 °C. The second supernatant was discarded and the pellet was carefully resuspended in ice-cold 0.3 ml 0.32 M sucrose buffer. Discontinuous sucrose gradient was prepared in 5 ml ultracentrifuge tubes (Beckman Coulter, C14279) with 2 ml of 1.2 M sucrose solution (1.2 M sucrose, 4 mM HEPES, 0.2 U/ μ L Ribolock, pH 7.4) at the bottom and 2 ml 0.8 M sucrose solution (0.8 M sucrose, 4 mM HEPES, 0.2 U/ μ L Ribolock, pH 7.4) at the top. The resuspended pellet was then carefully laid over the prepared gradient. The tubes were ultracentrifuged at 58,000 \times g for 45 min at 4 °C. After ultracentrifugation two layers of particles and a pellet appeared. The middle layer containing synaptic particles was collected with a syringe by piercing through the tube wall. Collected crude synaptosome sample was then diluted in 8 ml of ice-cold 0.22 μ m filtered PBS. This sample was then split and part of it was collected onto a 0.1 μ m polycarbonate filter and washed with Trizol reagent for RNA extraction. The second part was used for Fluorescence Activated Synaptosome Sorting (FASS) to prepare matching excitatory synaptosome-enriched samples.

2.8. Fluorescence Activated Synaptosome Sorting (FASS)

The prepared crude synaptosome sample was diluted in PBS and stained with SynaptoRed C2 (1 μ g/ml, Tocris Bioscience) to label all plasma membrane-containing particles to increase synaptosome detection sensitivity. The dilution was optimized every time to reach around 15 000 events per second at the flow rate between 3 and 4. A new sorting sample was prepared every 45 min and the collection tube was changed at the same time. Synaptosome sorting was performed as described previously (Luquet et al. 2017). For sorting we used BD FACSAria III Cell Sorter set as follows: 70 μ m Nozzle, sample shaking at 300 rpm, sample temperature at 4 °C, FSC

neutral density filter 1.0, 488 nm Laser on, Area Scaling 1.18, Window Extension 0.0, FSC Area Scaling 0.96, Sort Precision: 0-16-0. Thresholding on SynaptoRed C2 with a threshold value of 800. Synaptosomes were sorted into a 5 ml polystyrene round-bottom tubes (BD Falcon) and kept on ice. The synaptosomes were sorted and collected for at least 6 hours. Then synaptosomes were collected onto a 0.1 μ m polycarbonate filter and washed with Trizol reagent for RNA extraction.

2.9. Synaptosome analysis using Cytex Amnis FlowSight imaging flow cytometer

Collected synaptosomes were loaded and examined using the Cytex Amnis FlowSight imaging flow cytometer according to manufacturers instructions. Results were analyzed by IDEAS analysis software (Amnis Corporation, Seattle, WA, USA).

2.10. RNA extraction

Total RNA from mouse cortex, crude and enriched synaptosomal preparations and surgically resected human brain samples was extracted using TRIzol Plus RNA Purification Kit and Phasemaker Tubes Complete System (Invitrogen, cat. no. A33254). The remaining gDNA was removed using TURBO DNA-free Kit (Invitrogen, cat. no. AM1907) following the manufacturer's protocols.

2.11. Preparation of heat-degraded RNA samples

Mouse cortex RNA samples were diluted to 100 ng/ μ l. An aliquot (12 μ l) of each diluted RNA sample was taken into separate tubes. While one tube served as the control (heated at 70 °C for 2 min to denature RNA), the other tubes were exposed to 90 °C heat for 1, 2, 3, 4, 5, 10, or 15 min in a thermocycler. The same procedure was applied to human brain total RNA samples, which were kept at 90 °C for 1, 3, 5, or 10 min.

2.12. Evaluation of RNA concentration and rRNA integrity

A NanoDrop 2000 Spectrophotometer (Thermo Fisher Scientific, Waltham, MA USA) was used to measure the absorbance at 260 nm to evaluate RNA concentration. rRNA integrity was assessed by an Agilent 2100

Bioanalyzer system, using the Agilent RNA 6000 Pico Kit (Part Number: 5067-1513) (Agilent Technologies, Mississauga, ON, Canada) following the manufacturer's protocols.

2.13. cDNA synthesis and RT-qPCR

The reverse transcription reactions were performed in a total volume of 20 μ l using 1 μ g of total RNA (heated at 70 °C for 2 min to denature RNA), 2.5 μ g Anchored Oligo-dT primers (Invitrogen), 0.5 mM dNTP Mix (Thermo Scientific) and 200 U Thermo Scientific Maxima Reverse Transcriptase (Thermo Scientific) following manufacturer's first-strand cDNA synthesis protocol. All cDNA samples were diluted with nuclease-free water to the final cDNA concentration of 20 ng/ μ l.

Quantitative PCR was performed with The StepOne™ Real-Time PCR System or QuantStudio™ 3 System (Applied Biosystems™) using 5 μ l diluted cDNA, 0.3 μ M of the forward and reverse (5 μ l) primer mix (designed primer pairs targeting either 3' or 5' *Pgk1* cDNA ends are presented in **Table 1**), and 12.5 μ l 2 \times Thermo Scientific Maxima SYBR Green/ROX qPCR Master Mix (Thermo Scientific) and 2.5 μ l of nuclease-free water in a reaction volume of 25 μ l. The RT-qPCR reaction mix was denatured at 95 °C for 10 min and then subjected to 40 amplification cycles (15 s denaturation at 95 °C, 30 s annealing at 60 °C and 30 s extension at 72 °C) following manufacturer's protocols for the SYBR Green Master Mix. The reactions were run in triplicates. The specificity of the qPCR products was assessed by melting-curve analysis. No-template controls (NTC) did not record any positive Ct values. Maxima™ First Strand cDNA Synthesis Kit was used for reverse transcription followed by TaqMan PCR assay in accordance with manufacturer's first-strand cDNA synthesis protocol. The Ct values of *GAPDH* in surgically resected human brain tissue RNA samples were defined by TaqMAN qPCR assay. The following primers were used: *GAPDH* (Hs02758991_g1, #4331182, Thermo Fisher Scientific).

2.14. Integrity value correction for difference in amplification efficiency

To estimate amplification efficiency, seven serial 5-fold dilutions were prepared using constructed linearized plasmids or prepared mouse or human cDNA and RNase/DNase free water. For plasmid dilution series, the highest concentration was 1.04×10^8 plasmids per reaction. For cDNA dilution series the highest concentration was 170 ng of cDNA per 25 μ l q-PCR reaction. RT-

PCR was performed as described above. Acquired mean Ct values were plotted against concentration logarithm by 5 (the number of dilution factor) using Microsoft Excel Spreadsheet Software. Next, a linear regression curve was generated and the slope of the trend line was calculated. Amplification efficiency was estimated using the following equation:

$$\text{Amplification efficiency} = \left(5^{\frac{-1}{\text{Slope}}} - 1 \right) \times 100$$

Then the amplification factor was calculated and corrections for the expression were made as described by Damgaard and Treebak (Damgaard and Treebak 2022).

2.15. RNA next-generation sequencing

Total RNA from enriched synaptosome samples in Trizol reagent were extracted by RNA clean and Concentrator-5 kit (Zymo). Total RNA libraries were generated by using SmartSeq2 protocol. This protocol was selected for its robustness and high efficiency for library preparation with low amounts of RNA starting material (Picelli et al. 2014; Hennig et al. 2018). Twenty-five µl of RNase Free water were used for elution. Ten µl of starting RNA material was used for the input for library preparation. Twenty-two PCR cycles were used for cDNA amplification. Ultimately, cDNA libraries of ~500 bp were obtained, with each sample containing a specific barcode. All libraries were sequenced together in the same sequencing run. The RNA sequencing was carried using Illumina NextSeq 2000 System. The sequencing procedures were conducted at the EMBL GeneCore facility situated in Heidelberg, Germany.

2.16. RNA sequencing data analysis

For detection and annotation of the sequencing reads, the following pipeline was used.

Genome alignment

The reference genome was mouse version GRCm39 from Genome Reference Consortium (GCA_000001635.9). An annotation GTF file was

downloaded from the Ensembl database. Read alignment was conducted with the STAR aligner (Dobin et al. 2013).

Count matrix generation

Read counts and count matrix were assessed by using featureCounts on Galaxy EU which is community-driven web-based analysis platform for life science research (The Galaxy Community 2022).

Quality control

Gene body coverage plots were obtained with Galaxy EU using RSeQC Gene Body Coverage (BAM) tool with the BAM files. Calculations for density plots were made with R and ggplot2 package (Wilkinson 2011) was used for visualization. For normalized expression transcripts per million (TPM) were calculated. First, library sizes were calculated and the counts were normalized using the calcNormFactors function. Then cpm function was used to calculate counts per million (CPM). TPM then were calculated by dividing CPM by a scaling factor.

Differential expression analysis

Differential expression analysis was performed by using DESeq2 package in R (Love, Huber, and Anders 2014). Adjusted p-values from DESeq2 analysis were used for data visualization, which is the transformation of the p-value after accounting for multiple testing using Benjamini and Hochberg method. For differential expression visualization volcano plots were made with R using ggplot2 package.

Gene Ontology

Gene Ontology analysis was made using GOrilla (Gene Ontology enRichment anaLysis and visuaLizAtion tool) which is a web based bioinformatics tool used to identify enriched GO terms in ranked list of genes (Eden et al. 2009). For this analysis genes were ranked according to the fold change difference between analyzed groups with a cut-off of 2-fold change.

2.17. C2 cloning and fusion with tags

For recombinant protein expression, fused proteins were cloned into pET-21a(+) plasmid. The open reading frame of the C2 domain was amplified using mouse tissue DNA as a template and Thermo Scientific Phusion Flash High-Fidelity PCR Master Mix, following manufacturer recommendations. The pET-C2 plasmid was obtained by ligating NdeI and HindIII restriction fragments of pET21a(+) vector and C2 PCR product. For protein fusion, flexible peptide linker was used (Chen, Zaro, and Shen 2013). The SNAP-tag gene was amplified from a plasmid kindly gifted by Heppenstall (Dhandapani

et al. 2018) and the mKate gene was amplified from pAAV-GFAP-mKate plasmid (Addgene #99129, RRID:Addgene_99129) with primers that inserted XhoI and HindIII restriction sites. The SNAP-tag or mKate amplicons were ligated into the pET-21a(+) plasmid after restriction with HindIII and XhoI

2.18. The mutagenesis of C2 domain

To obtain the inactive C2 domain, substitutions were made at Lys24 and Lys45, replacing them with asparagines. Site-directed mutagenesis was performed for the Lys24 substitution using specific primers (F: 5'-CAGCTACAATACATGGAACC-3' and R: 5'-CTGGAGGCTGACATCTGGCT-3') for PCR amplification with Thermo Scientific Phusion Flash High-Fidelity PCR Master Mix. Similarly, site-directed mutagenesis for the Lys45 substitution was carried out using specific primers (F: 5'-TCAGGGCAATATCAATGCCT-3' and R: 5'-TTATCCAGCCTTCCCAAGTG-3'). The resulting pET21a-C2m2 plasmid was used to construct pET21a-C2m2-SNAP and pET21a-C2m2-mKate plasmids, following the procedure described above.

2.19. pAAV plasmid for virus production

The plasmids for virus production were designed to carry astrocyte specific promoter GFAP sequence from pAAV-GFAP-mKate plasmid (Addgene plasmid #99129, RRID:Addgene_99129). Signal peptide sequence (UniProtKB/Swiss-Prot Accession Number: P21956) was introduced to ensure the secretion of constructed proteins.

2.20. Protein expression and purification

The recombinant pET21a-C2-mKate, pET21a-C2m2-mKate, pET21a-C2-SNAP or pET21a-C2m2-SNAP expression plasmids were transformed into *E. coli* BL21(DE3), HMS174(DE3), C43(DE3)pLysS, NovaBlue(DE3), Rosetta-gami 2(DE3) or ArcticExpress (DE3) competent cells. Transformants were selected by plating cells on agar plates containing ampicillin (100 µg/ml). The expression of recombinant proteins was induced by either 0.5 mM or 1.0 mM (2R,3R,4S,5R,6S)-2-(hydroxymethyl)-6-(propan-2-ylsulfanyl)oxane-3,4,5-triol (IPTG) at different temperatures (13 °C, 20 °C, 25 °C, 16 °C) with continuous shaking. After 16 h, cells were harvested by centrifugation at 3000 × g for 20 min at 4 °C. The pellet was sonicated using

BANDELIN SONOPULS mini20 with VS70T probe for 5 min at an amplitude setting of 50%. Sonication was performed for 15 s with 15 s intervals to cool down the specimen. Cell debris was centrifuged at $3000 \times g$ for 25 min at 4 °C. The solubility of recombinant proteins was assessed by 14% SDS-PAGE. The recombinant proteins from the supernatant of ArcticExpress (DE3) biomass induced by 1 mM IPTG at 16 °C were purified by immobilized chelate affinity chromatography on HisPur™ Ni-NTA (Thermo Scientific) column using ÄKTATM avant 25 chromatography system (Cytiva). After loading the sample, the system was washed with NPI-10 buffer (50 mM Na₂HPO₄, 300 mM NaCl, 10 mM imidazole). The proteins with His-tag were eluted with NPI-400 buffer containing 400 mM imidazole. Elution fractions were loaded on 14% SDS-PAGE to select those containing purified fused recombinant proteins. Chosen fractions were concentrated using Amicon® Ultra-4 Centrifugal Filter Units 10 kDa (Millipore) in a buffer containing 20 mM NaPO₄, 20 mM NaCl, pH 6.5. The concentration of purified proteins was determined using NanoDrop™ 2000 (Thermo Scientific).

2.21. Cultivation of mammalian cell lines

HEK293T (RRID:CVCL_0063) and Neuro2a (RRID:CVCL_0470) cell lines were purchased from American Type Culture Collection (ATCC). Human embryo kidney HEK293T cells were maintained in T25 flasks with Dulbecco's Modified Eagle's Medium (DMEM) supplemented with GlutaMAX™, 5% fetal bovine serum (FBS), 100 U/ml penicillin, 100 µg/ml streptomycin, and 1% non-essential amino acids (Thermo Fisher Scientific). Mouse neuroblastoma Neuro2a cells were cultured in Eagle's Minimum Essential Medium (EMEM) supplemented with 10% FBS, and 100 U/ml penicillin, 100 µg/ml streptomycin. The cell cultures were maintained at 37 °C and 5% CO₂. The cells were harvested using TrypLE™ solution. To evaluate PS exposure, the cells were plated at a density of 400 cells/mm² onto 8-well plates (Nunc™ Lab-Tek™, Thermo Scientific) that were pre-coated with poly-L-lysine (0.001% in PBS) for at least 20 min at RT. Experiments were conducted by Eimina Dirvelyte.

2.22. Apoptosis assay

To induce apoptosis, 24 h after plating the cells were treated with 3 µM of staurosporine (Sigma Aldrich) for 16 h. PS exposure was then detected by

adding 100 µg/ml recombinant fusion proteins for 30 min. Excess protein was removed by rinsing with pre-warmed media, and then cells were fixed with 4% paraformaldehyde (PFA) in PBS for 20 min at RT. After rinsing with PBS, residual PFA was quenched with 30 mM glycine in PBS, and the cells were washed twice with PBS. To visualize C2-SNAP and C2m2-SNAP proteins, the cells were labelled with 3 µM of benzylguanine substrate SNAP-Surface® Alexa Fluor® 647 (NEB) for 30 min at RT. Excess substrate was removed by washing with PBS three times and then incubating in PBS for an additional 30 min. All cells were stained with DAPI (1 µg/ml) for 10 min at RT. After a final three washes with PBS, Lab-Tek chambers were removed, and the microscopic slide was coverslipped with Mowiol (Calbiochem). The imaging was performed on the confocal Leica TCS SP8 microscope with 63×/1.4 oil immersion objective (pixel size 0.481 × 0.481 µm). A diode laser with an excitation wavelength of 405 nm was used for DAPI excitation. The white light laser was used for the excitation of PSVue (λ = 553 nm), AlexaFluor647 (λ = 647 nm), and mKate (λ = 589 nm). DAPI fluorescence was collected using a photomultiplier tube (PMT) detector (415–550 nm). The fluorescence of AlexaFluor647 (657–680 nm), mKate (599–750 nm), and PSVue (563–660 nm) was collected using a hybrid detector with a gating of 0.3–6 ns. Experiments were conducted by Eimina Dirvelyte.

2.23. Cell image analysis

Confocal images were analysed using the open-source CellProfiler software (RRID:SCR_007358) (45). The integrated intensity of C2 probe-specific fluorescence was measured in each image (n = 10-15 images for each condition, all conditions were repeated in duplicates across three independent experiments). The intensity was estimated per cell by dividing the image fluorescence intensity by the count of nuclei in that image. Fluorescence values were normalized to the highest obtained values of C2-SNAP and C2-mKate, as required. Experiments were conducted by Eimina Dirvelyte.

2.24. Adeno-associated virus production

The production of adeno-associated viruses (AAVs) expressing C2 probes was performed as described previously (Challis et al. 2019). For viral packaging, HEK293T cells were plated at a density of 6×10⁴ cells/cm². After 24 h, cells were transfected by three plasmids: 1) pAAV encoding the C2 probe of interest, engineered in this study as described above, 2) capsid-

encoding plasmid pUCmini-iCAP-PHP.eB (a gift from Viviana Gradinaru, Addgene plasmid #103005; RRID: Addgene_103005), and 3) helper plasmid XX6-80 (received from The National Gene Vector Biorepository, NGVB) at the ratio of 1:4:2, with a total of 40 µg of DNA per dish. The transfection was mediated by polyethylenimine (linear, MW 25 000, Sigma Aldrich). After 72 h and 120 h post-transfection, cell media were collected and filtered through a 0.45 µm filter to remove cell debris and sterile filtered through 0.22 µm syringe filter. The AAV solution was concentrated by centrifugation in Amicon Ultra Centrifugal Filter Units 100 kDa (Merck Millipore) at 3000 × g for 8 min at RT or until the volume of the solution remaining in the top chamber of the Amicon filter device was 500–1500 µl. Then DPBS with 0.001% Pluronic F-68 (Thermo Fisher Scientific) was added to the AAV solution in Amicon filter device and centrifuged 3000 × g for 8 min at RT, repeating the washing three times. During the last spin 300-500 µl of AAV solution was collected. AAV titre was determined by quantitative PCR using SYBR Green. In brief, DNase I was added to degrade any unpacked DNA, which was then inactivated with EDTA. Viral DNA was released using proteinase K and detected by qPCR. The obtained Ct values were used to determine AAV titres.

2.25. The modelling of the structure of fused recombinant proteins

The structures of fused recombinant C2-mKate and C2-SNAP proteins were predicted using de novo modelling tools Robetta (Baek et al. 2021), Raptor-X (Källberg et al. 2012) and artificial intelligence tool AlphaFold 2 (Jumper et al. 2021). The quality of the obtained models was assessed using VoroMQA (Olechnovič and Venclovas 2017), ProSA (Wiederstein and Sippl 2007), QMEANDisCo (Studer et al. 2020), and ProQ2 (Ray, Lindahl, and Wallner 2012) values, and the optimal model for each protein was chosen. The selected protein models for C2-mKate and C2-SNAP were aligned to PDB structures of individual domains (C2 – PDB ID:2L9L, mKate – PDB ID:3BXC, SNAP-tag – PDB ID:3KZZ) using the PyMOL program. Experiments were conducted by Eimina Dirvelyte.

2.26. Organotypic hippocampus slice culture preparation

Organotypic hippocampal slice cultures (OHSC) were prepared using the interface method, as previously described (Gogolla et al. 2006; De Simoni and MY Yu 2006). Briefly, three-day-old pups of *Thy1::EGFP* mice were

decapitated after cervical dislocation. The isolated brain was placed in a Petri dish filled with ice-cold dissection medium (100 U/ml penicillin, 100 µg/ml streptomycin, 15 mM HEPES, 0.5% glucose in HBSS). The removed hippocampi were sliced at a thickness of 300 µm using a McIlwain tissue chopper. The intact slices were carefully planted on prepared 0.4 µm 30 mm diameter cell culture inserts with MCE membrane (Merck Millipore) while maintaining medium (25% 1X BME, 25% horse serum, 5 % 10X MEM, 100 U/ml penicillin, 100 µg/ml streptomycin, 2 mM GlutaMAX, 0.65% glucose, 9 mM sodium bicarbonate in ddH₂O) and maintained in 5% CO₂ incubator at 37 °C. The medium was changed 24 h after the plating and every 2-3 days during culture maintenance. Experiments were conducted by Eimina Dirvelyte.

2.27. PS labelling in AAV-transduced OHSC

OHSC were transduced with 6.7×10¹⁰ vg of AAV-C2-mKate, AAV-C2m2-mKate, AAV-C2-SNAP, or AAV-C2m2-SNAP at 5 days *in vitro* (DIV5). The medium was changed 2 days after treatment and then every 2-3 days. The selected treatment was performed 9 days after the transduction, at DIV14. To inhibit fused protein secretion, OHSC were treated with 10 µg/ml of brefeldin A (BFA) (Thermo Fisher Scientific) for 5 hours. To induce apoptosis, OHSC were treated with 100 µM of staurosporine (Sigma Aldrich) for 16 hours. After either treatment, slice cultures were washed with prewarmed media and fixed in 4% PFA in PBS for 30 min at RT. Next, slices were rinsed once with PBS and quenched with 30 mM glycine/PBS. OHSC expressing C2-SNAP and C2m2-SNAP were labelled with 3 µM benzylguanine substrate SNAP-Surface® Alexa Fluor® 647 for 2 h at RT. Nuclei were counterstained with DAPI (1 µg/ml) for 15 min at RT. Both apoptosis and protein localization experiments were performed in three independent cultures containing duplicates for each experimental condition. Experiments were conducted by Eimina Dirvelyte.

2.28. OHSC immunofluorescence labelling

To label different cell types in BFA-treated OHSC, fixed slices were permeabilized and blocked in 0.4% Triton-X/PBS with 20% normal goat serum (NGS) (Abcam). They were then incubated for 16 h on a shaker at 4 °C. Afterwards, the slices were incubated with primary antibodies (polyclonal rabbit anti-Iba1 or polyclonal chicken anti-GFAP (Table 2) in 0.1% Triton-X

with 5 % NGS for 24 h on a shaker at 4 °C. Following three washes with PBS, the slices were incubated with secondary antibodies (polyclonal goat anti-rabbit Alexa Fluor Plus 594, or polyclonal goat anti-chicken Alexa Fluor Plus 594 respectively (Table 2) in PBS with 5% NGS for 4 h on a shaker at RT. The nuclei were counterstained with DAPI (1 µg/ml) for 15 min at RT. After three more washes with PBS, the slices were mounted onto the microscope slides using Mowiol (Calbiochem). Images were acquired using Leica TCS SP8 confocal microscope with either 63×/1.4 oil immersion objective (pixel size 0.18 × 0.18 µm) for protein secretion experiments or dry 20×/0.75 objective (pixel size 1.137 × 1.137 µm) for apoptosis experiments. For DAPI excitation, a diode laser with a wavelength of 405 nm was used. A white light laser was used for the excitation of AlexaFluor647 (λ = 647 nm), mKate (λ = 589 nm), EGFP (λ = 488 nm), and AlexaFluor594 plus (λ = 594 nm). DAPI fluorescence was collected using a photomultiplier tube (PMT) detector (415–550 nm). The fluorescence of AlexaFluor647 (657–680 nm), mKate (599–750 nm), and AlexaFluor594 plus (604–650 nm) was collected using a hybrid detector under gating of 0.3–6 ns. Experiments were conducted by Eimina Dirvelyte.

Table 2. Primary and secondary antibodies used in this study.

Antibody	Source	Final conc.	Host	Resource Identifiers	Lot number
Anti-Iba1	FUJIFILM Wako Chemicals	1 µg/ml	Rabbit	RRID:AB_839504	LEK0542
Anti-GFAP	Abcam	36.8 µg/ml	Chicken	RRID:AB_1975558	GR3393187-1
Anti-rabbit Alexa Fluor Plus 594	Invitrogen	4 µg/ml	Goat	RRID:AB_2762824	2307236
Anti-chicken Alexa Fluor Plus 594	Invitrogen	4 µg/ml	Goat	RRID:AB_2762829	XE349349

2.29. OHSC image analysis

Image analysis was performed using ImageJ software (RRID:SCR_003070) (Schindelin et al. 2012). The accumulation of C2-SNAP, C2m2-SNAP, C2-mKate or C2m2-mKate fusion proteins in astrocytes was quantified by assessing SNAP-specific fluorescence within GFAP-specific signal. For both SNAP and GFAP channels, the background was removed using the Subtract background function (rolling ball radius 50 pixels). Images were smoothed with Gaussian Blur filter (sigma = 2) and thresholded using the Otsu algorithm with the Auto-Threshold function to obtain masks for further measurements. The image of SNAP signal within the astrocytes was obtained using the Process-Image Calculator function with the

selected operation as "AND," and the area of both GFAP and SNAP within GFAP was determined using Measure function. Experiments were conducted by Eimina Dirvelyte.

2.30. AAV transduction in vivo

Study design: Mice injected with AAV-C2-SNAP were compared to non-injected littermate control using a single mouse as an experimental unit. **Sample size:** Five mice were injected with AAV-C2-SNAP, one mouse was used as non-injected control. In total, six mice were used. The number of animals was chosen to be sufficient for qualitative analysis. **Inclusion and exclusion criteria:** No animals were excluded during the experiment. **Randomization:** Mice were allocated to the injection and control groups randomly. The cofounders were controlled by comparing littermate injected and control mice. **Blinding:** Blinding was not applied. **Outcome measures:** C2 labelling was qualitatively assessed by imaging fluorescent signal in the brain samples from AAV-C2-SNAP and control animals. **Statistical methods:** Only qualitative analysis was performed. **Experimental animals:** Three-day-old (P3) homozygous *Thy1::EGFP* mice. **Experimental procedures:** P3 mice were injected into the facial vein with 1×10^{11} vg of AAV-C2-SNAP in 0.9% saline, in a total volume of 20 μ l, using an insulin syringe with a 29G needle. After 2 weeks (at P17), mice were transcardially perfused with 0.9% saline for 2 minutes, followed by 4% PFA for 5 minutes. The brains were post-fixed for 24 hours and then sectioned at 50 μ m using a 5100mz vibratome (Campden Instruments). Free-floating brain sections were labeled with 3 μ M SNAP-Surface® Alexa Fluor® 647, counterstained with DAPI (1 μ g/ml) for 15 minutes and washed with PBS. Slices were mounted in Mowiol (Calbiochem), and images were acquired using a Leica TCS SP8 confocal microscope with a 63 \times /1.4 oil immersion objective (pixel size 0.18 \times 0.18 μ m). Experiments were conducted by Eimina Dirvelyte and Igor Nagula.

2.31. Statistical analysis

GraphPad Prism 8 software was used for statistical analysis. R-squared test was applied to determine the strength of the relationship between the linear model and the dependent variables. Prism's linear regression analysis was used to compare the slopes and the intercepts of two linear regression lines. Concordance between datasets was estimated through Pearson correlation. Outliers were defined as exceeding three interquartile ranges and removed

from the analysis. Shapiro-Wilk test was used to assess the normality of the datasets and all data was confirmed to have normal distribution except data from Figure 3 B ($p=0.011$). Paired t -test was used to compare RIN to 5':3' integrity values.

The amplification efficiency was calculated from two different human or mouse RNA samples. RNA samples from five mouse cortices were used for RIN and 5':3' integrity score evaluation. RNA samples from postsurgical brain tissue of three patients were used for RIN and 5':3' integrity score evaluation. Four crude and sorted synaptosome samples from four different animals were used for mRNA integrity study of subcellular samples.

Neuro2a and HEK293T cell culture, as well as OHSC experiments, were replicated in at least three independent cultures. Data presented were expressed as means \pm standard error of the mean. Fold change graphs were expressed as geometric means \pm 95% confidence intervals. The normality of the data was verified by Shapiro-Wilk test. The means were compared by one-way ANOVA and *post-hoc* Tukey test. The means of fold change were compared by Kruskal-Wallis one-way analysis of variance and *post-hoc* Dunn's test. p values < 0.05 were considered as significant.

3. RESULTS

3.1. The analysis of axonal boutons during cortex maturation

Critical period of plasticity at mouse V1 starts around day P21, peaks at P28 where synaptic plasticity is at its highest and closes at around P35. It is known that formation of presynaptic boutons increases during the critical period and then declines with maturation of the network (Sun et al. 2019). It is also known that the range of persistent axonal bouton sizes is network activity-dependent with bouton size becoming more similar to the mean when the activity is deprived (Sammons, Clopath, and Barnes 2018). However, to this day the morphology and dynamics of axonal boutons during normal and unperturbed critical period of plasticity is not described. Also, the precise mechanisms controlling morphological bouton changes and synaptic plasticity during cortex critical period remain unclear although several processes like local protein synthesis probably plays an important role. Therefore, the initial focus of this thesis was to describe the morphological changes of axonal boutons during the critical period in the mouse V1. Furthermore, I aimed to implement a modern research FASS technique to extract a labeled population of synapses to look at transcriptomic changes during the visual cortex period of plasticity.

3.1.1. Axon bouton and C1q dynamics during the critical period of plasticity in mouse visual cortex

Axon bouton size and density can vary heavily during different stages of network maturation (Grillo et al. 2013; Sammons, Clopath, and Barnes 2018). Therefore, as a first step in this study, axon bouton size and density changes were investigated in the mouse visual cortex before, during and after the critical period of plasticity. To accomplish that, fluorescent imaging and subsequent image analysis was used. Mice expressing fluorescent EGFP protein under *Thy1* promoter provided a sparse excitatory neuron-specific labeling. The brains from such mice were collected at P21 (immature cortex), P28 (the peak of plasticity) and at P35 (matured cortex). The axons in the layer 2/3 of the visual cortex were then imaged and axon bouton size and density were calculated (Figure 3.1.1.) A statistically significant increase in bouton size was observed at P35 when compared to P21 or P28 (ANOVA with *post-hoc* Scheffe's method, $p < 0.01$ and $p < 0.01$ respectively). On the contrary,

bouton density was significantly lower at P35 than at P21 or P28 (ANOVA with *post-hoc* Scheffe's method, $p<0.01$ and $p<0.01$ respectively). This data confirmed an immature state of the neuron network at P21 with high density of small axonal boutons. The lower density but larger boutons at P35 indicated strong, matured synapses while axons at P28 were in between of these states.

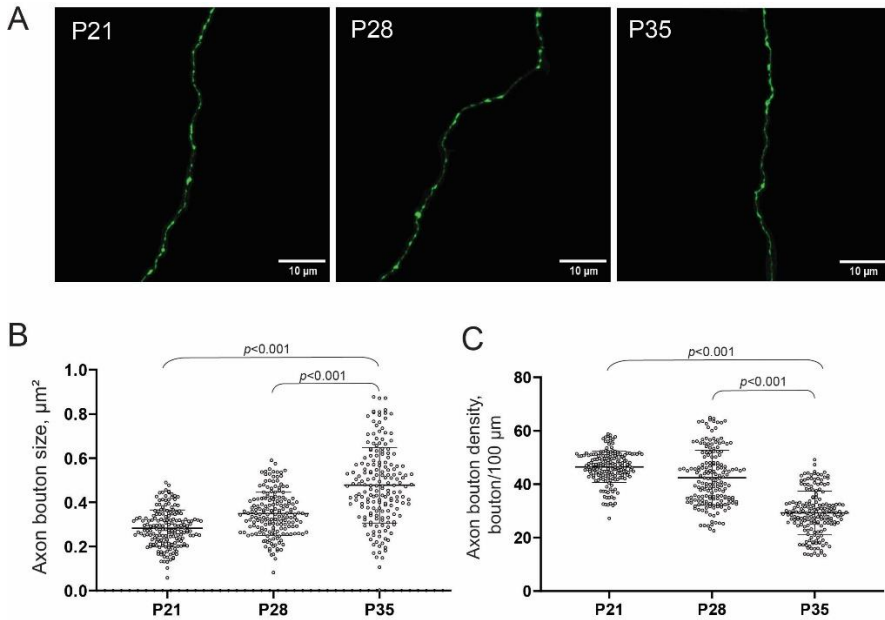


Figure 3.1.1. Visual cortex bouton size and density during critical period reflects immature, midway and mature states of the cortex. A) Representative fluorescence images of the axon of layer 2/3 excitatory neuron in the mouse visual cortex at P21, P28 and P35. Scale bar 10 μm. B) Axonal bouton size increased during visual cortex maturation, while the density decreased C). The sizes and densities of fluorescent EGFP axon boutons was calculated using optimized binary-processed image analysis with ImageJ. Each dot represents an individual image (n=180 in each group). ANOVA with *post-hoc* Scheffe's method.

Early neural development is marked by excessive outgrowth of neurons, leading to the formation of extensive networks of synapses. As development progresses, the redundant synaptic connections are selectively removed. One of the known “eat-me” signals for synapse elimination by microglia is C1q protein. Therefore, next C1q signal density was analysed during the same time points at P21, p28, and p35 in mice visual cortex. There was a significant increase in C1q signal density during the peak of critical period (P28)

compared to the samples before or after the critical period (ANOVA with *post-hoc* Scheffe's method, $p<0.01$ and $p<0.01$ respectively) (Figure 3.1.2.). Furthermore, C1q had higher colocalization with boutons at p28 then P21 or P35. This data suggests that C1q is involved in the network remodeling during the critical period of plasticity.

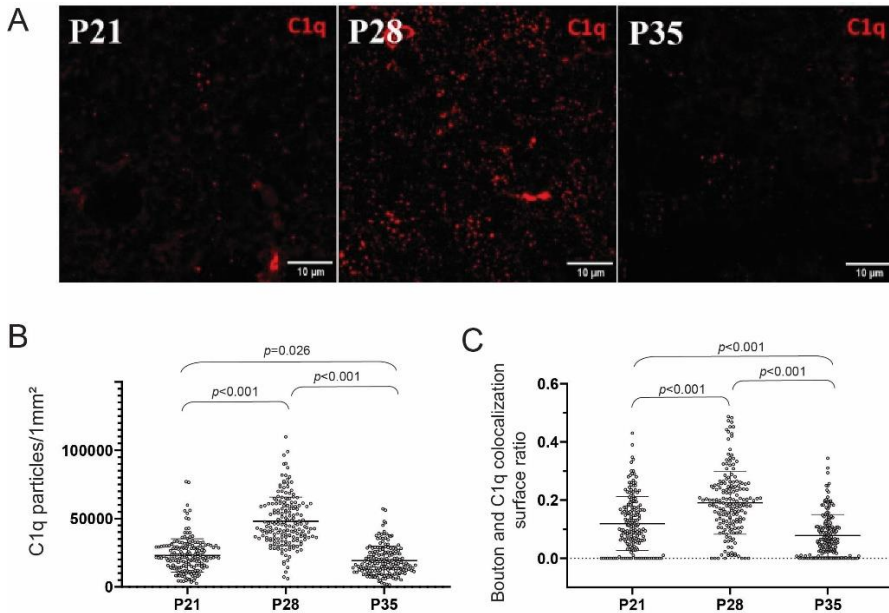


Figure 3.1.2. There is an increased labeling of complement component C1q during the peak of critical period. A) Representative images for immunofluorescence labelling of C1q protein in the mouse visual cortex at P21, P28 and P35. Scale bar 10 μm . B) The density of the C1q labelled particles increased during the peak of critical period. C). The colocalization surface ratio of axonal boutons and C1q signal. The C1q densities were calculated using optimized binary-processed image analysis with ImageJ and the colocalization was analyzed using Imaris microscopy image analysis software. Each dot represents an individual image ($n=180$ in each group). ANOVA with *post-hoc* Scheffe's method.

3.1.2. Implementation of Fluorescence Activated Synaptosome Sorting (FASS) for local transcriptome assessment

While the precise mechanisms controlling critical period of plasticity remain unclear, recent research highlights the involvement of local synaptic protein synthesis. Local protein synthesis is a process where synaptic proteins are produced locally at synaptic terminals. Excitatory presynaptic boutons as

well as postsynaptic spines carry out protein synthesis regularly and synthesis within these compartments is differentially recruited to modify local proteomes during synaptic plasticity (Hafner et al. 2019). Local protein synthesis adds spatial and temporal precision for proteome remodelling that can be exploited to rapidly modify synapses in specific subcellular compartments during critical plasticity period to adjust to external stimuli.

Local transcriptome and its regulation can be assessed using synaptosomes which are isolated synaptic terminals. Pure synaptosome sample can be obtained by using genetically engineered mouse where synapses are fluorescently labelled together with fluorescence-activated synaptosome sorting (FASS) technique (Figure 3.1.3.A) (Luquet et al. 2017). During this procedure, the neural tissue of interest was homogenized, centrifuged several times to remove unhomogenized larger particles and then ultracentrifuged in a sucrose gradient to acquire a layer of particles containing synaptosomes. Synaptosomes are very small particles (0.5–2 μm most of the time) and they fall below the detection limits of most cell sorters on standard thresholding methods using light scattering. Therefore, to achieve reliable particle detection in the cell sorter crude synaptosome sample was then dyed with lipophilic dye SynptoRed C2. Crude synaptosome sample contained a mixture of synaptosomes from different neuron types and particles from other cells. Therefore, sorting out the labeled excitatory synaptosomes ensured that pure excitatory synaptic samples were collected. After the sorting, 60–90 % of all the particles were mVenus+ compared to ~20% in crude preparations, indicating significant excitatory synapse enrichment (Figure 3.1.3.B). This ensured us that the fluorescent signals together with sensitive FACARIA III sorter was sufficient to sort out and collect the enriched mVenus+ excitatory synaptosome samples.

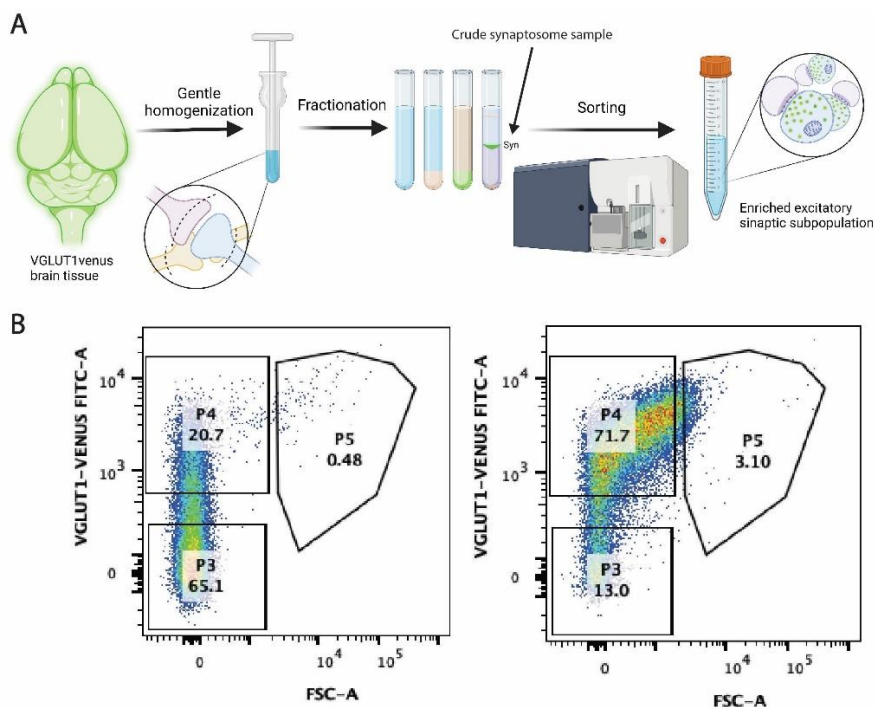


Figure 3.1.3. Fluorescence Activated Synaptosome Sorting (FASS) technique was implemented to collect enriched excitatory synaptosome samples. A) VGLUT1^{mVenus} mouse brain tissue was homogenized and the homogenate was serially fractionated to obtain the particles that have the size and the density corresponding to the synaptosomes. This crude synaptosome sample was then sorted according to mVenus fluorescence to get enriched excitatory synaptosome population. Created with Biorender.com. B) Analysis of synaptic particle distribution before and after sorting. In a crude synaptosome sample, there were ~20% mVenus+ synaptosomes. After FASS of mVenus+ excitatory synaptosomes, an enriched sample was prepared, where excitatory synaptosomes comprised more than 70% of all particles.

To further confirm that the sorted particles were Venus-fluorescent synaptosomes, Cytek Amnis FlowSight imaging flow cytometer was used which takes high quality images of moving particles in the stream and measures their fluorescence at the same time (Figure 3.1.4.) The acquired images showed that prepared mVenus and SynaptoRed C2 fluorescent particles were homogenous round particles reminiscent of synaptosomes and thus the implementation of elaborate technique for synaptosome enrichment by sorting was successful.

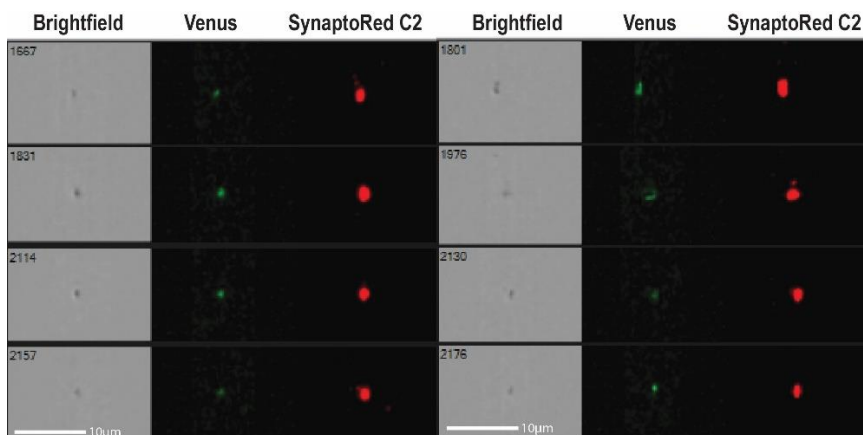


Figure 3.1.4. mVenus+ fluorescent excitatory synaptosomes can be visualized as round individual particles. Representative images of SynaptoRed C2+ and mVenus+ synaptosomes imaged on Cytex Amnis FlowSight imaging flow cytometer.

The next step in this study was collecting mVenus+ synaptosome samples for transcriptomic analysis. Since the procedure of preparing and sorting synaptosomes was lengthy (approximately 11-12 hours from dissecting the brain to collecting sorted mVenus+ synaptosome sample), it was important to measure and ensure high extracted synaptic RNA integrity. Currently, the most widely used method for RNA integrity evaluation is RIN calculation, which is based on the intactness of rRNA bands. Therefore, this method was used to evaluate the RNA integrity in our crude and sorted synaptosome samples. For this study RNA from eight matched synaptosomal preparations was used: four crude synaptosome samples and four FASS-enriched synaptosome samples. For these samples RIN value from 8.0 to 9.1 was acquired, which indicates good RNA quality. However, in the enriched synaptosomal samples RIN values could not be determined, because there was almost no ribosomal RNA and there were no detected rRNA bands in electrophoresis lanes (Figure 3.1.5.A) despite loading the same amount of sample RNA. It is known that synaptosomes do contain some ribosomes for local protein synthesis (Hafner et al. 2019). However, the reduced quantity of rRNA in the subcellular sample of synaptosomes was not sufficient to measure RNA integrity with RIN (Figure 3.1.5. B). Crude synaptosome samples were a mixture of particles similar in size and density still containing some rRNA which was enough to measure RIN value. However, after the enrichment the rRNA content was significantly reduced hindering the integrity evaluation

with this method. This identified problem demanded an alternative approach which would allow to measure sample RNA integrity independent of rRNA.

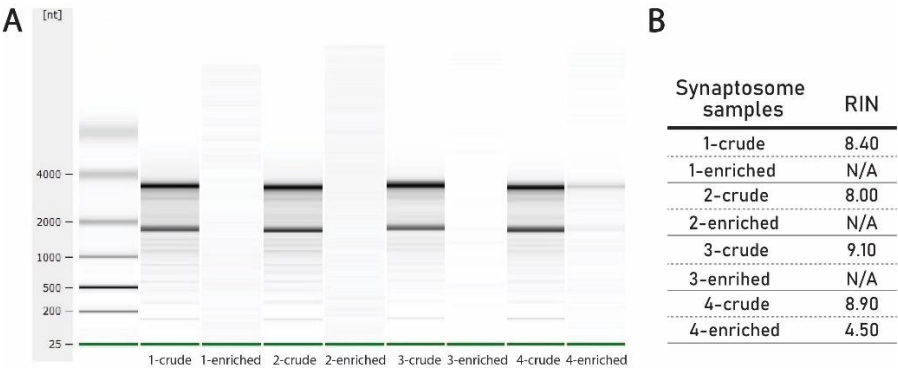


Figure 3.1.5. Evaluating RNA integrity in synaptosomes. A) Representative image of Agilent 2100 Bioanalyzer RNA Pico Chip gel of total RNA samples from crude and enriched mouse synaptosomal samples. B) RIN values of crude and enriched mouse synaptosomal samples.

3.2. 5':3' assay for direct mRNA integrity evaluation

Transcript integrity can be estimated by evaluating the length of reverse transcription products obtained from one of the transcript’s termini. Poor sample integrity is reflected in mRNA breaks that lead to shortened cDNAs, length of which can be assayed by quantitative PCR comparing the amounts of 3’ and 5’ fragments of assayed mRNA. The straightforward approach to reverse transcription of mRNA from one of its termini is to use oligo-dT primers that bind to the polyadenylated end of mature mRNA. Therefore, the 5’:3’ approach is based on using oligo-dT primers for reverse transcription and two sets of primers for qPCR to measure the relative expression of two amplicons located on the 3’ and 5’ regions of a long constitutively expressed mRNA of choice and then comparing the relative amounts of 3’- and 5’-ends of the transcript (**Figure 3.2.1.**) If mRNA in the sample is intact, reverse transcription from poly(A) tails goes on uninterrupted generating full-length cDNA. Therefore, following qPCR generates similar levels of 3’- and 5’-end products. In a partly degraded mRNA sample, cDNA synthesis from the poly(A) tail of fragmented mRNA leads to the truncated cDNA at the site of mRNA cleavage. This truncation depletes the binding sites for 5’-end primer pair resulting in a reduced amount of 5’-end product. The 5’:3’ integrity value for a sample is then quantified by dividing the amount of 5’-end amplicon amount by that of 3’-end amplicon and multiplying by 10 to get an integrity

score from 10 (intact mRNA) to 0 (totally degraded mRNA), in line with other RNA integrity assays that use 1–10 scales (Schroeder et al. 2006).

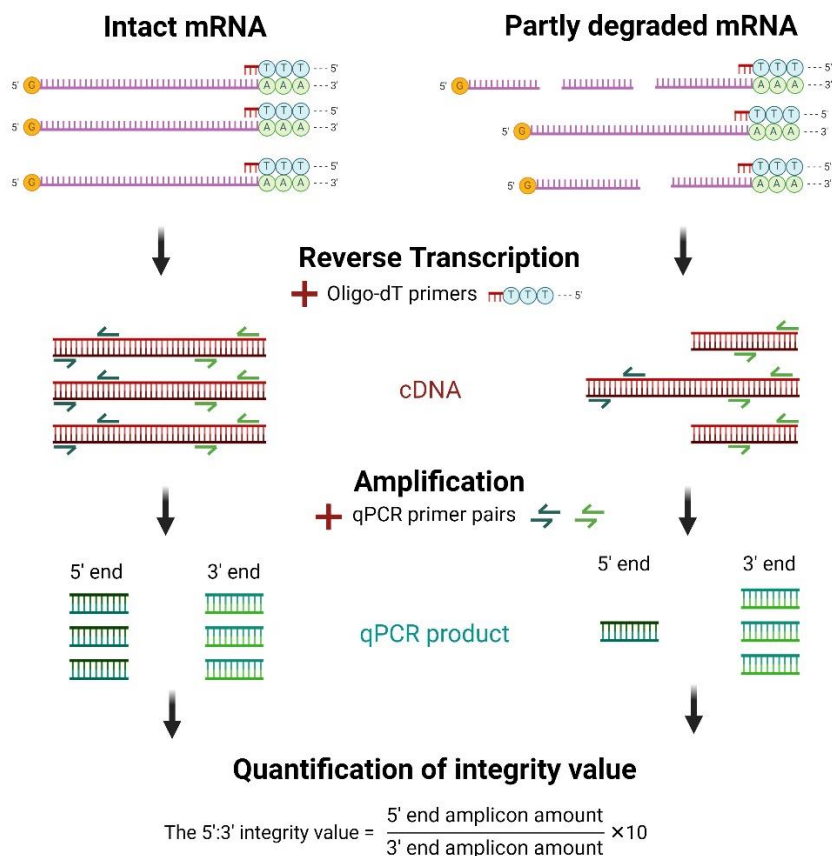


Figure 3.2.1. The principle of 5':3' assay for mRNA integrity evaluation. Reverse transcription reaction used oligo-dT primers to generate cDNA. In RNA samples of good quality, mRNA is intact and full-length cDNA is synthesized. In this case, both 3' and 5' pairs of qPCR primers have the same number of sites to attach and produce comparable amounts of 3'- and 5'-end PCR products. In contrast, in poor quality RNA samples with partly degraded mRNA, shorter cDNA is synthesized because of the breaks in mRNA. On truncated cDNA, PCR primer pair for the 5'-end of mRNA has lower number of binding sites compared to the 3'-end, close to the poly(A) tail of mRNA. After qPCR amplification, the 5':3' integrity value is calculated by dividing the amount of the 5'-end amplicon by that of the 3'-end amplicon and multiplying by 10, allowing the quantitative evaluation of mRNA quality in the sample. Created with Biorender.com.

3.2.1. 5':3' assay is based on PGK1 cDNA

The mRNA template for 5':3' assay has to be carefully selected and ideally should be a long transcript with a stable and abundant expression in the tissue of interest with as few pseudogenes as possible to ensure reliable results. The choice of a long transcript ensures that there is sufficient distance between 5' and 3' primer pair binding sites to capture the breaks in the mRNA caused by degradation. Here mouse and human *PGK1* cDNA was used as a template for the 5':3' assay. *PGK1* is ubiquitously expressed housekeeping gene that produces a relatively long transcript with a well-characterized exon-intron structure well suited for this assay (Padhi et al. 2018). Its product is an enzyme called phosphoglycerate kinase, which is involved in glycolysis (Rojas-Pirela et al. 2020). Due to its high and stable expression, *PGK1* has been recommended as a reference gene for quantitative measurements of gene expression in RNA samples isolated from human blood (Falkenberg et al. 2011). Moreover, *PGK1* gene is highly conserved and homologous between rats, mice and humans. In mice and humans, there are two *PGK* isozymes encoded by different genes: *PGK1* and *PGK2* but only *PGK1* is expressed ubiquitously (He Liu et al. 2022). *PGK1* transcripts have been previously used to measure mRNA integrity in rat toxicology studies (Padhi et al. 2018) and horse samples (Du Cheyne et al. 2021). Here the qPCR primers for 5':3' assay were designed based on mouse and human *PGK1* cDNA to measure mRNA integrity in mouse and human RNA samples (**Table 3**). To ensure that any remaining genomic DNA in mRNA sample does not interfere with the assay, samples were treated with DNase I and designed the primer pairs to be exclusively specific to mRNA. In particular, one primer in each primer pair used in this assay binds to an exon-exon junction to avoid any unwanted remnant genomic DNA amplification. The exon-exon junctions are marked in Table 3.

Table 3. Primer pair sequences for 5':3' assay in mouse and human RNA samples.

Species	Primer name	Primer sequence (5'-3')	Amplicon size (bp)
Mouse	mPgk1_5'For	TCGTGATGAGG / GTGGACTT	109
	mPgk1_5'Rev	GCTCCATTGTCCAAGCAGA	
	mPgk1_3'For	TGGGGTATTTGAATGGGAAG	107
	mPgk1_3'Rev	TGTCTCCACC / ACCTATGATAGT	
Human	hPGK1_5'For	GGTCGTTATGAG / AGTCGACTTC	109

	hPGK1_5'Rev	GCTCCATTGTCCAAGCAGA	
	hPGK1_3'For	TGGGGGTATTTGAATGGGAAG	107
	hPGK1_3'Rev	TGTCTCCACC / ACCTATGATGG	
/ - Exon-exon junction			

3.2.2. The integrity value of 5':3' assay should be corrected to reflect primer pair amplification efficiency

The 5':3' integrity assay relies heavily on the prerequisite that both 5'- and 3'-end fragments are amplified with equal efficiency. Therefore, it is important to assess the amplification efficiency of used primer pairs. To calculate the amplification efficiency of the designed primer pairs (**Table 3**) plasmids with cloned fragments of mice (55-1342 bp) and human *PGK1* (21-1270 bp) cDNA were used as a template for qPCR. Acquired Ct values of both 5'- and 3'-end amplicons were plotted against corresponding plasmid copy number and amplification efficiency (*E*) was calculated from the slope of linear regression equation. For both mouse and human *PGK1*, the primer pair for the 5'-end had lower amplification efficiency (**Figure 3.2.2.A, B**). The same pattern was observed when amplification efficiency was assessed in total RNA samples from mouse and human brain (**Figure 3.2.2.C, D**).

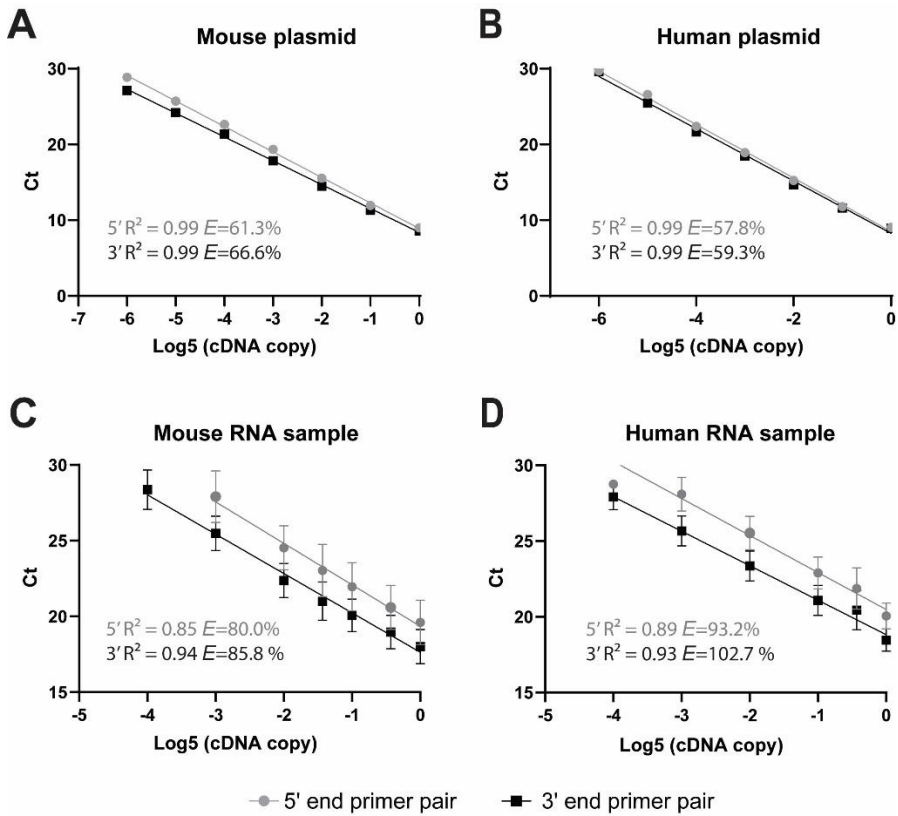


Figure 3.2.2. The amplification efficiency of the 5'-end and 3'-end primer pairs differs for both mouse and human 5':3' assay. Plasmids with cloned mouse (A) and human *PGK1* (B) cDNA or cDNA from mouse (C, n=2) and human (D, n=5) RNA samples were used for serial dilutions and following qPCR to determine primer amplification efficiency *E*.

Even a slight difference in the primer amplification efficiency between the primer pairs results in shifted integrity values of 5':3' assay. Therefore, a recently published STAR protocol for qPCR data analysis was applied that corrects the relative expression of the gene(s) of interest according to primer amplification efficiency¹². This protocol uses mathematical transformation to calculate amplification factor from the amplification efficiency (slope) for each primer pair that can be expressed as presented in the equation (1). Amplification factor is then used to correct the qPCR data, by defining a linear form of original gene expression (2). This approach was integrated to obtain adjusted 5':3' integrity values. To assess the outcome of this correction, uncorrected and corrected 5':3' integrity values were compared to RIN defined in the same set of RNA samples, isolated from surgically resected human brain tissue (Table 1). Paired *t*-test revealed that without the correction, the integrity values were significantly lower

than RIN values ($p<0.0001$, $n=16$), while 5':3' integrity values after correction were comparable to RIN values ($p=0.029$, $n=16$) (**Table 4**).

$$\text{Amplification factor} = \text{Dilution factor}^{\left(-\frac{1}{\text{slope}}\right)}$$

$$\text{Corrected expression} = \text{Amplification factor}^{-Ct}$$

Table 4. The comparison of 5':3' integrity values calculated without the primer amplification efficiency correction, the corrected 5':3' integrity values and RIN values. Original integrity values significantly lower than RIN ($p<0.0001$, paired t -test), while corrected 5':3' integrity values and RIN were comparable ($p=0.029$, paired t -test). The 5':3' integrity values and RIN were evaluated in RNA samples isolated from surgically resected human brain. List of samples and their clinical description is presented in Table 1

Sample ID	5':3' integrity value	5':3' corrected integrity value	RIN
#02	2.3	4.6	4.6
#03	2.5	6.4	6.0
#04	2.2	3.7	4.6
#05	2.4	4.1	5.8
#06	3.6	6.6	7.1
#07	2.8	6.5	6.9
#08	2.7	5.9	6.8
#09a	2.9	5.8	6.7
#09	2.7	5.8	6.2
#10a	2.3	4.4	5.9
#11	2.7	5.8	5.5
#12a	3.4	8.1	7.8
#12	3.1	6.8	6.5
#13	2.9	6.4	5.5
#13a	2.6	4.8	5.9
#14	1.9	4.2	5.6

3.2.3. The integrity value of 5':3' assay accurately represents different ratios of primer binding sites

To demonstrate that the calculated integrity value translates to the actual abundance of 3' and 5' binding sites, plasmids with truncated mouse and human *PGK1* cDNA were cloned. These plasmids contained 3' half of the cDNA (675-1342 bp of mouse *Pgk1* cDNA and 608-1270 bp of human *PGK1*

cDNA). By mixing different quantities of plasmids with cloned full-length *PGK1* and truncated 3'-end *PGK1* fragment, samples with known 3'- and 5'-end ratios were prepared to model variable cDNA sets resulting from RNA samples degraded to different extent. The 5':3' assay of these samples demonstrated a linear relationship between 5'- and 3'-end ratios and obtained integrity value ($R^2=0.93$, $p<0.0001$ for mouse *Pgk1* and $R^2=0.89$, $p<0.0001$ for human *PGK1*, Pearson's correlation) (**Figure 3.2.3**). These results showed that 5':3' assays integrity value can accurately represent the difference in the abundance of existing binding sites for created primer pairs.

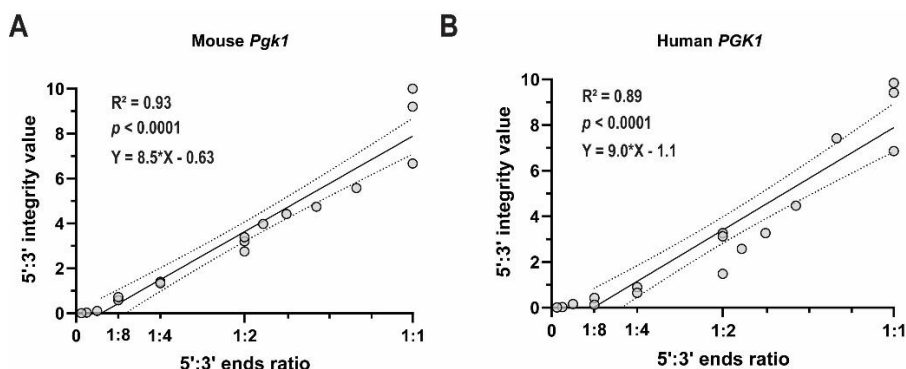


Figure 3.2.3. The calculated 5':3' integrity value represents the ratios of the binding sites for the used primer pairs. The different 5':3' ends ratios were acquired by mixing plasmids with cloned full length and truncated mouse and human *PGK1* cDNA to mimic a wide range of mRNA degradation. The 5':3' integrity value was calculated and plotted against the ends ratio for (A) mouse and (B) human assays. A linear relationship was observed for 5':3'ends ratios and integrity values for both mouse and human assays. Linear regression line is shown with 95% confidence interval of the true best-fit line.

3.2.4. 5':3' integrity value and RIN value correlate well in heat-treated RNA samples

Traditionally, RNA integrity is evaluated qualitatively by inspecting the intensities of the 28S and 18S ribosomal RNA (rRNA). This principle is used by currently most popular approach to assess RNA integrity – the Agilent Bioanalyzer system, which assigns RNA Integrity Number (RIN) to RNA sample. To assess the capacity of the 5':3' assay to detect the degradation in general RNA samples compared to RIN value, heat-degraded total RNA samples were used from mouse cortex. The samples were incubated for 1–15 min at 90 °C and then analyzed using mouse 5':3' RNA integrity assay and

Agilent Bioanalyzer. Both the 5':3' integrity values and RIN values gradually decreased with prolonged heat treatment (**Figure 3.2.4.A**). RIN values and 5':3' integrity values correlated well ($R^2=0.67$, $p<0.0001$, Pearson's correlation) and samples that had lower RIN value had lower 5':3' integrity value and *vice versa* (**Figure 3.2.4.B**). In primary not heated samples, the values calculated with both methods were comparable (from 7.2 to 8.5 for RIN and from 7.6 to 9.7 for 5':3' integrity values). However, with prolonged heating, 5':3' assays integrity values dropped faster than RIN values (**Figure 3.2.4.C, D**). Therefore, RIN cut-off value of 7.0, which is commonly used as a cut-off for good quality RNA samples suitable for further analysis, is equivalent to 5':3' assays integrity value of approximately 6.

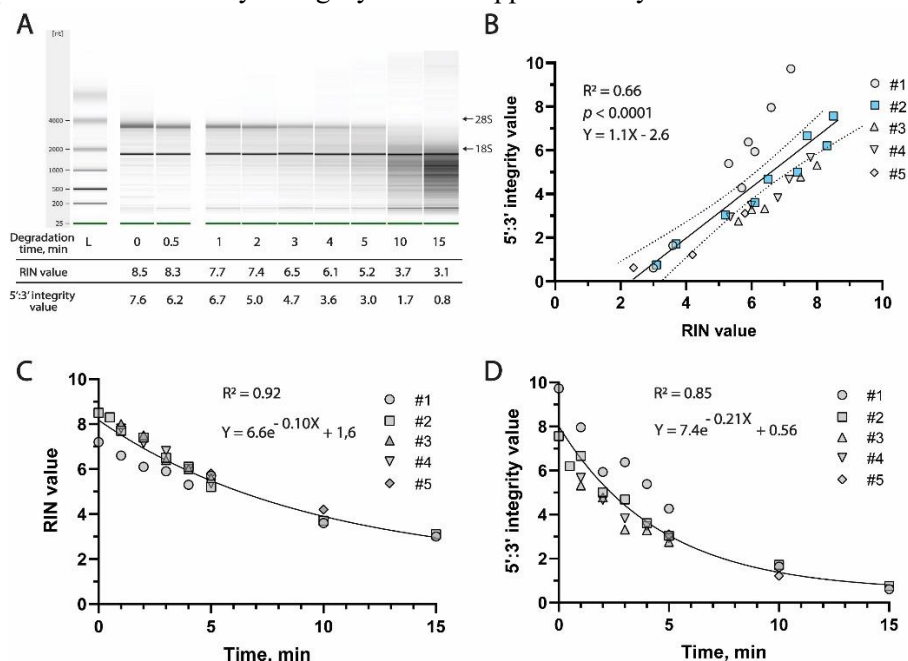


Figure. 3.2.4. Evaluating RNA integrity with 5':3' assay versus RIN values using heat-degraded mouse RNA samples. A Representative image of Agilent 2100 Bioanalyzer RNA Pico Chip gel of mouse brain sample #2 total RNA heat-degraded at 90 °C for 1, 2, 3, 4, 5, 10 and 15 min. At the bottom: RIN values and obtained 5':3' values. The displayed values are marked in blue on panel B. **B** There was a strong linear correlation between RIN value and 5':3' integrity value ($n=5$, individual mouse cortex samples labelled as #1, #2, #3, #4 and #5). Linear regression line is shown with 95% confidence interval of the true best-fit line. **C, D** Both RIN values (**C**) and

5':3' integrity values (**D**) decreased with longer heating duration. The lines in **C** and **D** represent one phase exponential decay of the data.

Next, the same principle was applied to assess 5':3' RNA integrity assay with human brain RNA samples. Three total RNA samples from surgically resected human brain tissue were heat-degraded for 1–10 min at 90 °C and then analyzed using the Agilent Bioanalyzer and human 5':3' RNA integrity assay. As seen with mouse RNA samples, both 5':3' integrity values and RIN values decreased with longer duration of sample heating (**Figure 3.2.5.A**). There was a very strong correlation between 5':3' RNA integrity values and RIN values ($R^2=0.86$, $p<0.0001$, Pearson's correlation) showing that both values reflect RNA degradation in samples comparatively (**Figure 3.2.5.B**). As with mouse RNA samples, heat degradation decreased human 5':3' integrity values faster than RIN values (**Figure 3.2.5.A, C, D**).

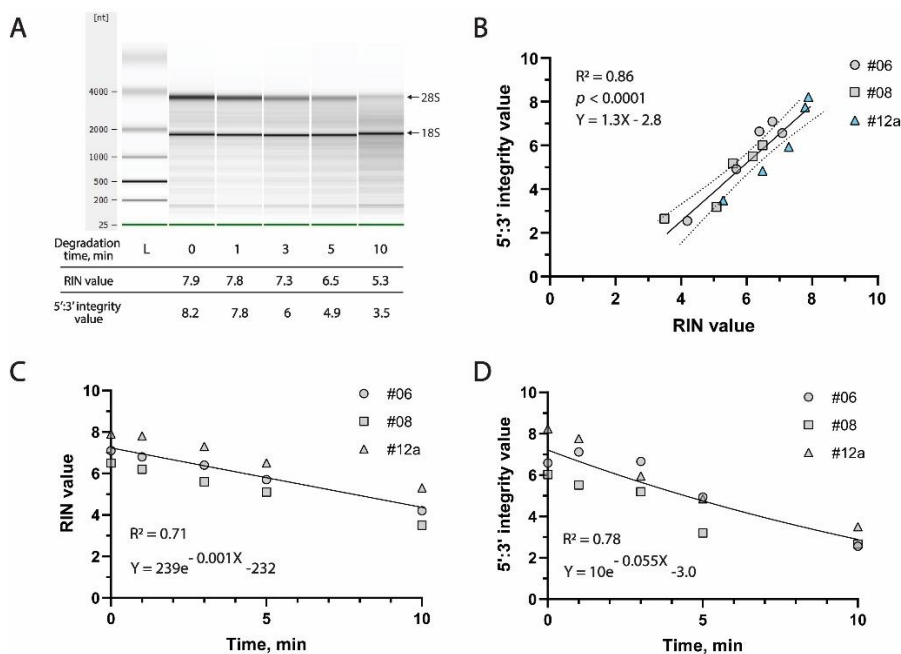


Figure 3.2.5. Evaluating RNA integrity with human 5':3' assay *versus* RIN values using heat-degraded human brain RNA samples. **A** Representative image of Agilent 2100 Bioanalyzer RNA Pico Chip gel of human brain sample #12a RNA heat-degraded at 90 °C for 1, 3, 5, and 10 min. At the bottom – RIN values and obtained 5':3' values. The displayed values are marked in blue in panel B. **B** Three total RNA samples from surgically resected human brain tissue were used to define 5':3' integrity values and RIN

values (#06, #08, #12a, **Table 1**). There was a strong linear correlation between RIN values and 5':3' integrity values in these samples. Linear regression line is shown with 95% confidence bands of the true best-fit line. **C, D** Both RIN values (C) and 5':3' integrity values (D) decreased with longer heating duration. The lines in **C** and **D** represent one phase exponential decay of the data.

3.2.5. In human post-surgical brain tissue samples, 5':3' integrity value represents the RNA integrity better than RIN

RT-qPCR based RNA integrity evaluation assay can be applied as an RNA quality control method for most medical laboratories working with human tissues. The increasing use of human tissue in research emphasizes the importance of developing appropriate and easy to use methods for tissue quality assessment. For that reason, human 5':3' assay was assessed to evaluate RNA integrity in human brain samples, obtained from the glioma or epilepsy surgery. RIN values were measured in the same samples for comparison. The surgically resected brain tissue was kept viable during transportation in cold artificial Cerebrospinal Fluid (aCSF) and then dissected immediately for homogenization, RNA extraction and both RNA integrity assays (**Figure 3.2.6.A**). Obtained 5':3' integrity values varied from 3.6 to 9.7 while RIN values varied from 4.6 to 7.8 in these samples. There was a significant moderate correlation between 5':3' integrity assay and RIN values ($R^2=0.59$, $p=0.0005$, Pearson's correlation) (**Figure 3.2.6.B**). This further supports our proposition that the 5':3' integrity value could be used to reliably evaluate RNA quality in clinical samples as an alternative to RIN.

For gene expression studies, it is important to define the integrity of mRNA in particular rather than total RNA or rRNA, which is defined by RIN. It is known that RNA integrity determines acquired Ct values in qPCR reactions for gene expression studies¹. For gene expression studies using qPCR, random hexamer primers are usually used to synthesize cDNA. These primers bind to random parts of mRNA independently of the primer binding site distance from the 3' or 5' end. However, this leads to higher Ct values when part of mRNA is degraded and the portion of binding sites for random hexamer primers is lowered. Therefore, RNA degradation lowers the cDNA quantity, length and abundance of the binding sites for qPCR primers. This in turn leads to higher Ct values in partially degraded mRNA samples compared to intact RNA samples. Therefore, 5':3' integrity values and RIN values were compared to the expression of a housekeeping gene *GAPDH* in the same clinical samples

as defined by real-time qPCR using Maxima First Strand cDNA Synthesis Kit with random hexamer primers and TaqMan system. The 5':3' integrity value correlated better with *GAPDH* Ct values than RIN values, which further supported our assertion that 5':3' assay reflected transcript quality in RNA samples better than RIN value ($R^2=0.48$, $p=0.0063$ for 5':3' integrity value and $R^2=0.34$, $p=0.0283$ for RIN value, Pearson's correlation) (**Figure 3.2.6.C, D**). This shows the credibility in observed integrity values, demonstrating that 5':3' assay can reliably predict the integrity of transcripts.

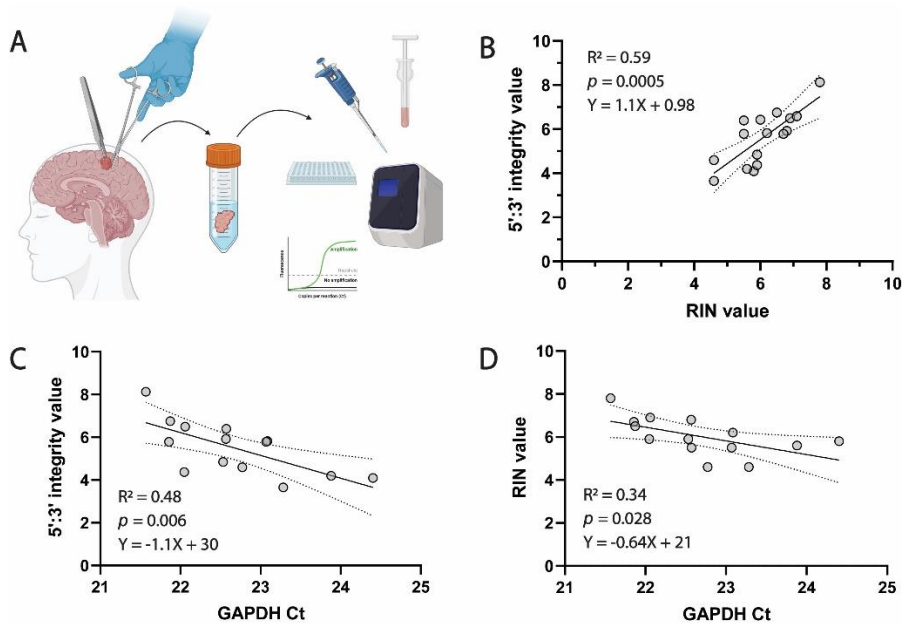


Figure 3.2.6. RNA integrity in total RNA samples from surgically resected human brain tissue. **A** Human post-surgical brain tissue from the glioma or epilepsy surgery was kept viable during transportation in artificial cerebrospinal fluid (aCSF). The sample was then immediately dissected and homogenized for RNA extraction and RNA integrity assays. Created with Biorender.com. **B** Relationship between 5':3' integrity value and RIN in RNA samples from human brain tissue (n=16). Linear regression line in **B** is shown with 95% confidence intervals of the true best-fit line. **C** There was a moderate linear correlation between the human brain tissue RNA sample 5':3' integrity values and Ct values from qPCR for *GAPDH* expression, while the correlation with RIN values was weak (**D**) (n=14).

3.2.6. 5':3' assay can be used to measure RNA integrity in synaptosomal preparations

Finally, developed 5':3' assay was used to measure the mRNA integrity of synaptosome samples. It has been shown that because of its ubiquitous expression *PGK1* is abundant in synaptosomes (Hafner et al. 2019). For this study RNA from eight matched synaptosomal preparations was used: four crude synaptosome samples and four FASS-enriched synaptosome samples as reported before (Figure 3.1.4.) In these samples, 5':3' integrity value was calculated and compared to the previously acquired RIN value. RNA integrity analysis in crude synaptosome samples demonstrated comparable values for 5':3' integrity assay and RIN. Even though in the enriched synaptosomal samples RIN values could not be determined, 5':3' assay, which is independent of rRNA, was suitable to evaluate mRNA integrity in enriched synaptosome samples with very low amount of rRNA (Figure 3.2.7.) demonstrating its applicability for the samples containing subcellular fractions.

Synaptosome samples	5':3' integrity value	RIN
1-crude	6.61	8.40
1-enriched	1.72	N/A
2-crude	6.95	8.00
2-enriched	2.40	N/A
3-crude	5.57	9.10
3-enriched	4.04	N/A
4-crude	6.99	8.90
4-enriched	3.69	4.50

Figure 3.2.7. 5':3' assay can evaluate mRNA integrity in synaptosomes. 5':3' integrity value and RIN value of crude and enriched mouse synaptosomal samples.

3.3. Local synaptic transcriptome

Each neuron may be connected to up to 10,000 other neurons, passing signals to each other via as many as 1,000 trillion synapses. These synapses might be relatively far from the neuron body and have to individually and quickly adapt to the received stimulus. To do that efficiently, synapses have been shown to significantly regulate their own proteome by local protein synthesis and this process is very important for their maintenance and synaptic plasticity (Van Driesche and Martin 2018). Hundreds of sequenced mRNA species, present within excitatory boutons, confirmed that protein synthesis

happens locally within synaptic particles and is regulated to modify local proteomes during the periods of synaptic plasticity (Hafner et al. 2019; C. Sun et al. 2021). However, it is still not known how the synaptic transcriptome changes in developing neural network and critical plasticity windows.

3.3.1. Synaptic RNA-sequencing and data quality control

To define local excitatory synaptic transcriptome and its changes during the refinement of cortical circuitry, RNA sequencing of enriched synaptosome samples was used. For this, 25 synaptosome samples were collected. Nine (5 male and 4 female) samples were from immature visual cortex at P21, 8 (4 male and 4 female) samples were from visual cortex during its peak of plasticity at P28 and the last 8 (4 male and 4 female) samples were from visual cortex after the critical period closure at P35. Synaptosome samples contain very low amounts of RNA – around 30 ng per sample. Therefore, SmartSeq2 protocol was used for sequencing library preparation as this protocol is robust and highly efficient for library preparation with low RNA starting material like RNA from single-cell experiments (Picelli et al. 2014; Hennig et al. 2018). The RNA sequencing was carried using Illumina NextSeq 2000 System. The gained reads per sample varied heavily from 0.7 to 32 million sequencing reads per sample. For that reason, to exclude low quality samples from further sequencing data analysis, 8 samples with lower than 10 million sequencing reads were removed.

Another step in the quality control (QC) of RNA sequencing data was checking for a 3' bias. Three prime end bias is an effect where significantly more gained reads map onto genes 3' end than 5' end. This is usually caused by RNA degradation. Typically, RNA-Seq libraries are prepared from total RNA using poly(A) enrichment of the mRNA to remove rRNA. However, when partially degraded samples are used with this protocol, only the transcript part near the 3' end and poly(A) tail is collected and used for the sequencing library leaving broken off parts of the transcript behind (H. Feng, Zhang, and Zhang 2015).

Three prime end bias can be observed from gene body coverage plots. Gene body coverage plots are a visualization tool used in genomics to assess the distribution of sequencing reads across the entire length of genes. The gene body coverage plots of enriched synaptosome RNA-seq data showed a similar distribution between 5' and 3' regions confirming high integrity of collected synaptic RNA samples (Figure 3.3.1).

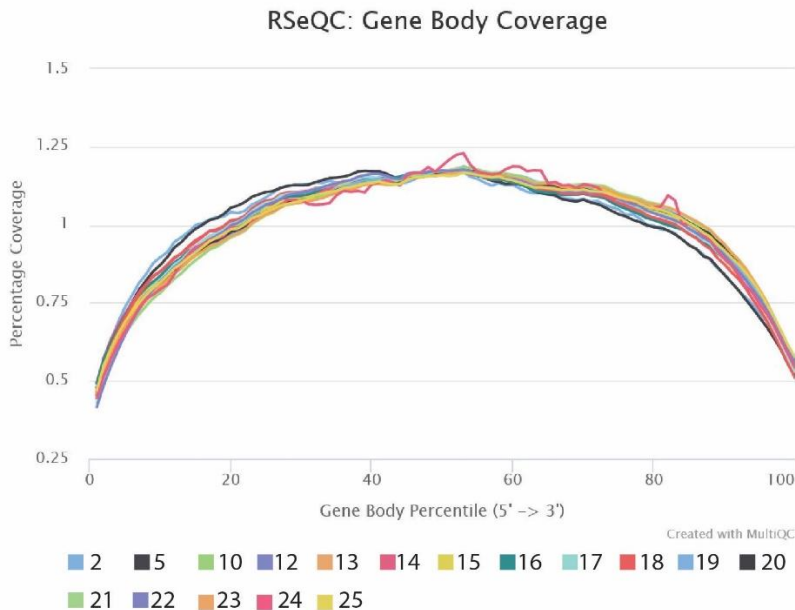


Figure 3.3.1. Synaptic mRNA integrity evaluation from RNA-seq data using gene body coverage plots. Gene body coverage plots showing the distribution of RNA-seq reads across the transcript length of enriched synaptosome samples and the percentage of coverage. The graphs for all samples were similar and did not show 3' bias.

Quality control in RNA-seq involves assessing read count distributions, often visualized using density plots. These plots highlight read count distribution across samples, aiding the evaluation of sequencing depth and overall data quality. In enriched synaptosome samples, typical patterns included two peaks: one representing lowly expressed transcripts near zero on the x-axis, and another denoting abundant transcripts around $3 \log_{10}(\text{read counts})$ (Figure 3.3.2.) Very low counts across genes may indicate poor sample quality, potentially biasing RNA-seq results. Samples #02 and #10 exhibited sharp peaks of very low read counts with an absence of discernible peaks indicative of high read counts. Consequently, sample #02 and #10 were excluded from further analysis to mitigate potential biases.

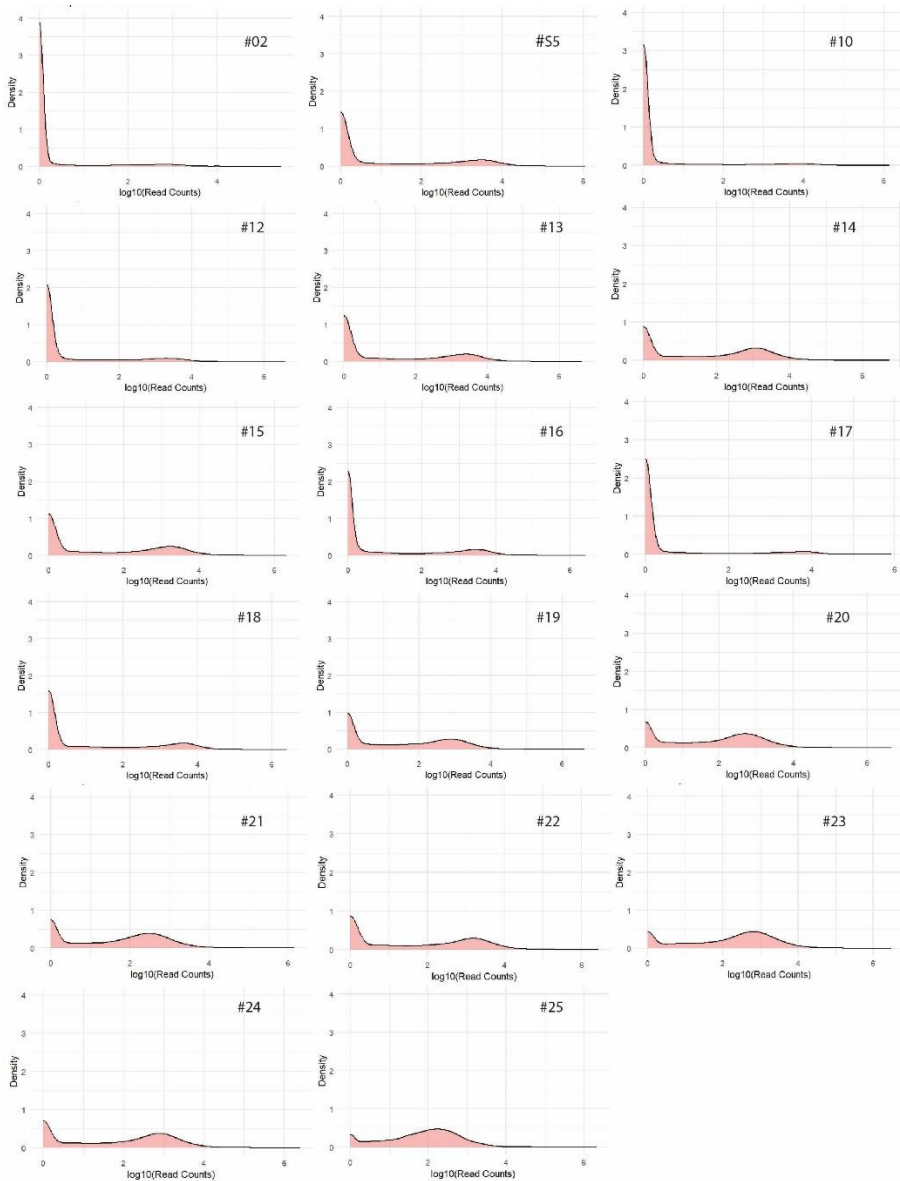


Figure 3.3.2. Sequencing data quality evaluation using read counts density plots. Density plot showing the distribution of RNA-seq read counts of collected enriched synaptosome samples.

Enriched synaptic samples were acquired with the aim of studying a predominantly excitatory synaptic population, minimizing impurities from other synaptic types or cellular constituents. To assess the efficacy of the sorting-based enrichment method and verify the predominance of excitatory synaptosomes in analysed samples, marker genes representative of various

cell types within brain tissue (including excitatory, inhibitory, and motor neurons, astrocytes, microglia, and epithelial cells) were selected (Zhu et al. 2023; E.-R. Martin, Gandawijaya, and Oguro-Ando 2022; Kuswanto et al. 2013; Niibori et al. 2023; H. J. Lee et al. 2014; Gerrits et al. 2020; Pan et al. 2020; Lawrence et al. 2023). Their expression was examined in sequenced synaptosome samples (Figure 3.3.3.A). As anticipated, the synaptosome samples exhibited notable expression of excitatory neuron marker genes (*Bsn*, *Glul*, *Grin2b*, and *Syt1*). Furthermore, no transcripts specific to inhibitory (*Gad2* and *Slc32a1*) or motor neurons (*Chat*, *Isl1*), microglia (*Tmem119*, *Siglech*, *P2ry12* and *Cx3cr1*), or epithelial cells (*Pecam1* and *Tie1*) were observed. Nonetheless, a presence of astrocytic transcripts was noted in the synaptosome samples. I hypothesize that this observation may stem from a tighter-than-expected junction between the synapse and astrocytic projection, a phenomenon known as the tripartite synapse (Farhy-Tselnick and Allen 2018). Therefore, at least part of the collected excitatory synaptosomes probably also contains an astrocytic transcripts as well (Figure 3.3.3.B).

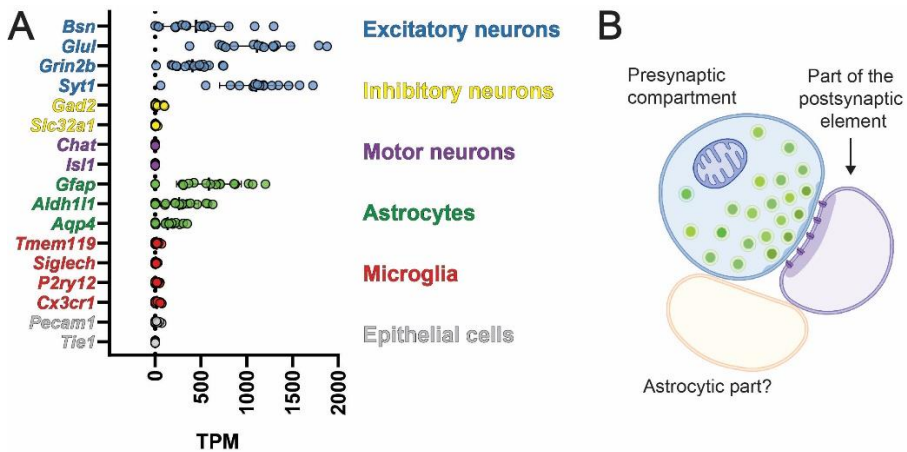


Figure 3.3.3. Synaptosomal transcriptome contain not only expected excitatory neuron marker genes but also some astrocyte-specific transcripts. A) Expression of marker genes specific for excitatory, inhibitory and motor neurons, astrocytes, microglia and epithelial cells in synaptosome samples. Expression shown as TPM. B) A proposed model of synaptosome containing part of connected astrocytic projection as a result of tripartite synapse.

3.3.2. Local excitatory synaptic transcriptome and its changes during cortex maturation

Recent evidence suggests that local translation occurs in the axons of excitatory and inhibitory neurons in the mature central nervous system (Hafner et al., 2019; Ostroff et al., 2019; Scarnati et al., 2018; Shigeoka et al., 2016; Younts et al., 2016). However, local excitatory synaptic transcriptome is still not well defined. Therefore, our subsequent focus was to elucidate the functional roles of the most highly expressed transcripts within synapses. Following quality control, a total of 15 synaptosome samples were retained for functional analysis, in which 15,716 distinct transcripts were identified. The transcripts were then ranked according to their expression levels. This ranked list was then used to identify enriched Gene Ontology (GO) terms using GOrilla, which is a web-based bioinformatics tool. Top 3 most significant GO terms were regulation of transport, modulation of chemical synaptic transmission and regulation of trans-synaptic signaling (Figure 3.3.4.A). Among the most significant GO terms of excitatory synaptic transcriptome many were similar or related to each other. Therefore, 20 top most significantly enriched GO terms were summarized as 5 following functions (Figure 3.3.4.B):

- Regulation of transport and localization
- Regulation of synaptic signaling and plasticity
- Intracellular transport and localization
- Translation
- Regulation of cellular organization

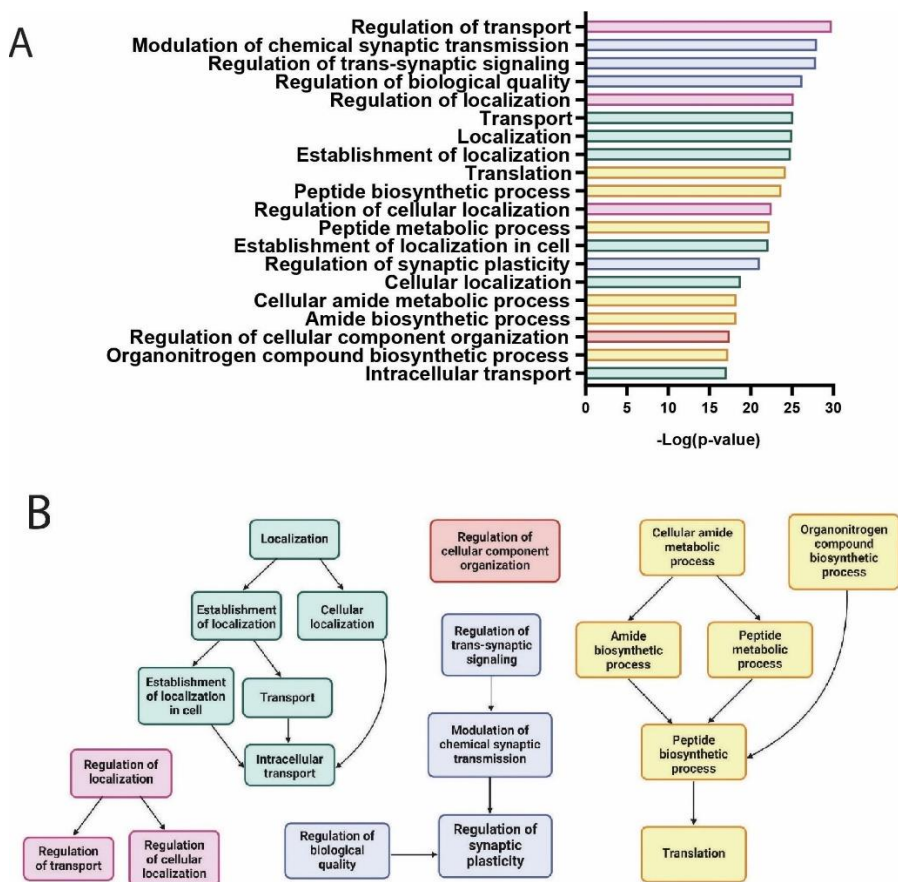


Figure 3.3.4. Excitatory synaptic transcriptome and its main functions. A) GO terms that are significantly overrepresented in general excitatory synaptosome transcriptome. B) The directed acyclic graphs of enriched GO terms, showing the main clusters.

To see what local transcriptomic changes are associated with visual cortex plasticity period, Differential Gene Expression (DGE) analysis was performed. At first, the synaptic transcriptome from the mature cortex (P35) was compared to the transcriptome from the cortex before the onset of critical period (P21). Out of 10267 transcripts detected within these groups, 180 transcripts were significantly upregulated and 109 transcripts were downregulated by two-fold or more in mature cortex samples compared to immature cortex (Figure 3.3.5.A).

Among the downregulated transcripts *Slc38a6* transcript was the most downregulated and was 24 times more abundant in immature cortex synaptic samples than in mature ones. This transcript encodes an amino acid transporter

that has selectivity for L-glutamine and L-glutamate, aiding in the uptake of glutamine in excitatory neurons (Bagchi et al. 2014). Due to pronounced downregulation of the *Slc38a6* transcript, the GO analysis identified the function of transporting glutamine as notably more common among the transcripts that are downregulated. Another GO term that was significantly overrepresented in downregulated transcript population was positive regulation of Interleukin-6 (IL-6) production with 7 downregulated transcripts assigned to this term (Figure 3.3.5.B). It is known that neurons do synthesize IL-6 and through classical and alternative signaling IL-6 promotes neurogenesis, neuron differentiation and maturation (Kummer et al. 2021). The high prevalence of transcripts responsible for IL-6 production in the immature cortex synapses indicates the importance of its local production while neurons are still developing.

The most upregulated transcript in the mature cortex synaptic samples was *Prkar2a* transcript, which produces a protein kinase, which is involved in the modulation of chemical transmission in glutamatergic synapses (Figure 3.3.5.C). Among all upregulated transcripts only one GO term was identified – membrane lipid metabolic process which incorporates 18 upregulated transcripts. This term combines transcripts participating in chemical reactions and pathways involving membrane lipids, any lipid found in or associated with a biological membrane. One of the transcripts within this term was *Pigv* transcript, which encodes glycosylphosphatidylinositol (GPI) mannosyltransferase 2 and was ten-fold more prevalent in mature cortex synaptosome samples than immature. This protein is involved in glycosylphosphatidylinositol-anchor biosynthesis and transfers the second mannose to the glycosylphosphatidylinositol during GPI precursor assembly. GPI-anchored proteins are a unique group of lipid-linked neuronal membrane proteins that play various roles in managing axon guidance, synaptic adhesion, cytoskeletal remodelling, and localized signal transduction, especially within lipid raft domains (Um and Ko 2017). Thus, the anchoring of diverse proteins via GPI likely represents a crucial local mechanism for ensuring robust adhesion and optimized signalling in mature synapses.

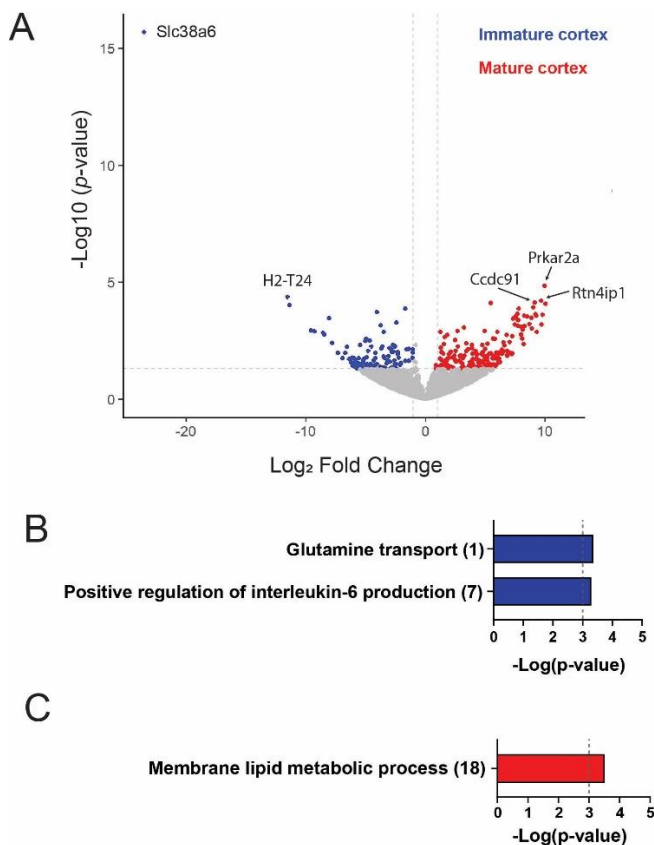


Figure 3.3.5. Differences between immature and mature visual cortex synaptic transcriptome. A) Volcano plot showing differentially expressed genes between synaptosome samples from immature visual cortex (P21) and mature visual cortex (P35). Upregulated genes in mature visual cortex synapses are shown in red while downregulated transcripts are shown in blue. Names of the five most significantly differentially expressed transcripts are displayed. B) Gene ontology terms that are significantly overrepresented in the transcripts downregulated at least two-fold. C) Gene ontology terms that are significantly overrepresented in the transcripts upregulated at least two-fold. Numbers in the brackets after the GO term indicate how many transcripts were assigned to that term. The dashed line in B and C shows a p -value threshold of 10^{-3} which was used to identify significantly enriched GO terms.

When the synaptic transcriptome from the immature cortex (P21) was compared to the transcriptome from the cortex during the critical period of plasticity (P28), there were 9370 transcripts identified in the samples of these

groups. 205 transcripts were downregulated and 196 transcripts were upregulated by two-fold or more in the cortex during the critical period peak.

A cluster of heavily downregulated transcripts in the cortex during its plasticity peak included *Slc38a6* (a predicted L-glutamine transmembrane transporter), *Gpr21* (G Protein-Coupled Receptor 21), and *Znfx1* (zinc finger NFX1-type containing 1) (Figure 3.3.6.A). *Slc38a6* transcript appeared to be specific to the immature cortex as it was only detected there and neither in the plastic nor mature cortex (Figure 3.3.5.A). This shows the possible importance of this L-glutamine transmembrane transporter for the activity of still-developing excitatory neurons. *Gpr21* and *Znfx1* functions in neurons have not been explored but might be very important locally for transmitting signals across cell membranes and maintaining cellular homeostasis (Wong et al. 2023; Liu et al., 2024.). There were four GO terms identified within the downregulated transcripts: regulation of insulin receptor signalling pathway, glutamine transport, negative regulation of transferase activity, and cellular lipid metabolic process with the first one being the most significant (Figure 3.3.6.B). Numerous studies have revealed insulin receptor (IR) involvement in a broad spectrum of functions in the CNS, with the majority of those appearing to be unrelated to metabolic functions of insulin. By now, the IR has been established as an important regulator of synapse formation and remodelling, neuronal survival and synaptic plasticity all of which seems to be regulated locally in the developing synapses (Pomytkin et al. 2018).

Two GO terms were identified between the transcripts upregulated in the synapses during critical period: regulation of nucleobase-containing compound metabolic process and alpha-beta T cell differentiation (Figure 3.3.6.C). The majority of transcripts from the first GO term encode proteins involved in controlling gene expression and might be produced locally and then delivered to neuronal soma to activate or repress transcription during the period of high plasticity (Goodwin and Picketts 2018). The later GO term was pointing at 3 transcripts - *Prr7* - proline rich 7, *Atp7a* and *Sema4a*. Apart from known or predicted function in T cell differentiation these genes are also involved in synapse-to-nucleus message delivering, copper transport from intracellular stores into the trans-Golgi network (TGN) and axonal guidance (Ito and Kumanogoh 2016; S. H. Lee et al. 2018; Polishchuk and Lutsenko 2013).

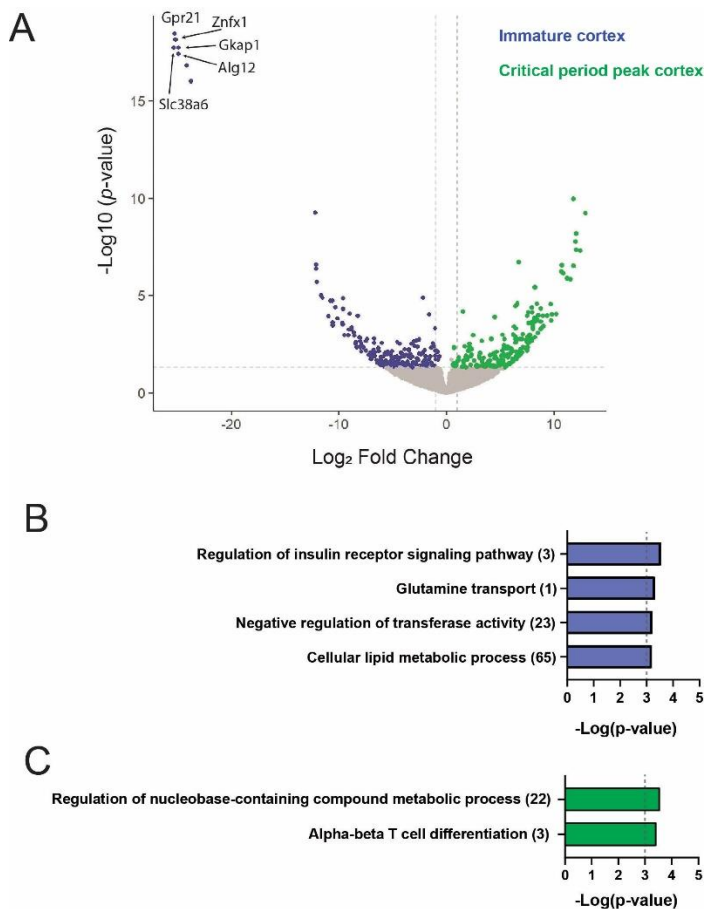


Figure 3.3.6. Differences between visual cortex during its plasticity peak and immature visual cortex synaptic transcriptome. A) Volcano plot showing differentially expressed genes between synaptosome samples from critical period peak visual cortex (P28) and immature visual cortex (P21). Upregulated genes in visual cortex synapses during the peak of plasticity are shown in green while downregulated transcripts are shown in blue. Names of five most significantly differentially expressed transcripts are displayed. B) Gene ontology terms that are significantly overrepresented in at least two-fold downregulated transcripts. C) Gene ontology terms that are significantly overrepresented in at least two-fold upregulated transcripts. Numbers in the brackets after GO term indicate how many transcripts were assigned to that term. The dashed line in B and C shows a p -value threshold of 10^{-3} which was used to identify significantly enriched GO terms.

At last, we compared the synaptic transcriptome from mature cortex (P35) and the cortex during its peak plasticity (P28). In these samples 9123

transcripts were identified. Out of these transcripts, 113 transcripts were significantly upregulated and 88 transcripts were downregulated by two-fold or more in mature cortex samples compared to the cortex during the peak of plasticity (Figure 3.3.7.A). The most significantly downregulated transcript in mature cortex compared to the peak plasticity period was *Mafk* transcript, from which transcription factor *MafK* can be synthesized. This transcription factor is a member of small Maf proteins (sMafs) which are basic region leucine zipper (bZIP)-type transcription factors. Small Mafs participate in transcriptional activation or repression depending on their heterodimeric partner molecules (Katsuoka and Yamamoto 2016).

GO analysis among the downregulated transcripts identified only two transcripts that are related in their function - *Map3k3* and *Fgf2*. The identified linking term was “positive regulation of cell migration in sprouting angiogenesis” which is process that increases the frequency, rate or extent of cell migration involved in the growth of new capillary vessels out of pre-existing ones (Figure 3.3.7.B). The most upregulated transcript in mature cortex synaptosome samples was *Tmem110*, which produces transmembrane protein. This protein regulates the long-term maintenance of ER-plasma membrane junctions and the short-term physiological remodelling of the junctions during store-dependent calcium signalling (Quintana et al. 2015). A significant part of upregulated transcripts was related to positive regulation of nucleobase-containing compound metabolic process and RNA metabolic process possibly because of intensified control of local synaptic protein synthesis in the matured neurons (Figure 3.3.7.C).

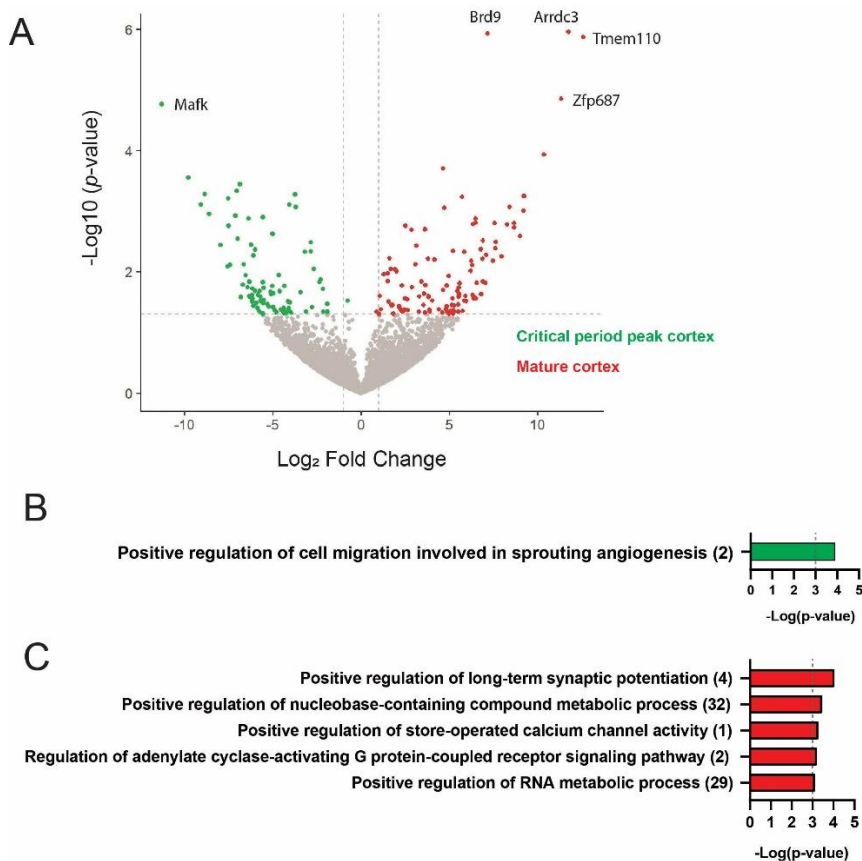


Figure 3.3.7. Differences between visual cortex during its plasticity peak and mature visual cortex synaptic transcriptome. A) Volcano plot showing differentially expressed genes between synaptosome samples from critical period peak visual cortex (P28) and mature visual cortex (P35). Upregulated genes in mature visual cortex synapses are shown in red while downregulated transcripts are shown in green. Names of five most significantly differentially expressed transcripts are displayed. B) Gene ontology terms that are significantly overrepresented in at least two-fold downregulated transcripts. C) Gene ontology terms that are significantly overrepresented in at least two-fold upregulated transcripts. Numbers in the brackets after GO term indicate how many transcripts were assigned to that term. The dashed line in B and C shows a p -value threshold of 10^{-3} which was used to identify significantly enriched GO terms.

Synaptic plasticity is known to be time-dependent, and in the mouse visual cortex, it is constrained to a critical period, with peak plasticity occurring around P28. Consequently, it can be informative to focus further on this specific time point and analyze its signature transcripts and biological

processes, in comparison with transcriptomes from both immature and mature synapses. In this study there were 500 genes identified that were uniquely upregulated at P28 by more than 1.5-fold compared to P21 and P35, and 402 genes that were significantly downregulated in plastic synapses. Gene Ontology analysis of the upregulated genes revealed that cellular metabolic processes, cellular component organization or biogenesis, and nucleobase-containing compound metabolic processes were the most enriched biological functions in plastic synapses. In contrast, the depleted transcripts were associated with cellular localization, intracellular transport, and positive regulation of biological processes. These findings further emphasize the distinct dynamics of the synaptic transcriptome during brain development.

3.3.3. Development of genetically encoded tool for the labelling of exposed synaptic phosphatidylserine

During critical periods of plasticity, the dynamic formation and elimination of synapses rely on molecular signals denoted as "don't eat-me" and "eat-me" necessary for efficient synaptic pruning and the optimization of network. Currently, the best-known "eat-me" signals are externalized phosphatidylserine (PS) and complement component 1q (C1q). The dynamics of phosphatidylserine in the plasma membrane is a tightly regulated feature of eukaryotic cells. Phosphatidylserine (PS) is found preferentially in the inner leaflet of the plasma membrane. Disruption of this asymmetry leads to the exposure of phosphatidylserine on the cell surface and is associated with such process as cell death or synaptic pruning. Due to the important role of phosphatidylserine in synaptic refinement and the small size of the synapses, an efficient phosphatidylserine probe is needed to study them. Currently, a few different phosphatidylserine labelling tools are available; however, these labels have unfavorable signal-to-noise ratios and are difficult to use in tissues due to limited permeability. Their application in living tissue requires injection procedures that damage the tissue and release damage associated molecular patterns, which in turn stimulates phosphatidylserine exposure. Thus, within this study, it was aimed to develop a novel genetically encoded phosphatidylserine probe based on the C2 domain of the lactadherin (MFG-E8) protein, suitable for labelling exposed phosphatidylserine in nervous tissue.

3.4. Local synaptic presence of transcripts involved in "don't eat-me" and "eat-me" signaling

Firstly, the local synaptic presence of transcripts involved in synaptic pruning was assessed. Synaptosomal RNA-seq data analysis revealed the presence of transcripts involved in phosphatidylserine (PS) biosynthesis, such as *Pisd*, *Ptdss2*, and *Ptdss1*, indicating its potential local synthesis mechanisms. However, the transcripts associated with PS externalization, such as scramblases *Xkr4*, *Xkr6*, *Xkr8*, *Tmem16D* or *Tmem16F* and flippases such as *Atp11A* or *Atp11C* were absent. Nevertheless, the transcripts of *Tmem16C* (known also as Anoctamin-3) which is calcium-dependent phospholipid scramblase were present in synaptosome samples suggesting its involvement in PS externalization in cortical excitatory synapses (Figure 3.4.1.A).

The presence of additional transcripts implicated in synaptic pruning was also assessed (Figure 3.4.1.B). Recent studies have indicated that caspases are involved in several neurodevelopmental processes, including axon guidance, synapse formation and pruning (Nguyen, Gillet, and Popgeorgiev 2021). Nevertheless, no transcripts for Caspase-3 or Caspase-7 were detected in the synaptic samples. The notable abundance of the *Cx3c11* transcript, also known as fractalkine, alongside transcripts associated with the formation and function of the C1q protein complex (*C1qa* and *C1qb*), underscores their potential significance in fostering microglial activation and phagocytosis of excitatory synapses within the visual cortex. Furthermore, the elevated expression of the *CD47* and *CD200* transcripts, linked to synaptic pruning as a "don't-eat-me" signal molecules, likely plays a crucial role in maintaining the persistent synapses (D. Feng et al. 2019). In conclusion, the intricate orchestration of "don't eat-me" and "eat-me" signals, exemplified by the interplay of molecules such as phosphatidylserine, C1q, fractalkine, and CD47, underscores their importance in mediating synaptic pruning and sculpting neural networks during critical period of plasticity.

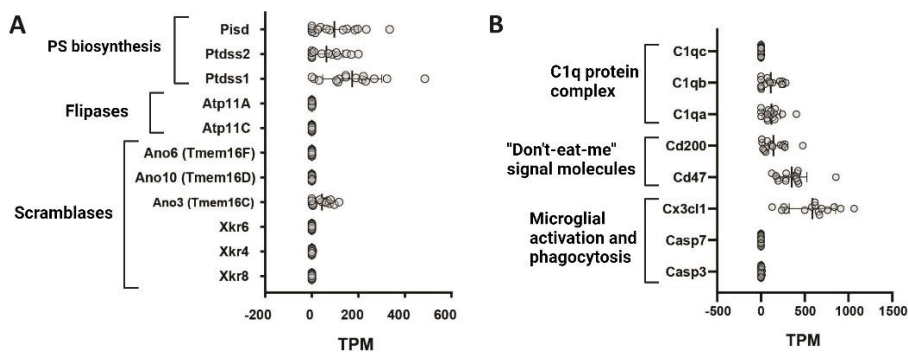


Figure 3.4.1. Local synaptic presence of transcripts associated with phosphatidylserine externalization and other synaptic pruning signalling molecules. A) Local synaptic expression of genes participating in PtdSer biosynthesis and externalization. B) Local synaptic expression of other genes participating in neuroinflammation and synaptic pruning. Expression shown as TPM.

3.4.1. PS labeling protein modelling suggests structural integrity of fused proteins

The precise local synaptic biochemical mechanisms triggering synapse elimination remain poorly understood. To address this inquiry, the labelling and extraction of synapses destined for pruning would be advantageous for the investigation of this process. Due to the well-known contribution of PS to synaptic pruning (Neniskyte et al. 2023b; Scott-Hewitt et al. 2020; Schafer et al. 2012), it was decided to use it as a target in labeling and extracting the population of synapses that have to be eliminated. Currently, a few different phosphatidylserine labelling tools are available; however, these labels have unfavourable signal-to-noise ratios and are difficult to use in tissues due to their limited permeability. Their application in living tissue requires injection procedures that damage the tissue and release damage associated molecular patterns, which in turn stimulates phosphatidylserine exposure. Due to the lack of specific PS probe for *in vivo* applications, our aim was to develop a genetically encoded tool. For this, C2 domain of the MFG-E8 protein was chosen as the basis for PS recognizing tool. It was fused with proteinaceous tags for visualization: either a fluorescent mKate protein or a self-labelling enzymatic SNAP-tag.

To assess whether C2 domain and the fluorescence tag can be compatible after the fusion, structural models of C2-mKate and C2-SNAP were created

using *de novo* modelling tools (Figure 3.4.2). It was demonstrated that the C2 domain in both fused proteins retained the same fundamental structural motifs as in PDB experimentally defined structures, namely a beta barrel core with seven loops. Importantly, the loops 1 – 3 that constitute the binding site for the PS were arranged as in native C2, suggesting that fused proteins should retain the affinity to the PS. Furthermore, the key lysine residues (K24 and K45) that are essential for PS binding (Ye et al. 2013) were in similar positions in the model of fused proteins as in the PDB structures, further suggesting that the fusion did not affect the structure of the active site of C2 domain.

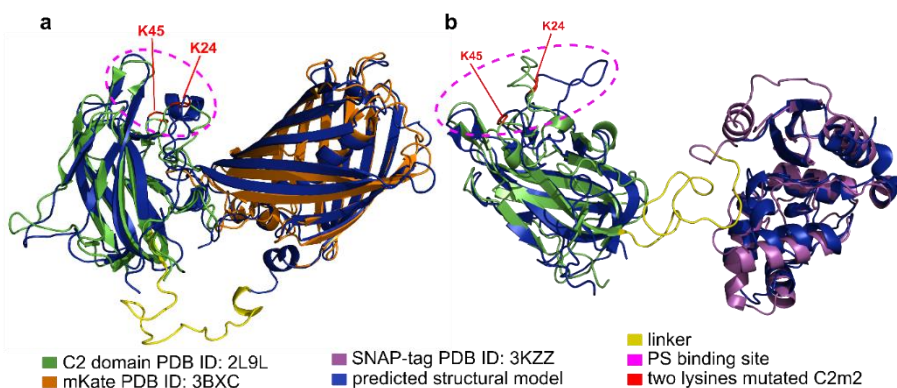


Figure 3.4.2. Structural models of recombinant C2 fusion proteins. A C2-mKate aligned to experimentally defined structures of C2 domain (PDB ID: 2L9L) and mKate (PDB ID: 3BXC). **B** C2-SNAP aligned to experimentally defined structures of C2 domain and SNAP-tag (PDB ID: 3KZZ). Purple dashed circle marks putative site of C2 and PS interaction, including critical amino acids K24 and K45 in red.

3.4.2. C2-mKate and C2-SNAP purification

To experimentally define the interaction of designed protein probes with PS, first recombinant proteins were expressed in bacteria using pET system plasmids and purified them chromatographically. To evaluate the specificity of the C2 probe, also mutated versions (C2m2) were developed of the designed fusion tools. In C2m2, the codons that specify previously identified key amino acids K24 and K45 (Ye et al. 2013) were substituted with asparagine codons. All of the proteins were fused with a six histidine residues tag for immobilized metal affinity chromatography.

To purify the fusion proteins, different *E.coli* strains were tested: BL21(DE3), Rosetta-gami 2(DE3), HMS174(DE3), NovaBlue(DE3),

C43(DE3)pLysS, ArcticExpress(DE3) and different induction conditions (temperature, IPTG concentration) as well as cell lysis conditions (NaCl concentration and pH of cell sonication buffer) to obtain the highest content of soluble recombinant protein. In all the strains, except for ArcticExpress(DE3), recombinant protein precipitated in the pellet rather than remaining in the soluble fraction, independently of other tested parameters. This precipitation rendered these strains unsuitable for the purification of recombinant fusion protein. Recombinant fusion proteins were successfully expressed in the ArcticExpress(DE3) strain after 1 mM IPTG induction at 16 °C using 300 mM NaCl and pH 8 cell lysis buffer. It is known that the ArcticExpress(DE3) strain produces exogenous chaperones Cpn10 and Cpn60, which facilitate protein folding (Ferrer et al. 2003). These chaperones are active at lower temperatures, which also slow down the expression of a recombinant protein, further contributing to correct protein folding. Using ArcticExpress(DE3) bacteria, C2, C2-mKate, C2m2-mKate, C2-SNAP and C2m2-SNAP recombinant proteins were purified, which were further used to characterize C2 fusion proteins as PS probes.

3.4.3. C2-mKate and C2-SNAP label apoptotic cells *in vitro*

To test whether PS-specific C2 fusion proteins are suitable for detecting the exposure of PS on the plasma membrane of cells *in vitro*, apoptosis was induced in the culture of mouse neuroblastoma cell line Neuro2a. The exposure of phosphatidylserine (PS) on the outer plasma membrane has long been considered a unique feature of apoptotic cells. The molecular pathways mediating apoptosis and synaptic pruning have distinct differences but also retain significant mechanistic overlap like PS externalization as an “eat-me” signal. Therefore, staurosporine induced apoptosis was used as a model system to test C2 fusion proteins ability to bind to externalized PS. After staurosporine treatment, apoptotic cells were labelled with either C2-SNAP or C2-mKate (Figure 3.4.3). In Neuro2a cell line C2 probes did not bind to non-apoptotic cells, while on apoptotic cells both C2-mKate and C2-SNAP decorated the cell membrane, revealing the cell contour. In contrast, mutated C2m2-mKate and C2m2-SNAP probes did not label apoptotic cells (Figure 3.4.3.), indicating that the binding of C2 probes on apoptotic cells was PS-dependent.

Next, the sensitivity of the designed C2 probes was compared to one of PS labelling tools that can be used for both *in vitro* and *in vivo* labelling – the organic label zinc dipicolamine known as PSVue (Scott-Hewitt et al. 2020;

Bhatta et al. 2021). In contrast to the C2 probes, PSVue labelling exhibited a high background signal on non-apoptotic cells (Figure 3.4.3.e, f). PSVue labelled apoptotic cells with an intensity above the background, but the contour of cell surface was not observed (Figure 3.4.3.e). Both C2-mKate and C2-SNAP probes had significantly higher signal-to-noise ratio compared to PSVue, whose signal on apoptotic cells was only 15% higher than that on non-apoptotic cells (Figure 3.4.3.f). Meanwhile, C2-SNAP demonstrated more than a 22-fold increase in fluorescence on apoptotic Neuro2a cells (Figure 3.4.3.d). C2-mKate had about 4-fold increased signal around apoptotic Neuro2a cells (Figure 3.4.3.b). C2-SNAP exhibited significantly stronger signal than C2-mKate, possibly due to favorable properties of the organic fluorophore used in SNAP-tag labelling: lower photobleaching and higher stability compared to auto fluorescent proteins (Deo and Lavis 2018). The *in vitro* experiments demonstrated that C2 fusion probes are specific and sensitive labelling tools for PS exposure on the external surface of cell plasma membrane.

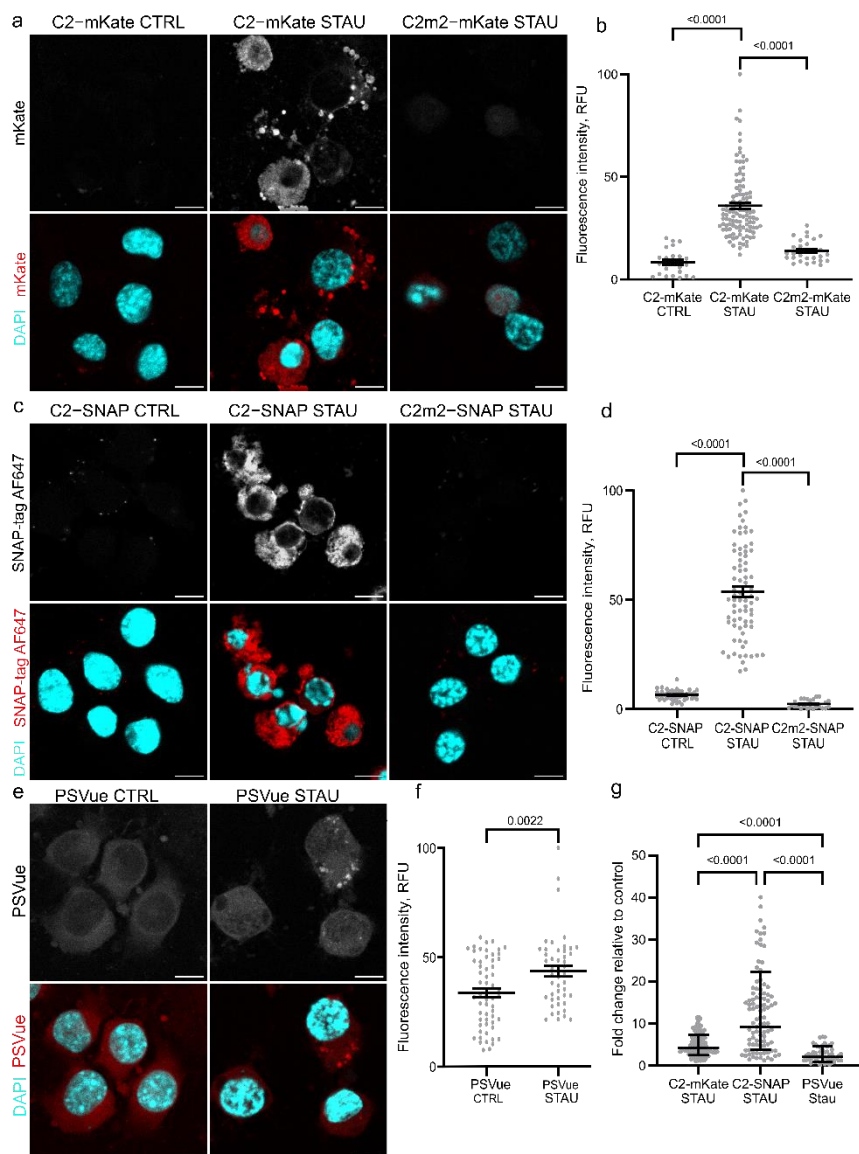


Figure 3.4.3. C2 fusion proteins label apoptotic Neuro2a cells *in vitro*.

a, c Confocal images of control (CTRL) and apoptotic (STAU, treated with 3 μ M staurosporine) Neuro2a cells labelled with either C2-mKate or C2-SNAP or their mutated counterparts C2m2-mKate and C2m2-SNAP; scale bar 10 μ m. **b, d** Quantification of mKate or SNAP-tag fluorescence intensity on Neuro2a cells with or without staurosporine treatment. **e** Confocal images of control (CTRL) or apoptotic (STAU, treated with 3 μ M staurosporine) Neuro2a cells labelled with PSVue. **f** Quantification of PSVue fluorescence intensity on Neuro2a cells with or without staurosporine treatment. **g** Comparative signal strength of mKate, SNAP and PSVue on apoptotic Neuro2

cells. Data presented as means \pm standard error of the mean (**b, d, f**) or geometrical means \pm 95% confidence intervals (**g**) (n=20-30 images per biological replicate, 3 independent biological replicates). Means were compared by one-way ANOVA and *post-hoc* Tukey test (**b, d, f**) or by Kruskal-Wallis one-way analysis of variance and *post-hoc* Dunn's test (**g**). *p* values < 0.05 were considered as significant. RFU – relative fluorescence units.

3.4.4. Expression of genetically encoded C2 probes in tissue culture

The investigation of PS exposure in 3D cellular models, tissue, or explant cultures poses further difficulties due to the limited permeability of externally applied PS probes. To overcome this limitation, adeno-associated viral (AAV) vectors were developed that genetically encode C2 probes and deliver them to the tissue without direct damage to the tissue of interest. Glial fibrillary acidic protein (GFAP) promoter was used to target C2 expression to astrocytes (Brenner et al. 1994). To ensure the release of C2 fusion proteins into the extracellular space for the labelling of exposed PS on the external membrane surface of the cells, a secretory signal peptide was introduced (Stubbs et al. 1990). Finally, for the packaging, the AAV-PHP.eB capsid was used, which was demonstrated to efficiently transduce the cells in the central nervous system after non-invasive delivery (Chan et al. 2017).

To test genetically encoded C2 probes, these engineered AAVs were used in organotypic hippocampal slice cultures – a well-established 3D tissue culture that closely resemble the development, cell physiology and intercellular interactions in the brain tissue (Linsley et al. 2019). AAV-delivered C2 fusion proteins were designed to be secreted. Therefore, to assess their expression in the *ex vivo* tissue, brefeldin A (BFA) was used to inhibit protein secretion and accumulate the recombinant protein in the Golgi–endoplasmic reticulum compartment of expressing cells (Nebenführ, Ritzenthaler, and Robinson 2002). By using immunolabelling the major nervous tissue cell types were identified to determine the cells expressing C2 probes in a tissue culture. OHSC slices were transduced with engineered AAVs at the fifth day *in vitro* (DIV5) (Figure 3.4.4.a). At DIV14, tissue cultures were treated with BFA for 5 h to inhibit protein secretion. After BFA treatment it was discovered that C2-SNAP, C2m2-SNAP, C2-mKate, and C2m2-mKate proteins accumulated in cells in organotypic slices (Figure 3.4.4.b). In contrast, in slices without the treatment to inhibit protein trafficking, no accumulation of C2 fusion probes was observed, indicative of

effective protein secretion (Figure 3.3.4.b). To determine what cells expressed C2 probes, C2 fusion proteins were colocalized with astrocytic (GFAP), microglial (Iba1) and neuronal (*Thy1*::GFP) markers. C2 was only found in astrocytes, but not microglia or neurons (Figure 3.4.4.b-d). These results revealed that AAV-delivered C2 probes are selectively expressed in astrocytes and are efficiently secreted into the extracellular space under normal conditions in 3D brain tissue cultures.

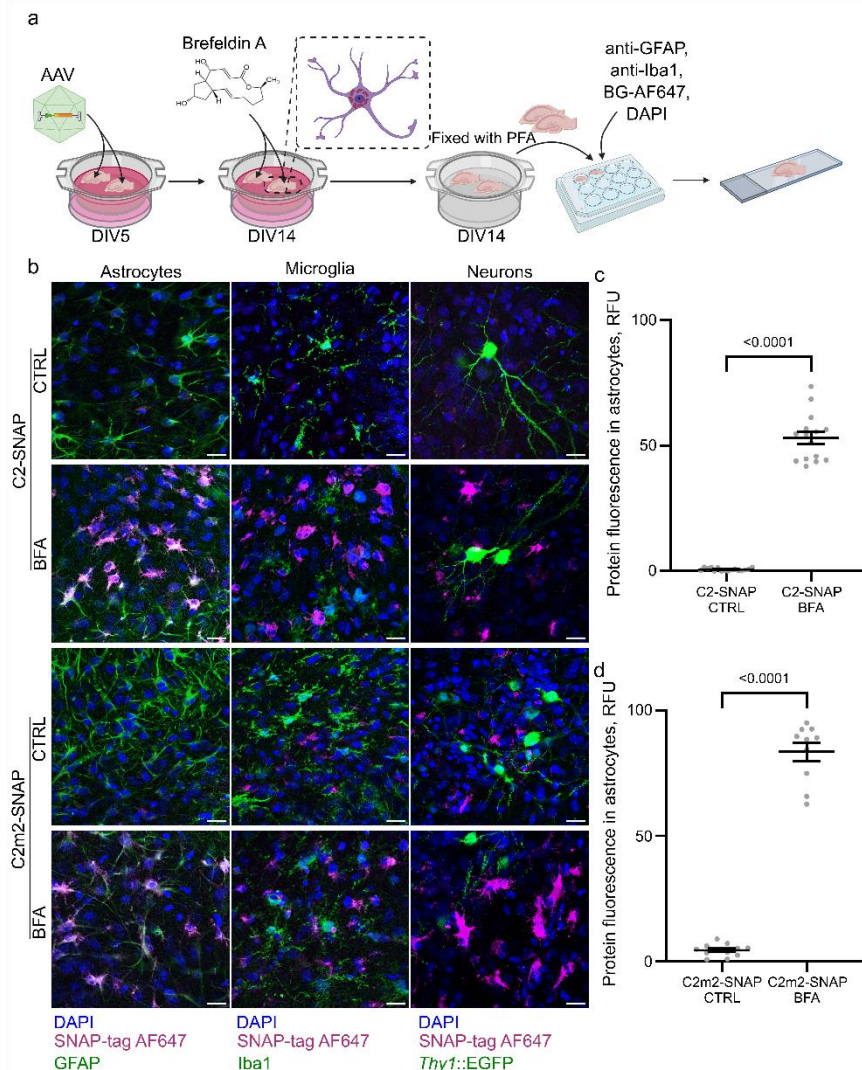


Figure 3.4.4. The expression of C2 fusion proteins in *ex vivo* organotypic hippocampal slices after AAV delivery. a OHSC were transduced with AAV carrying either C2-SNAP or C2m2-SNAP at 5 days *in vitro* (5DIV) and maintained for 9 days for protein expression. The secretion

of recombinant proteins was inhibited by 10 µg/ml brefeldin A (BFA) for 5 hours. Fixed control (CTRL) and inhibited (BFA) slices were labelled by immunohistochemistry and SNAP-tag substrate for fluorescent imaging. Created by Biorender.com. **b** Confocal images of OHSC transduced with either AAV-C2-SNAP or AAV-C2m2-SNAP. Cell nuclei were stained with DAPI, fused SNAP-tag was labelled with AlexaFluor647 (AF647). Astrocytes, microglia and neurons were labelled with GFAP, Iba1 antibodies, or expressed EGFP, respectively. Scale bar 20 µm. **c, d** Quantification of C2-SNAP and C2m2-SNAP fluorescence within astrocytes with or without BFA treatment. Data presented as means ± standard error of the mean (n=10-15 images per replicate, two independent replicates). Means were compared by one-way ANOVA and *post-hoc* Tukey test. *p* values < 0.05 were considered as significant. RFU – relative fluorescence units.

3.4.5. AAV-encoded C2 probes label apoptotic cells in tissue culture

Then the capacity of AAV-encoded C2 fusion probes was evaluated to label exposed PS in organotypic slices. OHSC were transduced with engineered AAVs on the fifth day *in vitro* (DIV5), and apoptosis was induced by staurosporine 9 days later (Figure 3.4.5.a). It was found that AAV-delivered C2-SNAP and C2-mKate fusion proteins efficiently labelled apoptotic cells in a tissue culture (Figure 3.4.5. b, c). The C2 probes visualized apoptotic neuron processes throughout the slice (Figure 3.4.5.b, c). Importantly, there was no labelling in viable organotypic slices without staurosporine treatment, indicating that AAV-delivered C2-SNAP and C2-mKate specifically bound to apoptotic cells (Figure 3.4.5.b, c). Furthermore, when AAVs delivered mutated C2m2 probes, neither cell bodies nor neuronal processes were labelled, and only a weak background signal was observed (Figure 3.4.5.b, c). Therefore, it was proposed that C2m2 probes could be used in parallel with C2 probes to serve as a negative control to evaluate any unspecific binding and to define thresholding for quantitative analysis. Our results revealed that C2 fusion probes can be efficiently expressed after AAV delivery and can be used to label exposed PS in a more complex experimental platform, such as tissue culture.

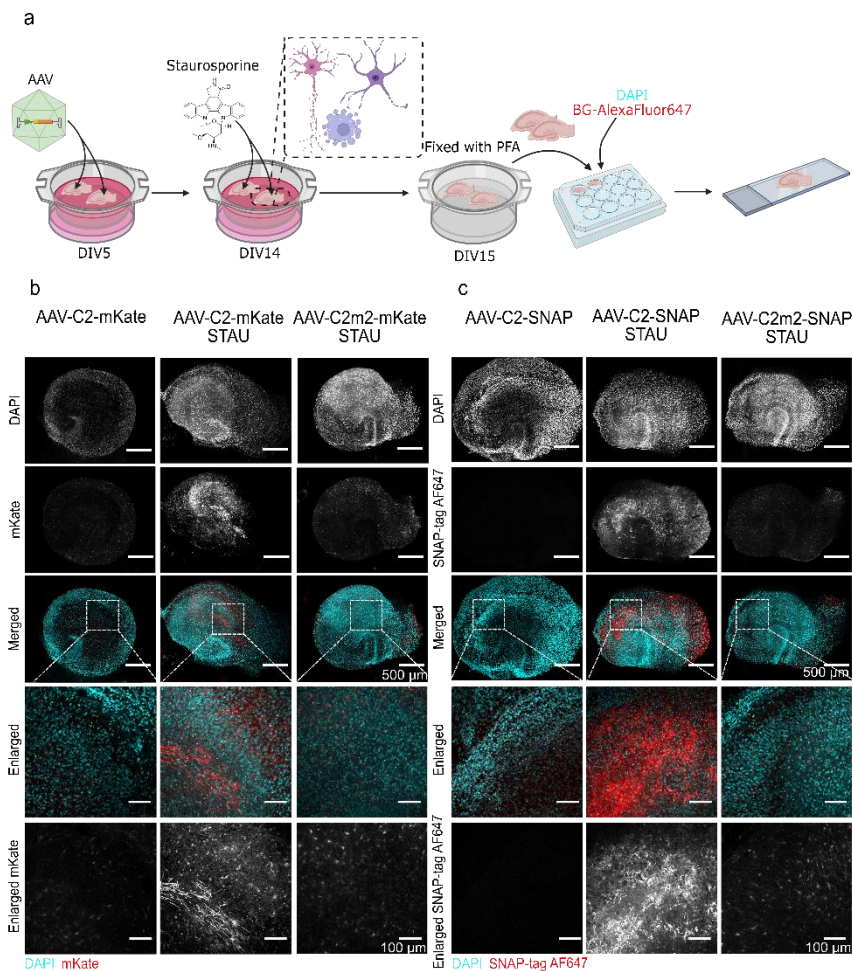


Figure 3.4.5. AAV-encoded C2 fusion probes label apoptotic cells in *ex vivo* organotypic hippocampal slices. **a** OHSC were transduced with AAVs carrying C2-SNAP, C2m2-SNAP, C2-mKate or C2m2-mKate at 5 days *in vitro* (5DIV) and maintained for 9 days for protein expression (n=3 biological replicates). Apoptosis was induced by the treatment with 10 μ M staurosporine for 16 hours. Created by Biorender.com. **b**, **c** Confocal images of OHSC transduced with AAV-C2-mKate vs. AAV-C2m2-mKate or AAV-C2-SNAP or AAV-C2m2-SNAP. Cell nuclei were counterstained with DAPI. Scale bars 500 μ m (whole slice) and 100 μ m (enlarged area).

3.4.6. AAV-C2-SNAP efficiently transduce the central nervous system *in vivo*

In order to investigate whether the genetically encoded C2-SNAP protein could be used for *in vivo* assays, perinatal (P3) mice were injected intravenously with neurotropic recombinant AAVs. After 2 weeks of *in vivo* expression, at P17, C2-SNAP expression was observed in hippocampus and visual cortex (Figure 3.4.6). These results confirm that intravenous AAV-C2-SNAP injection is sufficient for brain transduction.

No specific labelling was observed in brain sections of control mice treated with only SNAP-tag substrate, without C2-SNAP expression (Figure 3.4.6). These results demonstrated that genetically encoded C2-SNAP probe can be used for functional studies on PS exposure *in vivo* without invasive reagent delivery to the brain tissue.

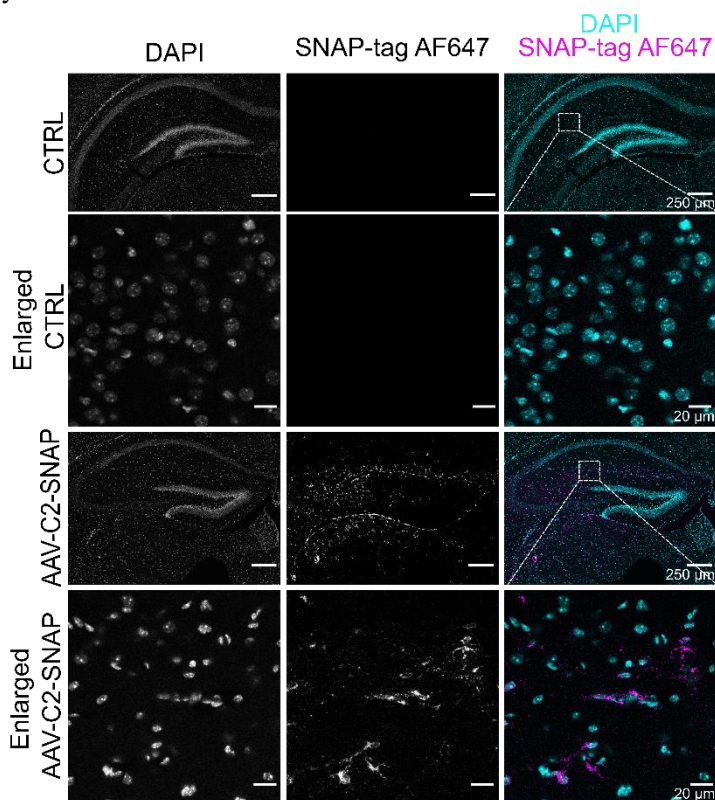


Figure 3.4.6. Application of adeno-associated viruses (AAV) for *in vivo* C2 domain-based probe delivery. At postnatal day 3 (P3) mice were injected with 1×10^{11} vg AAV-C2-SNAP virus. At the top of the panel are representative hippocampal area microscopy images after 2 weeks AAV-C2-SNAP expression (P17) (n=5 animals). On the right are enlarged hippocampus areas. Cell nuclei are stained with DAPI, fused SNAP-tag is labelled with AlexaFluor647 (AF647). Control images collected after BG-AF647 labelling

of not transduced brain tissue. Scale bar 250 μm (whole slice) and 20 μm (enlarged area).

Altogether, these results demonstrate high specificity of the designed C2-probe for PS. The developed genetically encoded PS biosensor can be utilized in a variety of assays as a two-component system of C2 and C2m2 fusion proteins. This system also allows for precise quantification and PS visualization at directly specified threshold levels, enabling the evaluation of PS exposure *in vivo* without any invasive procedures to the brain. This will facilitate the investigation of the synaptic pruning process mediated by externalized PS and aid in elucidating its role in neuronal network remodelling during the critical period of plasticity.

4. DISCUSSION

4.1. Dynamics of axonal bouton changes during critical periods and these changes can be studied by using extracted labelled synaptosome population

Sensory experiences during critical periods of plasticity play a crucial role in guiding the formation and maturation of neural circuits. During these periods, synaptic connections must be rapidly formed and restructured to accommodate dynamic changes. This study demonstrated that prior to the onset of the critical period, axonal boutons are predominantly small but densely packed (Figure 3.1.1.), likely forming various possible connections before the critical period begins and the network is later refined according to the stimuli presented. At the peak of the critical period, the average size of boutons increased while their density decreased, probably due to the stabilization of active pathways while removing unnecessary ones. After the critical period, the mean size of axonal boutons further increased, with the presence of both small boutons and exceptionally large boutons, indicating the formation and stabilization of strong, active connections. These findings suggest a reduction in the plasticity of cortical circuits post-critical period, characterized by fewer small connections but an enhancement of the remaining connectivity that compensates for a general synapse loss. Many studies have supported that there is a strong correlation between the size of a dendritic spine or axonal bouton and its synaptic strength (Murthy et al. 2001; Noguchi et al. 2011; Cheetham et al. 2014; Holler et al. 2021). Also, theoretical studies propose that the distribution of synaptic sizes and, therefore, strengths not only processes sensory input but also serves as a foundation for encoding experiences (Barbour et al. 2007; Stepanyants and Escobar 2011). Thus, while smaller boutons during the critical period may facilitate dynamic remodeling, the larger, stronger, and likely more persistent boutons are essential for storing sensory experiences in the mature cortex after the critical period concludes.

Changes in bouton size and plasticity require diverse protein combinations, and it is now understood that a significant portion of these proteins is synthesized locally at the synapse (Biever et al. 2020). This local synthesis likely determines the specificity, function, and plasticity potential of synapses. Consequently, the local synaptic transcriptome represents the synapse's capacity and readiness to produce necessary proteins on demand. However, synaptic terminals, being very small (0.5–2 μm) and delicate, are

challenging to study compared to whole cells (Luquet et al. 2017). Visualizing local synaptic processes necessitates specific approaches, such as preparing tissue using expansion microscopy to better visualize small structures like synapses (Hafner et al. 2019). To study the local synaptic transcriptome, pure synaptic extracts are required. Traditional biochemical methods for isolating synaptic terminals result in synapse-enriched fractions known as synaptosomes (Whittaker, Michaelson, and Kirkland 1964), which can be analyzed using next-generation sequencing. To isolate a well-defined synapse population encompassing all synaptic elements from *in vivo* brain structures Fluorescence Activated Synaptosome Sorting (FASS) technique was developed (Biesemann et al. 2014). Studies using this technique reported achieving 50-92% labelled synaptic enrichment in synaptosome samples after sorting (Biesemann et al. 2014; Luquet et al. 2017; Hafner et al. 2019; Paget-Blanc et al. 2022; Oostrum et al. 2023). In this study, this technique was implemented to sort labelled excitatory synaptosomes from the mouse V1 region to study their local transcriptome during brain circuit refinement. The FASS technique was optimized to achieve around 60-90% excitatory synaptosomes in the sorted samples (Figure 3.1.2.) which is comparable to mentioned results by other research groups. This indicates the high quality of the enriched excitatory synaptosome samples collected during this study.

4.2. Developed 5':3' assay can be applied to assess synaptic mRNA integrity

The degradation of RNA samples undermines the accuracy of gene expression analysis by qPCR or RNA sequencing (Fleige and Pfaffl 2006). RNA sequencing is particularly sensitive to mRNA degradation as mRNAs are usually captured by poly-dT probes in order to deplete overabundant rRNA. When an mRNA sample is degraded, only a few full length transcripts are captured, which leads to the 3' bias of RNA sequencing results (H. Feng, Zhang, and Zhang 2015; Gallego Romero et al. 2014). Due to this 3' bias, the reads are predominantly limited to the last exon of mRNA, which distorts gene expression profiles compared to not degraded RNA samples (H. Feng, Zhang, and Zhang 2015). Therefore, to obtain reliable and reproducible gene expression data, it is crucial to take into account the integrity of sample mRNA. Conventionally, RNA integrity is measured by RNA electrophoresis-based methods. However, these methods rely on the assumption that rRNA integrity represents the mRNA integrity well enough, even though it has been shown not to be the case (Sidova et al. 2015; Sonntag et al. 2016). Therefore,

a direct mRNA integrity evaluation assay was developed that does not require any specialized equipment and is based on the comparison of the abundance of 5':3' transcripts of housekeeping genes in mouse and human RNA samples.

This mouse and human 5':3' assay is based on *PGK1* mRNA as it is a long constitutively expressed transcript of a highly conserved gene (He Liu et al. 2022). The *PGK1* RNA was previously successfully used for designing 3':5' assay primers for rat and horse RNA samples (Padhi et al. 2018; Du Cheyne et al. 2021). Several other genes have also been tested in the past. The 3':5' assay was first published based on human *GAPDH* gene as it is a popular choice for endogenous control (Nolan, Hands, and Bustin 2006). There was also a variant of this method based on β -actin mRNA optimized for sea bass larvae (Schaeck et al. 2016). However, there have been reports demonstrating high expression variability of *GAPDH* (Dragon et al. 2023). It is also well known that *GAPDH* and β -actin have many pseudogenes (Tso et al. 1985; Hanauer and Mandel 1984; Y. Sun et al. 2012). This means that the results obtained using these genes as constitutive controls might not translate very well across different tissues or conditions and it will be more susceptible to errors caused by genomic DNA contamination.

An important improvement of 5':3' assay was the correction of the integrity score according to the amplification efficiency of used primer pairs. Primer amplification efficiency is known to fluctuate between different primers. This cannot be completely avoided during primer design process and highly depends on the qPCR machine, the choice of reagents for PCR, the presence of various inhibitors in the sample and even the sample volume used for the dilutions (Svec et al. 2015). Therefore, it is important to correct the real-time PCR data using primer amplification efficiency to enhance the analytical accuracy (Damgaard and Treebak 2022). This correction was added to our integrity value calculations ensuring a robust method for RNA integrity assessment. This will help to successfully establish this method in any other laboratory as the correction eliminates the bias introduced by using different primers, equipment or reagents.

To validate 5':3' assays ability to reflect the RNA integrity status our results were compared with widely used RIN value. 5':3' assay integrity value and RIN values were very comparable in heat-degraded mouse and human RNA samples (Figure 3.2.4. and Figure 3.2.5). In clinical samples the correlation was lower (Figure 3.2.6.) compared to the mouse and human heat-degraded RNA samples possibly indicating that enzymatic RNA degradation, which occurs during sample collection and preparation, might affect messenger and ribosomal RNA differently. Heat-induced RNA degradation does not depend on RNA structure and thus affects both rRNA and mRNA

similarly. However, mRNA is significantly more sensitive to enzymatic degradation by nuclease activity compared to rRNA (Sidova et al. 2015). In clinical samples or any other RNA samples, where RNA degradation is caused by endogenous nucleases, the results from rRNA-based methods can overestimate the RNA integrity. As sample collection in clinical settings and field studies are prone to rapid tissue necrosis, which is associated with enzymatic degradation of nucleic acids, 5':3' assay would be a better indicator of RNA quality in such samples.

Ribosomal RNA-based methods for RNA integrity evaluation cannot be applied for various subcellular samples, such as synaptosomes or extracellular vesicles. Such samples share similar features that affect the assessment of the expression of their local transcripts: prolonged processing of the sample, low yields of RNA and most importantly – lack of rRNA (Crescitelli et al. 2013). Despite the accumulating evidence on local protein synthesis and the presence of both ribosomal and messenger RNAs in synaptosomes, the RNA quality of synaptosomal preparations has not been previously reported, possibly due to the lack of suitable methods. Ribosomal RNA quantity in the synaptosomes is far lower than in general tissue RNA sample and that is usually not enough to calculate RIN even when the same amount of RNA sample is used (Figure 3.1.4). Messenger RNAs are very different in lengths and do not form distinct bands; therefore, mRNAs are not observed as a trail in capillary electrophoresis gels and cannot be used to calculate RIN. Therefore, RIN could not be determined in subcellular samples, but mRNA based 5':3' assay was suitable to measure the RNA integrity (Figure 3.2.7). This shows a huge advantage and potential of this method to be used to check RNA integrity on any sample that lacks high quantities of rRNA, making the use of common RNA integrity assays impossible. The analysis of subcellular samples requires a careful choice of reference transcript for 5':3' assay due to the compartmentalization of within the cell. For example, previous studies have found that the transcriptome in the synaptosomes is selectively enriched for specific mRNAs and therefore differs from total cortical transcriptome (Hafner et al. 2019). For this study, Pgk1 transcript was chosen for 5':3' assay, as it is ubiquitously expressed throughout neurons, including their presynaptic compartment. However, different subcellular samples may need other reference mRNAs and it is advisable to confirm their localization in advance.

Overall, the 5':3' assay is a promising method for assessing mRNA integrity for gene expression studies, offering advantages over conventional techniques. The assay, based on PGK1 mRNA, provides a user-friendly assessment system, aligning the integrity score with the widely used RIN values. Its correction for primer amplification efficiency enhances analytical

accuracy, addressing the variations in qPCR conditions. While validation against RIN values showed strong correlation in heat-degraded samples, a slight disparity of correlation in clinical samples emphasizes the likely impact of the differences in enzymatic degradation of mRNA and rRNA. Despite acknowledged limitations, the adaptability of the 5':3' assay by designing primers for specific transcripts holds high potential for personalized assessments, offering a step forward in refining the accuracy of mRNA integrity evaluations.

4.3. Local transcriptomic changes during visual cortex refinement

Neurons exhibit morphological complexity, consisting of a cell body from which intricately branching dendrites and axons extend. These projections with formed connections can be relatively far from the neuron body. Part of the needed proteins are brought to presynaptic compartment by well-documented system of axonal transport. However, to support their complex morphology, neurons also position mRNAs and ribosomes near synapses, enabling efficient local protein production when needed. Therefore, in neurons, prevalent local protein synthesis plays a crucial role in both the maintenance and plasticity of synapses.

In this study, enriched excitatory synaptosome samples were collected from the mouse primary visual cortex before, during, and after the critical period of plasticity, and their transcripts were identified using next-generation sequencing. GO analysis revealed that the majority of the identified local excitatory transcripts were involved in cellular transport and localization, regulation of synaptic signalling and plasticity, or local protein translation (Figure 3.3.4). This emphasizes the importance of presynaptic compartments in synthesizing proteins necessary for delivering specific molecules to other sub compartments or the neuron body. This local protein production enables neurons to respond to injury and communicate with the cell soma by expressing transcription factors and nucleocytoplasmic transport factors, which are assembled into retrograde signalling complexes that regulate transcription in the nucleus (Cox et al. 2008; Ben-Yaakov et al. 2012; Kar et al. 2013; Baleriola et al. 2014; Ji and Jaffrey 2014). The transport and translation of mRNAs in axons are thought to play a crucial role in the formation of growth cones and synapses and in maintaining neuronal viability. Consequently, impaired axonal transport, particularly of mRNAs and their local translation in axons, is speculated to be involved in the pathogenesis of several neurodegenerative diseases such as amyotrophic lateral sclerosis

(ALS), frontotemporal dementia (FTD), and fragile X syndrome (FXS) (Arai et al. 2006; Neumann et al. 2006; Maurin, Zongaro, and Bardoni 2014). This underscores the essential role of localization and its regulation in supporting normal neuronal function. The abundance of presynaptically located transcripts involved in synaptic signal transduction and plasticity confirms that these functions are also locally regulated. Finally, the data presented in this study indicate that local protein translation is a critical aspect of synapse function, as a significant portion of the local transcriptome supports this process, allowing axons to rapidly respond to environmental changes during development.

As the network matures during the critical period of plasticity, the local transcriptome of synapses also undergoes changes. Differential expression analysis of local transcriptomes from the visual cortex before, during, and after the critical period revealed numerous changes in transcript abundance corresponding to the evolving state of plasticity. One transcript found exclusively in the immature visual cortex before the critical period was *Slc38a6*, encoding the *SLC38A6* transporter, also known as SNAT6 (Figure 3.3.5. and 3.3.6). This transporter belongs to the *SLC38* family of glutamine transporters, which regulate the glutamate–glutamine cycle in the brain (Bagchi et al. 2014). SNAT6 is known to be uniquely expressed in the excitatory neurons of the brain and has a high specificity for glutamine and glutamate (Gandasi et al. 2021). In the glutamate–glutamine cycle of the nervous system, the primary mechanism for removing glutamate from the synaptic space is its uptake into glial cells by the transporters GLAST and GLT-1, where it is converted into glutamine and then transported back to neurons. Recent evidence suggests that the presynaptic uptake of glutamine, initially thought to be mediated by SNAT1 and SNAT2, is minimally contributed by these transporters, leaving the key neuronal transporter unidentified (Rae et al. 2003; Conti and Melone 2006; Gandasi et al. 2021). Therefore, SNAT6, expressed exclusively in immature excitatory neurons, can be a promising candidate for this crucial role in neuronal glutamine uptake during brain development.

Another process involving protein-encoding transcripts specifically located in immature excitatory neurons is the positive regulation of Interleukin-6 (IL-6) production (Figure 3.3.5). IL-6 is a multifunctional cytokine essential for the pathogenesis of inflammatory disorders and the physiological homeostasis of neural tissue (Kummer et al. 2021). It has been recently shown that prenatal IL-6 elevation increases excitatory synapse density and brain connectivity in adults by activating genetic programs of synaptogenesis in developing neurons (Mirabella et al. 2021). This process

involves the activation of the transcription factor STAT3 and the downstream gene *Rgs4* in neurons. Our data suggest that immature excitatory neurons harness the pro-synaptogenic effect of IL-6 by upregulating its production before the critical period, thereby forming densely packed boutons to facilitate network plasticity.

In the analysis of the transcripts specific to excitatory synapses during the peak of the critical plasticity window, the enriched functions in these transcripts appear primarily related to synapse-to-neuron soma signalling. Given that the critical period is characterized by rapid remodelling of synaptic connections in response to sensory experiences, it is fitting that there is an increased abundance of localized transcripts during this time, which can be synthesized and sent to cell soma to modify gene expression. One transcript, *Prr7* (proline-rich 7), shows elevated abundance at synaptic terminals during the peak of the critical period compared to immature neurons (Figure 3.3.6). *PRR7* protein is known to induce the removal of excitatory synapses and inhibit synaptogenic Wnt signaling (S. H. Lee et al. 2018). The opposing actions of Wnts and *PRR7*, promoting synaptogenesis and elimination respectively, are employed by synapses during the critical period to rapidly modify the network. Additionally, synapses require more oxygen and glucose during the peak of the critical period to support these dynamic changes compared to after maturation. Angiogenesis, the formation of new blood vessels, is highly active during brain development and becomes almost quiescent in the healthy adult brain (Wälchli et al. 2023). Therefore, data from this study suggest that developmental vascular growth in the CNS involves locally produced signaling molecules to meet the high energy demands during the highly plastic period (Figure 3.3.7). Hence, our findings highlight the crucial role of locally synthesized signaling molecules and increased metabolic demands in supporting the rapid synaptic remodeling and network modification characteristic of the critical period of plasticity.

The maturation and stabilization of excitatory synapses after the critical period lay the groundwork for the formation of neural circuits. The mature excitatory synaptic transcriptome showed higher levels of transcripts involved in membrane lipid metabolic processes, with many associated transcripts linking proteins to membranes via glycosylphosphatidylinositol (GPI) (Figure 3.3.5). GPI-anchored proteins are a specialized class of lipid-associated membrane proteins that perform diverse functions, including the dynamic control of axon guidance, synaptic adhesion, cytoskeletal remodelling, and localized signal transduction, particularly at lipid raft domains. Recent studies have shown that a subset of GPI-anchored proteins act as critical regulators of synapse development by modulating specific synaptic adhesion pathways

through direct interactions with key synapse-organizing proteins and by activating a set of intracellular signaling pathways (Um and Ko 2017). This synaptic adhesion and signaling modulated by GPI-anchored proteins is likely an understudied feature of mature neurons. Additionally, when comparing the mature synaptic transcriptome to synaptic samples collected during the peak of the critical period, positive regulation of nucleobase-containing compound metabolic processes and RNA metabolic processes were among the most enriched GO terms (Figure 3.3.7). This further underscores the necessity for locally produced signalling proteins and molecules that control local synaptic protein synthesis in mature neurons. These findings highlight the intricate molecular adaptations that occur to support synaptic stability and function in the mature neural network.

4.4. Genetically encoded PS labeling tool efficiently identifies exposed PS in the neurons

In this study, a two-component PS labelling system was developed based on the C2 domain of the MFG-E8 opsonin. The C2 probe that can be used either as a purified protein or genetically encoded and delivered by AAV. It is intended to be used in parallel with a C2m2 negative control, which was developed by mutating two amino acids in C2 domain, disabling the probe's binding to PS. The probes were tested on in vitro cell cultures and showcased that C2-SNAP and C2-mKate fusion proteins effectively labelled apoptosis in cell lines (Figure 3.4.3a-d). Also, C2 probes provided more precise and efficient visualization of PS-exposing cells compared to one of currently available tools, PSVue (Figure 3.4.3.g).

Cell monolayer cultures are insufficient when assessing complex physiological interactions. In contrast, 3D cell cultures, tissue cultures, or in vivo experiments can more accurately capture intracellular interactions. However, it is difficult to apply recombinant proteins or small molecule probes in 3D tissue due to limited access to cell membranes. The local injections of genetically encoded plasmids (Furuta et al. 2021; van Ham et al. 2010), chemical reagents (Scott-Hewitt et al. 2020) or proteins (Blankenberg et al. 1998) have limited permeability and can also cause tissue damage, potentially leading to apoptosis or necrosis, which in turn are marked by PS exposure (Sapar et al. 2018). This problem could be solved by using gene delivery tools. AAV delivery is a potential technique to label exposed PS ex vivo and in vivo. It was demonstrated that C2 probes can be designed to be selectively targeted to chosen cell type and can be efficiently secreted for PS

externalization assays (Figure 3.4.4. and Figure 3.4.5). It was observed that C2-SNAP proteins were expressed in AAVs transduced mouse brain two weeks after delivery (Figure 3.4.6.), consistent with other studies that used the same PHP.eB capsid in mice (Chan et al. 2017; Goertsen et al. 2022). Importantly, genetically encoded probes are readily modifiable and can be applied to any cell type of interest by changing the expression promoter (Becker, Fakhiri, and Grimm 2022) and the tropism of the used AAV capsid (Brown et al. 2021). AAVs with C2-probe genes could be applied in other areas than brain development research, such as blood clotting studies, by changing promoter to target blood or epithelium cells to further secreted C2 probe labelling of exposed PS on platelets. This system should then be supplemented with a specific AAV serotype for efficient transduction of the chosen cell type. Genetically encoded C2 fusion probes can be adapted for different visualization applications. If mKate could not be adapted for a particular experiment due to excitation and emission wavelengths of different fluorescent protein (e.g., green and yellow) or other red variants could be chosen. Also, to obtain different visualization spectra C2-SNAP probes could be easily modified by selecting a SNAP-tag substrate with required organic dye before conducting any experiment. This ensures the versatility of the C2 probe system presented in this paper.

It is known that the mouse brain is developing approximately until 30th day after birth (P30) (Mody et al. 2001; Navlakha, Barth, and Bar-Joseph 2015). During brain development, synaptic pruning is an important process in which PS-exposing synapses are eliminated (Kurematsu et al. 2022). Therefore, it is important to have PS labelling tools that can be delivered without disturbing nervous tissue. In our *in vivo* study, C2-SNAP protein labelling was localized in hippocampus during brain development (Figure 3.4.6). Thus, C2-SNAP could potentially be applied to label not only apoptotic cells, but also physiologically exposed PS.

Overall, the selectivity and specificity of the C2 domain have allowed us to create a genetically encodable and modifiable PS labelling probe for *in vitro*, *ex vivo* and *in vivo* applications. This tool can be applied in various assays as a two-component system consisting of C2 and C2m2 fusion proteins for PS visualization and precise quantification. By directly defining threshold levels, it enables to assess PS exposure both in cell death and in physiological processes.

CONCLUSIONS

1. Over 70 % enrichment of excitatory synaptosomes was achieved with FASS, allowing to collect and study bouton changes during cortex maturation.
2. Developed 5':3' assay demonstrated reliable assessment of mRNA integrity in mouse brain tissue and enriched synaptosomal samples lacking the prominent rRNA representation.
3. The synaptic transcriptome changes to enable efficient plasticity and network maturation.
4. Developed PS probe effectively labelled PS exposed on cellular membranes, enabling its visualization and quantification in various assays, including *in vivo* experiments.

BIBLIOGRAPHY

1. Aakalu, G., W. B. Smith, N. Nguyen, C. Jiang, and E. M. Schuman. 2001. "Dynamic Visualization of Local Protein Synthesis in Hippocampal Neurons." *Neuron* 30 (2): 489–502. [https://doi.org/10.1016/s0896-6273\(01\)00295-1](https://doi.org/10.1016/s0896-6273(01)00295-1).
2. Allen, Nicola J., and Cagla Eroglu. 2017. "Cell Biology of Astrocyte-Synapse Interactions." *Neuron* 96 (3): 697–708. <https://doi.org/10.1016/j.neuron.2017.09.056>.
3. Andrzejewska, Angelika, Małgorzata Zawadzka, and Katarzyna Pachulska-Wieczorek. 2020. "On the Way to Understanding the Interplay between the RNA Structure and Functions in Cells: A Genome-Wide Perspective." *International Journal of Molecular Sciences* 21 (18): 6770. <https://doi.org/10.3390/ijms21186770>.
4. Arai, Tetsuaki, Masato Hasegawa, Haruhiko Akiyama, Kenji Ikeda, Takashi Nonaka, Hiroshi Mori, David Mann, et al. 2006. "TDP-43 Is a Component of Ubiquitin-Positive Tau-Negative Inclusions in Frontotemporal Lobar Degeneration and Amyotrophic Lateral Sclerosis." *Biochemical and Biophysical Research Communications* 351 (3): 602–11. <https://doi.org/10.1016/j.bbrc.2006.10.093>.
5. Auguste, Yohan S. S., Austin Ferro, Jessica A. Kahng, Andre M. Xavier, Jessica R. Dixon, Uma Vrudhula, Anne-Sarah Nichitiu, et al. 2022. "Oligodendrocyte Precursor Cells Engulf Synapses during Circuit Remodeling in Mice." *Nature Neuroscience* 25 (10): 1273–78. <https://doi.org/10.1038/s41593-022-01170-x>.
6. Baek, Minkyung, Frank DiMaio, Ivan Anishchenko, Justas Dauparas, Sergey Ovchinnikov, Gyu Rie Lee, Jue Wang, et al. 2021. "Accurate Prediction of Protein Structures and Interactions Using a Three-Track Neural Network." *Science* 373 (6557): 871–76. <https://doi.org/10.1126/science.abj8754>.
7. Bagchi, Sonchita, Hajar Ali Baomar, Somar Al-Walai, Saifaddin Al-Sadi, and Robert Fredriksson. 2014. "Histological Analysis of SLC38A6 (SNAT6) Expression in Mouse Brain Shows Selective Expression in Excitatory Neurons with High Expression in the Synapses." *PLOS ONE* 9 (4): e95438. <https://doi.org/10.1371/journal.pone.0095438>.

8. Bai, Fengju, and Frank A. Witzmann. 2007. "Synaptosome Proteomics." *Sub-Cellular Biochemistry* 43:77–98. https://doi.org/10.1007/978-1-4020-5943-8_6.
9. Baleriola, Jimena, Chandler A. Walker, Ying Y. Jean, John F. Crary, Carol M. Troy, Peter L. Nagy, and Ulrich Hengst. 2014. "Axonally Synthesized ATF4 Transmits a Neurodegenerative Signal across Brain Regions." *Cell* 158 (5): 1159–72. <https://doi.org/10.1016/j.cell.2014.07.001>.
10. Ball, Jayson B., Suzanne M. Green-Fulgham, and Linda R. Watkins. 2022. "Mechanisms of Microglia-Mediated Synapse Turnover and Synaptogenesis." *Progress in Neurobiology* 218 (November):102336. <https://doi.org/10.1016/j.pneurobio.2022.102336>.
11. Barbour, Boris, Nicolas Brunel, Vincent Hakim, and Jean-Pierre Nadal. 2007. "What Can We Learn from Synaptic Weight Distributions?" *Trends in Neurosciences* 30 (12): 622–29. <https://doi.org/10.1016/j.tins.2007.09.005>.
12. Barkat, Tania Rinaldi, Daniel B. Polley, and Takao K. Hensch. 2011. "A Critical Period for Auditory Thalamocortical Connectivity." *Nature Neuroscience* 14 (9): 1189–94. <https://doi.org/10.1038/nn.2882>.
13. Bayer, K. Ulrich, and Howard Schulman. 2019. "CaM Kinase: Still Inspiring at 40." *Neuron* 103 (3): 380–94. <https://doi.org/10.1016/j.neuron.2019.05.033>.
14. Becker, Jonas, Julia Fakhiri, and Dirk Grimm. 2022. "Fantastic AAV Gene Therapy Vectors and How to Find Them-Random Diversification, Rational Design and Machine Learning." *Pathogens (Basel, Switzerland)* 11 (7): 756. <https://doi.org/10.3390/pathogens11070756>.
15. Ben-Yaakov, Keren, Shachar Y. Dagan, Yael Segal-Ruder, Ophir Shalem, Deepika Vuppalanchi, Dianna E. Willis, Dmitry Yudin, et al. 2012. "Axonal Transcription Factors Signal Retrogradely in Lesioned Peripheral Nerve." *The EMBO Journal* 31 (6): 1350–63. <https://doi.org/10.1038/emboj.2011.494>.
16. Bhatta, Maulasri, Gautam N. Shenoy, Jenni L. Loyall, Brian D. Gray, Meghana Bapardekar, Alexis Conway, Hans Minderman, et al. 2021. "Novel Phosphatidylserine-Binding Molecule Enhances Antitumor T-Cell Responses by Targeting Immunosuppressive Exosomes in Human Tumor Microenvironments." *Journal for Immunotherapy of Cancer* 9 (10): e003148. <https://doi.org/10.1136/jitc-2021-003148>.

17. Biesemann, Christoph, Mads Grønberg, Elisa Luquet, Sven P. Wichert, Véronique Bernard, Simon R. Bungers, Ben Cooper, et al. 2014. "Proteomic Screening of Glutamatergic Mouse Brain Synaptosomes Isolated by Fluorescence Activated Sorting." *The EMBO Journal*, January. <https://doi.org/10.1002/embj.201386120>.
18. Biever, Anne, Caspar Glock, Georgi Tushev, Elena Ciirdaeva, Tamas Dalmay, Julian D. Langer, and Erin M. Schuman. 2020. "Monosomes Actively Translate Synaptic mRNAs in Neuronal Processes." *Science (New York, N.Y.)* 367 (6477): eaay4991. <https://doi.org/10.1126/science.aay4991>.
19. Blankenberg, Francis G., Peter D. Katsikis, Jonathan F. Tait, R. Eric Davis, Louis Naumovski, Katsuichi Ohtsuki, Susan Kopiwoda, et al. 1998. "In Vivo Detection and Imaging of Phosphatidylserine Expression during Programmed Cell Death." *Proceedings of the National Academy of Sciences of the United States of America* 95 (11): 6349–54.
20. Boon, J. Middleton, and Bradley D. Smith. 2002. "Chemical Control of Phospholipid Distribution across Bilayer Membranes." *Medicinal Research Reviews* 22 (3): 251–81. <https://doi.org/10.1002/med.10009>.
21. Boyken, Janina, Mads Grønberg, Dietmar Riedel, Henning Urlaub, Reinhard Jahn, and John Jia En Chua. 2013. "Molecular Profiling of Synaptic Vesicle Docking Sites Reveals Novel Proteins but Few Differences between Glutamatergic and GABAergic Synapses." *Neuron* 78 (2): 285–97. <https://doi.org/10.1016/j.neuron.2013.02.027>.
22. Brenner, M., W. C. Kisseberth, Y. Su, F. Besnard, and A. Messing. 1994. "GFAP Promoter Directs Astrocyte-Specific Expression in Transgenic Mice." *The Journal of Neuroscience: The Official Journal of the Society for Neuroscience* 14 (3 Pt 1): 1030–37. <https://doi.org/10.1523/JNEUROSCI.14-03-01030.1994>.
23. Brown, David, Michael Altermatt, Tatyana Dobrova, Sisi Chen, Alexander Wang, Matt Thomson, and Viviana Gradinaru. 2021. "Deep Parallel Characterization of AAV Tropism and AAV-Mediated Transcriptional Changes via Single-Cell RNA Sequencing." *Frontiers in Immunology* 12 (October):730825. <https://doi.org/10.3389/fimmu.2021.730825>.
24. Burré, Jacqueline, Herbert Zimmermann, and Walter Volkhardt. 2007. "Immunoisolation and Subfractionation of Synaptic Vesicle

- Proteins.” *Analytical Biochemistry* 362 (2): 172–81.
<https://doi.org/10.1016/j.ab.2006.12.045>.
25. Cajigas, Iván J., Georgi Tushev, Tristan J. Will, Susanne tom Dieck, Nicole Fuerst, and Erin M. Schuman. 2012. “The Local Transcriptome in the Synaptic Neuropil Revealed by Deep Sequencing and High-Resolution Imaging.” *Neuron* 74 (3): 453–66.
<https://doi.org/10.1016/j.neuron.2012.02.036>.
 26. Challis, Rosemary C., Sripriya Ravindra Kumar, Ken Y. Chan, Collin Challis, Keith Beadle, Min J. Jang, Hyun Min Kim, et al. 2019. “Systemic AAV Vectors for Widespread and Targeted Gene Delivery in Rodents.” *Nature Protocols* 14 (2): 379–414.
<https://doi.org/10.1038/s41596-018-0097-3>.
 27. Chan, Ken Y., Min J. Jang, Bryan B. Yoo, Alon Greenbaum, Namita Ravi, Wei-Li Wu, Luis Sánchez-Guardado, et al. 2017. “Engineered AAVs for Efficient Noninvasive Gene Delivery to the Central and Peripheral Nervous Systems.” *Nature Neuroscience* 20 (8): 1172–79.
<https://doi.org/10.1038/nn.4593>.
 28. Cheetham, Claire E. J., Samuel J. Barnes, Giorgia Albieri, Graham W. Knott, and Gerald T. Finnerty. 2014. “Pansynaptic Enlargement at Adult Cortical Connections Strengthened by Experience.” *Cerebral Cortex (New York, N.Y.: 1991)* 24 (2): 521–31.
<https://doi.org/10.1093/cercor/bhs334>.
 29. Chen, Xiaoying, Jennica Zaro, and Wei-Chiang Shen. 2013. “Fusion Protein Linkers: Property, Design and Functionality.” *Advanced Drug Delivery Reviews* 65 (10): 1357–69.
<https://doi.org/10.1016/j.addr.2012.09.039>.
 30. Cho, Yong-Suk, Kyung Mi Kim, Duhwan Lee, Won Jong Kim, and Kyo Han Ahn. 2013. “Turn-on Fluorescence Detection of Apoptotic Cells Using a Zinc(II)-Dipicolylamine-Functionalized Poly(Diacetylene) Liposome.” *Chemistry, an Asian Journal* 8 (4): 755–59. <https://doi.org/10.1002/asia.201201139>.
 31. Chung, Won-Suk, Laura E. Clarke, Gordon X. Wang, Benjamin K. Stafford, Alexander Sher, Chandrani Chakraborty, Julia Joung, et al. 2013. “Astrocytes Mediate Synapse Elimination through MEGF10 and MERTK Pathways.” *Nature* 504 (7480): 394–400.
<https://doi.org/10.1038/nature12776>.
 32. Cioni, Jean-Michel, Max Koppers, and Christine E Holt. 2018. “Molecular Control of Local Translation in Axon Development and Maintenance.” *Current Opinion in Neurobiology, Cellular*

- <https://doi.org/10.1016/j.conb.2018.02.025>.
33. Cisneros-Franco, J. Miguel, Patrice Voss, Maryse E. Thomas, and Etienne de Villers-Sidani. 2020. “Chapter 8 - Critical Periods of Brain Development.” In *Handbook of Clinical Neurology*, edited by Anne Gallagher, Christine Bulteau, David Cohen, and Jacques L. Michaud, 173:75–88. Neurocognitive Development: Normative Development. Elsevier. <https://doi.org/10.1016/B978-0-444-64150-2.00009-5>.
34. Citri, Ami, and Robert C. Malenka. 2008. “Synaptic Plasticity: Multiple Forms, Functions, and Mechanisms.” *Neuropsychopharmacology* 33 (1): 18–41. <https://doi.org/10.1038/sj.npp.1301559>.
35. Condé, F., J. S. Lund, and D. A. Lewis. 1996. “The Hierarchical Development of Monkey Visual Cortical Regions as Revealed by the Maturation of Parvalbumin-Immunoreactive Neurons.” *Brain Research. Developmental Brain Research* 96 (1–2): 261–76. [https://doi.org/10.1016/0165-3806\(96\)00126-5](https://doi.org/10.1016/0165-3806(96)00126-5).
36. Conti, Fiorenzo, and Marcello Melone. 2006. “The Glutamine Commute: Lost in the Tube?” *Neurochemistry International* 48 (6–7): 459–64. <https://doi.org/10.1016/j.neuint.2005.11.016>.
37. Costa, Rui O., Helena Martins, Luís F. Martins, Andrzej W. Cwetsch, Miranda Mele, Joana R. Pedro, Diogo Tomé, et al. 2019. “Synaptogenesis Stimulates a Proteasome-Mediated Ribosome Reduction in Axons.” *Cell Reports* 28 (4): 864–876.e6. <https://doi.org/10.1016/j.celrep.2019.06.080>.
38. Cox, Llewellyn J., Ulrich Hengst, Nadya G. Gurskaya, Konstantin A. Lukyanov, and Samie R. Jaffrey. 2008. “Intra-Axonal Translation and Retrograde Trafficking of CREB Promotes Neuronal Survival.” *Nature Cell Biology* 10 (2): 149–59. <https://doi.org/10.1038/ncb1677>.
39. Crescitelli, Rossella, Cecilia Lässer, Tamas G. Szabó, Agnes Kittel, Maria Eldh, Irma Dianzani, Edit I. Buzás, and Jan Lötvall. 2013. “Distinct RNA Profiles in Subpopulations of Extracellular Vesicles: Apoptotic Bodies, Microvesicles and Exosomes.” *Journal of Extracellular Vesicles* 2 (September):10.3402/jev.v2i0.20677. <https://doi.org/10.3402/jev.v2i0.20677>.
40. Crowley, Lisa C., Brooke J. Marfell, Adrian P. Scott, and Nigel J. Waterhouse. 2016. “Quantitation of Apoptosis and Necrosis by Annexin V Binding, Propidium Iodide Uptake, and Flow Cytometry.” *Cold Spring Harbor Protocols* 2016 (11). <https://doi.org/10.1101/pdb.prot087288>.

41. Dachary-Prigent, J., J. M. Freyssinet, J. M. Pasquet, J. C. Carron, and A. T. Nurden. 1993. "Annexin V as a Probe of Aminophospholipid Exposure and Platelet Membrane Vesiculation: A Flow Cytometry Study Showing a Role for Free Sulfhydryl Groups." *Blood* 81 (10): 2554–65.
42. Dallérac, Glenn, Jonathan Zapata, and Nathalie Rouach. 2018. "Versatile Control of Synaptic Circuits by Astrocytes: Where, When and How?" *Nature Reviews. Neuroscience* 19 (12): 729–43. <https://doi.org/10.1038/s41583-018-0080-6>.
43. Damgaard, Mads V., and Jonas T. Treebak. 2022. "Protocol for qPCR Analysis That Corrects for cDNA Amplification Efficiency." *STAR Protocols* 3 (3): 101515. <https://doi.org/10.1016/j.xpro.2022.101515>.
44. De Simoni, Anna, and Lily MY Yu. 2006. "Preparation of Organotypic Hippocampal Slice Cultures: Interface Method." *Nature Protocols* 1 (3): 1439–45. <https://doi.org/10.1038/nprot.2006.228>.
45. Deglincerti, Alessia, and Samie R. Jaffrey. 2012. "Insights into the Roles of Local Translation from the Axonal Transcriptome." *Open Biology* 2 (6): 120079. <https://doi.org/10.1098/rsob.120079>.
46. Deo, Claire, and Luke D. Lavis. 2018. "Synthetic and Genetically Encoded Fluorescent Neural Activity Indicators." *Current Opinion in Neurobiology* 50 (June): 101–8. <https://doi.org/10.1016/j.conb.2018.01.003>.
47. Dhandapani, Rahul, Cynthia Mary Arokiaraj, Francisco J. Taberner, Paola Pacifico, Sruthi Raja, Linda Nocchi, Carla Portulano, et al. 2018. "Control of Mechanical Pain Hypersensitivity in Mice through Ligand-Targeted Photoablation of TrkB-Positive Sensory Neurons." *Nature Communications* 9 (1): 1640. <https://doi.org/10.1038/s41467-018-04049-3>.
48. Dobin, Alexander, Carrie A. Davis, Felix Schlesinger, Jorg Drenkow, Chris Zaleski, Sonali Jha, Philippe Batut, Mark Chaisson, and Thomas R. Gingeras. 2013. "STAR: Ultrafast Universal RNA-Seq Aligner." *Bioinformatics (Oxford, England)* 29 (1): 15–21. <https://doi.org/10.1093/bioinformatics/bts635>.
49. Dräger, Ursula C. 1975. "Receptive Fields of Single Cells and Topography in Mouse Visual Cortex." *Journal of Comparative Neurology* 160 (3): 269–89. <https://doi.org/10.1002/cne.901600302>.
50. Dragon, Andrea H., Cassie J. Rowe, Alisha M. Rhodes, Olivia L. Pak, Thomas A. Davis, and Elsa Ronzier. 2023. "Systematic Identification of the Optimal Housekeeping Genes for Accurate Transcriptomic and Proteomic Profiling of Tissues Following Complex Traumatic

- Injury.” *Methods and Protocols* 6 (2): 22. <https://doi.org/10.3390/mps6020022>.
51. Du Cheyne, Charis, Yao Chen, Jurgen De Craene, Olivier Thas, and Ward De Spiegelaere. 2021. “Development of a 3’:5’ Digital PCR Assay to Determine Horse mRNA Integrity.” *Analytical Biochemistry* 626 (August):114217. <https://doi.org/10.1016/j.ab.2021.114217>.
 52. Eden, Eran, Roy Navon, Israel Steinfeld, Doron Lipson, and Zohar Yakhini. 2009. “GOrilla: A Tool for Discovery and Visualization of Enriched GO Terms in Ranked Gene Lists.” *BMC Bioinformatics* 10 (1): 48. <https://doi.org/10.1186/1471-2105-10-48>.
 53. Erzurumlu, Reha S., and Patricia Gaspar. 2012. “Development and Critical Period Plasticity of the Barrel Cortex.” *The European Journal of Neuroscience* 35 (10): 1540–53. <https://doi.org/10.1111/j.1460-9568.2012.08075.x>.
 54. Espinosa, J. Sebastian, and Michael P. Stryker. 2012. “Development and Plasticity of the Primary Visual Cortex.” *Neuron* 75 (2): 230–49. <https://doi.org/10.1016/j.neuron.2012.06.009>.
 55. Falkenberg, Virginia R., Toni Whistler, Janna’ R. Murray, Elizabeth R. Unger, and Mangalathu S. Rajeevan. 2011. “Identification of Phosphoglycerate Kinase 1 (PGK1) as a Reference Gene for Quantitative Gene Expression Measurements in Human Blood RNA.” *BMC Research Notes* 4 (1): 324. <https://doi.org/10.1186/1756-0500-4-324>.
 56. Farhy-Tselnick, Isabella, and Nicola J. Allen. 2018. “Astrocytes, Neurons, Synapses: A Tripartite View on Cortical Circuit Development.” *Neural Development* 13 (1): 7. <https://doi.org/10.1186/s13064-018-0104-y>.
 57. Faust, Travis E., Georgia Gunner, and Dorothy P. Schafer. 2021. “Mechanisms Governing Activity-Dependent Synaptic Pruning in the Developing Mammalian CNS.” *Nature Reviews. Neuroscience* 22 (11): 657–73. <https://doi.org/10.1038/s41583-021-00507-y>.
 58. Feng, Depeng, Anqi Huang, Wei Yan, and Dezhe Chen. 2019. “CD200 Dysfunction in Neuron Contributes to Synaptic Deficits and Cognitive Impairment.” *Biochemical and Biophysical Research Communications* 516 (4): 1053–59. <https://doi.org/10.1016/j.bbrc.2019.06.134>.
 59. Feng, Huijuan, Xuegong Zhang, and Chaolin Zhang. 2015. “mRIN for Direct Assessment of Genome-Wide and Gene-Specific mRNA Integrity from Large-Scale RNA-Sequencing Data.” *Nature Communications* 6 (1): 7816. <https://doi.org/10.1038/ncomms8816>.

60. Ferrer, Manuel, Tatyana N. Chernikova, Michail M. Yakimov, Peter N. Golyshin, and Kenneth N. Timmis. 2003. "Chaperonins Govern Growth of Escherichia Coli at Low Temperatures." *Nature Biotechnology* 21 (11): 1266–67. <https://doi.org/10.1038/nbt1103-1266>.
61. Filipello, Fabia, Raffaella Morini, Irene Corradini, Valerio Zerbi, Alice Canzi, Bernadeta Michalski, Marco Erreni, et al. 2018. "The Microglial Innate Immune Receptor TREM2 Is Required for Synapse Elimination and Normal Brain Connectivity." *Immunity* 48 (5): 979–991.e8. <https://doi.org/10.1016/j.immuni.2018.04.016>.
62. Fine, Ione, Alex R. Wade, Alyssa A. Brewer, Michael G. May, Daniel F. Goodman, Geoffrey M. Boynton, Brian A. Wandell, and Donald I. A. MacLeod. 2003. "Long-Term Deprivation Affects Visual Perception and Cortex." *Nature Neuroscience* 6 (9): 915–16. <https://doi.org/10.1038/nn1102>.
63. Fleige, Simone, and Michael W. Pfaffl. 2006. "RNA Integrity and the Effect on the Real-Time qRT-PCR Performance." *Molecular Aspects of Medicine, Real-time Polymerase Chain Reaction*, 27 (2): 126–39. <https://doi.org/10.1016/j.mam.2005.12.003>.
64. Fonkeu, Yombe, Nataliya Kraynyukova, Anne-Sophie Hafner, Lisa Kochen, Fabio Sartori, Erin M. Schuman, and Tatjana Tchumatchenko. 2019. "How mRNA Localization and Protein Synthesis Sites Influence Dendritic Protein Distribution and Dynamics." *Neuron* 103 (6): 1109–1122.e7. <https://doi.org/10.1016/j.neuron.2019.06.022>.
65. Furuta, Yoshitaka, Omar Pena-Ramos, Zao Li, Lucia Chiao, and Zheng Zhou. 2021. "Calcium Ions Trigger the Exposure of Phosphatidylserine on the Surface of Necrotic Cells." *PLOS Genetics* 17 (2): e1009066. <https://doi.org/10.1371/journal.pgen.1009066>.
66. Gallego Romero, Irene, Athma A. Pai, Jenny Tung, and Yoav Gilad. 2014. "RNA-Seq: Impact of RNA Degradation on Transcript Quantification." *BMC Biology* 12 (1): 42. <https://doi.org/10.1186/1741-7007-12-42>.
67. Gandasi, Nikhil R., Vasiliki Arapi, Michel E. Mickael, Prajakta A. Belekar, Louise Granlund, Lakshmi Kothegala, Robert Fredriksson, and Sonchita Bagchi. 2021. "Glutamine Uptake via SNAT6 and Caveolin Regulates Glutamine–Glutamate Cycle." *International Journal of Molecular Sciences* 22 (3): 1167. <https://doi.org/10.3390/ijms22031167>.

68. Gerrits, Emma, Yang Heng, Erik W. G. M. Boddeke, and Bart J. L. Eggen. 2020. "Transcriptional Profiling of Microglia; Current State of the Art and Future Perspectives." *Glia* 68 (4): 740–55. <https://doi.org/10.1002/glia.23767>.
69. Goertsen, David, Nicholas C. Flytzanis, Nick Goeden, Miguel R. Chuapoco, Alexander Cummins, Yijing Chen, Yingying Fan, et al. 2022. "AAV Capsid Variants with Brain-Wide Transgene Expression and Decreased Liver Targeting after Intravenous Delivery in Mouse and Marmoset." *Nature Neuroscience* 25 (1): 106–15. <https://doi.org/10.1038/s41593-021-00969-4>.
70. Gogolla, Nadine, Pico Caroni, Andreas Lüthi, and Cyril Herry. 2009. "Perineuronal Nets Protect Fear Memories from Erasure." *Science* 325 (5945): 1258–61. <https://doi.org/10.1126/science.1174146>.
71. Gogolla, Nadine, Ivan Galimberti, Vincenzo DePaola, and Pico Caroni. 2006. "Preparation of Organotypic Hippocampal Slice Cultures for Long-Term Live Imaging." *Nature Protocols* 1 (3): 1165–71. <https://doi.org/10.1038/nprot.2006.168>.
72. Goodwin, Laura R., and David J. Picketts. 2018. "The Role of ISWI Chromatin Remodeling Complexes in Brain Development and Neurodevelopmental Disorders." *Molecular and Cellular Neuroscience*, Chromatin in nervous system development and disease, 87 (March):55–64. <https://doi.org/10.1016/j.mcn.2017.10.008>.
73. Govindarajan, Arvind, Inbal Israely, Shu-Ying Huang, and Susumu Tonegawa. 2011. "The Dendritic Branch Is the Preferred Integrative Unit for Protein Synthesis-Dependent LTP." *Neuron* 69 (1): 132–46. <https://doi.org/10.1016/j.neuron.2010.12.008>.
74. Green, Michael Richard, and Joseph Sambrook. 2012. *Molecular Cloning: A Laboratory Manual*. 4th ed. Cold Spring Harbor: Cold Spring Harbor laboratory press.
75. Grillo, Federico W., Sen Song, Leonor M. Teles-Grilo Ruivo, Lieven Huang, Ge Gao, Graham W. Knott, Bohumil Maco, et al. 2013. "Increased Axonal Bouton Dynamics in the Aging Mouse Cortex." *Proceedings of the National Academy of Sciences of the United States of America* 110 (16): E1514–23. <https://doi.org/10.1073/pnas.1218731110>.
76. Hafner, Anne-Sophie, Paul G. Donlin-Asp, Beulah Leitch, Etienne Herzog, and Erin M. Schuman. 2019. "Local Protein Synthesis Is a Ubiquitous Feature of Neuronal Pre- and Postsynaptic

- Compartments.” *Science (New York, N.Y.)* 364 (6441): eaau3644. <https://doi.org/10.1126/science.aau3644>.
77. Ham, Tjakko J. van, James Mapes, David Kokel, and Randall T. Peterson. 2010. “Live Imaging of Apoptotic Cells in Zebrafish.” *FASEB Journal: Official Publication of the Federation of American Societies for Experimental Biology* 24 (11): 4336–42. <https://doi.org/10.1096/fj.10-161018>.
 78. Hanauer, A., and J.I. Mandel. 1984. “The Glyceraldehyde 3 Phosphate Dehydrogenase Gene Family: Structure of a Human cDNA and of an X Chromosome Linked Pseudogene; Amazing Complexity of the Gene Family in Mouse.” *The EMBO Journal* 3 (11): 2627–33. <https://doi.org/10.1002/j.1460-2075.1984.tb02185.x>.
 79. Harauzov, Alexey, Maria Spolidoro, Graziella DiCristo, Roberto De Pasquale, Laura Cancedda, Tommaso Pizzorusso, Alessandro Viegi, Nicoletta Berardi, and Lamberto Maffei. 2010. “Reducing Intracortical Inhibition in the Adult Visual Cortex Promotes Ocular Dominance Plasticity.” *The Journal of Neuroscience* 30 (1): 361–71. <https://doi.org/10.1523/JNEUROSCI.2233-09.2010>.
 80. Hartshorne, Joshua K., Joshua B. Tenenbaum, and Steven Pinker. 2018. “A Critical Period for Second Language Acquisition: Evidence from 2/3 Million English Speakers.” *Cognition* 177 (August):263–77. <https://doi.org/10.1016/j.cognition.2018.04.007>.
 81. Henn, F. A., D. J. Anderson, and D. G. Rustad. 1976. “Glial Contamination of Synaptosomal Fractions.” *Brain Research* 101 (2): 341–44. [https://doi.org/10.1016/0006-8993\(76\)90274-2](https://doi.org/10.1016/0006-8993(76)90274-2).
 82. Hennig, Bianca P., Lars Velten, Ines Racke, Chelsea Szu Tu, Matthias Thoms, Vladimir Rybin, Hüseyin Besir, Kim Remans, and Lars M. Steinmetz. 2018. “Large-Scale Low-Cost NGS Library Preparation Using a Robust Tn5 Purification and Tagmentation Protocol.” *G3 (Bethesda, Md.)* 8 (1): 79–89. <https://doi.org/10.1534/g3.117.300257>.
 83. Hensch, Takao K. 2005. “Critical Period Plasticity in Local Cortical Circuits.” *Nature Reviews. Neuroscience* 6 (11): 877–88. <https://doi.org/10.1038/nrn1787>.
 84. Hobson, Benjamin D., Linghao Kong, Maria Florencia Angelo, Ori J. Lieberman, Eugene V. Mosharov, Etienne Herzog, David Sulzer, and Peter A. Sims. 2022. “Subcellular and Regional Localization of mRNA Translation in Midbrain Dopamine Neurons.” *Cell Reports* 38 (2): 110208. <https://doi.org/10.1016/j.celrep.2021.110208>.
 85. Holler, Simone, German Köstinger, Kevan A. C. Martin, Gregor F. P. Schuhknecht, and Ken J. Stratford. 2021. “Structure and Function of

- a Neocortical Synapse.” *Nature* 591 (7848): 111–16. <https://doi.org/10.1038/s41586-020-03134-2>.
86. Holt, Christine E., Kelsey C. Martin, and Erin M. Schuman. 2019. “Local Translation in Neurons: Visualization and Function.” *Nature Structural & Molecular Biology* 26 (7): 557–66. <https://doi.org/10.1038/s41594-019-0263-5>.
 87. Hooks, Bryan M., and Chinfai Chen. 2007. “Critical Periods in the Visual System: Changing Views for a Model of Experience-Dependent Plasticity.” *Neuron* 56 (2): 312–26. <https://doi.org/10.1016/j.neuron.2007.10.003>.
 88. Hu, T., J. Shi, X. Jiao, J. Zhou, and X. Yin. 2008. “Measurement of Annexin V Uptake and Lactadherin Labeling for the Quantification of Apoptosis in Adherent Tca8113 and ACC-2 Cells.” *Brazilian Journal of Medical and Biological Research = Revista Brasileira De Pesquisas Medicas E Biologicas* 41 (9): 750–57. <https://doi.org/10.1590/s0100-879x2008000900002>.
 89. Hubel, D. H., and T. N. Wiesel. 1970. “The Period of Susceptibility to the Physiological Effects of Unilateral Eye Closure in Kittens.” *The Journal of Physiology* 206 (2): 419–36.
 90. Ito, Daisuke, and Atsushi Kumanogoh. 2016. “The Role of Sema4A in Angiogenesis, Immune Responses, Carcinogenesis, and Retinal Systems.” *Cell Adhesion & Migration* 10 (6): 692–99. <https://doi.org/10.1080/19336918.2016.1215785>.
 91. Ji, Sheng-Jian, and Samie R. Jaffrey. 2014. “Axonal Transcription Factors: Novel Regulators of Growth Cone-to-Nucleus Signaling.” *Developmental Neurobiology* 74 (3): 245–58. <https://doi.org/10.1002/dneu.22112>.
 92. Jumper, John, Richard Evans, Alexander Pritzel, Tim Green, Michael Figurnov, Olaf Ronneberger, Kathryn Tunyasuvunakool, et al. 2021. “Highly Accurate Protein Structure Prediction with AlphaFold.” *Nature* 596 (7873): 583–89. <https://doi.org/10.1038/s41586-021-03819-2>.
 93. Källberg, Morten, Haipeng Wang, Sheng Wang, Jian Peng, Zhiyong Wang, Hui Lu, and Jinbo Xu. 2012. “Template-Based Protein Structure Modeling Using the RaptorX Web Server.” *Nature Protocols* 7 (8): 1511–22. <https://doi.org/10.1038/nprot.2012.085>.
 94. Kar, Amar N., Margaret A. MacGibeny, Noreen M. Gervasi, Anthony E. Gioio, and Barry B. Kaplan. 2013. “Intra-Axonal Synthesis of Eukaryotic Translation Initiation Factors Regulates Local Protein Synthesis and Axon Growth in Rat Sympathetic Neurons.” *The*

- Journal of Neuroscience* 33 (17): 7165–74.
<https://doi.org/10.1523/JNEUROSCI.2040-12.2013>.
95. Katsuoka, Fumiki, and Masayuki Yamamoto. 2016. “Small Maf Proteins (MafF, MafG, MafK): History, Structure and Function.” *Gene* 586 (2): 197–205. <https://doi.org/10.1016/j.gene.2016.03.058>.
 96. Kay, Jason G., Mirkka Koivusalo, Xiaoxiao Ma, Thorsten Wohland, and Sergio Grinstein. 2012. “Phosphatidylserine Dynamics in Cellular Membranes.” *Molecular Biology of the Cell* 23 (11): 2198–2212. <https://doi.org/10.1091/mbc.E11-11-0936>.
 97. Kim, Yujin E., Jeannie Chen, Jonah R. Chan, and Ralf Langen. 2010. “Engineering a Polarity-Sensitive Biosensor for Time-Lapse Imaging of Apoptotic Processes and Degeneration.” *Nature Methods* 7 (1): 67–73. <https://doi.org/10.1038/nmeth.1405>.
 98. Kim, Yujin E., Jeannie Chen, Ralf Langen, and Jonah R. Chan. 2010. “Monitoring Apoptosis and Neuronal Degeneration by Real-Time Detection of Phosphatidylserine Externalization Using a Polarity-Sensitive Indicator of Viability and Apoptosis.” *Nature Protocols* 5 (8): 1396–1405. <https://doi.org/10.1038/nprot.2010.101>.
 99. Kummer, Kai K., Maximilian Zeidler, Theodora Kalpachidou, and Michaela Kress. 2021. “Role of IL-6 in the Regulation of Neuronal Development, Survival and Function.” *Cytokine* 144 (August):155582. <https://doi.org/10.1016/j.cyto.2021.155582>.
 100. Kurematsu, Chihiro, Masato Sawada, Masaki Ohmuraya, Motoki Tanaka, Kazuya Kuboyama, Takashi Ogino, Mami Matsumoto, et al. 2022. “Synaptic Pruning of Murine Adult-Born Neurons by Microglia Depends on Phosphatidylserine.” *The Journal of Experimental Medicine* 219 (4): e20202304. <https://doi.org/10.1084/jem.20202304>.
 101. Kuswanto, Carissa Nadia, Min Yi Sum, Christopher Ren Zhi Thng, Yi Bin Zhang, Guo Liang Yang, Wieslaw Lucjan Nowinski, Yih Yian Sitoh, Chian Ming Low, and Kang Sim. 2013. “GRIN2B Gene and Associated Brain Cortical White Matter Changes in Bipolar Disorder: A Preliminary Combined Platform Investigation.” *BioMed Research International* 2013. <https://doi.org/10.1155/2013/635131>.
 102. Kwong, Jacky M. K., Celia Hoang, Reshil T. Dukes, Richard W. Yee, Brian D. Gray, Koon Y. Pak, and Joseph Caprioli. 2014. “Bis(Zinc-Dipicolylamine), Zn-DPA, a New Marker for Apoptosis.” *Investigative Ophthalmology & Visual Science* 55 (8): 4913–21. <https://doi.org/10.1167/iovs.13-13346>.

103. Lawrence, Jill M., Kayla Schardien, Brian Wigdahl, and Michael R. Nonnemacher. 2023. "Roles of Neuropathology-Associated Reactive Astrocytes: A Systematic Review." *Acta Neuropathologica Communications* 11 (1): 42. <https://doi.org/10.1186/s40478-023-01526-9>.
104. Lee, Hong J., Kwang S. Kim, Jin Ahn, Hye M. Bae, Inja Lim, and Seung U. Kim. 2014. "Human Motor Neurons Generated from Neural Stem Cells Delay Clinical Onset and Prolong Life in ALS Mouse Model." *PLOS ONE* 9 (5): e97518. <https://doi.org/10.1371/journal.pone.0097518>.
105. Lee, Sang H., Seung Min Shin, Peng Zhong, Hyun-Taek Kim, Dong-Il Kim, June Myoung Kim, Won Do Heo, et al. 2018. "Reciprocal Control of Excitatory Synapse Numbers by Wnt and Wnt Inhibitor PRR7 Secreted on Exosomes." *Nature Communications* 9 (1): 3434. <https://doi.org/10.1038/s41467-018-05858-2>.
106. Lewis, Terri L., and Daphne Maurer. 2005. "Multiple Sensitive Periods in Human Visual Development: Evidence from Visually Deprived Children." *Developmental Psychobiology* 46 (3): 163–83. <https://doi.org/10.1002/dev.20055>.
107. Li, Shuxin, Betty P. Liu, Stephane Budel, Mingwei Li, Benxiu Ji, Lee Walus, Weiwei Li, et al. 2004. "Blockade of Nogo-66, Myelin-Associated Glycoprotein, and Oligodendrocyte Myelin Glycoprotein by Soluble Nogo-66 Receptor Promotes Axonal Sprouting and Recovery after Spinal Injury." *The Journal of Neuroscience* 24 (46): 10511–20. <https://doi.org/10.1523/JNEUROSCI.2828-04.2004>.
108. Li, Tao, Brian Chiou, Casey K. Gilman, Rong Luo, Tatsuhiko Koshi, Diankun Yu, Hayeon C. Oak, et al. 2020. "A Splicing Isoform of GPR56 Mediates Microglial Synaptic Refinement via Phosphatidylserine Binding." *The EMBO Journal* 39 (16): e104136. <https://doi.org/10.15252/embj.2019104136>.
109. Lim, Tony KY, and Edward S Ruthazer. n.d. "Microglial Trophocytosis and the Complement System Regulate Axonal Pruning in Vivo." *eLife* 10:e62167. <https://doi.org/10.7554/eLife.62167>.
110. Linsley, Jeremy W., Atmiyata Tripathi, Irina Epstein, Galina Schmunk, Elliot Mount, Matthew Campioni, Viral Oza, et al. 2019. "Automated Four-Dimensional Long Term Imaging Enables Single Cell Tracking within Organotypic Brain Slices to Study Neurodevelopment and Degeneration." *Communications Biology* 2 (1): 1–13. <https://doi.org/10.1038/s42003-019-0411-9>.

111. Liu, He, Xingchen Wang, Peibo Shen, Yingqian Ni, and Xiuzhen Han. 2022. "The Basic Functions of Phosphoglycerate Kinase 1 and Its Roles in Cancer and Other Diseases." *European Journal of Pharmacology* 920 (April):174835. <https://doi.org/10.1016/j.ejphar.2022.174835>.
112. Liu, Honglin, Zhenyu Han, Liru Chen, Jing Zhang, Zhanqing Zhang, Yaoxin Chen, Feichang Liu, et al. n.d. "ZNFX1 Promotes AMPK-Mediated Autophagy against Mycobacterium Tuberculosis by Stabilizing Prkaa2 mRNA." *JCI Insight* 9 (1): e171850. <https://doi.org/10.1172/jci.insight.171850>.
113. Lodato, Simona, Caroline Rouaux, Kathleen B. Quast, Chanati Jantrachotechatchawan, Michèle Studer, Takao K. Hensch, and Paola Arlotta. 2011. "Excitatory Projection Neuron Subtypes Control the Distribution of Local Inhibitory Interneurons in the Cerebral Cortex." *Neuron* 69 (4): 763–79. <https://doi.org/10.1016/j.neuron.2011.01.015>.
114. Logue, Susan E., Mohamed Elgendy, and Seamus J. Martin. 2009. "Expression, Purification and Use of Recombinant Annexin V for the Detection of Apoptotic Cells." *Nature Protocols* 4 (9): 1383–95. <https://doi.org/10.1038/nprot.2009.143>.
115. Love, Michael I., Wolfgang Huber, and Simon Anders. 2014. "Moderated Estimation of Fold Change and Dispersion for RNA-Seq Data with DESeq2." *Genome Biology* 15 (12): 550. <https://doi.org/10.1186/s13059-014-0550-8>.
116. Luquet, Elisa, Christoph Biesemann, Annie Munier, and Etienne Herzog. 2017. "Purification of Synaptosome Populations Using Fluorescence-Activated Synaptosome Sorting." *Methods in Molecular Biology (Clifton, N.J.)* 1538:121–34. https://doi.org/10.1007/978-1-4939-6688-2_10.
117. Ma, Xiaokuang, Ke Chen, Yuehua Cui, Guanqun Huang, Antoine Nehme, Le Zhang, Handong Li, et al. 2020. "Depletion of Microglia in Developing Cortical Circuits Reveals Its Critical Role in Glutamatergic Synapse Development, Functional Connectivity, and Critical Period Plasticity." *Journal of Neuroscience Research* 98 (10): 1968–86. <https://doi.org/10.1002/jnr.24641>.
118. Majewska, Ania, and Mriganka Sur. 2003. "Motility of Dendritic Spines in Visual Cortex in Vivo: Changes during the Critical Period and Effects of Visual Deprivation." *Proceedings of the National Academy of Sciences* 100 (26): 16024–29. <https://doi.org/10.1073/pnas.2636949100>.

119. Maneta-Peyret, L., G. Freyburger, J. J. Bessoule, and C. Cassagne. 1989. "Specific Immunocytochemical Visualization of Phosphatidylserine." *Journal of Immunological Methods* 122 (2): 155–59. [https://doi.org/10.1016/0022-1759\(89\)90259-7](https://doi.org/10.1016/0022-1759(89)90259-7).
120. Martin, Emily-Rose, Josan Gandawijaya, and Asami Oguro-Ando. 2022. "A Novel Method for Generating Glutamatergic SH-SY5Y Neuron-like Cells Utilizing B-27 Supplement." *Frontiers in Pharmacology* 13 (October). <https://doi.org/10.3389/fphar.2022.943627>.
121. Martin, K. C., A. Casadio, H. Zhu, E. Yaping, J. C. Rose, M. Chen, C. H. Bailey, and E. R. Kandel. 1997. "Synapse-Specific, Long-Term Facilitation of Aplysia Sensory to Motor Synapses: A Function for Local Protein Synthesis in Memory Storage." *Cell* 91 (7): 927–38. [https://doi.org/10.1016/s0092-8674\(00\)80484-5](https://doi.org/10.1016/s0092-8674(00)80484-5).
122. Martin, O. C., and R. E. Pagano. 1987. "Transbilayer Movement of Fluorescent Analogs of Phosphatidylserine and Phosphatidylethanolamine at the Plasma Membrane of Cultured Cells. Evidence for a Protein-Mediated and ATP-Dependent Process(es)." *The Journal of Biological Chemistry* 262 (12): 5890–98.
123. Martins Rosa, Andreia, Maria Fátima Silva, Sónia Ferreira, Joaquim Murta, and Miguel Castelo-Branco. 2013. "Plasticity in the Human Visual Cortex: An Ophthalmology-Based Perspective." *BioMed Research International* 2013:568354. <https://doi.org/10.1155/2013/568354>.
124. Maurin, Thomas, Samantha Zongaro, and Barbara Bardoni. 2014. "Fragile X Syndrome: From Molecular Pathology to Therapy." *Neuroscience and Biobehavioral Reviews* 46 Pt 2 (October):242–55. <https://doi.org/10.1016/j.neubiorev.2014.01.006>.
125. McGee, Aaron W., Yupeng Yang, Quentin S. Fischer, Nigel W. Daw, and Stephen M. Strittmatter. 2005. "Experience-Driven Plasticity of Visual Cortex Limited by Myelin and Nogo Receptor." *Science (New York, N.Y.)* 309 (5744): 2222–26. <https://doi.org/10.1126/science.1114362>.
126. Meers, P., and T. Mealy. 1994. "Phospholipid Determinants for Annexin V Binding Sites and the Role of Tryptophan 187." *Biochemistry* 33 (19): 5829–37. <https://doi.org/10.1021/bi00185a022>.
127. Mirabella, Filippo, Genni Desiato, Sara Mancinelli, Giuliana Fossati, Marco Rasile, Raffaella Morini, Marija Markicevic, et al.

2021. "Prenatal Interleukin 6 Elevation Increases Glutamatergic Synapse Density and Disrupts Hippocampal Connectivity in Offspring." *Immunity* 54 (11): 2611-2631.e8. <https://doi.org/10.1016/j.immuni.2021.10.006>.
128. Mody, M., Y. Cao, Z. Cui, K. Y. Tay, A. Shyong, E. Shimizu, K. Pham, P. Schultz, D. Welsh, and J. Z. Tsien. 2001. "Genome-Wide Gene Expression Profiles of the Developing Mouse Hippocampus." *Proceedings of the National Academy of Sciences of the United States of America* 98 (15): 8862-67. <https://doi.org/10.1073/pnas.141244998>.
129. Mordelt, Annika, and Lot D. de Witte. 2023. "Microglia-Mediated Synaptic Pruning as a Key Deficit in Neurodevelopmental Disorders: Hype or Hope?" *Current Opinion in Neurobiology* 79 (April): 102674. <https://doi.org/10.1016/j.conb.2022.102674>.
130. Muddashetty, Ravi S., Sofija Kelić, Christina Gross, Mei Xu, and Gary J. Bassell. 2007. "Dysregulated Metabotropic Glutamate Receptor-Dependent Translation of AMPA Receptor and Postsynaptic Density-95 mRNAs at Synapses in a Mouse Model of Fragile X Syndrome." *The Journal of Neuroscience: The Official Journal of the Society for Neuroscience* 27 (20): 5338-48. <https://doi.org/10.1523/JNEUROSCI.0937-07.2007>.
131. Murthy, V. N., T. Schikorski, C. F. Stevens, and Y. Zhu. 2001. "Inactivity Produces Increases in Neurotransmitter Release and Synapse Size." *Neuron* 32 (4): 673-82. [https://doi.org/10.1016/s0896-6273\(01\)00500-1](https://doi.org/10.1016/s0896-6273(01)00500-1).
132. Navlakha, Saket, Alison L. Barth, and Ziv Bar-Joseph. 2015. "Decreasing-Rate Pruning Optimizes the Construction of Efficient and Robust Distributed Networks." *PLOS Computational Biology* 11 (7): e1004347. <https://doi.org/10.1371/journal.pcbi.1004347>.
133. Nebenführ, Andreas, Christophe Ritzenthaler, and David G. Robinson. 2002. "Brefeldin A: Deciphering an Enigmatic Inhibitor of Secretion." *Plant Physiology* 130 (3): 1102-8. <https://doi.org/10.1104/pp.011569>.
134. Neniskyte, Urte, Ugnė Kuliesiute, Auguste Vadisiute, Kristina Jevdokimenko, Ludovico Coletta, Senthilkumar Deivasigamani, Daina Pamedytyte, et al. 2023a. "Phospholipid Scramblase Xkr8 Is Required for Developmental Axon Pruning via Phosphatidylserine Exposure." *The EMBO Journal* 42 (14): e111790. <https://doi.org/10.15252/embj.2022111790>.

135. ———. 2023b. “Phospholipid Scramblase Xkr8 Is Required for Developmental Axon Pruning via Phosphatidylserine Exposure.” *The EMBO Journal* 42 (14): e111790. <https://doi.org/10.15252/emboj.2022111790>.
136. Neumann, Manuela, Deepak M. Sampathu, Linda K. Kwong, Adam C. Truax, Matthew C. Micsenyi, Thomas T. Chou, Jennifer Bruce, et al. 2006. “Ubiquitinated TDP-43 in Frontotemporal Lobar Degeneration and Amyotrophic Lateral Sclerosis.” *Science (New York, N.Y.)* 314 (5796): 130–33. <https://doi.org/10.1126/science.1134108>.
137. Nguyen, Trang Thi Minh, Germain Gillet, and Nikolay Popgeorgiev. 2021. “Caspases in the Developing Central Nervous System: Apoptosis and Beyond.” *Frontiers in Cell and Developmental Biology* 9 (July). <https://doi.org/10.3389/fcell.2021.702404>.
138. Nichols, J. Wylie. 2002. “Internalization and Trafficking of Fluorescent-Labeled Phospholipids in Yeast.” *Seminars in Cell & Developmental Biology* 13 (3): 179–84. [https://doi.org/10.1016/s1084-9521\(02\)00046-0](https://doi.org/10.1016/s1084-9521(02)00046-0).
139. Nihonmatsu, Itsuko, Noriaki Ohkawa, Yoshito Saitoh, Reiko Okubo-Suzuki, and Kaoru Inokuchi. 2020. “Selective Targeting of mRNA and the Following Protein Synthesis of CaMKII α at the Long-Term Potentiation-Induced Site.” *Biology Open* 9 (1): bio042861. <https://doi.org/10.1242/bio.042861>.
140. Niibori, Yosuke, Robert Duba-Kiss, Joseph T. Bruder, Jared B. Smith, and David R. Hampson. 2023. “In Silico Prediction and in Vivo Testing of Promoters Targeting GABAergic Inhibitory Neurons.” *Molecular Therapy Methods & Clinical Development* 28 (March):330–43. <https://doi.org/10.1016/j.omtm.2023.01.007>.
141. Noguchi, Jun, Akira Nagaoka, Satoshi Watanabe, Graham C R Ellis-Davies, Kazuo Kitamura, Masanobu Kano, Masanori Matsuzaki, and Haruo Kasai. 2011. “In Vivo Two-Photon Uncaging of Glutamate Revealing the Structure–Function Relationships of Dendritic Spines in the Neocortex of Adult Mice.” *The Journal of Physiology* 589 (Pt 10): 2447–57. <https://doi.org/10.1113/jphysiol.2011.207100>.
142. Nolan, Tania, Rebecca E. Hands, and Stephen A. Bustin. 2006. “Quantification of mRNA Using Real-Time RT-PCR.” *Nature Protocols* 1 (3): 1559–82. <https://doi.org/10.1038/nprot.2006.236>.

143. Noller, Harry F. 2005. "RNA Structure: Reading the Ribosome." *Science* 309 (5740): 1508–14. <https://doi.org/10.1126/science.1111771>.
144. Olechnovič, Kliment, and Česlovas Venclovas. 2017. "VoroMQA: Assessment of Protein Structure Quality Using Interatomic Contact Areas." *Proteins* 85 (6): 1131–45. <https://doi.org/10.1002/prot.25278>.
145. Oostrum, Marc van, Thomas M. Blok, Stefano L. Giandomenico, Susanne tom Dieck, Georgi Tushev, Nicole Fürst, Julian D. Langer, and Erin M. Schuman. 2023. "The Proteomic Landscape of Synaptic Diversity across Brain Regions and Cell Types." *Cell* 186 (24): 5411–5427.e23. <https://doi.org/10.1016/j.cell.2023.09.028>.
146. Oshima, Kenzi, Takehiko Yasueda, Shunsuke Nishio, and Tsukasa Matsuda. 2014. "MFG-E8: Origin, Structure, Expression, Functions and Regulation." In *MFG-E8 and Inflammation*, edited by Ping Wang, 1–31. Dordrecht: Springer Netherlands. https://doi.org/10.1007/978-94-017-8765-9_1.
147. Ouyang, Y., A. Rosenstein, G. Kreiman, E. M. Schuman, and M. B. Kennedy. 1999. "Tetanic Stimulation Leads to Increased Accumulation of Ca(2+)/Calmodulin-Dependent Protein Kinase II via Dendritic Protein Synthesis in Hippocampal Neurons." *The Journal of Neuroscience: The Official Journal of the Society for Neuroscience* 19 (18): 7823–33. <https://doi.org/10.1523/JNEUROSCI.19-18-07823.1999>.
148. Padhi, Bhaja K., Manjeet Singh, Marianela Rosales, Guillaume Pelletier, and Sabit Cakmak. 2018. "A PCR-Based Quantitative Assay for the Evaluation of mRNA Integrity in Rat Samples." *Biomolecular Detection and Quantification* 15 (May):18–23. <https://doi.org/10.1016/j.bdq.2018.02.001>.
149. Paget-Blanc, Vincent, Marlene E. Pfeffer, Marie Pronot, Paul Lapios, Maria-Florencia Angelo, Roman Walle, Fabrice P. Cordelières, et al. 2022. "A Synaptic Analysis Reveals Dopamine Hub Synapses in the Mouse Striatum." *Nature Communications* 13 (June):3102. <https://doi.org/10.1038/s41467-022-30776-9>.
150. Pan, Jie, Nana Ma, Bo Yu, Wei Zhang, and Jun Wan. 2020. "Transcriptomic Profiling of Microglia and Astrocytes throughout Aging." *Journal of Neuroinflammation* 17 (1): 97. <https://doi.org/10.1186/s12974-020-01774-9>.

151. Paredes, Mercedes F., David James, Sara Gil-Perotin, Hosung Kim, Jennifer A. Cotter, Carissa Ng, Kadellyn Sandoval, et al. 2016. "Extensive Migration of Young Neurons into the Infant Human Frontal Lobe." *Science (New York, N.Y.)* 354 (6308): aaf7073. <https://doi.org/10.1126/science.aaf7073>.
152. Perez-Catalan, Nelson A., Chris Q. Doe, and Sarah D. Ackerman. 2021. "The Role of Astrocyte-mediated Plasticity in Neural Circuit Development and Function." *Neural Development* 16 (1): 1. <https://doi.org/10.1186/s13064-020-00151-9>.
153. Picelli, Simone, Omid R. Faridani, Åsa K. Björklund, Gösta Winberg, Sven Sagasser, and Rickard Sandberg. 2014. "Full-Length RNA-Seq from Single Cells Using Smart-Seq2." *Nature Protocols* 9 (1): 171–81. <https://doi.org/10.1038/nprot.2014.006>.
154. Pizzorusso, Tommaso, Paolo Medini, Nicoletta Berardi, Sabrina Chierzi, James W. Fawcett, and Lamberto Maffei. 2002. "Reactivation of Ocular Dominance Plasticity in the Adult Visual Cortex." *Science (New York, N.Y.)* 298 (5596): 1248–51. <https://doi.org/10.1126/science.1072699>.
155. Polishchuk, Roman, and Svetlana Lutsenko. 2013. "GOLGI IN COPPER HOMEOSTASIS: A VIEW FROM THE MEMBRANE TRAFFICKING FIELD." *Histochemistry and Cell Biology* 140 (3): 285–95. <https://doi.org/10.1007/s00418-013-1123-8>.
156. Pomytkin, Igor, João P. Costa-Nunes, Vladimir Kasatkin, Ekaterina Veniaminova, Anna Demchenko, Alexey Lyundup, Klaus-Peter Lesch, Eugene D. Ponomarev, and Tatyana Strekalova. 2018. "Insulin Receptor in the Brain: Mechanisms of Activation and the Role in the CNS Pathology and Treatment." *CNS Neuroscience & Therapeutics* 24 (9): 763–74. <https://doi.org/10.1111/cns.12866>.
157. Presumey, Jessy, Allison R. Bialas, and Michael C. Carroll. 2017. "Chapter Two - Complement System in Neural Synapse Elimination in Development and Disease." In *Advances in Immunology*, edited by Frederick W. Alt, 135:53–79. Academic Press. <https://doi.org/10.1016/bs.ai.2017.06.004>.
158. Prinzen, Lenneke, Robbert-Jan J. H. M. Miserus, Anouk Dirksen, Tilman M. Hackeng, Niko Deckers, Nicole J. Bitsch, Remco T. A. Megens, et al. 2007. "Optical and Magnetic Resonance Imaging of Cell Death and Platelet Activation Using Annexin A5-Functionalized Quantum Dots." *Nano Letters* 7 (1): 93–100. <https://doi.org/10.1021/nl062226r>.

159. Quintana, Ariel, Vangipurapu Rajanikanth, Suzette Farber-Katz, Aparna Gudlur, Chen Zhang, Ji Jing, Yubin Zhou, Anjana Rao, and Patrick G. Hogan. 2015. "TMEM110 Regulates the Maintenance and Remodeling of Mammalian ER–Plasma Membrane Junctions Competent for STIM–ORAI Signaling." *Proceedings of the National Academy of Sciences* 112 (51): E7083–92. <https://doi.org/10.1073/pnas.1521924112>.
160. Rae, Caroline, Nathan Hare, William A. Bubb, Sally R. McEwan, Angelika Bröer, James A. McQuillan, Vladimir J. Balcar, Arthur D. Conigrave, and Stefan Bröer. 2003. "Inhibition of Glutamine Transport Depletes Glutamate and GABA Neurotransmitter Pools: Further Evidence for Metabolic Compartmentation." *Journal of Neurochemistry* 85 (2): 503–14. <https://doi.org/10.1046/j.1471-4159.2003.01713.x>.
161. Rajgor, Dipen, Alicia M. Purkey, Jennifer L. Sanderson, Theresa M. Welle, Joshua D. Garcia, Mark L. Dell'Acqua, and Katharine R. Smith. 2020. "Local miRNA-Dependent Translational Control of GABAAR Synthesis during Inhibitory Long-Term Potentiation." *Cell Reports* 31 (12): 107785. <https://doi.org/10.1016/j.celrep.2020.107785>.
162. Rajgor, Dipen, Theresa M. Welle, and Katharine R. Smith. 2021. "The Coordination of Local Translation, Membranous Organelle Trafficking, and Synaptic Plasticity in Neurons." *Frontiers in Cell and Developmental Biology* 9:711446. <https://doi.org/10.3389/fcell.2021.711446>.
163. Ray, Arjun, Erik Lindahl, and Björn Wallner. 2012. "Improved Model Quality Assessment Using ProQ2." *BMC Bioinformatics* 13 (1): 224. <https://doi.org/10.1186/1471-2105-13-224>.
164. Reddy Nanga, Ravi Prakash, Subramanian Vivekanandan, and Ho Sup Yoon. 2007. "Expression, Purification and Characterization of C2 Domain of Milk Fat Globule-EGF-Factor 8-L." *Protein Expression and Purification* 52 (2): 329–33. <https://doi.org/10.1016/j.pep.2006.08.018>.
165. Reh, Rebecca K., Brian G. Dias, Charles A. Nelson, Daniela Kaufer, Janet F. Werker, Bryan Kolb, Joel D. Levine, and Takao K. Hensch. 2020. "Critical Period Regulation across Multiple Timescales." *Proceedings of the National Academy of Sciences of the United States of America* 117 (38): 23242–51. <https://doi.org/10.1073/pnas.1820836117>.

166. Reichelt, Amy C., Dominic J. Hare, Timothy J. Bussey, and Lisa M. Saksida. 2019. "Perineuronal Nets: Plasticity, Protection, and Therapeutic Potential." *Trends in Neurosciences* 42 (7): 458–70. <https://doi.org/10.1016/j.tins.2019.04.003>.
167. Ribot, Jérôme, Rachel Breton, Charles-Félix Calvo, Julien Moulard, Pascal Ezan, Jonathan Zapata, Kevin Samama, et al. 2021. "Astrocytes Close the Mouse Critical Period for Visual Plasticity." *Science* 373 (6550): 77–81. <https://doi.org/10.1126/science.abf5273>.
168. Rojas-Pirela, Maura, Diego Andrade-Alviárez, Verónica Rojas, Ulrike Kemmerling, Ana J. Cáceres, Paul A. Michels, Juan Luis Concepción, and Wilfredo Quiñones. 2020. "Phosphoglycerate Kinase: Structural Aspects and Functions, with Special Emphasis on the Enzyme from Kinetoplastea." *Open Biology* 10 (11): 200302. <https://doi.org/10.1098/rsob.200302>.
169. Rowlands, Daire, Kristian K. Lensjø, Tovy Dinh, Sujeong Yang, Melissa R. Andrews, Torkel Hafting, Marianne Fyhn, James W. Fawcett, and Gunnar Dick. 2018. "Aggrecan Directs Extracellular Matrix-Mediated Neuronal Plasticity." *The Journal of Neuroscience: The Official Journal of the Society for Neuroscience* 38 (47): 10102–13. <https://doi.org/10.1523/JNEUROSCI.1122-18.2018>.
170. Sammons, Rosanna P., Claudia Clopath, and Samuel J. Barnes. 2018. "Size-Dependent Axonal Bouton Dynamics Following Visual Deprivation In Vivo." *Cell Reports* 22 (3): 576–84. <https://doi.org/10.1016/j.celrep.2017.12.065>.
171. Sanz, Elisenda, Linghai Yang, Thomas Su, David R. Morris, G. Stanley McKnight, and Paul S. Amieux. 2009. "Cell-Type-Specific Isolation of Ribosome-Associated mRNA from Complex Tissues." *Proceedings of the National Academy of Sciences of the United States of America* 106 (33): 13939–44. <https://doi.org/10.1073/pnas.0907143106>.
172. Sapor, Maria L., Hui Ji, Bei Wang, Amy R. Poe, Kush Dubey, Xingjie Ren, Jian-Quan Ni, and Chun Han. 2018. "Phosphatidylserine Externalization Results from and Causes Neurite Degeneration in *Drosophila*." *Cell Reports* 24 (9): 2273–86. <https://doi.org/10.1016/j.celrep.2018.07.095>.
173. Scarnati, Matthew S., Rahul Kataria, Mohana Biswas, and Kenneth G. Paradiso. 2018. "Active Presynaptic Ribosomes in the Mammalian Brain, and Altered Transmitter Release after Protein Synthesis Inhibition." *eLife* 7 (October): e36697. <https://doi.org/10.7554/eLife.36697>.

174. Schaeck, M., W. De Spiegelaere, J. De Craene, W. Van den Broeck, B. De Spiegeleer, C. Burvenich, F. Haesebrouck, and A. Decostere. 2016. "Laser Capture Microdissection of Intestinal Tissue from Sea Bass Larvae Using an Optimized RNA Integrity Assay and Validated Reference Genes." *Scientific Reports* 6 (February):21092. <https://doi.org/10.1038/srep21092>.
175. Schafer, Dorothy P, Emily K Lehrman, Amanda G Kautzman, Ryuta Koyama, Alan R Mardinly, Ryo Yamasaki, Richard M Ransohoff, Michael E Greenberg, Ben A Barres, and Beth Stevens. 2012. "Microglia Sculpt Postnatal Neural Circuits in an Activity and Complement-Dependent Manner." *Neuron* 74 (4): 691–705. <https://doi.org/10.1016/j.neuron.2012.03.026>.
176. Schafer, Dorothy P, Emily K Lehrman, and Beth Stevens. 2013. "The 'Quad-Partite' Synapse: Microglia-Synapse Interactions in the Developing and Mature CNS." *Glia* 61 (1): 24–36. <https://doi.org/10.1002/glia.22389>.
177. Schick, P K, K B Kurica, and G K Chacko. 1976. "Location of Phosphatidylethanolamine and Phosphatidylserine in the Human Platelet Plasma Membrane." *Journal of Clinical Investigation* 57 (5): 1221–26.
178. Schindelin, Johannes, Ignacio Arganda-Carreras, Erwin Frise, Verena Kaynig, Mark Longair, Tobias Pietzsch, Stephan Preibisch, et al. 2012. "Fiji: An Open-Source Platform for Biological-Image Analysis." *Nature Methods* 9 (7): 676–82. <https://doi.org/10.1038/nmeth.2019>.
179. Schroeder, Andreas, Odilo Mueller, Susanne Stocker, Ruediger Salowsky, Michael Leiber, Marcus Gassmann, Samar Lightfoot, Wolfram Menzel, Martin Granzow, and Thomas Ragg. 2006. "The RIN: An RNA Integrity Number for Assigning Integrity Values to RNA Measurements." *BMC Molecular Biology* 7 (1): 3. <https://doi.org/10.1186/1471-2199-7-3>.
180. Scott, Haden L., Frederick A. Heberle, John Katsaras, and Francisco N. Barrera. 2019. "Phosphatidylserine Asymmetry Promotes the Membrane Insertion of a Transmembrane Helix." *Biophysical Journal* 116 (8): 1495–1506. <https://doi.org/10.1016/j.bpj.2019.03.003>.
181. Scott-Hewitt, Nicole, Fabio Perrucci, Raffaella Morini, Marco Erreni, Matthew Mahoney, Agata Witkowska, Alanna Carey, et al. 2020. "Local Externalization of Phosphatidylserine Mediates

- Developmental Synaptic Pruning by Microglia.” *The EMBO Journal* 39 (16): e105380. <https://doi.org/10.15252/embj.2020105380>.
182. Shi, Lv, Xin Du, Hong Zhou, Changlu Tao, Yuntao Liu, Fantao Meng, Gao Wu, et al. 2014. “Cumulative Effects of the ApoE Genotype and Gender on the Synaptic Proteome and Oxidative Stress in the Mouse Brain.” *International Journal of Neuropsychopharmacology* 17 (11): 1863–79. <https://doi.org/10.1017/S1461145714000601>.
 183. Shigeoka, Toshiaki, Hosung Jung, Jane Jung, Benita Turner-Bridger, Jiyeon Ohk, Julie Qiaojin Lin, Paul S. Amieux, and Christine E. Holt. 2016. “Dynamic Axonal Translation in Developing and Mature Visual Circuits.” *Cell* 166 (1): 181–92. <https://doi.org/10.1016/j.cell.2016.05.029>.
 184. Shigeoka, Toshiaki, Jane Jung, Christine E. Holt, and Hosung Jung. 2018. “Axon-TRAP-RiboTag: Affinity Purification of Translated mRNAs from Neuronal Axons in Mouse In Vivo.” *Methods in Molecular Biology (Clifton, N.J.)* 1649:85–94. https://doi.org/10.1007/978-1-4939-7213-5_5.
 185. Sidova, Monika, Silvie Tomankova, Pavel Abaffy, Mikael Kubista, and Radek Sindelka. 2015. “Effects of Post-Mortem and Physical Degradation on RNA Integrity and Quality.” *Biomolecular Detection and Quantification* 5 (August):3–9. <https://doi.org/10.1016/j.bdq.2015.08.002>.
 186. Skoe, Erika, and Nina Kraus. 2013. “Musical Training Heightens Auditory Brainstem Function during Sensitive Periods in Development.” *Frontiers in Psychology* 4 (September). <https://doi.org/10.3389/fpsyg.2013.00622>.
 187. Sonntag, Kai-C., George Tejada, Sivan Subburaju, Sabina Berretta, Francine M. Benes, and Tsung-Ung W. Woo. 2016. “Limited Predictability of Postmortem Human Brain Tissue Quality by RNA Integrity Numbers.” *Journal of Neurochemistry* 138 (1): 53–59. <https://doi.org/10.1111/jnc.13637>.
 188. Southwell, Derek G., Robert C. Froemke, Arturo Alvarez-Buylla, Michael P. Stryker, and Sunil P. Gandhi. 2010. “Cortical Plasticity Induced by Inhibitory Neuron Transplantation.” *Science (New York, N.Y.)* 327 (5969): 1145–48. <https://doi.org/10.1126/science.1183962>.
 189. Stedehouder, Jeffrey, Demi Brizee, Guy Shpak, and Steven A. Kushner. 2018. “Activity-Dependent Myelination of Parvalbumin Interneurons Mediated by Axonal Morphological Plasticity.” *The*

- Journal of Neuroscience* 38 (15): 3631–42.
<https://doi.org/10.1523/JNEUROSCI.0074-18.2018>.
190. Stepanyants, Armen, and Gina Escobar. 2011. “Statistical Traces of Long-Term Memories Stored in Strengths and Patterns of Synaptic Connections.” *Journal of Neuroscience* 31 (21): 7657–69.
<https://doi.org/10.1523/JNEUROSCI.0255-11.2011>.
 191. Stevens, Beth, Nicola J. Allen, Luis E. Vazquez, Gareth R. Howell, Karen S. Christopherson, Navid Nouri, Kristina D. Micheva, et al. 2007. “The Classical Complement Cascade Mediates CNS Synapse Elimination.” *Cell* 131 (6): 1164–78.
<https://doi.org/10.1016/j.cell.2007.10.036>.
 192. Stubbs, J D, C Lekutis, K L Singer, A Bui, D Yuzuki, U Srinivasan, and G Parry. 1990. “cDNA Cloning of a Mouse Mammary Epithelial Cell Surface Protein Reveals the Existence of Epidermal Growth Factor-like Domains Linked to Factor VIII-like Sequences.” *Proceedings of the National Academy of Sciences of the United States of America* 87 (21): 8417–21.
 193. Studer, Gabriel, Christine Rempfer, Andrew M. Waterhouse, Rafal Gumieny, Juergen Haas, and Torsten Schwede. 2020. “QMEANDisCo-Distance Constraints Applied on Model Quality Estimation.” *Bioinformatics (Oxford, England)* 36 (6): 1765–71.
<https://doi.org/10.1093/bioinformatics/btz828>.
 194. Sun, Chao, Andreas Nold, Claudia M. Fusco, Vidhya Rangaraju, Tatjana Tchumatchenko, Mike Heilemann, and Erin M. Schuman. 2021. “The Prevalence and Specificity of Local Protein Synthesis during Neuronal Synaptic Plasticity.” *Science Advances* 7 (38): eabj0790. <https://doi.org/10.1126/sciadv.abj0790>.
 195. Sun, Yuan, Yan Li, Dianzhong Luo, and D. Joshua Liao. 2012. “Pseudogenes as Weaknesses of ACTB (Actb) and GAPDH (Gapdh) Used as Reference Genes in Reverse Transcription and Polymerase Chain Reactions.” *PLOS ONE* 7 (8): e41659.
<https://doi.org/10.1371/journal.pone.0041659>.
 196. Sun, Yujiao Jennifer, J. Sebastian Espinosa, Mahmood S. Hoseini, and Michael P. Stryker. 2019. “Experience-Dependent Structural Plasticity at Pre- and Postsynaptic Sites of Layer 2/3 Cells in Developing Visual Cortex.” *Proceedings of the National Academy of Sciences* 116 (43): 21812–20.
<https://doi.org/10.1073/pnas.1914661116>.
 197. Svec, David, Ales Tichopad, Vendula Novosadova, Michael W. Pfaffl, and Mikael Kubista. 2015. “How Good Is a PCR Efficiency

- Estimate: Recommendations for Precise and Robust qPCR Efficiency Assessments.” *Biomolecular Detection and Quantification* 3 (March):9–16. <https://doi.org/10.1016/j.bdq.2015.01.005>.
198. Takesian, Anne E., and Takao K. Hensch. 2013. “Balancing Plasticity/Stability across Brain Development.” *Progress in Brain Research* 207:3–34. <https://doi.org/10.1016/B978-0-444-63327-9.00001-1>.
 199. Tang, Yunshuo, Michael P. Stryker, Arturo Alvarez-Buylla, and Juan Sebastian Espinosa. 2014. “Cortical Plasticity Induced by Transplantation of Embryonic Somatostatin or Parvalbumin Interneurons.” *Proceedings of the National Academy of Sciences of the United States of America* 111 (51): 18339–44. <https://doi.org/10.1073/pnas.1421844112>.
 200. Taylor, Anne M., Mathew Blurton-Jones, Seog Woo Rhee, David H. Cribbs, Carl W. Cotman, and Noo Li Jeon. 2005. “A Microfluidic Culture Platform for CNS Axonal Injury, Regeneration and Transport.” *Nature Methods* 2 (8): 599–605. <https://doi.org/10.1038/nmeth777>.
 201. The Galaxy Community. 2022. “The Galaxy Platform for Accessible, Reproducible and Collaborative Biomedical Analyses: 2022 Update.” *Nucleic Acids Research* 50 (W1): W345–51. <https://doi.org/10.1093/nar/gkac247>.
 202. Tropea, Daniela, Ania K. Majewska, Rodrigo Garcia, and Mriganka Sur. 2010. “Structural Dynamics of Synapses in Vivo Correlate with Functional Changes during Experience-Dependent Plasticity in Visual Cortex.” *The Journal of Neuroscience* 30 (33): 11086–95. <https://doi.org/10.1523/JNEUROSCI.1661-10.2010>.
 203. Tso, J. Yun, Xiao-Hong Sun, Teh-hui Kao, Kimberly S. Reece, and Ray Wu. 1985. “Isolation and Characterization of Rat and Human Glyceraldehyde-3-Phosphate Dehydrogenase cDNAs: Genomic Complexity and Molecular Evolution of the Gene +.” *Nucleic Acids Research* 13 (7): 2485–2502. <https://doi.org/10.1093/nar/13.7.2485>.
 204. Tucker, K. L., M. Meyer, and Y. A. Barde. 2001. “Neurotrophins Are Required for Nerve Growth during Development.” *Nature Neuroscience* 4 (1): 29–37. <https://doi.org/10.1038/82868>.
 205. Um, Ji Won, and Jaewon Ko. 2017. “Neural Glycosylphosphatidylinositol-Anchored Proteins in Synaptic

- Specification.” *Trends in Cell Biology* 27 (12): 931–45. <https://doi.org/10.1016/j.tcb.2017.06.007>.
206. Van Driesche, Sarah J., and Kelsey C. Martin. 2018. “New Frontiers in RNA Transport and Local Translation in Neurons.” *Developmental Neurobiology* 78 (3): 331–39. <https://doi.org/10.1002/dneu.22574>.
 207. Villers-Sidani, Etienne de, Edward F. Chang, Shaowen Bao, and Michael M. Merzenich. 2007. “Critical Period Window for Spectral Tuning Defined in the Primary Auditory Cortex (A1) in the Rat.” *Journal of Neuroscience* 27 (1): 180–89. <https://doi.org/10.1523/JNEUROSCI.3227-06.2007>.
 208. Wager, E., N. J. Mangini, and A. L. Pearlman. 1980. “Retinotopic Organization of Striate and Extrastriate Visual Cortex in the Mouse.” *The Journal of Comparative Neurology* 193 (1): 187–202. <https://doi.org/10.1002/cne.901930113>.
 209. Wälchli, Thomas, Jeroen Bisschop, Peter Carmeliet, Gelareh Zadeh, Philippe P. Monnier, Katrien De Bock, and Ivan Radovanovic. 2023. “Shaping the Brain Vasculature in Development and Disease in the Single-Cell Era.” *Nature Reviews Neuroscience* 24 (5): 271–98. <https://doi.org/10.1038/s41583-023-00684-y>.
 210. Weingarten, Jens, Melanie Lassek, Benjamin F. Mueller, Marion Rohmer, Ilaria Lunger, Dominic Baeumlisberger, Simone Dudek, Patricia Gogesch, Michael Karas, and Walter Volkhardt. 2014. “The Proteome of the Presynaptic Active Zone from Mouse Brain.” *Molecular and Cellular Neurosciences* 59 (March):106–18. <https://doi.org/10.1016/j.mcn.2014.02.003>.
 211. Weinhard, Laetitia, Giulia di Bartolomei, Giulia Bolasco, Pedro Machado, Nicole L. Schieber, Urte Neniskyte, Melanie Exiga, et al. 2018. “Microglia Remodel Synapses by Presynaptic Trogocytosis and Spine Head Filopodia Induction.” *Nature Communications* 9 (1): 1228. <https://doi.org/10.1038/s41467-018-03566-5>.
 212. Werker, Janet F., and Takao K. Hensch. 2015. “Critical Periods in Speech Perception: New Directions.” *Annual Review of Psychology* 66 (January):173–96. <https://doi.org/10.1146/annurev-psych-010814-015104>.
 213. White, Erin Jacquelyn, Stefanie Andrea Hutka, Lynne J. Williams, and Sylvain Moreno. 2013. “Learning, Neural Plasticity and Sensitive Periods: Implications for Language Acquisition, Music Training and Transfer across the Lifespan.” *Frontiers in Systems*

<https://doi.org/10.3389/fnsys.2013.00090>.

214. Whittaker, V. P., I. A. Michaelson, and R. Jeanette A. Kirkland. 1964. "The Separation of Synaptic Vesicles from Nerve-Ending Particles ('synaptosomes')." *Biochemical Journal* 90 (2): 293–303.
215. Wiederstein, Markus, and Manfred J. Sippl. 2007. "ProSA-Web: Interactive Web Service for the Recognition of Errors in Three-Dimensional Structures of Proteins." *Nucleic Acids Research* 35 (suppl_2): W407–10. <https://doi.org/10.1093/nar/gkm290>.
216. Wiesel, T. N., and D. H. Hubel. 1963a. "EFFECTS OF VISUAL DEPRIVATION ON MORPHOLOGY AND PHYSIOLOGY OF CELLS IN THE CATS LATERAL GENICULATE BODY." *Journal of Neurophysiology* 26 (November):978–93. <https://doi.org/10.1152/jn.1963.26.6.978>.
217. ———. 1963b. "SINGLE-CELL RESPONSES IN STRIATE CORTEX OF KITTENS DEPRIVED OF VISION IN ONE EYE." *Journal of Neurophysiology* 26 (November):1003–17. <https://doi.org/10.1152/jn.1963.26.6.1003>.
218. Wilhelm, Benjamin G., Sunit Mandad, Sven Truckenbrodt, Katharina Kröhnert, Christina Schäfer, Burkhard Rammner, Seong Joo Koo, et al. 2014. "Composition of Isolated Synaptic Boutons Reveals the Amounts of Vesicle Trafficking Proteins." *Science (New York, N.Y.)* 344 (6187): 1023–28. <https://doi.org/10.1126/science.1252884>.
219. Wilkinson, Leland. 2011. "Ggplot2: Elegant Graphics for Data Analysis by WICKHAM, H." *Biometrics* 67 (2): 678–79. <https://doi.org/10.1111/j.1541-0420.2011.01616.x>.
220. Williams, Alex H., Cian O'Donnell, Terrence J. Sejnowski, and Timothy O'Leary. 2016. "Dendritic Trafficking Faces Physiologically Critical Speed-Precision Tradeoffs." *eLife* 5. <https://doi.org/10.7554/eLife.20556>.
221. Wilton, Daniel K., Lasse Dissing-Olesen, and Beth Stevens. 2019. "Neuron-Glia Signaling in Synapse Elimination." *Annual Review of Neuroscience* 42 (July):107–27. <https://doi.org/10.1146/annurev-neuro-070918-050306>.
222. Wong, Thian-Sze, Wei Gao, Geng Chen, Chen Qiu, Guodong He, Fang Ye, Zhangsong Wu, Zicheng Zeng, and Yang Du. 2023. "Cryo-EM Structure of Orphan G Protein-coupled Receptor GPR21." *MedComm* 4 (1): e205. <https://doi.org/10.1002/mco2.205>.

223. Xiao, Yan, Luigi Petrucco, Laura J. Hoodless, Ruben Portugues, and Tim Czopka. 2022. "Oligodendrocyte Precursor Cells Sculpt the Visual System by Regulating Axonal Remodeling." *Nature Neuroscience* 25 (3): 280–84. <https://doi.org/10.1038/s41593-022-01023-7>.
224. Ye, Hong, Baihong Li, Vivekanandan Subramanian, Bo-Hwa Choi, Yu Liang, Amaravadhi Harikishore, Goutam Chakraborty, Kwanghee Baek, and Ho Sup Yoon. 2013. "NMR Solution Structure of C2 Domain of MFG-E8 and Insights into Its Molecular Recognition with Phosphatidylserine." *Biochimica Et Biophysica Acta* 1828 (3): 1083–93. <https://doi.org/10.1016/j.bbamem.2012.12.009>.
225. Yeung, Tony, Gary E. Gilbert, Jialan Shi, John Silvius, Andras Kapus, and Sergio Grinstein. 2008. "Membrane Phosphatidylserine Regulates Surface Charge and Protein Localization." *Science (New York, N.Y.)* 319 (5860): 210–13. <https://doi.org/10.1126/science.1152066>.
226. Yeung, Tony, Bryan Heit, Jean-Francois Dubuisson, Gregory D. Fairm, Basil Chiu, Robert Inman, Andras Kapus, Michele Swanson, and Sergio Grinstein. 2009. "Contribution of Phosphatidylserine to Membrane Surface Charge and Protein Targeting during Phagosome Maturation." *The Journal of Cell Biology* 185 (5): 917–28. <https://doi.org/10.1083/jcb.200903020>.
227. Younts, Thomas J., Hannah R. Monday, Barna Dudok, Matthew E. Klein, Bryen A. Jordan, István Katona, and Pablo E. Castillo. 2016. "Presynaptic Protein Synthesis Is Required for Long-Term Plasticity of GABA Release." *Neuron* 92 (2): 479–92. <https://doi.org/10.1016/j.neuron.2016.09.040>.
228. Zhang, Li I., Shaowen Bao, and Michael M. Merzenich. 2002. "Disruption of Primary Auditory Cortex by Synchronous Auditory Inputs during a Critical Period." *Proceedings of the National Academy of Sciences of the United States of America* 99 (4): 2309–14. <https://doi.org/10.1073/pnas.261707398>.
229. Zhou, Yanmei, Baoling Lai, and Wen-Biao Gan. 2017. "Monocular Deprivation Induces Dendritic Spine Elimination in the Developing Mouse Visual Cortex." *Scientific Reports* 7 (1): 4977. <https://doi.org/10.1038/s41598-017-05337-6>.
230. Zhu, Na, Charles A. LeDuc, Ilene Fennoy, Blandine Laferrère, Claudia A. Doege, Yufeng Shen, Wendy K. Chung, and Rudolph L. Leibel. 2023. "Rare Predicted Loss of Function Alleles in

Bassoon (BSN) Are Associated with Obesity.” *Npj Genomic Medicine* 8 (1): 1–6. <https://doi.org/10.1038/s41525-023-00376-7>.

SANTRAUKA

Įvadas

Normaliam smegenų vystymuisi labai svarbūs yra kritiniai laikotarpiai (KL), kuriems būdingas padidėjęs sinapsinis plastiškumas, palengvinantis struktūrinius ir funkcinis tinklo pokyčius reaguojant į aplinkos dirgiklius. Dėl šio sustiprėjusio plastiškumo kritiniu laikotarpiu patirtys yra labai svarbios ugdant sudėtingus įgūdžius, tokius kaip kalba ir muzikiniai gebėjimai. Šiuos gebėjimus suaugus tampa sunkiau išugdyti dėl stabilesnių nervinių tinklų (Skoe ir Kraus 2013; White et al. 2013; Hartshorne, Tenenbaum, ir Pinker 2018). Kai kritinis laikotarpis baigiasi sinapsinis plastiškumas žymiai susilpnėja. Naujausi tyrimai rodo, kad šiam procesui reguliuoti svarbi yra neuronų sąveika su glijos ląstelėmis, signalo slopinimo ir sužadavimo pusiausvyra, mielino dangos ir perineuroninių tinklų susidarymas bei lokali baltymų gamyba sinapsėse (Takesian and Hensch 2013; Schafer et al. 2012; Reichelt et al. 2019; Stedehouder et al. 2018; Rajgor, Welle, and Smith 2021). Kritiniu vystymosi laikotarpiu taip pat svarbus yra greitas sinapsių atsiradimas ir pašalinimas, kuris priklauso nuo tam tikrų „valgyk mane“ ir „nevalgyk manęs“ molekulinį signalų. Keletas tokių žinomų signalų yra į išorinę plazminės membranos pusę perkeltas fosfatidilserinas (FS) ir komplemento sistemos opsoninai C1q ir C3, kuriuos atpažįsta mikroglijos ląstelės (Mordelt and de Witte 2023). Sinapsinio plastiškumo reguliavime svarbų, tačiau menkai ištirtą vaidmenį, atlieka lokali baltymų sintezė sinapsėse. Neuronų struktūra yra sudėtinga dėl savo poliarizacijos ir ilgų projekcijų. Dėl to lokali baltymų gamyba presinapsiniuose ir posinapsiniuose galuose jiems yra reikalinga, kad būtų greitai atnaujinamas vietinis proteomas užtikrinant greitus funkcinis pokyčius itin plastišku kritiniu laikotarpiu (Rajgor, Welle, and Smith 2021). Nepaisant to, lokalūs biocheminiai pokyčiai sinapsėse, kurie lemia sinapsių išsaugojimą ar šalinimą, yra menkai suprasti.

Tyrinėti lokalią baltymų sintezę ir sinapsines informacines RNR (iRNR) anksčiau buvo itin sudėtinga dėl aksonų gležnumo ir dėl sunkumų išskiriant ir surenkant grynus aksonų mėginius. Sinaptosomų (išskirtų nervinių galūnių) mėginiai buvo naudingi tiriant sinapses ir lokalią baltymų sintezę, nepaisant to, kad šie mėginiai nebūdavo grynai ir turėdavo gana daug įvairių nesinapsinių priemaišų (Bai and Witzmann 2007; Burré, Zimmermann, and Volkandt 2007; Boyken et al. 2013; Weingarten et al. 2014; Wilhelm et al. 2014). Fluorescencija Pagrįstas Sinaptosomų Rūšiavimas (FPSR, angl. *Fluorescence Activated Synaptosome Sorting, FASS*) stipriai pagerino išskiriamų sinapsinių

mėginių specifiškumą ir grynumą. Tai lėmė tikslesnių duomenų gavimą apie lokalią baltymų sintezę sinapsėse ir sinapsėms būdingus baltymus (Biesemann et al. 2014). Vis dėlto, iki šios trūksta kokybės kontrolės metodų tokiems mėginiams vertinti. Pavyzdžiui, įprastai RNR kokybė ir vientisumas yra vertinamas pagal ribosominę RNR (rRNR). Tačiau, įvairiems genų raiškos tyrimams, tarp jų ir lokaliai sinapsių transkriptomui, daug svarbiau yra įvertinti baltymus koduojančios iRNR kokybę ir degradacijos laipsnį. Kadangi rRNR ir iRNR turi skirtingą struktūrą ir funkcijas, prielaida, kad iš rRNR kokybės ir vientisumo galima spręsti apie iRNR kokybę gali būti neteisinga (Fleige and Pfaffl 2006; Sidova et al. 2015; Sonntag et al. 2016). Be to, priešingai nei RNR išskirta iš audinio, ląstelių dalių preparatai tokie kaip sinaptosomos turi reikšmingai mažiau rRNR, dėl ko tradiciniai RNR kokybės vertinimo metodai tokiems mėginiams negali būti panaudoti. Taip pat, kadangi yra žinoma, jog įvairūs molekuliniai signalai ant sinapsių yra labai svarbūs tinklo remodeliavimui, labai reikalingi yra nauji ypatingai jautrūs įrankiai tyrinėti šių signalų dalyvavimą sinapsinio plastiškumo procesuose. Genetiškai koduojami biojutikliai yra būtini tokių signalų kaip FS vizualizavimui ant sinapsių išorės. Vienas iš kandidatų tokiam įrankiui kurti yra prie FS efektyviai ir specifiškai prisikabinantis C2 domenas, kuris yra MFG-E8 baltymo dalis (Reddy Nanga, Vivekanandan, and Yoon 2007; Ye et al. 2013). Nauji ir patobulinti kokybės kontrolės metodai ir biojutikliai daug prisidėtų prie detalesnių ir tikslesnių lokalių baltymų sintezės ir sinapsių genėjimo tyrimų kritiniu nervų sistemos plastiškumo laikotarpiu.

Tyrimo tikslas

Šio tyrimo tikslas buvo apibūdinti lokalų transkriptomą ir jo pokyčius sužadinaimosiose pelių regos žievės sinapsėse kritiniu vystymosi laikotarpiu ir sukurti įrankį, kuris leistų pažymėti ir tirti šalinamas sinapses.

Uždaviniai

1. Apibūdinti aksonų gumbelių dinamiką ir pritaikyti FPRS sinapsinio transkriptomo tyrimui kritiniu vystymosi laikotarpiu pelės regos žievėje.
2. Sukurti metodą tiesioginiam informacinės RNR kokybės vertinimui, kuris būtų tinkamas sinaptosomų mėginiams neturintiems didelio ribosominės RNR kiekio.
3. Apibūdinti lokalaus sinapsių transkriptomo pokyčius pelės regos žievės vystymosi metu.
4. Sukurti genetiškai koduojamą fosfatidilserino žymėjimo įrankį, kuris leistų žymėti ir tirti žievės vystymosi metu šalinamas sinapses.

Gyvūnai

Tyrimė naudojamos pelės buvo gautos iš Gyvybės Mokslų Centre veisiamų pelių kolonijų. *VGLUT1^{mVenus}* pelės buvo naudotos homozigotinės. *Thy1::EGFP;Cx3cr1::CreER;RC::LSL-tdTomato* trigubai transgeninės pelės buvo naudojamos homozigotinės pagal *Thy1::EGFP* ir heterozigotinės pagal *Cx3cr1::CreER* ir *RC::LSL-tdTomato*. *Thy1::EGFP* pelės buvo naudotos heterozigotinės. RNR integralumo tyrimui, C57BL/6 pelių smegenys buvo surinktos atlikus cervikalinę dislokaciją. Tuomet reikalinga smegenų žievės dalis buvo išpjauta ir homogenizuota su Trizol reagentu. Surinkti smegenų mėginiai buvo laikomi -80 °C šaldiklyje, kol išskirta RNR. 21, 28 ir 35 dienų amžiaus *VGLUT1^{mVenus}* pelės buvo naudojamos sinaptosomų išskyrimui. Tyrimai su gyvūnais buvo atlikti laikantis 2010/63/EU direktyvos ir patvirtinti Lietuvos maisto ir veterinarijos tarbybos (Leidimo Nr. G2-92).

Pelių smegenų pjūvių ruošimas

21, 28 ir 35 dienų amžiaus *Thy1::EGFP;Cx3cr1::CreER;RC::LSL-tdTomato* pelės buvo anestezuotos intraperitonine injekcija naudojant 2.5% Avertin (Sigma-Aldrich) ir perfuzuotos su 4% paraformaldehido (PFA) tirpalu. Išimtos smegenys buvo toliau fiksuotos laikant jas per naktį 4% PFA tirpale 4 °C. Koronaliniai 100 µm smegenų pjūviai buvo surinkti naudojant vibratomą (Leica Microsystems) ir permeabilizuoti PBS tirpalu su 20% normalaus ožkos serumu ir 0.4% Triton X-100 laikant pjūvius tirpale dvi valandas kambario temperatūroje.

Fluorescencinis vaizdinimas ir kiekybinis vertinimas

Fluorescuojančiam aksonuose esančiam EGFP vaizdinimui ir C1q žymėjimui ir vaizdinimui koronaliniai *Thy1::EGFP;Cx3cr1::CreER;RC::LSL-tdTomato* pelių smegenų pjūviai buvo nudažyti naudojant DAPI (1 µg/ml), pirminius triušio anti-C1q antikūnus (ab182451) ir antrinius monokloninius Alexa Fluor Plus 647 antikūnus prieš triušį (A32733). Nudažyti pjūviai fiksuoti naudojant Mowiol. Smegenų pjūviai vaizdinti naudojant TCS SP8 rezonansinį skenerio konfokalinį mikroskopą (Leica Microsystems) naudojant 63×/1.4NA įmersinį aliejaus objektyvą. Aksonų gumbelių dydžio ir C1q žymėjimo vertinimui pagal z-sukrauti vaizdai, apimantys aksoną regos žievės 2/3 sluoksnyje, buvo gauti su 0,3 µm z žingsniu. Vaizdai buvo išanalizuoti naudojant optimizuotą dvejetainiu būdu apdoroto vaizdo analizę su ImageJ programa. Po fono apdorojimo buvo apskaičiuotas vidutinis aksono šakos intensyvumas ir

padaugintas iš 1, 4. Tada pritaikius „Watershed“ ir „Fill holes“ funkcijas, funkcijų „Analizuoti daleles“ dydžio ir apvalumo parametrai buvo nustatyti nuo 0,06 iki begalybės ir nuo 0,02 iki 1,00, kad būtų galima apskaičiuoti gumbelių dydį ir tankį. Kiekvienoje amžiaus grupėje (P21, P28 ir P35) buvo išanalizuota 180 vaizdų, kur 30 vaizdų išanalizuoti iš kiekvienos pelės. Šie eksperimentai buvo atlikti kartu su bakalauru studente Monika Kušeliauskyte.

PGK1 kopijinės DNR (kDNR) plazmidžių ruošimas

Pelės *PGK1* kDNR fragmentai buvo nukopijuoti ir padauginti naudojant PGR iš pelės smegenų RNR mėginio. Naudoti pradmenys: *Pgk1_For_MMPCR*: 5'- GGAGGCCCGGCATTCTGCAC-3' ir *Pgk1_Rev_MMPCR*: 5'- ACCGCCCCCAGTGCTCACATG-3'. PGR padauginti fragmentai tada buvo įklijuoti į pJET1.2 plazmidę bukais galais naudojant CloneJET PGR klonavimo rinkinį (Thermo Scientific). Plazmidėms, kurios turėtų tik 3' *PGK1* kDNR galą, sukurti, 5' galas nuo amplifikuoto pilno ilgio *PGK1* kDNR fragmento buvo nukirptas naudojant *NcoI* restriktazę. Visos plazmidės eksperimentams buvo linearizuotos naudojant *XhoI* restriktazę.

Sinaptosomų ruošimas

Pelės smegenys buvo nuplautos ir atvėsintos lediniame PBS tirpale. Visi tolesni veiksmai buvo atlikti ant ledo. Pelės regos žievė buvo išpjauta ir įdėta į 2 ml švarų ledo šaltumo stiklo-Teflono homogenizavimo indą. Audinys buvo homogenizuojamas 1 ml šalto 32 M sukrozės tirpalo (0.32 M sukrozės, 4 mM HEPES, 4 U/μL Ribolock, pH 7.4) tefloninę piestelę sukančią 900 rpm apsisukimų greičiu 15 s. Gautas žievės homogenatas buvo nucentrifuguotas 1000×g, 5 min 4 °C. Atskirtas supernatantas centrifuguotas 12,500×g, 8 min, 4 °C. Antrą kartą gautas supernatantas pašalintas, o gautos nuosėdos buvo sumaišytos su 0.3 ml šaltu 0.32 M sukrozės tirpalu. Sukrozės gradientas paruoštas 5 ml ultracentrifuginiuose mėgintuvėliuose (Beckman Coulter, C14279), kurių dugne buvo 2 ml 1.2 M sukrozės tirpalo (1.2 M sukrozės, 4 mM HEPES, 0.2 U/μL Ribolock, pH 7.4), o viršuje 2 ml 0.8 M sukrozės tirpalo (0.8 M sukrozės, 4 mM HEPES, 0.2 U/μL Ribolock, pH 7.4). Sumaišytos nuosėdos buvo užlietos ant paruošto sukrozės gradiento. Mėgintuvėliai buvo ultracentrifuguoti 24,000 rpm, 45 min, 4 °C. Po ultracentrifugavimo 1.2 M ir 0.8 M sukrozės tirpalų sandūroje buvo sinapsinių dalelių sluoksnis, kuris surinktas mėgintuvėlį praduriant ir sinaptosomas surenkant su švirkštu. Surinktos sinaptosomos buvo atskiestos su 8 ml šalto PBS tirpalo. Pusė paruošto mėginio buvo sukonzentruota ant 0.1 μm polikarbonatinio filtro. Filtras tada nuplautas su Trizol reagentu mėginio

laikymui ir vėlesniam RNR gryninimui. Likusi gautų sinaptosomų dalis buvo panaudota Fluorescencija Pagrįstam Sinaptosomų Rūšiavimui (FPSR).

Fluorescencija Pagrįstas Sinaptosomų Rūšiavimas

Paruoštame sinaptosomų mėginyje, kad būtų pagerintas dalelių atpažinimas, visos membrininės dalelės buvo nudažytos naudojant SynaptoRed C2 (1 µg/ml, Tocris Bioscience). Mėginio skiedimas su šaltu PBS buvo kiekvieną kartą koreguojamas, kad rūšiavimo metu prietaisas detektuotų apie 15 000 įvykių per sekundę, kai tėkmės greitis yra nuo 3 iki 4. Naujas mėginys sortiravimui buvo paruošiamas kas 45 min. Sinaptosomų rūšiavimas buvo atliktas, kaip aprašyta anksčiau (Luquet et al. 2017). Sortiravimui naudotas BD FACSAria III ląstelių rūšioklis. Naudoti prietaiso parametrai: 70 µm Nozlas, mėginys purtytas 300 rpm dažniu, palaikyta 4 °C temperatūra, FSC neutralaus tankio filtras 1.0, 488 nm, kai lazeris įjungtas, ploto mastelio keitimas 1.18, Lango pratesimas 0.0, FSC ploto mastelio keitimas 0.96, rūšiavimo tikslumas: 0-16-0. Slenkstinė SynaptoRed C2 fluorescencijos riba laikyta 800. Sinaptosomos rūšiuotos į 5 ml polistireninius mėgintuvėlius apvaliu dugnu ir laikytos ant ledo. Sinaptosomos rūšiuotos ir rinktos bent 6 val. Tuomet sinaptosomos buvo sukonzentruotos ant 0.1 µm polikarbonatinio filtro ir nuplautos bei surinktos naudojant Trizol reagentą.

RNR išskyrimas

Bendra RNR iš pelės žievės, bendro ar rūšiuotų sinaptosomų mėginio buvo išskirta naudojant TRIzol Plus RNR išskyrimo rinkinį su fazių atskyrimo mėgintuvėliais (Invitrogen, cat. no. A33254). Po gryninimo likusios genominės DNR priemaišos buvo iš RNR mėginio pašalintos naudojant TURBO DNA-free rinkinį (Invitrogen, cat. no. AM1907) naudojantis gamintojo rekomendacijomis.

Karščių suardytų RNR mėginių ruošimas

RNR mėginiai iš pelės žievės buvo atskiesti iki 100 ng/µl koncentracijos ir išpilstyti po 12 µl. Kontrolinis mėginys buvo pakaitintas 70 °C 2 min RNR išlydymui. Kiti mėginiai buvo kaitinti 90 °C temperatūroje 1, 2, 3, 4, 5, 10, arba 15 min.

RNR koncentracijos ir rRNR integralumo vertinimas

NanoDrop 2000 Spektrofotometras (Thermo Fisher Scientific, Waltham, MA USA) buvo naudojamas įvertinti RNR koncentraciją. rRNR integralumas buvo vertinamas naudojant Agilent 2100 Bioanalyzer sistemą ir Agilent RNA

6000 Pico Rinkinį (Part Number: 5067-1513) (Agilent Technologies, Mississauga, ON, Canada) vadovaujantis gamintojo nurodymais.

Kopijinės DNR (kDNR) sintezė ir realaus laiko kiekybinė PGR

Atvirkštinė transkripcija buvo vykdoma 20 µl tūrio reakcijose, kurias sudarė 1 µg RNR, 2.5 µg Inkaruotų Oligo-dT pradmenų (Invitrogen), 0.5 mM dNTP Mišinio (Thermo Scientific) ir 200 U Thermo Scientific Maxima Atvirkštinės Transkriptazės naudojantis gamintojo nurodymais. Gauti kDNR mėginiai buvo atskiesti vandeniu iki 20 ng/µl koncentracijos.

Kiekybinė PGR (kPGR) buvo atlikta naudojantis The StepOne™ Real-Time PCR Sistema arba QuantStudio™ 3 Sistema (Applied Biosystems™). Reakcijoms naudoti 5 µl paruoštos kDNR, 0.3 µM pirminio ir atvirkštinio pradmenų, 12.5 µl 2× Thermo Scientific Maxima SYBR Green/ROX qPCR Master Mišinio (Thermo Scientific) ir 2.5 µl vandens. Bendras reakcijos tūris - 25 µl. kPGR reakcijų mišiniai buvo išlydyti 95 °C laikant 10 min ir tuomet vykdyta 40 padauginimo ciklą (15 s išlydymas 95 °C, 30 s pradmenų prikibimas 60 °C ir 30 s prailginimas 72 °C). Visos reakcijos turėjo tris pakartojimus.

Kitos kartos RNR sekoskaita

Bendra RNR iš Trizol reagento saugotų sinaptosomų buvo išskirta naudojant „RNA clean and Concentrator-5“ rinkinį (Zymo). RNR sekoskaitos bibliotekos buvo sukurtos naudojant SmartSeq2 protokolą. Šis protokolas buvo pasirinktas dėl didelio patikimumo ir efektyvumo ruošiant bibliotekas su mažais pradinės RNR kiekiais (Picelli et al. 2014; Hennig et al. 2018). Dvidešimt penki µl vandens be nukleazų buvo naudoti eliuavimui. Iš gautos RNR 10 µl tada buvo panaudoti sekoskaitos bibliotekai sukurti. Dvidešimt du PGR ciklai buvo naudoti bibliotekos pagausinimui. Galiausiai gautos ~500 bp dydžio kDNR fragmentų bibliotekos. Kiekvienam mėginiui buvo priskirtas unikalus barkodas. Sekoskaita atlikta visų mėginių bibliotekoms vienu metu naudojant Illumina NextSeq 2000 Sistemą. Visi sekoskaitos žingsniai atlikti EMBL GeneCore padalinyje Heidelberge, Vokietijoje.

RNR sekoskaitos duomenų analizė

Gautų sekų sulysinimas su genomu

Sulyginimui naudotas GRCm39 pelės genomas iš Genomo Nuorodos Konsorciumo (GCA_000001635.9). Reikalingas genomu failas GTF formatu parsisiųstas iš Ensembl duomenų bazės. Sekų sulysinimas atliktas naudojant STAR bioinformatinį įrankį (Dobin et al. 2013).

Skaičių matricos sukūrimas

Sekos buvo suskaičiuotos ir skaičių matrica sukurta naudojant featureCounts įrankį Galaxy EU platformoje (The Galaxy Community 2022).

Raiškos normalizavimas

Raiška buvo normalizuota apskaičiuojant transkriptus per milijoną (TPM). Pirmiausia buvo apskaičiuotas bibliotekos dydis ir sekų skaičiai buvo normalizuojami naudojant calcNormFactors funkciją. Tuomet cpm funkcija panaudota apskaičiuoti sekas per milijoną. TPM tada buvo apskaičiuoti padalijant sekas per milijoną iš mastelio koeficiento.

Raiškos skirtumų analizė

Raiškos skirtumų analizė buvo atlikta naudojant DESeq2 įrankį R programine kalba (Love, Huber, and Anders 2014). Raiškos skirtumai buvo vizualizuoti su volkano grafikais naudojantis ggplot2 įrankiu.

Genų Ontologija

Genų Ontologijos analizė atlikta naudojant GOrilla (angl. *Gene Ontology enrichment analysis and visualization*) įrankį (Eden et al. 2009). Šiai analizei genai buvo sureitinguoti pagal raiškos skirtumų dydį tarp grupių naudojant du kartus didesnę raišką kaip ribinę vertę.

C2 klonavimas ir suliejimas su žymenimis

Rekombinantinių baltymų raiškai baltymų sekos buvo įklonuotos į pET-21a(+) plasmides. C2 domeno atviro skaitymo rėmelis buvo padaugintas nuo pelės audinio DNR mėginio naudojant Thermo Scientific Phusion Flash High-Fidelity PGR Master Mišinį, vadovaujantis gamintojo rekomendacijomis. pET-C2 plasmidės buvo gautos sujungiant NdeI ir HindIII restriktazėmis sukarpytą pET21a(+) vektorių ir C2 PGR produktą. Baltymų sujungimui buvo įterpta lanksti peptidinė seka (Chen, Zaro, and Shen 2013). SNAP-tag genas buvo padaugintas nuo plazmidės gautos iš Heppenstall (Dhandapani et al. 2018). Pagausintos SNAP-tag sekos buvo įklijuotos į pET-21a(+) plazmidę po apkarpyimo su HindIII ir XhoI restriktazėmis.

C2 domeno mutavimas

Tam kad būtų gautas neaktyvus C2 domenas, Lys24 ir Lys45 aminorūgštys buvo pakeistos asparagais. Lys24 aminorūgštis pakeista naudojant specifinius PGR pagausinimui skirtus pradmenis (F: 5'-CAGCTACAATACATGGAACC-3' ir R: 5'-CTGGAGGCTGACATCTGGCT-3') ir Thermo Scientific Phusion Flash High-Fidelity PGR mišinį. Analogiškai viskas buvo atlikta ir Lys45 aminorūgščiai pakeisti naudojant specifinius pradmenis (F: 5'-TCAGGGCAATATCAATGCCT-3' ir R: 5'-TTATCCAGCCTTCCCAAGTG-3').

pAAV plazmidžių gavimas

Plazmidės reikalingos virusams pasigaminti buvo sukurtos taip, kad turėtų astroцитams specifinį promotorių GFAP, kurio seka gauta iš pAAV-GFAP-mKate plazmidės (Addgene plasmid #99129, RRID:Addgene_99129). Signalinė peptidų seka buvo pridėta, kad būtų užtikrinta konstrukto sekrecija į aplinką (UniProtKB/Swiss-Prot Accession Number: P21956).

Baltymų raiška ir gryninimas

Rekombinantinėmis pET21a-C2-SNAP arba pET21a-C2m2-SNAP raiškos plazmidėmis buvo transformuotos ArcticExpress (DE3) *E. coli* ląstelės. Transformuotos kolonijos atrinktos lėkštelėse su ampicilinu (100 µg/ml). Rekombinantinių baltymų raiška buvo sukelta į auginimo terpę pridedant 1.0 mM (IPTG) ląsteles auginant 16 °C temperatūroje su purtymu. Po 16 valandų auginimo ląstelės surinktos centrifuguojant 3000 × g greičiu 20 min, 4 °C temperatūroje. Nuosėdos suardytos naudojant BANDELIN SONOPULS mini20 prietaisą su VS70T sonikavimo galu ardant 5 min su 50% amplitude. Po ardymo ląstelių nuosėdos atskirtos centrifuguojant 3000 × g greičiu 25 min, 4 °C. Rekombinantinių baltymų tirpumas buvo patikrintas su 14% SDS-PAGE. Rekombinantiniai baltymai gauti iš biomasės tirpios frakcijos, buvo išgryninti naudojant HisPur™ Ni-NTA (Thermo Scientific) kolonėles ir ÄKTATM avant 25 chromatografijos sistemą (Cytiva). Išgryninti baltymai sukonzentruoti naudojant Amicon® Ultra-4 mėgintuvėlius 10 kDa (Millipore) ir 20 mM NaPO₄, 20 mM NaCl tirpalą, pH 6.5. Baltymų koncentracija pamatuota naudojant NanoDrop™ 2000 (Thermo Scientific).

Žinduolių ląstelių auginimas

Neuro2a (RRID:CVCL_0470) ląstelių linija nusipirkta iš Amerikos Tipinių Kultūrų Kolekcijos (angl. *American Type Culture Collection, ATCC*). Pelės neuroblastomos Neuro2a ląstelės buvo auginamos DMEM terpėje su 10% FBS, 100 U/ml penicilino ir 100 µg/ml streptomicino. Ląstelių kultūros buvo laikomos 37 °C temperatūroje su 5% CO₂. Ląstelės buvo surinktos naudojant TrypLE™ tirpalą. FS ekspozicijos stebėjimui, ląstelės buvo užsėtos 400 ląstelių/mm² tankiu 8-šulinėlių lėkštelėse (Nunc™ Lab-Tek™, Thermo Scientific). Lėkštelės buvo padengtos poli-L-lizinu (0.001% PBS tirpale) inkubuojant 20 min kambario temperatūroje (KT).

Apoptozės vertinimas

Apoptozė ląstelėms buvo sukelta po 24 h auginimo į terpę pridedant 3 µM staurosporino (Sigma Aldrich) ir inkubuojant su juo 16 h. FS ekspozicija buvo

vertinama pridedant 100 µg/ml rekombinantinio baltymo ir laikant 30 min. Baltymų perteklius buvo pašalintas nuplaunant ląsteles su sušildyta terpe. Tada ląstelės buvo užfiksuotos su 4% paraformaldehidu (PFA) PBS tirpale laikant 20 min KT. Po praplovimo PBS tirpalu, likęs PFA buvo inaktyvuotas su 30 mM glicino PBS ir ląstelės vėl nuplaautos PBS tirpalu. C2-SNAP ir C2m2-SNAP baltymų vizualizavimui, ant ląstelių buvo uždėta 3 µM benzilguanino substrato SNAP-Surface® Alexa Fluor® 647 (NEB), su kuriuo ląstelės inkubuotos 30 min KT. Substrato perteklius buvo pašalintas nuplaunant ląsteles tris kartus su PBS tirpalu bei galiausiai inkubuojant PBS tirpale 30 min. Visos ląstelės buvo nudažytos su DAPI (1 µg/ml) laikant 10 min KT. Tuomet mikroskopinis stiklelis buvo padengtas Mowiol (Calbiochem). Vaizdinimui naudotas konfokalinis Leica TCS SP8 mikroskopas su 63×/1.4 su į aliejų įmerkiamu objektyvu (pixelio dydis 0.481 × 0.481 µm). Diodinis lazeris sužadintas 405 nm bangos ilgiu buvo naudotas DAPI sužadinimui. Baltos šviesos lazeris buvo naudotas AlexaFluor647 (λ = 647 nm) sužadinimui. DAPI fluorescencija buvo surinkta naudojant fotodaugintojo vamzdelinį (PMT) detektorių (415–550 nm). AlexaFluor647 (657–680 nm) fluorescencija surinkta naudojant hibridinį detektorių apribojant ties 0.3–6 ns.

Ląstelių vaizdų analizė

Vaizdai buvo analizuoti naudojant laisvai prieinamą CellProfiler programinę įrangą (RRID:SCR_007358). Integruota C2 žymeniui specifinė fluorescencija buvo matuojama kiekviename vaizde (n = 10-15 vaizdų kiekvienai sąlygai, nepriklausomi eksperimentai atlikti po du kartus). Intensyvumas buvo apskaičiuotas kiekvienai ląstelei padalinant vaizdo fluorescencijos intensyvumą iš matomų branduolių skaičiaus vaizde. Fluorescencijos skaičiai buvo normalizuoti pagal didžiausią nustatytą C2-SNAP fluorescenciją.

Adeno-asocijuotų virusų gaminimas

Adeno-asocijuoti virusai (AAVs) reiškiantys C2-SNAP žymenis buvo gaminami kaip aprašyta anksčiau (Challis et al. 2019). Virusų surinkimui HEK293T ląstelės buvo užsėtos 6×10⁴ ląstelių/cm² tankiu. Po 24 h ląstelės buvo trasfekuotos trimis plazmidėmis: 1) pAAV plazmidė, kuri turėjo C2 žymens seką, 2) plazmidė koduojanti kapsidei reikalingus baltymus pUCmini-iCAP-PHP.eB (dovana nuo Viviana Gradinaru, Addgene plazmidė #103005; RRID: Addgene_103005), ir 3) pagalbinė plazmidė XX6-80 (gauta iš „The National Gene Vector Biorepository“, NGVB). Plazmidės sumaišytos 1:4:2 santykiu iki 40 µg DNR vienai lėkštei. Trasfekcijai palengvinti naudotas

poliethileniminas (linearizuotas, MW 25 000, Sigma Aldrich). Po 72 h ir vėliau po 120 h transfekcijos ląstelių terpė buvo surenkama ir filtruojama pro 0.45 µm filtrą, kad būtų pašalintos ląstelių priemonės. Surinkta terpė sterilizuota filtruojant su 0.22 µm švirkštiniu filtru. Gautas AAV tirpalas buvo sukonzentruotas jį centrifuguojant su Amicon Ultra Centrifugal Filter Units 100 kDa (Merck Millipore) 3000 × g greičiu 8 min KT. Tada į AAV tirpalą Amicon filtriniame mėgintuvėlyje buvo pridėta DPBS su 0.001% Pluronic F-68 (Thermo Fisher Scientific) ir mėgintuvėlis centrifuguotas 3000 × g greičiu 8 min kambario temp. Plovimai buvo pakartoti tris kartus. Po paskutinio centrifugavimo buvo surinkta 300-500 µl AAV tirpalo. AAV titras buvo nustatytas naudojant kiekybinę PGR.

Sulietų rekombinantinių baltymų struktūros modeliavimas

Sulietų rekombinantinių C2-SNAP baltymų struktūros buvo nuspėtos naudojant *de novo* modeliavimo įrankius Robetta (Baek et al. 2021), RaptorX (Källberg et al. 2012) ir dirbtinio intelekto įrankį AlphaFold 2 (Jumper et al. 2021). Gauti baltymų modeliai buvo įvertinti naudojant VoromQA (Olechnovič and Venclovas 2017), ProSA (Wiederstein ir Sippl 2007), QMEANDisCo (Studer et al. 2020) ir ProQ2 (Ray, Lindahl, ir Wallner 2012) įverčius, pagal kuriuos buvo atrinkti optimalūs modeliai. Šie C2-SNAP modeliai buvo tada palyginti su individualiomis domenų struktūromis iš PDB (C2 – PDB ID:2L9L, SNAP-tag – PDB ID:3KZZ) naudojant PyMOL programą.

Organotipinių hipokampo pjūvių kultūrų ruošimas

Organotipinės hipokampo pjūvių kultūros (OHPK) buvo paruoštos naudojant interfazės metodą, kaip paskelbta anksčiau (Gogolla et al. 2006; De Simoni ir MY Yu 2006). Trumpai, trijų dienų amžiaus *Thy1::EGFP* linijos peliukams buvo atskirta galva atliekant cervikalinę dislokaciją. Išimtos smegenys buvo perkeltos į Petri lėkštelę pripildytą šaltos pjaustymo terpės (100 U/ml penicilino, 100 µg/ml streptomicino, 15 mM HEPES, 0.5% gliukozės HBSS tirpale). Išimti hipokampai buvo supjaustyti 300 µm storiu naudojant McIlwain audinių pjaustymo prietaisą. Gauti pjūviai buvo atsargiai perkelti į paruoštus 0.4 µm 30 mm diametrų ląstelių kultūrų insertus su MCE membrana (Merck Millipore), kurioje buvo palaikomoji terpė (25% 1X BME, 25% arklio serumo, 5 % 10X MEM, 100 U/ml penicilino, 100 µg/ml streptomicino, 2 mM GlutaMAX, 0.65% gliukozė, 9 mM natrio bikarbonato ddH2O). Insertai buvo laikomi 37 °C inkubatoriuje su 5% CO₂. Terpė buvo pakeičiama 24 h po pjūvių paruošimo ir tada kas 2-3 dienas pjūvių palaikymui.

PS žymėjimas naudojant AAV ir OHKP

Penkias dienas *in vitro* (DIV5) laikyti OHKP buvo transdukuoti uždedant 6.7×10^{10} vg AAV-C2-SNAP arba AAV-C2m2-SNAP. Terpė buvo pakeista praėjus dviem dienoms po transdukcijos ir vėliau keista kas 2-3 dienas. DIV14 pjūviai 16 h buvo veikiami 100 μ M staurosporino (Sigma Aldrich) apoptozei sukelti. Po paveikimo pjūviai buvo nuplauti su sušildyta terpe ir 30 min fiksuoti naudojant 4% PFA PBS tirpale KT. Po to pjūviai buvo dar kartą praplauti su PBS tirpalu ir fiksacija sustabdyta naudojant 30 mM glicino/PBS. OHKP, kuriuose vyko C2-SNAP ir C2m2-SNAP raiška, buvo pažymėti pjūvius 2 h KT laikant su 3 μ M benzilguanino substrato SNAP-Surface® Alexa Fluor® 647. Ląstelių branduoliai buvo nudažyti pjūvius 15 min KT palaikant su DAPI (1 μ g/ml). Apoptozės eksperimentai buvo atlikti paruošiant tris nepriklausomas kultūras ir dublikatus kiekvienai sąlygai.

Transdukcija naudojant AAV *in vivo* sistemoje

Tyrimo eiga: Trijų dienų amžiaus (P3) homozigotinės *Thy1::EGFP* pelės gavusios AAV-C2-SNAP injekciją buvo lyginamos su tos pačios vados neinjekuotomis pelėmis (kontrolė). Vadoje 5 pelės gavo AAV-C2-SNAP injekciją ir viena neinjekuota pelė buvo laikoma kaip neigiama kontrolė (iš viso šešios pelės). Injekcijai pelės buvo pasirinktos atsitiktinai. P3 pelėms injekcija buvo atlikta suleidžiant 20 μ l dozę 1×10^{11} vg AAV-C2-SNAP 0.9% fiziologiniame tirpale į veido veną naudojant insulino švirkštą su 29G adata. Po dviejų savaičių (P17) pelėms buvo atlikta perfuzija 2 minutes naudojant 0.9% fiziologinį tirpalą ir 5 minutes naudojant 4% PFA. Išimtos smegenys 24 h fiksuotos 4% PFA ir tuomet supjaustytos 50 μ m storiu naudojant 5100mz vibratomą (Campden Instruments). Smegenų pjūviai buvo nudažyti su 3 μ M SNAP-Surface® Alexa Fluor® 647 dažų ir DAPI (1 μ g/ml). Nudažyti pjūviai užfiksuoti ant mikroskopavimo stiklėlių naudojant Mowiol (Calbiochem). Pjūvių vaizdai gauti naudojant Leica TCS SP8 konfokalinį mikroskopą su 63 \times /1.4 imersiniu aliejaus objektyvu (pikselių dydis $0.18 \times 0.18 \mu$ m).

Statistinė analizė

GraphPad Prism 8 programinė įranga naudota statistinei duomenų analizei. Ryšio tarp tiesinio modelio ir priklausomų kintamųjų stiprumui nustatyti buvo pritaikytas R kvadrato testas. Duomenų rinkinių atitikimas buvo įvertintas naudojant Pearsono koreliaciją. Išskirtys buvo apibrėžtos kaip viršijančios tris tarpkvartilinius diapazonus ir pašalintos iš analizės. Duomenų rinkinių normalumui įvertinti buvo naudojamas Shapiro-Wilk testas. RNR mėginiai iš penkių pelių žievės buvo naudojami RIN ir 5':3' RNR integralumo vertės paltginimui. Keturi bendri ir išrūšiuoti sinaptosomų mėginiai iš keturių

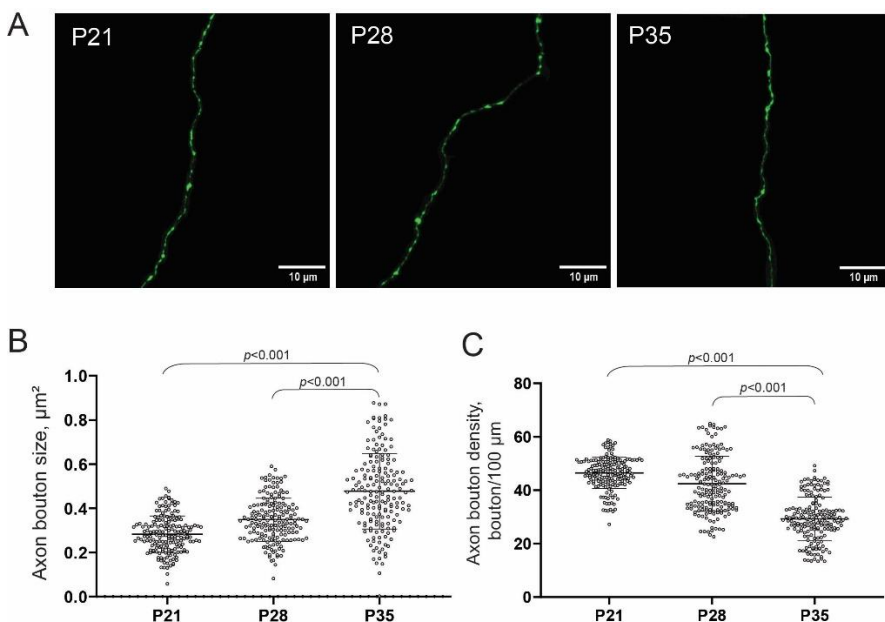
skirtingų gyvūnų buvo naudojami tarpląstelinių mėginių iRNR integralumui vertinti. Eksperimentai su Neuro2a ląstelių kultūromis ir OHKP buvo atlikti ruošiant mažiausiai tris nepriklausomas kultūras. Duomenys iš eksperimentų pateikti kaip vidurkis \pm standartinė vidurkio paklaida. Vidurkiai buvo palyginti naudojant vienpusį ANOVA ir post-hoc Tukey testą. p reikšmės $< 0,05$ buvo laikomos reikšmingomis.

Rezultatai

Aksonų gumbelių pokyčiai žievės brendimo metu

Pelės pirminės regos žievės (V1) kritinis vystymosi laikotarpis prasideda 21 gyvenimo dieną, jautriausias būna apie 28 dieną ir pasibaigia apie 35 dieną. Yra žinoma, jog kritiniu vystymosi laikotarpiu presinapsinių gumbelių formavimasis suintensyvėja, bet tinklui subrendus nuslopsta (Sun et al. 2019). Vis dėlto, iki pat šiol mažai yra žinoma apie aksonų gumbelių morfologiją ir dinamiką normaliu kritiniu vystymosi laikotarpiu. Be to, nors yra duomenų, kad lokali baltymų transliacija yra svarbi sinapsiniam plastiškumui ir morfologiniams pokyčiams, tikslūs šių procesų mechanizmai nėra išaiškinti. Dėl to, vienas iš šio tyrimo tikslų buvo apibūdinti morfologinius aksonų gumbelių pokyčius normaliu V1 kritiniu vystymosi laikotarpiu. Be to, specifinei sinapsių populiacijai išskirti ir lokaliai transkriptomui kritiniu vystymosi laikotarpiu tirti buvo siekiama pritaikyti modernų Fluorescencija Pagrįstą Sinaptosomų Rūšiavimo (FPSR) metodą.

Pirmiausia buvo įvertinti aksonų gumbelių dydžio ir tankio pokyčiai V1 prieš, per ir po kritinio vystymosi laikotarpio. Tam buvo naudota fluorescencinė mikroskopija ir gautų aksonų vaizdų analizė. Šiam tyrimui naudotos pales turėjo pažymėtus pavienius sužadinamuosius neuronus, kur fluorescuojantis EGFP buvo reiškiamas nuo *Thy1* promotoriaus. Tokių pelių smegenys surinktos 21 (prieš kritinį laikotarpį, P21), 28 (kritinio laikotarpio piku, P28) ir 35 (po kritinio laikotarpio, P35) gyvenimo dieną. Naudojant šias smegenis surinkti V1 2/3 sluoksnių aksonų vaizdai, jie išanalizuoti ir apskaičiuoti gumbelių dydžiai bei tankis (**1 pav.**). Statistiškai reikšmingas gumbelių padidėjimas buvo pastebėtas P35, lyginant su P21 ar P28 (ANOVA su *post-hoc* Scheffe testu, $p < 0.01$ ir $p < 0.01$ atitinkamai). Priešingai nei dydis, gumbelių tankis reikšmingai sumažėjo P35 lyginant su P21 arba P28 (ANOVA su *post-hoc* Scheffe testu, $p < 0.01$ and $p < 0.01$ atitinkamai). Šie duomenys patvirtino, kad P21 neuroninis tinklas vis dar yra nesubrendęs ir turi didelį mažų gumbelių tankį. Mažesnis tankis, bet didesni P35 gumbeliai parodė šiam laikotarpiui būdingas stiprias, subrendusias sinapses, o P28 aksonų gumbeliai buvo tarp šių būsenų.

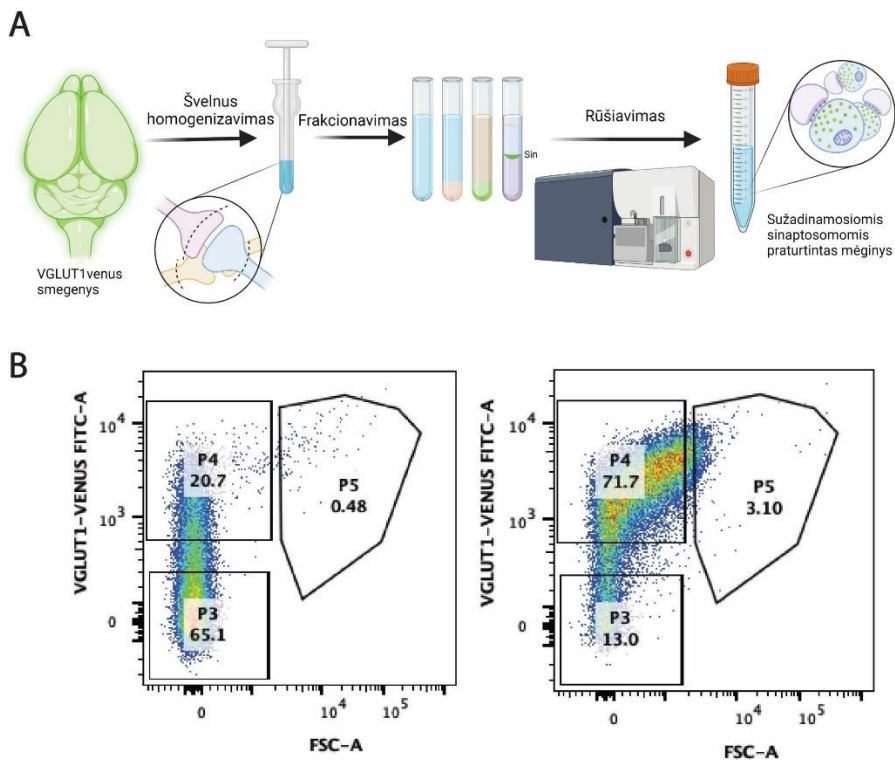


1 paveikslas. Regos žievės gumbelių dydis ir tankis kritiniu laikotarpiu atspindi nesubrendusią, pereinamąją ir subrendusią žievės būseną. A) Reprezentatyvūs 2/3 pelės regos žievės sluoksnio sužadinamųjų neuronų aksonų fluorescenciniai vaizdai P21, P28 ir P35. Skalė 10 μm. **B)** Aksonų gumbeliai padidėjo regos žievės brendimo metu, o tankis sumažėjo **C)**. Kiekvienas taškas reiškia atskirą vaizdą (n=180 kiekvienoje grupėje). ANOVA su *post-hoc* Scheffe testu.

Nors tikslūs mechanizmai, kontroliuojantys kritinį plastiškumo laikotarpį, lieka neaiškūs, naujausi tyrimai pabrėžia lokalsios sinapsinių baltymų transliacijos svarbą. Lokali baltymų transliacija yra procesas, kurio metu sinapsiniai baltymai gaminami pačiuose sinapsiniuose galuose. Sužadinamieji presinapsiniai gumbeliai ir postsinapsiniai spygliukai pastoviai vykdo baltymų sintezę ir šis procesas nuo ląstelės kūno nutolusiose dalyse yra pasitelkiamas, kad sinapsinio plastiškumo metu būtų greitai keičiamas lokalus proteomas (Hafner et al. 2019). Lokali baltymų transliacija leidžia specifiskai kontroliuoti proteomo pokyčius laike ir erdvėje, o tai yra svarbu greitiems sinapsių pokyčiams kritiniu plastiškumo laikotarpiu, kad šios spėtų reaguoti į gaunamus signalus.

Lokalų transkriptomą ir jo reguliavimą galima tirti naudojant sinaptosomas, kurios yra izoliuotų sinapsių mėginiai. Gryną sinaptosomų mėginį galima gauti naudojant genetiškai modifikuotas peles, kuriose sinapsės

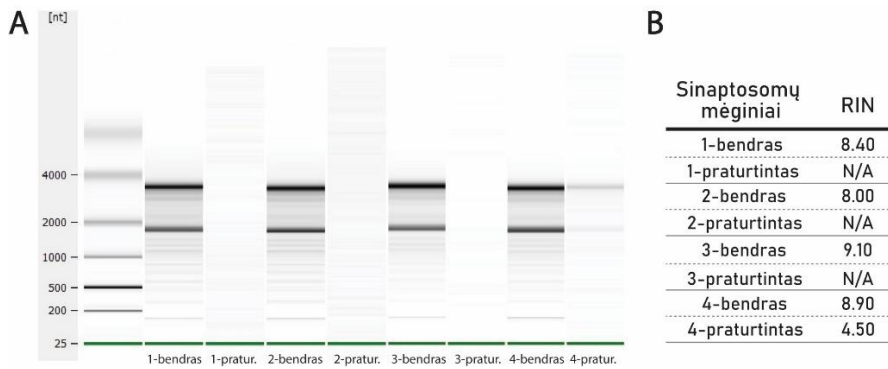
yra fluorescenciškai pažymėtos, kartu su Fluorescencija Pagrįstu Sinaptosomų Rūšiavimo (FPSR) metodu (**2 pav. A**) (Luquet et al. 2017), kuris panaudotas šiame tyrime gryniems sinapsių mėginiams gauti. Šios procedūros metu pelės regos žievė buvo suhomogenizuota, keletą kartų centrifuguota ir galiausiai ultracentrifuguota sacharozės gradientu, kad būtų atskirtas dalelių sluoksnis, kuriame yra sinaptosomos. Sinaptosomos yra labai mažos dalelės (dažniausiai 0,5–2 μm). Dėl to, siekiant padidinti dalelių matomumą ir rūšiavimo efektyvumą, bendras sinaptosomų mėginys buvo nudažytas SynaptoRed C2 lipofiliniu dažu. Bendrame sinaptosomų mėginyje buvo sinaptosomų iš įvairių neuronų tipų ir priemaišų iš kitų ląstelių. Fluorescenciškai pažymėtų sužadinamųjų sinaptosomų rūšiavimas užtikrino, kad surinkti mėginiai bus praturtinti būtent šiomis sinapsėmis. Po rūšiavimo 60–90 % visų dalelių buvo fluorescuojančios mVenus+, palyginti su ~ 20 % bendruose sinaptosomų mėginiuose, o tai rodo reikšmingą sužadinamųjų sinapsių praturtinimą (**2 pav. B**). Tai parodė, kad fluorescencinis sinapsių žymėjimas kartu su FPSR metodu gali būti naudojami išskirti ir surinkti sužadinamųjų sinapsių mėginius.



2 paveikslas. Fluorescencija Pagrįstas Sinaptosomų Rūšiavimas (FPSR) panaudotas gauti sužadinamosiomis sinaptosomomis praturtintus mėginius. A) VGLUT1^{mVenus} pelės smegenų audinys buvo

suhomogenizuotas ir homogenatas nuosekliai frakcionuotas, kad būtų gautos dalelės, kurių dydis ir tankis atitinka sinaptosomas. Tada iš šio bendro sinaptosomų mėginio išrūšiuotos ir surinktos mVenus+ fluorescencuojančios sinaptosomos. Sukurta su Biorender.com. **B)** Sinaptosomų mėginio analizė prieš ir po rūšiavimo. Bendrame sinaptosomų mėginyje buvo ~20% mVenus+ fluorescencuojančių sinaptosomų. Po rūšiavimo pagal mVenus+ fluorescenciją buvo gautas mėginys praturtintas sužadinamosiomis sinaptosomomis, kur jos sudarė daugiau nei 70% visų dalelių.

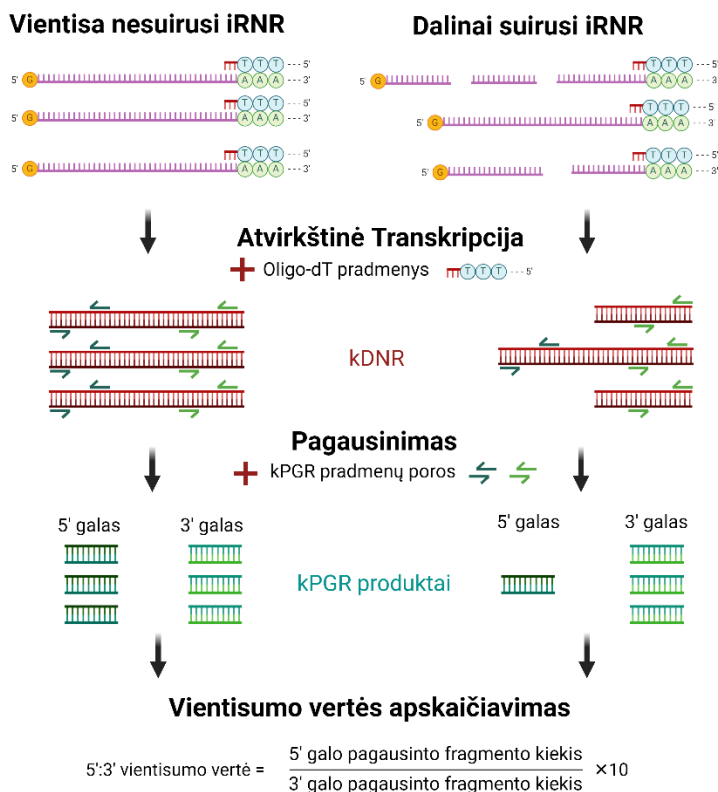
Kitas šio tyrimo žingsnis buvo mVenus+ sinaptosomų mėginių rinkimas transkriptomo analizei. Kadangi sinaptosomų paruošimas yra itin ilga procedūra (maždaug 11-12 h nuo smegenų išėmimo iki rūšiuotų sinaptosomų gavimo) prieš atliekant transkriptomo analizę buvo svarbu įvertinti gautų sinapsinių RNR mėginių kokybę. Šiuo metu tam dažniausiai naudojamas metodas yra RIN vertės apskaičiavimas, kuris nurodo mėginio degradacijos laipsnį. Šio metodo veikimas yra pagrįstas rRNR juostelėmis matomomis po kapiliarinės RNR elektroforezės. Šis metodas buvo panaudotas bendrų ir praturtintų sinaptosomų RNR kokybei įvertinti. Tam panaudoti aštuoni poriniai sinaptosomų mėginiai, iš kurių keturi buvo bendri ir keturi praturtinti sužadinamosiomis sinaptosomomis. Bendrų sinaptosomų RNR mėginių RIN vertės buvo nuo 8.0 iki 9.1, kas rodė gerą RNR kokybę. Vis dėlto, RIN verčių nebuvo įmanoma nustatyti praturtintuose sinaptosomų mėginiuose. Taip nutiko dėl reikšmingai sumažėjusio rRNR kiekio, dėl ko rRNR juostelės nebuvo detektuojamos elektroforezės takeliuose (**3 pav. A**) nepaisant to, kad į takelius buvo įneštas toks pats kiekis RNR mėginio kaip ir bendrų sinaptosomų atveju. Yra žinoma, kad sinaptosomose yra ribosomų, kurios yra reikalingos lokaliai baltymų transliacijai (Hafner et al. 2019). Nepaisant to, sinaptosomose esančios rRNR kiekis buvo per mažas RNR kokybės matavimui naudojant RIN (**3 pav. B**). Šiai problemai spręsti ir sinaptosomų RNR kokybei įvertinti reikėjo alternatyvaus metodo, kuris leistų išmatuoti mėginio RNR vientisumą nepriklausomai nuo rRNR.



3 paveikslas. Sinaptosomų RNR kokybės vertinimas. **A)** Reprezentaciniai mikrokapiliarinės elektroforezės vaizdai iš bendrų ir praturtintų sinaptosomų mėginių RNR kokybės analizės naudojant Agilent 2100 Bioanalyzer sistemą su RNA Pico Chip rinkiniu. **B)** Gautos RIN vertės bendruose ir sužadinamosiomis sinaptosomomis praturtintuose sinaptosomų RNR mėginiuose.

5':3' metodas iRNR kokybei įvertinti

Transcriptų kokybę ir vientisumą galima įvertinti pamatuojant po atvirkštinės transkripcijos reakcijos gautų produktų ilgį, jei reakcija buvo vykdoma tik nuo vieno iRNR galo. Kai mėginys yra prastos kokybės ir dalis iRNR yra sudegradavusi, iRNR trūkiai lemia sutrumpėjusią kopijinę DNR (kDNR) po atvirkštinės transkripcijos. Šis kDNR sutrumpėjimas gali būti įvertinamas naudojant kokybinę PGR (kPGR), kai yra vertinamas nuo kDNR 5' galo ir 3' galo pagausintų fragmentų kiekis. Dažniausiai naudojamas būdas iRNR paversti į kDNR tik nuo vieno galo yra atvirkštinės transkripcijos metu naudoti oligo-dT pradmenis, kurie kimba tik prie poliadenilinto subrendusios iRNR galo. Todėl 5':3' metodas pagrįstas oligo-dT pradmenų naudojimu atvirkštinei transkripcijai ir dviem pradmenų poromis kPGR, kad būtų galima išmatuoti santykinę dviejų amplikonų, esančių 3' ir 5' iRNR galuose (**4 pav.**). Jei iRNR mėginyje yra nepažeista, atvirkštinė transkripcija nuo poliadenilinto galo vyksta nepertraukiamai generuodama viso ilgio kDNR. Dėl to po kPGR gaunami panašūs padaugintų 3' ir 5' galų fragmentų kiekiai. Dalinai sudegradavusiame RNR mėginyje dėl trūkių iRNR sekoje kDNR susintetinama tik iki trūkio, o ne pilna. Šis procesas lemia sumažėjusį 5' sričių, kur turi prisijungti kPGR pradmenys, skaičių ir atitinkamai sumažėjusį pagausintų 5' fragmentų kiekį. Tada mėginio vientisumo vertė 5':3' metodu kiekybiškai įvertinama 5' galo amplikono kiekį padalijus iš 3' galo amplikono kiekio ir padauginus iš 10, kad vientisumo balas būtų nuo 10 (nepažeista iRNR) iki 0 (visiškai suardyta iRNR), kas atitinka kitas RNR kokybės tyrimų vertinimo skales, kuriose naudojamos 1–10 vertės.



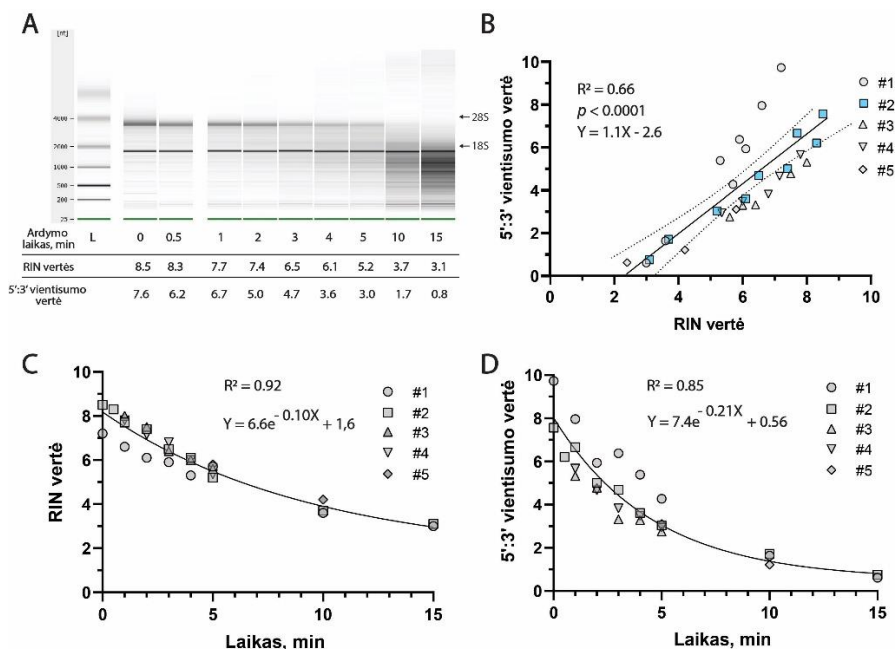
4 paveikslas. 5':3' metodo principas iRNA vientisumui įvertinti.

Atvirkštinės transkripcijos reakcijai naudojami oligo-dT pradmenys, kad būtų susintetinta kDNR nuo vieno iRNA galo. Geros kokybės iRNA mėginiuose iRNA yra vientisa ir dėl to kDNR yra susintetinama pilno subrendusios iRNA ilgio. Tokiu atveju tiek 3' galo tiek 5' galo kPGR pradmenų poros turi vienodą prisikabinimo sričių skaičių dėl ko gaunami panašūs kPGR pagausintų 3' galo ir 5' galo fragmentų kiekiai. Kai iRNA mėginys yra dalinai suiręs, dėl esančių trūkių iRNA susintetinamos trumpesnės kDNR. Kai kPGR naudojamas toks mėginys 5'-galo kPGR pradmenų pora turi mažiau prisikabinimo vietų lyginant su 3'-galo pradmenų pora, kurios prisikabinimo saitas yra arti iRNA poli(A) uodegos. Po fragmentų pagausinimo kPGR, yra apskaičiuojama 5':3' vientisumo vertė padalijant nuo 5'-galo pagausinto fragmento kiekį iš nuo 3'-galo pagausinto fragmento kiekį ir padauginant gautą vertę iš 10, kas leidžia kiekybiškai įvertinti iRNA vientisumą ir mėginio kokybę. Sukurta su Biorender.com.

5':3' tyrimui pasirinkta iRNA idealiu atveju turi būti ilga ir stabiliai bei gausiai sintetinama dominančiame audinyje. Ilgo transkripto pasirinkimas užtikrintų pakankamą atstumą tarp 5' ir 3' pradmenų porų prikibimo vietų, ko

reikia, kad būtų efektyviai pastebėti iRNR degradacijos sukelti trūkiai. Šiame tyrime 5':3' metodas pagrįstas pelės *PGK1* kDNR. *PGK1* yra gausiai reiškiamas ląstelėms būtinas genas, nuo kurio yra sintetinamas ilgas transkriptas su gerai apibūdinta egzono-intronų struktūra. Šio geno produktas yra fermentas pavadinimu fosfoglicerato kinazė, kuri dalyvauja glikolizės procesuose. *PGK1* genas yra homologiškas tarp žiurkių, pelių ir žmonių. *PGK1* transkriptai buvo jau anksčiau panaudoti iRNR vientisumui vertinti žiurkių toksikologiniuose tyrimuose ir su arklių mėginiais. Dėl to šiam tyrimui ir 5':3' metodo kPGR pradmenų poroms sukurti kaip pagrindas taip pat pasirinkta pelės *PGK1* kDNR.

Tradicškai, RNR vientisumas yra kokybiškai įvertinamas pagal 28S ir 18S rRNR juostelių aiškumą ir intensyvumą. Šiuo principu paremta taip pat yra Agilent Bioanalyzer Sistema, kuri šiuo metu yra populiariausias būdas RNR vientisumui nustatyti. Ši sistema mėginiui priskiria RNR Vientisumo Skaičių - RIN vertę (angl. *RNA Integrity Number*). Norint įvertinti 5':3' metodo gebėjimą aptikti degradaciją RNR mėginiuose ir palyginti gautas vientisumo vertes su RIN, buvo naudojami karščiu suskaidyti pelės žievės audinio RNR mėginiai. Mėginiai buvo 1–15 min kaitinami 90 °C ir tuomet analizuojami naudojant 5':3' RNR vientisumo metodą ir Agilent Bioanalyzer sistemą. Tiek 5':3' vientisumo vertė tiek RIN mažėjo kartu su kaitinimo laiku (**5 pav. A**). RIN verčių ir 5':3' vientisumo verčių koreliacija tarpusavyje buvo gera ($R^2=0.67$, $p<0.0001$, Pearsono koreliacija) ir mėginiai, kurių RIN buvo maži turėjo mažesnes ir 5':3' vientisumo vertes (**5 pav. B**). Kontroliniuose karščiu neveiktuose mėginiuose abiejais metodais apskaičiuotos RNR vientisumo vertės buvo panašios (nuo 7.2 iki 8.5 RIN ir nuo 7.6 iki 9.7 5':3' vietisumo vertės). Vis dėlto, ilgiau kaitintų mėginių 5':3' metodu gautos vientisumo vertės mažėjo greičiau nei RIN vertės (**5 pav. C, D**). Dėl to, nors įprastai kokybiškais RNR mėginiais laikomi tokie, kurių RIN yra 7 ar daugiau, 5':3' metodu apskaičiuota vientisumo ribinė vertė kokybiškiems RNR mėginiams būtų apie 6.



5 paveikslas. RNR vientisumo vertinimas naudojant 5':3' metodą ir RIN karščiu suardytuose pelės RNR mėginiuose. **A** Representaciniai Agilent 2100 Bioanalyzer sistemos mikrokapiliarinės elektroforezės takelių vaizdai, kuriuose matyti 1, 2, 3, 4, 5, 10 ir 15 min 90 °C ardyti RNR mėginiai. Apačioje: RIN ir 5':3' vientisumo vertės. **A** dalyje Rodomos vertės taip pat pažymėtos mėlynai **B** dalyje. **B** Buvo stipri koreliacija tarp RIN ir 5':3' vientisumo verčių (n=5, atskiri pelės žievės RNR mėginiai pažymėti #1, #2, #3, #4 ir #5). Tiesinės regresijos linija rodoma su 95 % patikimumo intervalu tikrosios geriausiai atitinkančios linijos. **C**, **D** Tiek RIN (**C**) tiek 5':3' vientisumo vertės (**D**) mažėjo kaitinant mėginius. Linijos **C** ir **D** dalyse rodo vienos fazės eksponentinį verčių mažėjimą.

Sukurtas 5':3' metodas tuomet panaudotas sinaptosomų RNR mėginių kokybei įvertinti. Yra žinoma, jog dėl savo universalios gausios raiškos *PGK1* yra taip pat aptinkamas ir sinaptosomose (Hafner et al. 2019). Šiam tyrimui buvo panaudoti aštuoni RNR mėginiai išskirti iš keturių bendrų sinaptosomų mėginių ir keturių praturtintų sužadinamųjų sinaptosomų mėginių kaip aprašyta prieš tai (**3 pav.**). Šiuose mėginiuose apskaičiuotos 5':3' vientisumo vertės buvo palygintos su anksčiau gautomis RIN vertėmis. RNR vientisumo analizė bendruose sinaptosomų mėginiuose parodė, kad vientisumo vertės gautos tiek 5':3' metodu tiek RIN buvo panašios. Vis dėlto, nors praturtintuose sinaptosomų mėginiuose buvo neįmanoma pamatuoti RIN dėl itin mažo rRNR

kiekio, 5':3' metodas, kuris nepriklauso nuo rRNR, sėkmingai įvertino šių mėginių iRNR vientisumą. (**6 pav.**). Tai rodo 5':3' metodo potencialią naudą ir pritaikomumą tyrimams su subląstelinių frakcijų mėginiais.

Sinaptosomų mėginiai	5':3' vientisumo vertė	RIN
1-bendras	6.61	8.40
1-praturtintas	1.72	N/A
2-bendras	6.95	8.00
2-praturtintas	2.40	N/A
3-bendras	5.57	9.10
3-praturtintas	4.04	N/A
4-bendras	6.99	8.90
4-praturtintas	3.69	4.50

6 paveikslas. 5':3' metodu galima įvertinti sinaptosomų iRNR vientisumą. Pelės bendrų ir praturtintų sinaptosomų mėginių 5':3' vientisumo vertės ir RIN.

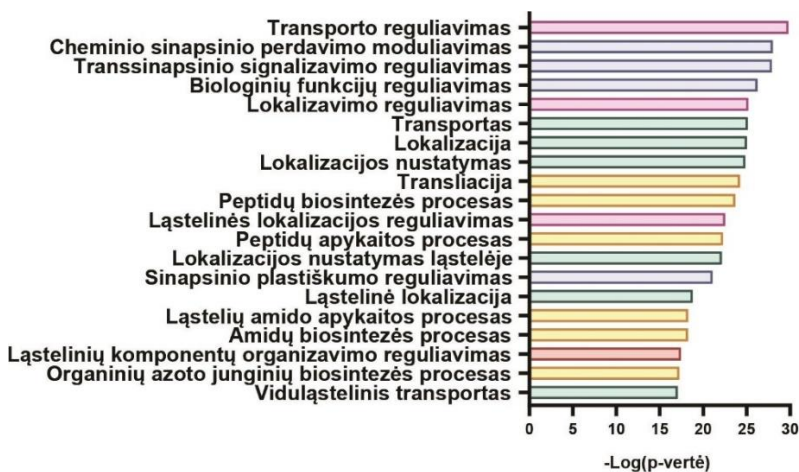
Lokalus sinapsių transkriptomas ir jo pokyčiai brendimo metu

Kiekvienas neuronas gali sudaryti iki 10 000 jungčių su kitais neuronais ir perduoti signalus vienas kitam per 1 000 trilijonų sinapsių. Šios sinapsės gali būti sąlyginai toli nuo neurono kūno, tačiau turi individualiai ir greitai keistis priklausomai nuo gaunamų signalų. Norint tai padaryti efektyviai sinapsės reguliuoja didelę dalį savo proteomo gaminant reikalingus baltymus lokaliai ir šis procesas yra labai svarbus jų palaikymui ir sinapsiniam plastiškumui (Van Driesche and Martin 2018). Šimtai nuskaitytų iRNR aptiktų sužadinamosiose sinapsėse patvirtino, kad baltymų sintezė vyksta sinaptinėse ir yra reguliuojama priklausomai nuo vystymosi stadijos (Hafner et al. 2019; C. Sun et al. 2021). Nepaisant to, vis dar yra nežinoma, kaip sinapsinis transkriptomas keičiasi vystantis neuroniam tinklui kritiniais laikotarpiais.

Norint apibrėžti lokalų sužadinamųjų sinapsių transkriptomą ir jo pokyčius bręstant regos žievei, buvo surinkti sužadinamosiomis sinaptosomomis praturtinti mėginiai ir išskirta jų RNR. Sužadinamųjų sinaptosomų mėginiai iš pelės regos žievės buvo renkami prieš prasidedant kritiniam vystymosi periodui (P21), jo viduryje (P28) ir jam pasibaigus (P35). Iš praturtintų sinaptosomų mėginių gauti labai maži RNR kiekiai – apie 30 ng iš vieno mėginio. Dėl to sekoskaitos bibliotekai paruošti buvo naudojamas SmartSeq2 protokolas, kuris yra žinomas kaip labai efektyvus bibliotekų ruošimui su mažais pradiniais RNR kiekiais (Picelli et al. 2014; Hennig et al. 2018). RNR sekoskaita atlikta naudojant Illumina NextSeq 2000 sistemą.

Pirmiausia šiame tyrime buvo charakterizuotas pats sužadinanųjų sinapsių transkriptomas bendrai. 15 sinaptosomų mėginių buvo aptikta 15,716 skirtingų genų transkriptų. Šie transkriptai buvo tuomet sureitinguoti pagal jų raiškos dydį. Toks sureitinguotas sąrašas buvo panaudotas identifikuoti praturtintus Genų Ontologijos (GO) terminus naudojant GOrilla. 3 sužadinanosioms sinapsėms svarbiausi GO terminai buvo transporto reguliavimas, cheminio sinapsinio perdavimo moduliavimas ir transsinapsinio perdavimo reguliavimas (7 pav.). Tarp svarbiausių sužadinanųjų sinapsių transkriptomo GO terminų daugelis buvo panašūs arba susiję vienas su kitu. Dėl to, 20 svarbiausių labiausiai praturtintų GO terminų buvo apibendrinti kaip šios 5 sužadinanųjų sinapsių transkriptų funkcijos:

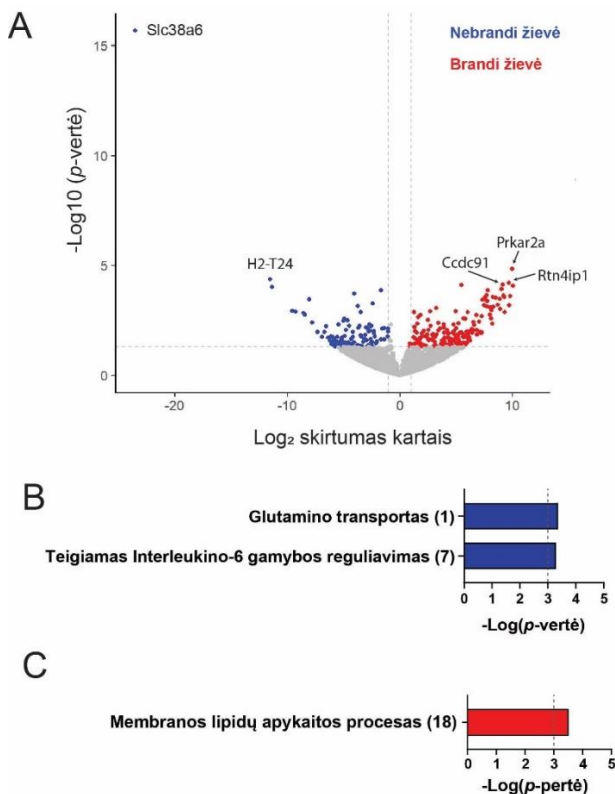
Transporto ir lokalizacijos reguliavimas
 Sinapsinio signalo perdavimo ir plastiškumo reguliavimas
 Viduląstelinis transportas ir lokalizacija
 Transliacija
 Ląstelės kompartmentų organizavimas ir reguliacija



7 paveikslas. Lokalus sužadinanųjų sinapsių transkriptomas ir jo pagrindinės funkcijos. GO terminai ir funkcijos, už kurias atsakingi gausiausi sužadinanųjų sinaptosomų transkriptai.

Norint suprasti, kokie lokalaus transkriptomo pokyčiai yra susiję su regos žievės plastiškumu kritiniu laikotarpiu, buvo atlikta genų raiškos pokyčių analizė. Pirmiausia buvo palyginti subrendusios žievės sinapsiniai transkriptai (P35) su transkriptais iš regos žievės prieš kritinį plastiškumo laikotarpį (P21). *Slc38a6* transkripto kiekis labiausiai skyrėsi tarp minėtų grupių ir jo buvo 24 katus daugiau nesubrendusioje žievėje nei brandžioje. Šis transkriptas

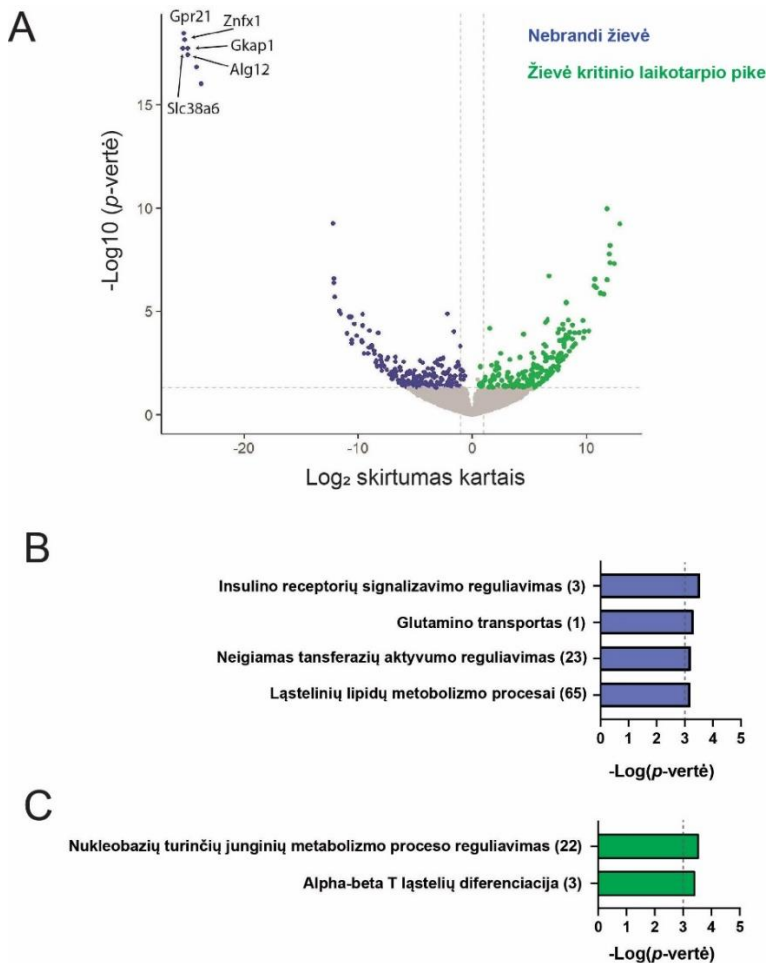
koduoja aminorūgščių transporterį, kuris yra specifiškas L-glutaminui ir L-glutamatui, padedantis glutaminui patekti į sužadinausias sinapses neuronuose (Bagchi et al. 2014) (**8 pav. A**). Dėl ryškių *Slc38a6* transkripto skirtumų tarp grupių GO analizė įvardijo glutamino transportavimą kaip reiškingai išsiskiriančią nesubrendusios žievės sinapsių funkciją. Kita identifikuota nebrandžioms sinapsėms būdinga GO funkcija buvo teigiamas Interleukino-6 (IL-6) gamybos reguliavimas (**8 pav. B**). Dažniausiai subrendusios žievės sinapsėse lyginant su nesubrendusia aptiktas transkriptas buvo *Prkar2a*, kurio koduojama kinazė dalyvauja signalo perdavimo sinapsėse moduliavime (**8 pav. A**). Subrendusios žievės sinapsėms buvo identifikuota tik viena specifinė funkcija - membranų lipidų apykaitos procesas, kuriame dalyvauja net 18 brandžiose sinapsėse aptiktų transkriptų (**8 pav. C**). Šis terminas apjungia transkriptus, dalyvaujančius cheminėse reakcijose ir molekuliniuose keliuose su membraniniais lipidais. Vienas iš tokių lokalių transkriptų buvo *Pigv*, kuris koduoja glikosilfosfatidilinositolio (GPI) manosiltransferazę 2. Šio transkripto brandžiose sinapsėse aptikta dvigubai daugiau nei nebrandžiose.



8 paveikslas. Brandžių ir nebrandžių regos žievės sinapsių transkriptomo skirtumai. **A)** Vulkano grafikas vaizduojantis skirtingą transkriptų kiekį tarp nebrandžių (P21) ir brandžių (P35) regos žievės sinaptosomų. Brandžiose sinapsėse aptikti genai pavaizduoti raudonai, o nebrandžiose sinapsėse – mėlynai. Taip pat atvaizduoti 5 labiausiai besiskiriančių transkriptų pavadinimai. **B)** Genų ontologijos terminai nurodantys identifikuotas nebrandžioms sinapsėms būdingas funkcijas. **C)** Genų ontologijos terminai nurodantys identifikuotas brandžioms sinapsėms būdingas funkcijas. Skaičiai skliausteliuose nurodo kiek aptiktų transkriptų yra susiję su nurodyta funkcija. Punktyrinė linija B ir C dalyse rodo 10^{-3} ribinę *p*-vertę naudotą atskirti reikšmingai besiskiriančius transkriptus GO analizei.

Lyginant nebrandžių regos žievės sinapsių transkriptomą su transkriptomu iš sinapsių surinktų kritiniu vystymosi periodu identifikuota grupėlė nebrandžioms sinapsėms būdingų transkriptų, tarp kurių - *Slc38a6*, *Gpr21* ir *Znfx1* (**9 pav. A**). *Slc38a6* transcriptas vėl identifikuotas kaip specifiškas nebrandžiai smegenų žievei, nes šio transkripto buvo aptikta tik šioje grupėje kas parodė galimą šio transkripto svarbą besivystančių neuronų aktyvumui. *Gpr21* ir *Znfx1* funkcijos neuronuose nėra ištirtos, tačiau šio tyrimo duomenys rodo, kad šie transkriptai gali būti labai svarbūs perduodant signalus lokaliai per ląstelių membranas ir palaikant ląstelių homeostazę. (Wong et al. 2023; Liu et al., 2024.). Tarp visų reikšmingai didesnę raišką nebrandžiose sinapsėse turinčių transkriptų GO analizė nustatė 4 terminus: insulino receptorių signalizavimo reguliavimas, glutamino transportas, neigiamas transferazių aktyvumo reguliavimas ir ląstelių lipidų metabolizmo procesai (**9 pav. B**). Insulino receptoriai (IR) dalyvauja daugelyje CNS procesų. Yra žinoma, jog IR yra svarbus normaliam sinapsių formavimuisi ir remodeliavimui bei reguliuoja sinapsinį plastiškumą (Pomytkin et al. 2018). Šis tyrimas parodo, kad visi šie procesai iš dalies gali būti reguliuojami lokaliai sinapsėse ir svarbūs nebrandžioms sinapsėms.

Du GO terminai buvo identifikuoti tarp reikšmingai didesnę raišką sinapsėse kritiniu vystymosi laikotarpiu turėjusių transkriptų: nukleobazių turinčių junginių metabolizmo proceso reguliavimas ir alfa-beta T ląstelių diferenciacija (**9 pav. C**). Dauguma pirmojo GO termino transkriptų kodavo baltymus, dalyvaujančius kontroliuojant genų raišką. Tokie baltymai galimai yra gaminami lokaliai sinapsėse, o po to pristatomi į neurono kūną, kad būtų suaktyvinta arba slopinama transkripcija kritiniu plastiškumo laikotarpiu (Goodwin and Picketts 2018).

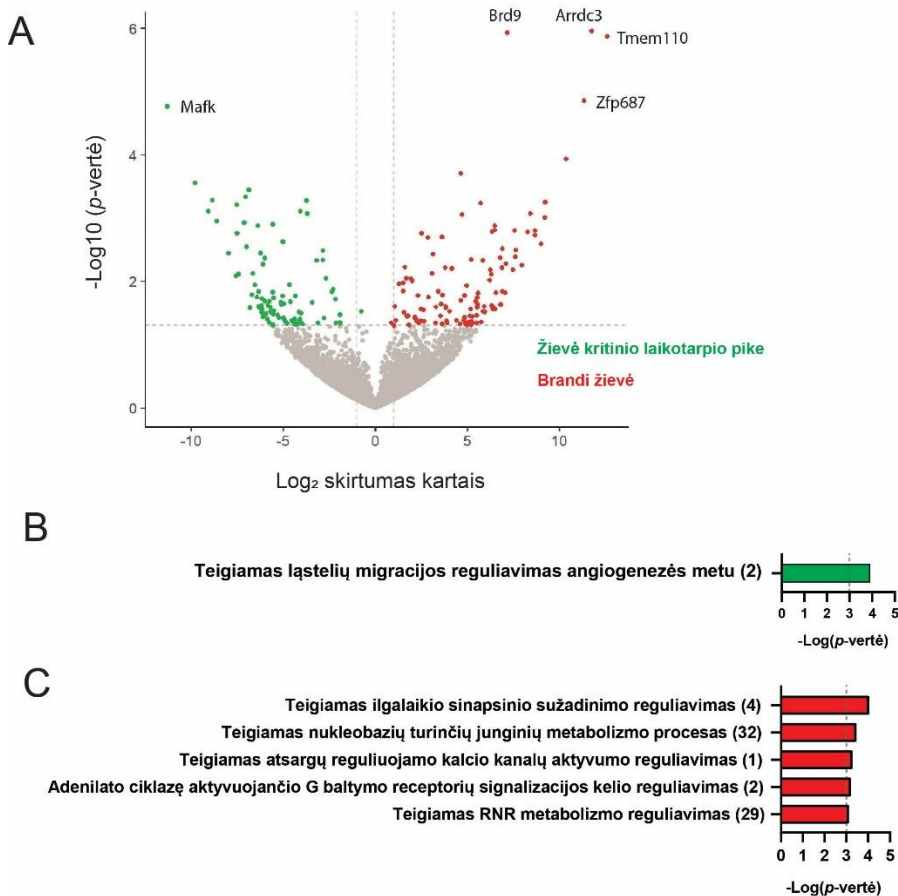


9 paveikslas. Nebrandžių ir plastiškų regos žievės sinapsių transkriptomų skirtumai. A) Vulkano grafikas vaizduojantis skirtingą transkriptų kiekį tarp nebrandžių (P21) ir itin plastiškų (P28) regos žievės sinapsių. Plastiškose kritinio laikotarpio sinapsėse aptikti genai pavaizduoti žaliai, o nebrandžiose sinapsėse – mėlynai. Taip pat atvaizduoti 5 labiausiai besiskiriančių transkriptų pavadinimai. B) Genų ontologijos terminai nurodantys identifikuotas nebrandžioms sinapsėms būdingas funkcijas. C) Genų ontologijos terminai nurodantys identifikuotas plastiškoms sinapsėms būdingas funkcijas. Skaičiai skliausteliuose nurodo kiek aptiktų transkriptų yra susiję su nurodyta funkcija. Punktyrinė linija B ir C dalyse rodo 10^{-3} ribinę p -vertę naudotą atskirti reikšmingai besiskiriančius transkriptus GO analizei.

Galiausiai buvo palyginti transkriptomai iš brandžių (P35) ir plastiškų sinapsių kritinio laikotarpio viduryje (P28). Lyginant šias grupes plastiškose

sinapsėse labiausiai išsiskyrė reikšmingai didesnis *Mafk* transkripto kiekis (**10 paveikslas, A dalis**). Šis transkriptas reikalingas *MafK* transkripcijos faktoriui sintetinti. Šis transkripcijos faktorius priklauso mažų Maf baltymų (sMafs) šeimai, kurie yra pagrindinio regiono leucino užtrauktuko (bZIP) tipo transkripcijos faktoriai. Maži Maf baltymai dalyvauja transkripcijos aktyvavime arba slopinime, priklausomai nuo jų heterodimerinių partnerių molekulių (Katsuoka and Yamamoto 2016). GO analizė tarp transkriptų, kurių kiekis yra reikšmingai didesnis plastiškose sinapsėse lyginant su brandžiomis identifikavo tik du transkriptus susijusius atliekama funkcija - *Map3k3* ir *Fgf2*. Juos jungiantis GO terminas buvo teigiamas ląstelių migracijos reguliavimas angiogenezės metu (**10 pav. B**).

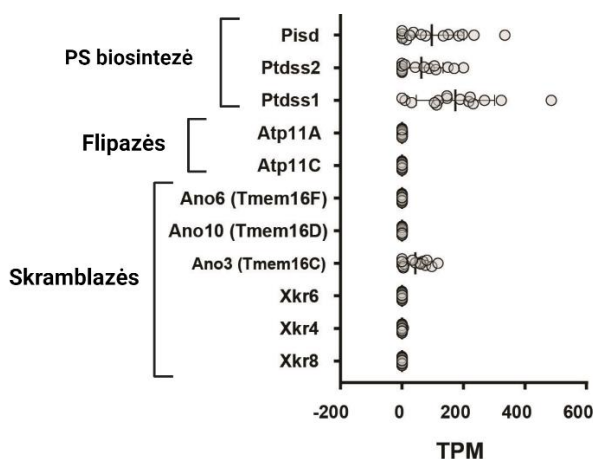
Brandžiose sinapsėse lyginant su plastiškomis labiausiai išsiskyrė *Tmem110* transkripto kiekis. *Tmem110* reikalingas susintetinti transmembraninį baltymą, kuris reguliuoja ilgalaikį jungčių palaikymą tarp endoplazminio tinklo ir plazminės membranos, bei trumpalaikį fiziologinį jungčių remodeliavimą kalcio signalo perdavimo metu (Quintana et al. 2015). Didelė dalis brandžioms sinapsėms specifinių transkriptų buvo susiję su teigiamu nukleobazių turinčių junginių metabolizmo procesais ir RNR apykaitos reguliavimu, galbūt dėl to, kad subrendusių neuronų lokali sinapsinė baltymų sintezė buvo suaktyvinta (**10 pav. C**).



10 paveikslas. Brandžių ir plastiškų regos žievės sinapsių transkriptomo skirtumai. A) Vulkano grafikas vaizduojantis skirtingą transkriptų kiekį tarp brandžių (P35) ir itin plastiškų (P28) regos žievės sinapsosomų. Plastiškose kritinio laikotarpio sinapsėse aptikti genai pavaizduoti žaliai, o brandžiose sinapsėse – raudonai. Taip pat atvaizduoti 5 labiausiai besiskiriančių transkriptų pavadinimai. B) Genų ontologijos terminai nurodantys identifiкуotas plastiškoms sinapsėms būdingas funkcijas. C) Genų ontologijos terminai nurodantys identifiкуotas brandžioms sinapsėms būdingas funkcijas. Skaiciai skliausteliuose nurodo kiek aptiktų transkriptų yra susiję su nurodyta funkcija. Punktyrinė linija B ir C dalyse rodo 10^{-3} ribinę p -vertę naudotą atskirti reikšmingai besiskiriančius transkriptus GO analizei.

Kritiniais smegenų plastiškumo laikotarpiais dinamiškas sinapsių susidarymas ir pašalinimas priklauso nuo molekulinų signalų, vadinamų „nevalgyk manęs“ ir „valgyk mane“, kurie yra būtini efektyviam sinapsių

genėjimui ir tinklo optimizavimui. Šiuo metu geriausiai žinomi „valgyk mane“ signalai yra ląstelės paviršiuje eksponuotas fosfatidilserinas (FS) ir komplemento komponentas 1q (C1q). Normaliai ląstelėse FS yra randamas vidinėje plazminės membranos pusėje ir šios asimetrijos sutrikdymas, bei FS atsiradimas išorinėje membranos pusėje yra siejamas su ląstelės mirtimi ar sinapsių genėjimu. Dėl šių priežasčių buvo patikrinta ar lokaliai sinapsėse yra transkriptų susijusių su sinapsių genėjimu ir FS perkėlimu į kitą membranos pusę. Sinaptosomų RNA-sekoskaitos duomenų analizė parodė, kad sinapsėse yra transkriptų atsakingų už FS biosintezę, *Pisd*, *Ptdss2*, ir *Ptdss1*. Vis dėlto, skrambrazių *Xkr4*, *Xkr6*, *Xkr8*, *Tmem16D*, *Tmem16F* ar flipazių *Atp11A*, *Atp11C* transkriptų, kurių koduojami baltymai yra atsakingi už FS perkėlimą į išorinę membranos pusę, sinapsėse nebuvo. Sinapsių mėginiuose buvo aptikta tik vienos skramblazės *Tmem16C* (dar žinomos kaip Anoctamin-3) transkriptų. Šios nuo kalcio priklausomos skramblazės transkriptų buvimas lokaliai sinapsėse parodė jos galimą svarbą PS perkėlime ir sinapsių genėjime vystantis regos žievei (**11 pav.**).

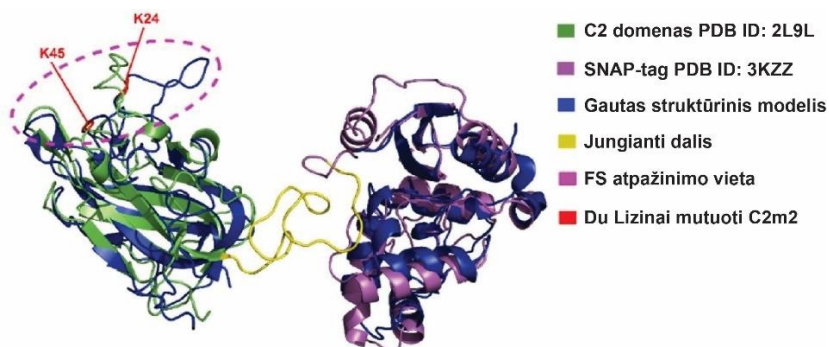


11 paveikslas. Su fosfatidilserino ekspozicija ant membranos susijusių transkriptų raiška sinapsėse. Su FS biosinteze ir ekspozicija susijusių transkriptų kiekiai sužadinamosiose sinaptosomose. Raiška atidėta TPM.

Dėl svarbaus FS vaidmens sinapsių remodeliavimo metu ir itin mažo sinapsių dydžio, šiems procesams tirti reikalingas efektyvus ir jautrus PS žymuo. Šiuo metu prieinami FS žymenys pasižymi gan mažu specifiskumu ir žema skvarba į audinius. Be to, norint juos naudoti su gyvūnais, reikalingos injekcijos į smegenis, o tai pažeidžia audinį ir įjungia su pažeidimu susijusius signalinius kelius, o tai savo ruožtu skatina FS perkėlimą iš vidinės į išorinę ląstelės membranos pusę. Dėl šių priežasčių, šiame tyrime buvo siekta sukurti

naują genetiškai koduojamą ir tyrimams smegenyse tinkamą FS žymenį, kuris būtų paremtas laktadherino (MFG-E8) C2 domenu. FS atpažįstantis C2 domenas vizualizavimui buvo sujungtas su fermentiniu žymeniu SNAP-tag.

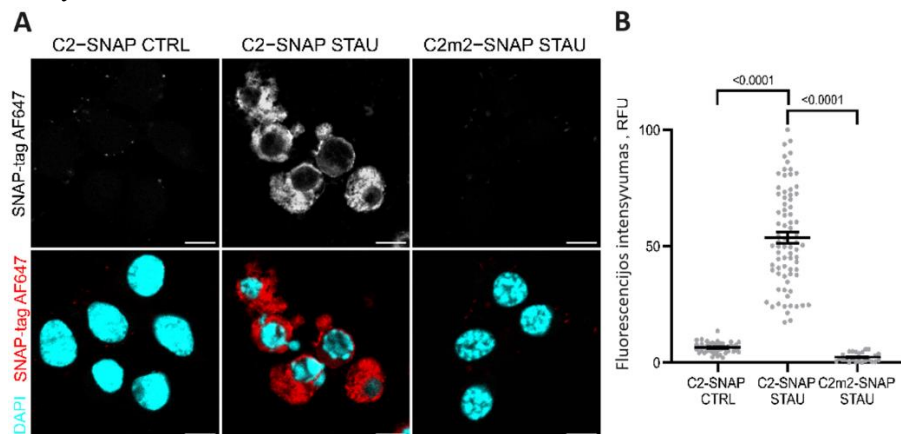
Norint įvertinti, ar C2 domenas ir parinktas žymuo gali būti suderinami po suliejimo, naudojant *de novo* modeliavimo įrankius buvo sukurtas C2-SNAP struktūrinis modelis (**12 pav.**). Gautas modelis pademonstravo, kad C2 domenas po suliejimo išlaikė visus fundamentinius struktūrinius motyvus, kurie buvo matomi PDB eksperimentiškai nustatytoje struktūroje. Svarbu tai, kad 1–3 kilpos, sudarančios kritinę FS prisijungimo vietą, buvo išdėstytos taip, kaip natūraliame C2, o tai rodo, kad sulieti baltymai turėtų išlaikyti gebėjimą prisikabinti prie FS. Be to, prisijungimui kritinės lizino aminorūgštys (K24 ir K45) išliko panašiose vietose kaip ir PDB duomenų bazėje esančioje struktūroje taip dar kartą patvirtinant, jog baltymų suliejimas neturėtų paveikti C2 domeno funkcionalumo.



12 paveikslas. C2-SNAP struktūrinis modelis. C2-SNAP išlaikė tokią pačią struktūrą kaip ir eksperimentiškai apibudinta C2 domeno (PDB ID: 2L9L) ir SNAP-tag žymens struktūra (PDB ID: 3KZZ). Violetinė punktyrinė linija žymi C2 ir FS prisijungimo zoną. Prisijungimui kritinės aminorūgštys K24 ir K45 pažymėtos raudonai.

C2-SNAP baltymų gebėjimas prisikabinti prie eksponuojamo FS *in vitro* buvo įvertintas naudojant apoptozines pelės neuroblastomos ląsteles Neuro2a. Apoptozei sukelti ląstelės paveiktos staurosporinu ir pažymėtos naudojant išgrynintus C2-SNAP baltymus. Sveikų, staurosporinu nepaveiktų Neuro2a ląstelių C2-SNAP nežymėjo (**13 pav. A**). Tačiau prie paveiktų apoptuojančių ląstelių C2-SNAP prisikabino pažymėdamas ląstelių membraną. Mutuotas C2m2-SNAP baltymas neprisijungė prie apoptuojančių ląstelių membranos parodydamas, kad rekombinantinių baltymų sąveika su membrana yra specifiška FS. Kiekybinė analizė parodė ypatingą žymenų specifiskumą, nes

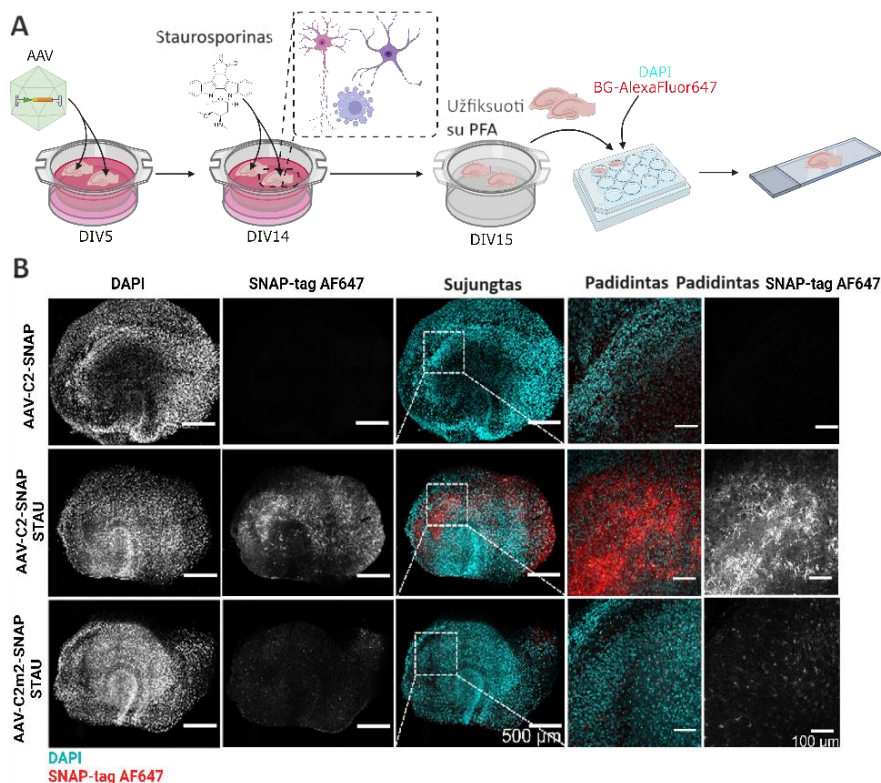
gauta fluorescencija buvo 22 kartus didesnė nei fonas (**13 pav. B**). Toks rezultatas gautas dėl puikių SNAP-tag žymėjime naudojamo organinio fluoroforo savybių: žemo fotobalinimo ir didelio stabilumo lyginant su fluorescuojančiais baltymais (Deo and Lavis 2018). Šie *in vitro* eksperimentai parodė, kad C2-SNAP yra jautrus ir specifiškas ant ląstelių išorės eksponuoto FS žymuo.



13 paveikslas. C2-SNAP baltymai pažymi apoptuojančias Neuro2a ląsteles *in vitro*. **A** Reprezentaciniai kontrolinių (CTRL) ir apoptotinių (STAU, paveiktos 3 μ M staurosporino) Neuro2a ląstelių vaizdai žymėjimui naudojant C2-SNAP arba C2m2-SNAP; Skalė 10 μ m. **B** Kiekybinė SNAP-tag fluorescencijos intensyvumo analizė. Duomenys pavaizduoti kaip vidurkis \pm standartinė vidurkio paklaida. Vidurkiai palyginti naudojant vienpusę ANOVA ir *post-hoc* Tukey testą (**B**). *p* vertės < 0.05 laikytos statistiškai reikšmingomis. RFU – santykiniai fluorescencijos vienetai.

FS ekspozicijos tyrimai yra ypač sudėtingi 3D ląstelių modeliuose ir audiniuose dėl mažo išoriškai naudojamų FS žymenų prasiskverbimo. Šitam trūkumui pašalinti buvo sukurti adeno-asocijuoti virusiniai (AAV) vektoriai, koduojantys C2-SNAP žymenis ir galintys be audinio pažeidimo nukeliauti į reikiamą vietą ir ten juos pristatyti. Kad žymenų raiška vyktų tik astrocituose, buvo panaudotas glijos fibrilinio rūgštinio baltymo (GFAP) promotorius (Brenner et al. 1994). Taip pat, kad rekombinantiniai baltymai būtų sekretuojami į tarpląstelinę erdvę, kur jie galėtų pažymėti ant ląstelių ekspuojamą FS, buvo įterpta sekreciją užtikrinanti signalinė peptidų seka (Stubbs et al. 1990). Galiausiai, virusinių dalelių surinkimui buvo pasirinkta AAV-PHP.eB kapsidė, kadangi buvo parodyta, jog ši kapsidė geba efektyviai patekti į nervų sistemos ląsteles, po virusinių dalelių suleidimo į kraują (Chan et al. 2017).

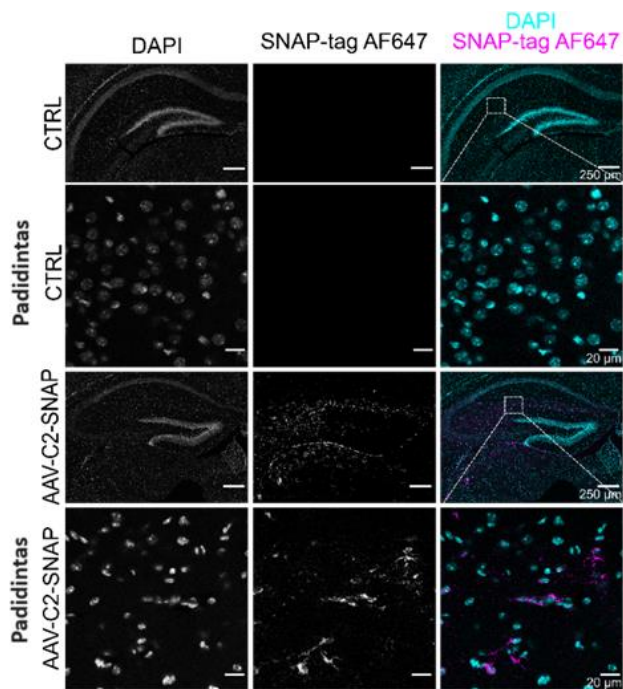
Tam, kad patikrinti AAV genetiškai užkoduoto C2-SNAP žymens gebėjimą atpažinti FS audinyje, sukurti AAV buvo panaudoti su organotipinių hipokampo pjūvių kultūromis (OHSC). Šios gerai žinomos 3D kultūros yra labai panašios savo vystymuisi, ląstelių fiziologija ir sąveikomis į smegenų audinį (Linsley et al. 2019). Paruošti AAV buvo uždėti and OHSC penktą pjūvių dieną *in vitro* (DIV5). Apoptozė naudojant staurosporiną organotipiniuose pjūviuose buvo sukurta dar po devynių dienų (**14 pav. A**). Parodyta, kad AAV koduojami C2-SNAP baltymai efektyviai pažymėjo apoptuojančias ląsteles audinyje (**14. B**). C2-SNAP žymuo leido vizualizuoti apoptuojančių neuronų atšakas hipokampo pjūvyje. Svarbu tai, kad sveikuose, staurosporinu nepaveikuose pjūviuose ląstelių žymėjimo nebuvo matyti, o tai parodė, kad AAV pristatytas C2-SNAP specifiškai jungėsi tik prie apoptuojančių ląstelių. Tik labai silpnas foninis signalas buvo aptiktas naudojant AAV su mutantiniu C2m2-SNAP žymeniu. Dėl to mutantinis C2m2-SNAP galėtų būti naudojamas paraleliai su C2-SNAP kaip neigiama kontrolė vertinant nespecifinį žymėjimą ar norint nustatyti fluorescencijos slenkstinę ribą kiekybinėje analizėje. Šie rezultatai atskleidė, kad C2-SNAP žymuo buvo efektyviai pagamintas po koduojančių sekų pernešimo AAV ir susintetintas žymuo gebėjo pažymėti audinyje ant ląstelių ekponuojamą FS.



14 paveikslas. AAV-koduojamas C2-SNAP žymuo pažymėjo apoptotines ląsteles organotipiniuose hipokampo pjūviuose *ex vivo*. **A)** Ant 5 dienas laikomų (DIV5) organotipinių hipokampo pjūvių buvo uždėta sukurtų C2-SNAP koduojančių AAV. Po 9 dienų baltymų raiškai ($n=3$ biologiniai pakartojimai) audinyje buvo sukurta ląstelių apoptozė naudojant 10 μM staurosporino laikant su juo 16 val. Sukurta naudojant Biorender.com. **B)** Reprezentaciniai organotipinių pjūvių, paveiktų AAV-C2-SNAP arba AAV-C2m2-SNAP, vaizdai. Ląstelių branduoliai nudažyti naudojant DAPI. Skalė 500 μm (visas pjūvis) ir 100 μm (padidinta zona).

Siekiant ištirti, ar genetiškai užkoduotas C2-SNAP baltymas gali būti naudojamas tyrimams *in vivo*, trijų dienų amžiaus pelėms į veną buvo suleista neurotropinių rekombinantinių AAV. Po dviejų savaičių baltymų raiškos *in vivo*, C2-SNAP baltymų raiška ir fluorescencija buvo stebėta hipokampe ir regos žievėje (**15 pav.**). Šie rezultatai patvirtino, kad smegenų transdukcijai pakanka intraveninės AAV-C2-SNAP injekcijos. Jokio fluorescencinio žymėjimo nebuvo pastebėta kontrolinėse pelėse, ant kurių smegenų pjūvių buvo uždėtas SNAP-tag substratas. Šie rezultatai parodė, kad genetiškai

užkoduotas C2-SNAP žymuo gali būti naudojamas funkciniais FS tyrimams *in vivo* be invazinio reagento tiekimo į smegenų audinį.



15 paveikslas. Adeno-asocijuotų virusų (AAV) panaudojimas C2-SNAP žymenims pristatyti *in vivo*. Trečią postnatalinę dieną (P3) pelėms buvo suleista 1×10^{11} vg AAV-C2-SNAP virusų. Viršuje pateikti reprezentaciniai hipokampo vaizdai po dviejų savaičių (P17) C2-SNAP baltymų raiškos (n=5 gyvūnai). Dešinėje pateikti padidinti hipokampo vaizdai. Ląstelių branduoliai nudažyti naudojant DAPI, C2-SNAP nudažytas naudojant AlexaFluor647 (AF647). Kontroliniai vaizdai gauti nudažant virusais nepaveiktų pelių pjūvius BG-AF647 substratu. Skalė 250 μm (visas pjūvis) ir 20 μm (padidinta zona).

Apibendrinant, šių tyrimų rezultatai rodo didelį sukurto C2-SNAP žymens specifiškumą FS. Sukurti genetiškai koduojami FS žymenys įveiriuose tyrimuose taip pat gali būti naudojami kaip dviejų komponentų, funkcionalaus S2-SNAP ir išveiklinto kontrolinio C2m2-SNAP, sistema. Tokia Sistema leidžia jautriai ir patikimai vizualizuoti ir apskaičiuoti FS signalą *in vivo* be jokių invazyvių procedūrų smegenims. Tai palengvins sinapsinio genėjimo, kurį skatina eksternalizuotas FS, tyrimus ir padės išsiaiškinti jo vaidmenį neuronų tinklo remodeliavime kritiniu plastiškumo laikotarpiu.

Išvados

1. Daugiau nei 70 % mėginių praturtinimas sužadinamosiomis sinaptosomomis buvo pasiektas naudojant FPSR metodą, kas leido tirti šių sinapsių pokyčius žievės brendimo metu.
2. Sukurtas 5':3' metodas geba patikimai įvertinti iRNR vientisumą tiek pelės smegenų RNR mėginiuose tiek išskirtų sinaptosomų mėginiuose, kuriuose yra itin mažas rRNR kiekis.
3. Sinapsinis transkriptomas kinta, kad būtų užtikrintas plastiškumas ir tinklo brendimas
4. Sukurtas FS žymuo specifiškai pažymi ant ląstelių membranų eksponuojamą FS, kas leidžia jo vizualizaciją ir kiekybinį vertinimą įskaitant ir *in vivo* eksperimentus.

ACKNOWLEDGEMENTS

First and foremost, I want to express my gratitude to my supervisor, Dr. Urtė Neniškytė, for trusting me with this project, guiding me and constantly pushing me to improve. I have learned an incredible amount from you and have significantly grown as a researcher.

I also extend my thanks to my lab colleagues, Lina, Ugnė, Gintarė, Dovydas, Eimina, Neringa, Simas and Viktorija. Thank you for your answers, discussions and support when I was stuck or discouraged. Special thanks to the Neurokontora team for being the best office mates.

My students during my PhD greatly contributed with their skills and hard work. A big thank you to Eimina and Monika, who accepted me as their supervisor, did an outstanding work and exceeded my expectations.

Synaptosome preparation and sorting were among the most challenging experiments. Therefore, I am grateful to Maria Florencia Angelo and Etienne Herzog for teaching me everything about this technique and setting me up for success. Additionally, thanks to Jaroslav Denkovskij for assisting me at the Innovative Medicine Centre, helping me with parking, dealing with the administration and all the supervision with FACS Aria III.

A big thank you to Vladimir Benes and his team at GeneCore EMBL for welcoming me with RNA samples and patiently teaching me how to prepare sequencing libraries and conducting sequencing as well.

Throughout my studies, my husband Modestas looked after my sanity and well-being like no one else. He always boosted my confidence when it was low, cheered me up and believed in me. Thank you for putting up with all the tiredness and never ending complains that I would bring home. Love you a lot. Also, a shout-out to my cat, Mitten, for being the best emotional support animal.

I also want to thank my mom and dad, who never fully understood what I was studying for twelve years, but who would always ask and try to grasp the complex things I wanted to do and why. Thank you for always being amazed at how did I become so smart.

Lastly, I want to thank my friends, Saulė, Danguolė, Lina and my therapist for listening to me, wanting the best for me and offering endless encouragement and empathy.

LIST OF PUBLICATIONS

Bujanauskiene D, Merkevičius K, Kuliesiute U, Denkovskij J, Kutanasovas S, Luksys G, Ročka S, Bernotiene E, Neniskyte U. Integrity Assay for Messenger RNA in Mouse and Human Brain Samples and Synaptosomal Preparations. IScience, Volume 27, Issue 8, 2024, 110419, ISSN 2589-0042.

<https://doi.org/10.1016/j.isci.2024.110419>

Dirvelyte, E., **Bujanauskiene, D.**, Jankaityte, E. Daugelaviciene N, Kisieliute U, Nagula I, Budvytyte R, Neniskyte U. Genetically encoded phosphatidylserine biosensor for in vitro, ex vivo and in vivo labelling. Cell Mol Biol Lett 28, 59 (2023). <https://doi.org/10.1186/s11658-023-00472-7>

Neniskyte U, Kuliesiute U, Vadisiute A, Jevdokimenko K, Coletta L, Deivasigamani S, **Pamedytyte D**, Daugelaviciene N, Dabkeviciene D, Perlas E, Bali A, Basilico B, Gozzi A, Ragozzino D, Gross CT. Phospholipid scramblase Xkr8 is required for developmental axon pruning via phosphatidylserine exposure. EMBO J. 2023 Jul 17;42(14):e111790. [doi: 10.15252/emboj.2022111790](https://doi.org/10.15252/emboj.2022111790). Epub 2023 May 22. PMID: 37211968; PMCID: PMC10350823

CONFERENCE PROCEEDINGS

2023.11.24 15th international conference of lithuanian neuroscience association, Kaunas, Lithuania. Poster “Integrity assay for messenger RNA in ribosome-depleted subcellular samples” D. Bujanauskiene (presenter), K. Merkevicius, U. Kuliesiute, J. Denkovskij, S. Kutanovas, G. Luksys, S. Rocka, E. Bernotiene, U. Neniskyte.

2023.11.23 16th Lithuanian Young Scientists' Conference “Biofuture: Perspectives of Natural and Life Sciences”, Vilnius, Lithuania. Oral presentation “Genetically encoded phosphatidylserine biosensor for in vitro, ex vivo and in vivo labelling”; E. Dirvelyte, D. Bujanauskiene, E. Jankaityte, N. Daugelaviciene, U. Kisieliute, I. Nagula, R. Budvytyte, U. Neniskyte.

2023.08.08-13 11th IBRO WORLD CONGRESS OF NEUROSCIENCE, Granada, Spain. Poster “RT-qPCR-based assay to measure the integrity of mRNA in synaptosomal RNA samples from mouse and human brain tissue “. D. Pamedytyte (presenter), K. Merkevicius, U. Kuliesiute, J. Denkovskij, S. Kutanovas, G. Luksys, S. Rocka, E. Bernotiene, U. Neniskyte.

2023.05.23 Jędrzej Sniadecki’s Memorial Conference "Frontiers in Molecular Life Sciences (JSMC2023)", Vilnius, Lithuania. Poster “Genetically encoded phosphatidylserine biosensor for in vitro, ex vivo and in vivo labelling” E. Dirvelyte, D. Pamedytyte, E. Jankaityte, N. Daugelaviciene, U. Kisieliute, I. Nagula, R. Budvytyte, U. Neniskyte.

2022.07.09-13 Fens forum 2022, Paris, France. Poster “RT-qPCR-based assay for mRNA integrity evaluation in mouse and human brain tissue and synaptosomal preparations “. D. Pamedytyte (presenter), U. Neniskyte.

2021.10.20-23 The Brain Conference on RNA Mechanisms and Brain Disease, Copenhagen, Denmark. Poster “ RT-qPCR-based assay for mRNA integrity evaluation in mouse brain tissue and synaptosomal preparations“. D. Pamedytyte (presenter), U. Neniskyte.

CURRICULUM VITAE

EDUCATION

2018 10 –	PhD Student in Biochemistry
2024 09	Dr. Urte Neniskyte group, Department of Neurobiology and Biophysics, Life Sciences Center, Vilnius University, Vilnius, Lithuania
2016 09 –	MSc in Molecular Biology
2018 01	Prof. Aurelija Zvirbliene group, Department of Immunology and Cell Biology, Life Sciences Center, Vilnius, Lithuania
2012-09 –	BSc in Molecular Biology
2016 06	Prof. Aurelija Zvirbliene group, Department of Immunology and Cell Biology, Life Sciences Center, Vilnius, Lithuania

RESEARCH EXPERIENCE

2023 10 –	Junior Researcher
2024 09	Dr. Urte Neniskyte group, Institute of Biosciences, Life Sciences Center, Vilnius University, Vilnius, Lithuania
2021 10 –	Junior Researcher
2023 09	Dr. Urte Neniskyte group, VU-EMBL partnership institute, Life Sciences Center, Vilnius University, Vilnius, Lithuania
2019-10 –	Junior Researcher
2021 09	Dr. Urte Neniskyte group, Department of Neurobiology and Biophysics, Life Sciences Center, Vilnius University, Vilnius, Lithuania
2016-10 –	Junior Researcher
2018 09	Prof. Aurelija Zvirbliene group, Department of Immunology and Cell Biology, Life Sciences Center, Vilnius, Lithuania

RESEARCH INTERNSHIPS

2023 04 24 –	Internship
2023 05 05	EMBL GeneCore, Heidelberg, Germany. A collaborative project where I brought purified synaptic samples to do general RNA and miRNA sequencing with the help of the experts at EMBL GeneCore under supervision of Vladimir Benes
2022 08 19 –	Young Investigator Training Programme (YITP)
2022 09 09	Institut NeuroMyoGène, Lyon, France. YITP sponsored by IBRO-PERC was a 3-week internship at a chosen host laboratory in France
2020 02 04 –	Internship
2020 02 07	SONY CENTER, Berlin, Germany. The goal of the internship was to bring prepared presorted synaptosomes to try new SH800S Cell Sorter for Fluorescence Activated Synaptosome Sorting
2018-12 02 –	Internship
2018 12 08	University of Bordeaux, France. The goal of the internship was to learn Fluorescence Activated Synaptosome Sorting (FASS) technique and apply it to our research in Lithuania

PROFESSIONAL TRAINING

2023 03 27 –	VIZBI – visualizing biological data masterclass (EMBO
2023 03 28	wokshop), online
2022 06 13 –	CAJAL advanced neuroscience training course on single cell
2022 07 01	profiling and analysis in neuroscience. Held at Bordeaux Scholl of Neuroscience, Bordeaux, France
2022 07 01 –	R for Biochemists course , online, held by the Biochemical
2022 08 01	Society

SCOLARSHIPS AND AWARDS

2023 08 16	Early Career Scientist Grant From HELLOBIO To attend 11th International IBRO world congress in Granada, Spain
2023 08 09	FENS travel grant for the IBRO World Congress 2023 To attend 11th International IBRO world congress in Granada, Spain
2023 06 12	Christian Boulin Fellowship For internship at EMBL GeneCore in Heidelberg, Germany
2022 08 04	Lithuanian Neuroscience Association Scholarship For internship at Institute NeuroMyoGene in Lyon, France
2022 06 30	Grant for (doctoral) academic visit by Research Council of Lithuania To attend FENS forum 2022 in Paris, France
2022 06 10	Travel Grant from the Boehringer Ingelheim Fonds (BIF) To attend the CAJAL course held in Bordeaux school of Neuroscience, Bordeaux, France
2021 10 20	FENS, the Brain Prize and IBRO-PERC stipend To attend the Brain Conference on RNA mechanisms and brain disease, Copenhagen, Denmark

SCIENTIFIC COMMUNICATION

An interview in HelloBio website as part of accepting Early Career Scientist grant. (2023.08.16) <https://hellobio.com/blog/meet-our-early-career-scientist-grant-winner-daina-pamedytyte.html?fbclid=IwAR2imOVDD7xDkNxrpNyX3J6phQfxVkfCWsGdFOXgA8V7mICISj1tOc1RSy8>

TEACHING EXPERIENCE

Transcriptomics and modeling neurodevelopment disorders lectures and several seminars as part of Neuromethods course, Neurobiology and Biophysics BSc programme (since 2022)

Consultant for 1 master's student (2021-2023)

Supervisor/Consultant of 5 bachelor students (since 2015)

VOLUNTEERING AND SOCIAL PROJECTS

2021 11 20 –	Jubilee Lithuanian Scout camp program organizer
2023 07 15	Camp for children 10 to 14 years old. There were 600 children participating in our program through the camp. One activity there I was leading myself
2022 02 11 –	ERASMUS + youth exchange project “Peaceful leadership”
2022 02 15	in Estonia
and 2022 03	The project aim was to inspire youth to lead and build confidence
22 – 2022 03	by providing space to create and lead various collaborative
30	activities and discussions. I was the program organizer and
	Lithuanian team leader
2021 09 07 –	ERASMUS + youth exchange project “Language Learning
2021 09 13	to support active Social Inclusion” in Poland
	The training course aim was to promote collaboration, improve
	creativity and public speaking skills

NOTES

NOTES

NOTES

NOTES

Vilniaus universiteto leidykla
Saulėtekio al. 9, III rūmai, LT-10222 Vilnius
El. p. info@leidykla.vu.lt, www.leidykla.vu.lt
bookshop.vu.lt, journals.vu.lt
Tiražas 15 egz.